MULTIFUNCTIONAL CONDUCTIVE CEMENTITIOUS COMPOSITES INCLUDING PHASE CHANGE MATERIALS WITH SNOW/ICE MELTING CAPABILITY

KAR/BUZ ERİTME ÖZELLİĞİNE SAHİP, FAZ DEĞİŞTİREN MALZEME İÇEREN MULTİFONKSİYONEL İLETKEN ÇİMENTO ESASLI KOMPOZİTLER

FATİH ACIKÖK

PROF. DR. MUSTAFA ŞAHMARAN

Supervisor

Submitted to

Graduate School Of Science and Engineering of Hacettepe Universtiy

as a Partial Fulfilment to the Requirements

for be Award of the Degree of **Doctor of Philosopy**

in Civil Engineering

2024

ABSTRACT

MULTIFUNCTIONAL CONDUCTIVE CEMENTITIOUS COMPOSITES INCLUDING PHASE CHANGE MATERIALS WITH SNOW/ICE MELTING CAPABILITY

Fatih ACIKÖK

Doctor of Philosophy, Department of Civil Engineering

Supervisor: Prof. Dr. Mustafa ŞAHMARAN

December 2023, 156 pages

In winter, snowfall and icing below 0 °C cause disruption of transportation on roads and airlines, as well as accidents with loss of life and property damage. Within the scope of the mechanical methods (ploughing, sweeping, etc.) applied for cleaning snow and ice, labor, equipment and operator costs affect the resources of our country negatively. On the other hand, the deicing salt method, which is frequently used to melt snow and ice, when applied to asphalt pavements, can cause disintegration, deterioration, and the adherence between aggregates and bituminous mixture significantly weakening and decomposition of aggregates, together with freeze-thaw effects. In addition, freezing and thawing cycles and de-icing salts cause spalling damage on concrete pavements, causing significant damage to the surface of the pavement, and in later stages, the de-icing salt solution leaks into the pavement and causes reinforcement corrosion. In order to eliminate the negative properties of mechanical methods and deicing salts, which are within the scope of

traditional applications, Phase Change Materials (PCM), which is a renewable energy source and has the ability to store and release the heat energy of the sun, potential of melting snow and ice in concrete and asphalt road pavements has been started to be investigated in recent years. However, some problems with the direct use of PCM on asphalt and concrete pavements need to be eliminated. If PCM is used in hot bituminous mixtures, it is necessary to produce microencapsulated PCMs resistant to high temperatures (140-160°C) during the mixing, placing and compaction stages of these mixtures. Otherwise, it is expected that the PCMs will leak from the microcapsules and lose their effectiveness and affect the physical and rheological properties of the asphalt mixture. In case PCMs are used directly on concrete pavements, it is predicted that the heat energy that will be released or absorbed at the phase change temperature will remain at low levels due to the insulating nature of the concrete material. On the other hand, in recent years, the structural performance, energy consumption, sustainability, safety and efficiency of infrastructure and superstructures have been improved thanks to multifunctional cementitious composites. It is known that conductive cementitious materials, which are classified as multifunctional cementitious composites and obtained by incorporating different types of functional materials into the composite, find applications in heating systems, which are generally costly, in order to melt snow and ice.

Within the scope of the thesis, a new approach was exhibited by departing from the previous studies. In the first part of the thesis, cement-based composites with self-levelling properties and sufficient strength were produced. In the second part, multifunctional cement-based composites with increased thermal conductivity were developed by adding conductive materials to this composite produced. In the third part, microencapsulated organic PCM were included in the multifunctional cement-based composites developed. Thus, it is aimed to produce pavements that can melt snow and ice by providing rapid transfer of the heat energy to the surface where the snow/ice is found thanks to the improved thermal conductivity of the composite. In addition, thanks to the improved conductive feature, it is aimed to achieve snow/ice melting performance with a lower amount of PCM compared to the usage rates in the literature. In the last section, studies were carried out to create sufficient bond strength with the substrate

concrete and asphalt in order to apply the composite, which has the ability to melt snow/ice on its own, as a pavement on asphalt and concrete roads.

Keywords: De-icing salts, Phase Change Materials, Multifunctionality, Conductive cementitious composites, Strength and durability

ÖZET

KAR/BUZ ERİTME ÖZELLİĞİNE SAHİP, FAZ DEĞİŞTİREN MALZEME İÇEREN MULTİFONKSİYONEL İLETKEN ÇİMENTO ESASLI KOMPOZİTLER

Fatih ACIKÖK

Doktora, İnşaat Mühendisliği Bölümü

Tez Danışmanı: Prof. Dr. Mustafa ŞAHMARAN

Aralık 2023, 156 sayfa

Kış mevsiminde oluşan kar yağışları ve 0 °C'nin altında meydana gelen buzlanma, karayolu ve havayollarında ulaşımın aksamasına ve bununla birlikte can kayıplı ve maddi hasarlı kazalara sebep olmaktadır. Kar ve buzun temizlenmesi amacıyla uygulanan mekanik yöntemler (küreme, süpürme vs.) kapsamında iş gücü, ekipman ve operatör maliyetleri ülkemizin kaynaklarını olumsuz anlamda etkilemektedir. Diğer yandan kar ve buzu eritmek için sıklıkla kullanılan buz çözücü tuz yöntemi, asfalt kaplamalara uygulandığında donma çözülme etkileriyle birlikte parçalanmaya, bozulmaya ve agregalar ile bitümlü karışım arasındaki aderansı önemli derecede zayıflatıp agregaların ayrışmasına sebep olabilmektedir. Bununla birlikte donma çözülme çevrimlerinin ve buz çözücü tuzların beton kaplamalarda pullanma hasarı meydana getirmesi sonucu öncelikle üstyapının yüzeyinde önemli seviyede hasarlar oluşturup ileri ki aşamalarda tuzlu su çözeltisinin üstyapının içerisine sızıp donatı korozyonuna neden olmaktadır. Geleneksel

uygulamalar kapsamında olan mekanik yöntemlerin ve buz çözücü tuzların belirtilen olumsuz özelliklerini gidermek amacıyla yenilenebilir enerji kaynağı sınıfına giren ve güneşin ısı enerjisini depolayıp salabilme özelliğine sahip olan Faz Değiştiren Malzemelerin (FDM) beton ve asfalt yol kaplamalarında kar ve buzu eritebilme potansiyeli son yıllarda araştırılmaya başlanmıştır. Fakat FDM'nin asfalt ve beton kaplamalarda doğrudan kullanılmasıyla ile ilgili bazı problemlerin giderilmesi gerekmektedir. FDM'nin bitümlü sıcak karışımlarda kullanılması durumunda bu karışımların karıştırma, yerleştirme ve sıkıştırma aşamalarında yüksek sıcaklıklara (140-160°C) dayanıklı mikrokapsüllü FDM'lerin üretilmesi gerekmektedir. Aksi takdirde mikrokapsüllerin içerisinden FDM'lerin sızması ve etkinliğini yitirmesiyle birlikte asfalt karışımının fiziksel ve reolojik özelliklerini etkilemesi beklenmektedir. FDM'lerin doğrudan beton kaplamalarda kullanılması durumunda ise faz değişim sıcaklığında salacağı veya absorbe edeceği ısı enerjisinin beton malzemesinin yalıtkan yapısı nedeniyle düşük seviyelerde kalacağı öngörülmektedir. Diğer yandan son yıllarda altyapı ve üstyapıların yapısal performansı, enerji tüketimi, sürdürülebilirliği, güvenliği ve verimliliği multifonksiyonel çimentolu kompozitler sayesinde geliştirilmektedir. Multifonksiyonel çimentolu kompozitler sınıfına giren ve farklı tipte fonksiyonel malzemelerin kompozite dahil edilmesiyle elde edilen iletken çimentolu malzemelerin kar ve buzu eritmek amacıyla genellikle maliyeti yüksek olan ısıtmalı kaplama sistemlerinde uygulama alanı bulduğu bilinmektedir.

Tez kapsamında ise geçmiş çalışmalardan ayrışarak, yeni bir yaklaşım sergilenmiştir. Tezin ilk bölümünde kendiliğinden seviyelenebilme özelliğine ve yeterli dayanıma sahip çimento bağlayıcılı kompozitler üretilmiştir. İkinci bölümünde ise üretilen bu kompozite iletken özellikte malzemeler dahil edilerek ısıl iletkenliği arttırılmış multifonksiyonel çimento bağlayıcılı kompozitler geliştirilmiştir. Üçüncü bölümde ise geliştirilen multifonksiyonel çimento bağlayıcılı kompozitlere mikrokapsüllenmiş organik FDM dahil edilmiştir. Böylelikle FDM'nin salacağı ısı enerjisinin kompozitin geliştirilmiş ısıl iletkenliği sayesinde kar/buzun bulunduğu yüzeye hızlı transferinin sağlanarak kendiliğinden kar ve buz eritebilen kaplamaların üretilmesi amaçlanmıştır. Ayrıca geliştirilmiş iletken özellik sayesinde literatürdeki kullanım oranlarına kıyasla daha düşük miktarda FDM oranı ile kar/buz eritme performansı alınması hedeflenmiştir. Son

bölümde ise kendilinden kar/buz eritebilme özelliğine sahip olarak üretilen kompozitin asfalt ve beton yollar üzerinde kaplama olarak uygulanması için alt tabaka beton ve asfaltı ile yeterli bağ dayanımı oluşturmasına yönelik çalışmalar yapılmıştır.

Anahtar Kelimeler: Buz çözücü tuzlar, Faz değiştiren malzemeler, Multifonksiyonellik, İletken çimento bağlayıcılı kompozitler, Dayanım ve durabilite

ACKNOWLEDGEMENT

I would first want to express my sincere gratitude to my supervisor, Prof. Dr. Mustafa ŞAHMARAN, for supporting and guiding me during the course of my thesis study with his enormous knowledge and expertise. Working with him was a great honor and joy.

I also want to express my gratitude to Prof. Dr. İlhami DEMİR, Assoc. Prof. Dr. Mustafa Kerem KOÇKAR, Assoc. Prof. Dr. Gürkan YILDIRIM and Assist. Prof. Hüseyin ULUGÖL for being on my thesis jury.

For their assistance and enduring friendship, I would like to thank every single person who works at the Advanced Concrete Research Laboratory at Hacettepe University. Especially, I would like to thank Res. Asst. Mehmet Kemal Ardoğa for his contributions through the process.

I would like to thank TÜBİTAK (The Scientific and Technological Research Council Of Türkiye) for its support within the scope of the 1002 - Short Term R&D Funding Program scholarship.

I would also like to thank my beloved wife who supported me wholeheartedly throughout the thesis process.

FATİH ACIKÖK

December 2023, Ankara

TABLE OF CONTENTS

ABSTRACT i

ÖZET iv

ACKNOWLEDGEMENT vii

LIST OF FIGURES xii

LIST OF TABLES xviii

SYMBOLS AND ABBREVIATIONS xxi

1. INTRODUCTION 1

1.1. Problem Definition 1

1.2. Scope and Objectives 2

1.3. Thesis Outline 4

2. LITERATURE REVIEW 5

2.1. Snow/Ice Melting 5

2.1.1. De-icing Salts 8

2.1.2. Heated Pavement Systems 12

2.1.3. Phase Change Materials 13

2.2. Multifunctional Cementitious Materials 22

2.2.1. Electrical Conductive Cementitious Composites 23

2.2.2. Thermal Conductive Cementitious Composites 29

3. EXPERIMENTAL STUDIES 33

3.1. Materials 33

3.1.1. Binder 33

3.1.2. Aggregates 33

3.1.3. Mineral Additives 34

3.1.4. Chemical Additives 35

3.1.5. Carbon Fiber 36

3.1.6. Steel Fiber 36
3.1.7. Phase Change Materials 37
3.2. Methodology 43
3.2.1. Production of Reference Composite 43
3.2.2. Production of Conductive Composites 44
3.2.3. Production of Composites with Self-Melting Capability of Snow/Ice 45
3.3. Testing 48
3.3.1. Mini Slump Flow Spread Test and T_{500} Tests 49
3.3.2. Compressive Strength Test 50
3.3.3. Electrical Resistivity and Thermal Conductivity Tests 50
3.3.4. Freeze-Thaw Performance Test 53
3.3.4.1. First Procedure-Different PCM Ratios by Cement Weight 55
3.3.4.2. Second Procedure-Composites of Different Thicknesses Containing 6% PCM of the Cement Weight 55
3.3.5. Ice Melting Performance Test 57
3.3.5.1. First Procedure-Different PCM Ratios by Cement Weight 57
3.3.5.2. Second Procedure-Composites of Different Thicknesses Containing 6% PCM of the Cement Weight 57
3.3.6. Scaling Test 58
3.3.7. Bond Strength Tests 59
3.3.7.1. Slant Shear Test 60
3.3.7.2. Pull-Off Test 62
3.3.8. Microstructural Analysis 64
4. RESULTS AND DISCUSSION 66
4.1. Results of Mini Slump Flow Spread and T_{500} Tests 66
4.2. Results of Compressive Strength Test 70
4.3. Results of Electrical Resistivity and Thermal Conductivity Tests 75
4.4. Results of Freeze-Thaw Performance Test 83
4.4.1. First Procedure-Different PCM Ratios by Cement Weight 83
4.4.1.1. Samples Containing 8% PCM By Weight of Cement 83
4.4.1.2. Samples Containing 6% PCM By Weight of Cement 90
4.4.1.3. Samples Containing 4% PCM By Weight of Cement 92

4.4.1.4. Samples Containing 2% PCM By Weight of Cement 94
4.4.1.5. PCM-Free Samples 96
4.4.2. Second Procedure-Composites of Different Thicknesses Containing 6% PCM of the Cement Weight 99
4.4.2.1. Samples with 50 mm Thickness 100
4.4.2.2. Samples with 40 mm Thickness 101
4.4.2.3. Samples with 30 mm Thickness 103
4.4.2.4. Samples with 20 mm Thickness 105
4.5. Results of Ice Melting Performance Test 108
4.5.1. First Procedure-Different PCM Ratios by Cement Weight 108
4.5.1.1. Samples Containing 8% PCM By Weight of Cement 109
4.5.1.2. Samples Containing 6% PCM By Weight of Cement 110
4.5.1.3. Samples Containing 4% PCM By Weight of Cement 112
4.5.1.4. Samples Containing 2% PCM By Weight of Cement 113
4.5.1.5. PCM-Free Samples 115
4.5.2. Second Procedure-Composites of Different Thicknesses Containing 6% PCM of the Cement Weight 118
4.5.2.1. Samples with 50 mm Thickness 118
4.5.2.2. Samples with 40 mm Thickness 119
4.5.2.3. Samples with 30 mm Thickness 121
4.5.2.4. Samples with 20 mm Thickness 122
4.5.2.5. Samples with 10 mm Thickness 123
4.6. Results of Scaling Test 126
4.7. Results of Bond Strength Tests 128
4.7.1. Slant Shear Test 128
4.7.2. Pull-Off Test 130
4.8. Microstructural Analysis Results of Cementitious Composites 134
5. CONCLUSION 142
6. REFERENCES 148
APPENDICES 157
APPENDIX 1 – Published articles from thesis work 157
APPENDIX 2 – Thesis Originality Report 176

CIRRICULUM VITAE 177

LIST OF FIGURES

Figure 1.1. Multifunctional conductive overlay containing PCM with melting snow/ice capability 3
Figure 2.1. Analysis of Türkiye Annual Average Number of Snow Covered Days (1970- 2020) (MS, 2021) 5
Figure 2.2. 2020-2021 winter season minimum temperature map (Extreme temperature map) (MS, 2021) 6
Figure 2.3. Vehicles of dealing with snow and ice a.) Trucks with snow blade equipment b.) Rotary snowplow (Karayolları Genel Müdürlüğü, 2018) 7
Figure 2.4. GDH Safety Road Maintenance and Operation Costs in 2020 (Karayolları Genel Müdürlüğü, 2021) 8
Figure 2.5. Typical surface scaling on concrete pavements as a result of freeze-thaw cycles and bursting of aggregate particles forming cavities on the concrete surface (Damage at an airport in our country after two years) 10
Figure 2.6. Damages in a test sample containing sodium chloride (NaCl) solution and exposed to freeze-thaw cycles (GDH Concrete Laboratory) 11
Figure 2.7. Caused by ASR damage in airport rigid pavements; a) Cracking b) Expansion of concrete pavement adjacent to asphalt pavement (Shi, 2008) 12
Figure 2.8. Energy-temperature relationship of PCMs (Fernandes et al., 2014) 14
Figure 2.9. Effect of PCMs on temperature amplitudes in asphalt and concrete pavements (Manning et al., 2015) 15
Figure 2.10. Effect of PCM on heat of hydration (Hunger et al., 2009) 19
Figure 2.11. Effect of PCM in concrete on snow melting (Farnam et al., 2017) 20
Figure 2.12. Methods of incorporation of PCM into concrete and cement-based composites; a) Using pipes filled with PCM b) Using lightweight aggregate particles saturated with PCM c) Using microcapsules containing PCM d) Filling surface voids with PCM absorption (Savija, 2018) 21

Figure 2.13. Effect of PCM on compressive and flexural strength of concrete (Yeon and Kim, 2018) 22
Figure 2.14. De-icing time of composites containing carbon nanotubes and carbon nanofibers (Gomis et al., 2015) 25
Figure 2.15. The relationship between conductivity and the rate of contact between fibers (Xie et al., 1996) 26
Figure 2.16. Electrical resistance values of conductive composites containing different volumes of CF depending on the hydration age (Wu, Liu and Yang, 2015) 27
Figure 2.17. Temperature change in the center of mass concrete with increasing k value (Folliard et al., 2017) 31
Figure 2.18. Effect of SF volume on the thermal conductivity of concrete (Liu et al., 2017) 32
Figure 3.1. Digital camera of QS 34
Figure 3.2. Digital camera photo and SEM analysis image of CF 36
Figure 3.3. Digital camera image of SF 37
Figure 3.4. Digital camera view of PCM 38
Figure 3.5. SEM analysis image of PCM 38
Figure 3.6. DSC analysis of PCM 40
Figure 3.7. PCM particles in fluorescent microscopy 41
Figure 3.8. The cumulative particle size distribution of microencapsulated PCMs 41
Figure 3.9. FTIR spectra of PCM 42
Figure 3.10. Scheme of synthesis of melamine formaldehyde resins 43
Figure 3.11. Addition of PCM dispersion to the mortar mix 46
Figure 3.12. Flow diagram of tests applied to produced mixture 48
Figure 3.13. Determination of the consistency of mixtures with the mini slump flow spread test 49
Figure 3.14. a) Placing the mortar in the mold b) Subjecting the sample to the compressive strength test 50
Figure 3.15. Resistivity meter with the test specimen 51
Figure 3.16. a.) Core drilling machine b.) Cutting machine c.) Abrasion machine d.) Thermal conductivity samples of Ø50×25 mm obtained after coring, cutting and abrasion processes (GDH-Concrete Laboratory) 52

Figure 3.17. Heat Flow Meter (Lasercomp Fox-50 device).....53
Figure 3.18. Graph of the cycle systems created on the reference sample 54
Figure 3.19. a) Ready-made freeze-thaw molds b) Samples placed in molds and siliconized on the edges c) Drilling process from the middle of the sample in the mold d) The samples placed in the cabinet with a thermocouple in their center e) Freeze-Thaw cabinet. 56
Figure 3.20. Samples with a thickness of 10, 20, 30, 40, 50 mm.....57
Figure 3.21. The process of placing ice on the samples in the cabinet 58
Figure 3.22. Scaling test cycle plot 59
Figure 3.23. a) Substrate concrete samples cut at an angle of 30 °C b) Monolithic state of PCM(6)CF(0.1) mixture and substrate concrete sample 61
Figure 3.24. a) Substrate asphalt samples cut at an angle of 30 °C b) Monolithic state of PCM(6)CF(0.1) mixture and substrate asphalt sample.....61
Figure 3.25. Pull-Off Test Device.....63
Figure 3.26. Substrate concrete casting.....63
Figure 3.27. Substrate concrete sample with 5 cm thickness PCM(6)CF(0.1) coded composite.....63
Figure 3.28. a) 1 cm thick PCM(6)CF(0.1) coded composite and substrate asphalt sample b) Core taked and metal ring attached sample 64
Figure 3.29. SEM analysis device.....65
Figure 4.1. Results of mini slump flow spread and T_{500} test.....68
Figure 4.2. Clustering of SFs collapsing to the substrate in a mixture with a mini flow diameter of 360 mm 69
Figure 4.3. Visual determination of the homogeneous distribution of SFs a.) Distribution of SFs in the mixture with code SF(5) broken with a hammer b.) Distribution of SFs in a sample cored for thermal conductivity test.....69
Figure 4.4. Compressive strength results of conductive composites 72
Figure 4.5. Compressive strength results of conductive composites containing PCM ...74
Figure 4.6. Electrical resistance values of composites containing CF and SF.....77
Figure 4.7. Electrical Thermal conductivity values of composites containing CF and SF.....77
Figure 4.8. Relationship between ER and thermal conductivity for 7th day 80

Figure 4.9. Relationship between ER and thermal conductivity for 28th day 80
Figure 4.10. Electrical resistance values of composites containing PCM 82
Figure 4.11. +20/-20 °C temperature cycle for the reference composite 84
Figure 4.12. The shoulders formed in the PCM(8)CF(0) composite 84
Figure 4.13. PCM(0)CF(0) and PCM(8)CF(0.1) in the first simulation..... 85
Figure 4.14. Determining the regions where the PCM emits and absorbs heat energy and the effect of the PCM on the temperature amplitudes for first simulation 86
Figure 4.15. PCM(0)CF(0) and PCM(8)CF(0.3) in the first simulation..... 86
Figure 4.16. PCM(0)CF(0), PCM(8)CF(0), PCM(8)CF(0.1) and PCM(8)CF(0.1) in the first simulation 87
Figure 4.17. Zones 1 and 2 where temperature data are taken for the first simulation .. 87
Figure 4.18. Second simulation for composites which containing 8% PCM by weight of cement. 90
Figure 4.19. First simulation for composites which containing 6% PCM by weight of cement 91
Figure 4.20. Second simulation for composites which containing 6% PCM by weight of cement 91
Figure 4.21. First simulation for composites which containing 4% PCM by weight of cement 93
Figure 4.22. Second simulation for composites which containing 4% PCM by weight of cement. 93
Figure 4.23. First simulation for composites which containing 2% PCM by weight of cement 95
Figure 4.24. Second simulation for composites which containing 2% PCM by weight of cement. 95
Figure 4.25. First simulation for composites which containing 0% PCM by weight of cement 97
Figure 4.26. Second simulation for composites which containing 0% PCM by weight of cement 97
Figure 4.27. Temperature differences compared to the reference sample 99
Figure 4.28. Sample thickness of 50 mm in first simulation 100
Figure 4.29. Sample thickness of 50 mm in second simulation 101

Figure 4.30. Sample thickness of 40 mm in first simulation.....102
Figure 4.31. Sample thickness of 40 mm in second simulation.....102
Figure 4.32. Sample thickness of 30 mm in first simulation.....104
Figure 4.33. Sample thickness of 30 mm in second simulation.....104
Figure 4.34. Sample thickness of 20 mm in first simulation.....106
Figure 4.35. Sample thickness of 20 mm in second simulation.....106
Figure 4.36. Variation of temperature differences compared to the reference sample according to sample thicknesses.....108
Figure 4.37. Melting Ice Amounts In The Samples Containing 8% PCM Relative to Cement Weight.....110
Figure 4.38. Melting Ice Amounts In The Samples Containing 6% PCM Relative to Cement Weight.....111
Figure 4.39. Condition of the ice layers on the samples at the 24th hour of the test 112
Figure 4.40. Melting Ice Amounts In The Samples Containing 4% PCM Relative to Cement Weight.....113
Figure 4.41. Melting Ice Amounts In The Samples Containing 2% PCM Relative to Cement Weight.....115
Figure 4.42. Melting Ice Amounts In The Samples Containing 0% PCM Relative to Cement Weight.....116
Figure 4.43. Ice melting rates of composites 118
Figure 4.44. Melting Ice Amounts in Samples with a Thickness of 50 mm.....119
Figure 4.45. Melting Ice Amounts in Samples with a Thickness of 40 mm.....120
Figure 4.46. Melting Ice Amounts in Samples with a Thickness of 30 mm.....122
Figure 4.47. Melting Ice Amounts in Samples with a Thickness of 20 mm.....123
Figure 4.48. Melting Ice Amounts in Samples with a Thickness of 10 mm.....124
Figure 4.49. Ice melting rates of samples with different thickness.....125
Figure 4.50. Results of scaling test 127
Figure 4.51. The spalling material from the PCM(6)CF(0.3) coded composite 128
Figure 4.52. Stages of slant shear test 130
Figure 4.53. The rupture patterns formed on the 28th day in the 4 cm-thick sample 132
Figure 4.54. The rupture patterns formed on the 28th day in 1 cm and 5 cm samples ..133
Figure 4.55. Samples that broke off as a result of the test on the 28th day in the sample with a thickness of 2 cm.....134

Figure 4.56. First image of reference sample with 10000x magnification 135
Figure 4.57. Second image of reference sample with 10000x magnification..... 135
Figure 4.58. Third image of reference sample with 10000x magnification 135
Figure 4.59. 500x magnification image of CF(0.1) composite..... 136
Figure 4.60. 500x magnification image of CF(0.3) composite..... 136
Figure 4.62. 2500x magnification image of PCM(2)CF(0) composite..... 138
Figure 4.63. 5000x magnification image of PCM(4)CF(0) composite..... 138
Figure 4.64. Ettringite formation around microcapsules for PCM(6)CF(0)..... 138
Figure 4.65. Distribution of PCM microcapsules for the PCM(6)CF(0) composite 139
Figure 4.66. Flexible structure of microcapsules for the PCM(6)CF(0) composite 139
Figure 4.67. 10000x magnification image of PCM(6)CF(0) composite..... 139
Figure 4.68. SEM image of the PCM(8)CF(0) composite at different magnification factors..... 140
Figure 4.69. 2500x magnification image of PCM(2)CF(0.1) composite..... 141
Figure 4.70. 5000x magnification image of PCM(4)CF(0.1) composite..... 141
Figure 4.71. 5000x magnification image of PCM(6)CF(0.1) composite..... 141
Figure 4.72. 1000x magnification image of PCM(8)CF(0.1) 141

LIST OF TABLES

Table 2.1. Deicing Chemicals (Berberoğlu, 2011; Zhang and Das, 2009; Yehia and Tuan, 1998) 9
Table 2.2. Costs and power consumptions of various heating systems (Seferoğlu, Seferoğlu and Akpınar, 2015; Yehia and Tuan, 1998) 13
Table 2.3. Data on the number of locations predicted to extend the service life by at least 1 year as the thermal conductivity of bridge deck composites with different PCM types increases from 1.5 W/m.k to 3 W/m.k in the simulation model (Sakulich and Bentz, 2012) 17
Table 2.4. Classification and technical specifications of PCMs (Savija, 2018) 17
Table 3.1 Chemical and physical properties of PC, GGBFS, and QS 34
Table 3.2. Technical characteristics of HRWRA 35
Table 3.3. Properties of VM (Culminal) 35
Table 3.4. Physical properties of CF 36
Table 3.5. Physical properties of SF 37
Table 3.6. Technical data of PCM dispersion 38
Table 3.7. Heat properties of PCM 40
Table 3.8. Weight ratios of compounds for the reference mixture composite 44
Table 3.9. Volumetric incorporation rates of fibers into referenc mixture 45
Table 3.10. Conductive composites containing PCM and CF 47
Table 3.11. Spalling resistance test cycle intervals 59
Table 4.1. Consistency properties of cementitious composites 67
Table 4.2. Compressive strength of cementitious composites 71
Table 4.3. Electrical resistance and thermal conductivity avarage results of composites containing CF and SF 76
Table 4.4. Electrical resistance avarage results of PCM containing composites 82
Table 4.5. Freeze-thaw performance test results of composites which containing 8% PCM by weight of cement 88
Table 4.6. Freeze-thaw performance test results of composites which containing 6% PCM by weight of cement 92

Table 4.7. Freeze-thaw performance test results of composites which containing 4% PCM by weight of cement 94
Table 4.8. Freeze-thaw performance test results of composites which containing 2% PCM by weight of cement 96
Table 4.9. Freeze-thaw performance test results of composites which containing 0% PCM by weight of cement 98
Table 4.10. The difference in temperature amplitudes at 50 mm sample thickness 101
Table 4.11. The difference in temperature amplitudes at 40 mm sample thickness 103
Table 4.12. The difference in temperature amplitudes at 30 mm sample thickness 105
Table 4.13. The difference in temperature amplitudes at 20 mm sample thickness 107
Table 4.14. Time-dependent cumulative ice melting of conductive samples containing 8% of the cement weight of PCM and the reference sample . 109
Table 4.15. Time-dependent cumulative ice melting of conductive samples containing 6% of the cement weight of PCM and the reference sample . 111
Table 4.16. Time-dependent cumulative ice melting of conductive samples containing 4% of the cement weight of PCM and the reference sample . 113
Table 4.17. Time-dependent cumulative ice melting of conductive samples containing 2% of the cement weight of PCM and the reference sample . 114
Table 4.18. Time-dependent cumulative ice melting of conductive samples containing 0% of the cement weight of PCM and the reference sample . 116
Table 4.19. Cumulative ice melting amounts of samples with a thickness of 50 mm depending on time 119
Table 4.20. Cumulative ice melting amounts of samples with a thickness of 40 mm depending on time 120
Table 4.21. Cumulative ice melting amounts of samples with a thickness of 30 mm depending on time 121
Table 4.22. Cumulative ice melting amounts of samples with a thickness of 20 mm depending on time 123
Table 4.23. Cumulative ice melting amounts of samples with a thickness of 10 mm depending on time 124
Table 4.24. The amount of material that scaling as a result of the test cycles 126
Table 4.25. Results of slant shear strength test 129
Table 4.26. Results of pull-off test for asphalt substrate 131

Table 4.27. Results of pull-off test for concrete substrate 133

SYMBOLS AND ABBREVIATIONS

Symbols

Ω	Electrical resistance (ohm)
Hz	Hertz
k	Thermal conductivity
kHz	Kilohertz
Mpa	Megapascal
Pa	Pascal
τ	Shear stress
τ_0	Yield stress
μ	Shear rate
γ	Plastic viscosity

Abbrevations

ASR	Alkali Silica Reaction
$Ca(OH)_2$	Calcium Hydroxide
$CaCl_2$	Calcium Chloride
CF	Carbon Fiber
CMA	Calcium Magnesium Acetate
C-S-H	Calcium Silicate Hydrate Gel
DSC	Differantial Scanning Calorimetry
FTIR	Fourier Transform Infrared Spectroscopy
GGBFS	Ground Granulated Blast Furnace Slag

GDH	General Directorate of Highways
HRWRA	High-Range Water Reducing Admixture
KAc	Potassium Acetate
KF	Potassium Formate
MS	Meteorological Service
NaAc	Sodium Acetate
NaCl	Sodium Chloride
NaOH	Sodium Hydroxide
$MgCl_2$	Magnesium Chloride
PCM	Phase Change Material
PVA	Poly-vinyl-alcohol
SEM	Scanning Electron Microscope,
SF	Steel Fiber
VM	Viscosity Modifier

1. INTRODUCTION

1.1. Problem Definition

In our country and around the world, cement-based composites are widely used because they are affordable, simple to make and use, and have a high compressive strength. However, factors including high brittleness, low toughness, and low tensile strength have a negative impact on the durability of these materials. In order to avoid the aforementioned drawbacks, multifunctional cementitious composites with high durability and enhanced mechanical properties have been developed (Yildirim et al., 2015; Gomis et al., 2015). Multifunctionality refers to the ability to assess and use non-structural functions without the usage of an external power source or device. Creating multifunctional cementitious composites with the extra features is the goal in order to achieve high durability, sustainability, safety and efficiency together with satisfying structural performance and low energy consumption. Conductive cementitious materials, on the other hand, are employed in heating, anti-static, anti-corrosion, and electromagnetic protection applications and are also categorized as multifunctional cementitious composites. The production of conductive composites is often achieved with steel fibers/powders, but mostly, carbon-based materials (carbon fibers, carbon nanotubes and nanofibers, carbon black etc.) (Faneca et al., 2018). One of the aims using conductive composites is to melt the snow/ice on superstructures such as highways, bridges and airports. Thanks to its conductivity, electrical or heat energy is transferred in the pavement surface rapidly allowing snow/ice to melt faster (Wu, Liu and Yang, 2015).

Snow/ice melting applications are becoming important in Türkiye which many regions and cities where long-term snowfalls are effective in. Especially in Central Anatolia and Eastern Anatolia, which have continental climates, the snow thickness and the duration of snow on the ground cause transportation challenges for village roads, city roads and highways, and accidents resulted from the ice formation at temperatures below 0 °C. In Türkiye, the General Directorate of Highways (GDH) is responsible for preventing accidents and reopening snow-covered roads as soon as feasible. GDH has a hierarchical action plan, and it begins with preventive maintenance (anti-icing) prior to snowfall and icing. After snowfall and icing, within the scope of de-icing application, snowplow and

snow removal operators serve (mechanical methods) and de-icing salt method (chemical methods) is applied (KGM, 2018). De-icing salts, however, damage metal components, environment, plants (Seferoğlu, Seferoğlu and Akpınar, 2015; KGM, 2018) and cause spalling and disintegration in concrete pavements with freeze-thaw cycles, and over time, they leach into the pavement, causing rust in reinforcements, if any (Neville, 2011). Furthermore, particularly the chemicals, used to deice airport concrete pavements and based on alkali metal salts (potassium acetate-KAc, sodium acetate-NaAc, etc.), cause alkali-silica reactions (ASR) (Rangaraju et al., 2006). The use of heated pavement systems (electrical heating, hydraulic heating etc.) as an alternative to mechanical and chemical processes is still limited because of their expensive installation/maintenance requirements (Zhang ve Das, 2009; Anand et al., 2014). Due to the drawbacks of mechanical methods, de-icing salts and heating system methods, the needs of other ways for melting snow and ice on roads have emerged.

1.2. Scope and Objectives

In recent years, phase change materials (PCM), which are used for thermal purposes in many industries and have the ability to store and release the solar energy depending on weather conditions, have been studied for their potential to melt snow/ice. The PCMs tend to reduce the temperature variations of the system they were involved in, by releasing and absorbing heat energy at the phase change temperature and thus minimizing freeze-thaw damage in concrete structures (Fernandes et al., 2014; Manning et al., 2015; Gao et al., 2016; Savija, 2018). PCM is used in cement-based composites in snow/ice melting applications, it is expected that the heat energy efficiency of PCM will be low due to the insulating property of composites. If PCMs are used in hot bituminous mixtures, it affects the physical and rheological properties of the asphalt pavement (Anupam, Sahoo and Rath, 2020).

The goal of this study is to create new PCM-containing cement-based composites that can be used as an overlay for concrete and asphalt pavements having high thermal conductivity because of the inclusion of carbon fiber (CF) and steel fiber (SF). In addition, it is also aimed that the proposed design has self-leveling, high strength and durability

properties. Thanks to the increased thermal conductivity in overlay, the heat energy that PCM will release at the phase change temperature reaches the surface where snow and ice is located in a much shorter time and more effectively, even in the case of much lower dosages of PCM. The drawbacks of using PCMs on concrete and asphalt pavements are anticipated to be eliminated by this overlay, which is designed for usage on roadways, airports, and bridges. Furthermore, this composite is anticipated to offer self-leveling, high strength, and durability qualities. In Figure 1.1, the visual of the conductive cement-based composite overlay containing PCM which is aimed to be produced within the scope of the thesis, is given.

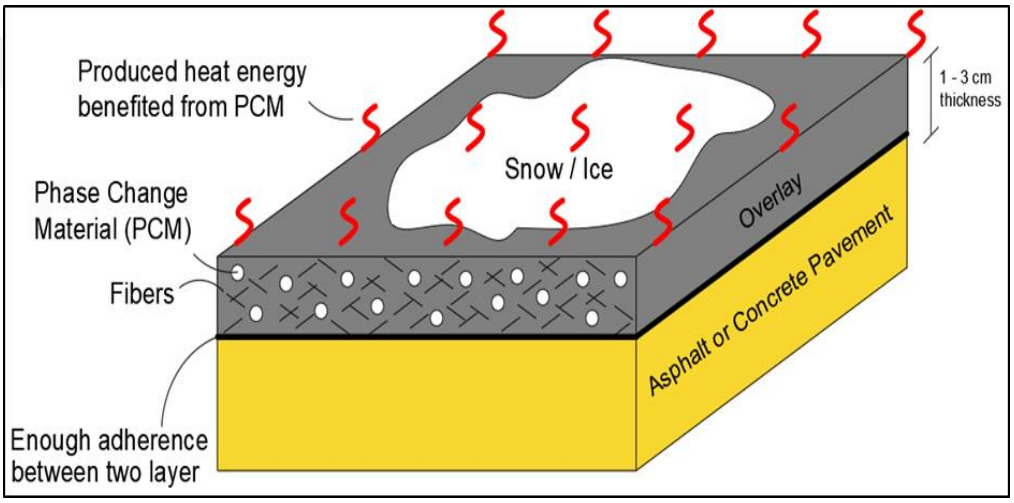

Figure 1.1. Multifunctional conductive overlay containing PCM with melting snow/ice capability

The following specific objectives have been set in order to get to the aim of this thesis study;

- To determine the appropriate matrix content (reference matrix) that has the self-leveling ability and sufficient strength.
- To create composites with low, medium and high thermal conductivity levels by adding CF and SF to the reference matrix.
- By adding certain amounts of PCM to these composites to produce composites that have snow/ice melting capacity reducing the freeze-thaw effect.

- To ensure adequate adherence between composites produced with PCM and the concrete/asphalt road pavement.

1.3. Thesis Outline

The are five main sections in this thesis.

The purpose, scope, and objectives of the thesis study are described in the "Introduction" part.

Extensive literature review about the multifunctional cementitious materials, conductive cementitious composites, thermal conductivity, snow/ice melting methods, PCMs are given in the 2nd part of the thesis , titled "Literature Review".

Detailed informations are presented regarding the materials utilized, specimen preparation, mixing techniques examined, and tests conducted in the 3rd part, titled "Materials and Methods".

The results of the experimental research are reported in the 4th section, titled "Results and Discussion". This section includes the developed of (i) composites with appropriate consistency and sufficient strength (ii) conductive composites with optimum fiber ratio (iii) composites with abilitye snow/ice melting feature (iv) composites of sufficient strength with substrate concrete/asphalt.

The 5th part, “Conclusion” includes a summary of the results and discussion.

2. LITERATURE REVIEW

2.1. Snow/Ice Melting

As a result of snowfall in winter, roads are covered with snow and transportation problems arise. Türkiye has many places with a great number of snow-covered days. According to Turkish Meteorological Service (MS), while the average number of days covered with snow is around 100 days in the last 50 years in the elevated parts of the Eastern Anatolia Region such as Erzurum, Kars and Muş, this number can reach up to 125 days in Hakkari and Ardahan. Again, while the provinces of Van and Erzincan in Eastern Anatolia are covered with snow for an average of 75 days, this is the case for an average of 60 days in the provinces of Sivas and Yozgat in Central Anatolia. An average of 25-30 days of snow cover is effective in a large part of the Western Black Sea and Eastern Black Sea Region, Central Anatolia (Figure 2.1) (MS, 2021).

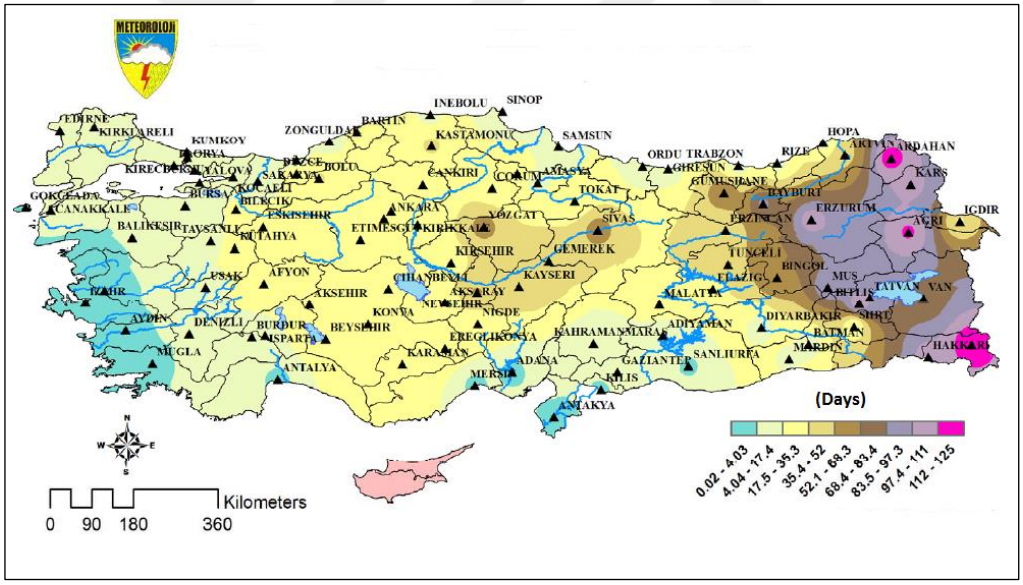

Figure 2.1. Analysis of Türkiye Annual Average Number of Snow Covered Days (1970-2020) (MS, 2021)

Eastern Anatolia, Central Anatolia, and the Eastern Black Sea Region of Türkiye, have high snow thicknesses. The highest snow thicknesses measured in the period between 1970-2011 belongs to the Eastern Anatolia Region (Bitlis: 341 cm, Ağrı: 225 cm, Tunceli: 285 cm etc.) and the Black Sea Region (Artvin: 142 cm, Bayburt: 110 cm, Zonguldak: 91 cm etc.). In the Central Anatolia Region, the average snow thickness varies between 30-

80 cm (Günal, 2013). On the other hand, apart from snowfalls, icing is also effective in this country. In Figure 2.2, the "2020-2021 Winter Season Minimum Temperature Map" is given. According to the map, temperatures in almost all parts of the country fall below 0°C, even at least once in winter (MS, 2021). It is predicted that especially the Central Anatolia and Eastern Anatolia Regions, which have heavy snowfall, are exposed to icing in a large part of the winter season according to Figure 2.2.

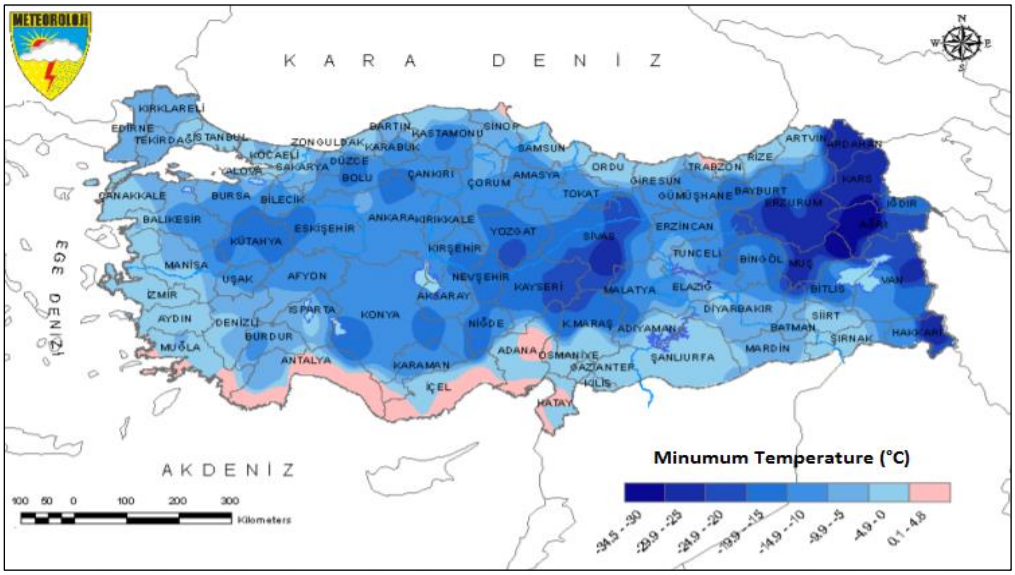

Figure 2.2. 2020-2021 winter season minimum temperature map (Extreme temperature map) (MS, 2021)

The icing, which is resulted from the collected snow on roadways, with weather conditions is responsible from the 10-15 % of traffic accidents which cause fatalities and property damage in winter seasons (Yehia and Tuan, 2000). In order to eliminate this drawbacks, the GDH of Türkiye acts with a series of action plans detailed in the "Dealing with Snow and Ice Guide" (Karayolları Genel Müdürlüğü, 2018). In accordance with this strategy, the "Pre-Icing Application (Anti-icing)" approach is used, initially. De-icers (wet salt or liquid solution) are used prior to snowfall to prevent ice formation on pavement. If de-icers are not applied before snowfall, icing must be removed after snowfall, and this application is called "After Snowfall and Icing Application (De-icing)". In this method, de-icing materials (wetted salt, NaCl, $MgCl_2$, $CaCl_2$) penetrate into ice and snow, lowering the freezing point of water. This breaks the bond between the road and the snow/ice, allowing snowplows to remove it from the surface of the road. The anti-

icing method requires less material consumption and labor force than the de-icing method. Furthermore, instead of using de-icers during snowfall, as stated in the guide, it is more appropriate to remove snow from the road surface with mechanical methods to reduce the amount of salt to be used. Trucks with snow blades are used as snowplow vehicles, and in regions experienced with heavy snowfall, rotary snowplow that removes snow by spraying or self-propelled rotary trucks are used (Figure 2.3) (Karayolları Genel Müdürlüğü, 2018). According to GDH 2020 State and Provincial Roads Maintenance - Operation Costs data, 8.309 TL is spent per kilometer within the scope of dealing snow and ice. Also, it is well known that the damages caused by de-icing salts to the road pavement also cause asphalt road maintenance costs (Figure 2.4). For snow/ice removal, GDH spent approximately 74.5 million TL in 2020, and also the costs of the tendered were about 283.5 million TL. (Karayolları Genel Müdürlüğü, 2021).

a.) b.)

Figure 2.3. Vehicles of dealing with snow and ice a.) Trucks with snow blade equipment b.) Rotary snowplow (Karayolları Genel Müdürlüğü, 2018)

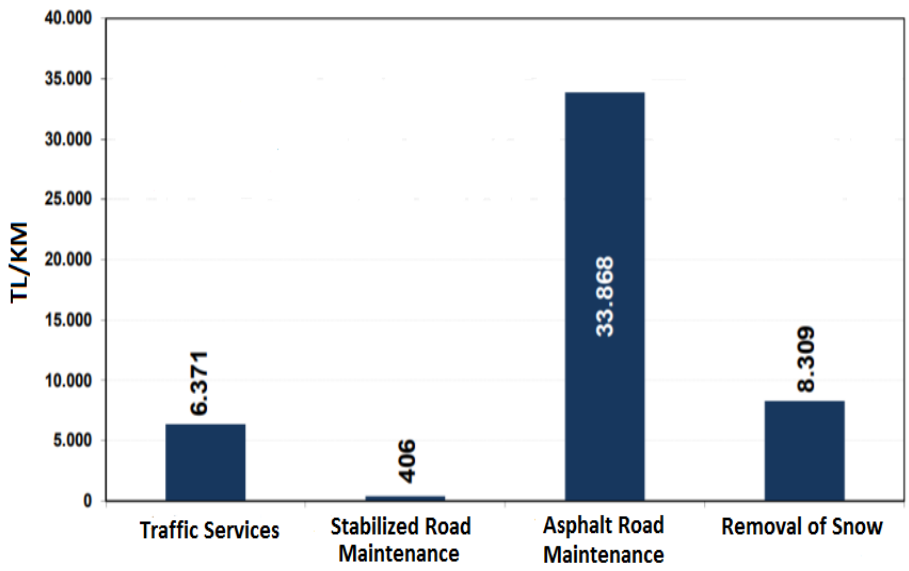

Figure 2.4. GDH Safety Road Maintenance and Operation Costs in 2020 (Karayolları Genel Müdürlüğü, 2021)

2.1.1. De-icing Salts

To remove snow and ice on roads, the de-icing salts are used in conjunction with costly and labor-intensive mechanical methods (Farnam et al., 2017; Ding et al., 2023). These can cause, however, damages in metal components as well as the environment (Seferoğlu, Seferoğlu and Akpınar; Karayolları Genel Müdürlüğü, 2018). It also brings out spalling and disintegration in concrete pavements with freeze-thaw cycles, and over time, they leach into the pavement, rusting the reinforcement, if any (Abdulla, 2018). Furthermore, particularly the deicers used to deice airport concrete pavements and based on alkali metal salts (potassium acetate-KAc, sodium acetate-NaAc, etc.) can lead to alkali-silica reactions (ASR) (Rangaraju et al., 2006). General properties of alkali metal salts and other deicing chemicals used in roads/airports are given in Table 2.1. Studies have shown that these salts also weaken the asphalt pavements technically. As de-icing salt solutions, potassium acetate, sodium formate, urea, sodium chloride, calcium chloride, and distilled water solutions were utilized in the study of Hassan (2002), and limestone and quartzite were used as aggregates. The bituminous mixture with urea solution and quartzite aggregate was the most fragmented sample after 30 freeze-thaw cycles, with approximately 70% material loss, while the bituminous mixture with pure water solution and limestone aggregate was the least affected, with 5-10% material loss. This shows that de-icing salts caused the asphalt mixture to breakdown by reducing the bond between the

aggregate and the bitumen. In another study, it was found that especially potassium acetate (KAc) and potassium formate (KF)-based deicing salts caused the asphalt binder to soften and separate from the aggregate (Fay et al., 2008). As a result of this situation, both road pavements (Shi et al., 2009) and airport pavements (Shi, 2008) can suffer serious damage. In addition, de-icing salts cause loss of skid resistance on asphalt surfaces (Shi et al., 2009).

Table 2.1. Deicing Chemicals (Berberoğlu, 2011; Zhang and Das, 2009; Yehia and Tuan, 1998)

Material type		**Operating range of temperature (°C)**	**Cost**	**Properties**
Chloride based salts	Sodium chloride (NaCl)	Between 1°C and -10 °C	$26/ton	1)They are more economic. 2)They have corrosive effects on steel. 3) They are harmful for living environment.
	Calcium chloride ($CaCl_2$)	-25 °C	$267/ton	
	Magnesium Chloride ($MgCl_2$)	-15 °C	not available	
Organic products	Calcium magnesium acetate (CMA)	Between 0°C and -5 °C	$670/ton	1)They are not corrosive. 2)Their effect on living environment is lower. 3)Their performance is lower. 4.)They are expensive.
	Potassium acetate (KAc)	Between -30°C and -60 °C (at solution concentration between 35-50%)	not available	
	Agricultural products	-	not available	-
	Manufactured organic products (Glycol, methanol)	-	not available	-
Nitrogen products	Urea	-9 °C	$130-260/ton	-

The water present in air/capillary voids of concrete is highly sensitive against variable air conditions. The cold weather, which the concrete is exposed to, causes the freezing of

water and forms ice in its pores of a limited volume. Because of its expansive nature, this newly formed ice creates tensile stresses to the pore walls, and correspondingly, causes damage and even strength reduction. However, when the temperature warms up, the ice melts and the pores is filled with water, again. The experience of concrete against that cycle is called "freeze-thaw effect" or "frost action" and for a durable concrete, the concrete should have sufficient resistance to it (Powers and Helmuth, 1953; Neville, 2011). In cold climates, the frost action causes serious problems such as cracking and spalling of concrete surfaces for important infrastructures (e.g., bridges, roads and airport pavements) (Mehta and Monterio, 2011) (Figure 2.5).

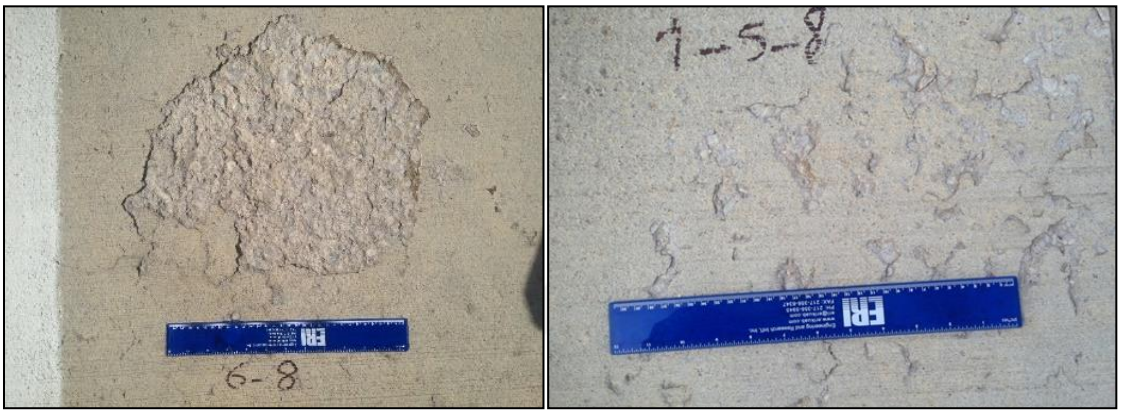

Figure 2.5. Typical surface scaling on concrete pavements as a result of freeze-thaw cycles and bursting of aggregate particles forming cavities on the concrete surface (Damage at an airport in our country after two years)

De-icing salts, cause substantial damage to the concrete material when combined with the frost action. The osmotic pressure created by the salts on the pavement surface pulls the water in the concrete towards upper layer of the pavement. As a result of re-freezing of the water on upper layer and creating hydraulic pressure, scaling damage occurs (Figure 2.6). Additionally, it is well known that reinforcement corrosion is resulted from salt solutions that leak into the pavement (Neville, 2011). The frost action damage in concrete structures is generally reduced by a uniform air void system, produced adding air-entrainment agent to the fresh state of concrete (Du and Folliard, 2005). In addition, the anti-freezing agents (Polat, 2016) and mineral additives (Whiting, 1989; Acikok, 2019) are also used to increase freeze-thaw resistance of concrete. Acikok (2019) produced three mixes with no mineral additions, 20 % fly ash (by weight of cement), and 20% slag (by

weight of cement) to measure the effect of different types of mineral additives with de-icing salts under the influence of freeze-thaw cycles. Under the effect of a 3% NaCl solution, 28 freeze-thaw cycles were applied. It was found that material loss was 0.10 kg / m^2 in the reference mixture, 0.09 kg / m^2 in the mixture with 20% fly ash, and 0.05 kg / m^2 in the mixture with 20% slag. It was determined that mineral admixtures increase the freeze-thaw resistance by filling the pores of the concrete due to their very fine grains.

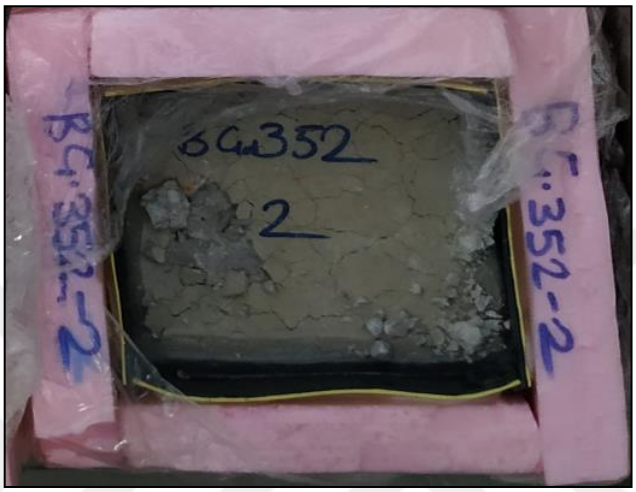

Figure 2.6. Damages in a test sample containing sodium chloride (NaCl) solution and exposed to freeze-thaw cycles (GDH Concrete Laboratory)

The formation of snow/ice on airport runways make landing and take-off operations dangerous, and can cause flights to be cancelled and postponed (Seferoğlu, Seferoğlu and Akpınar, 2015). Furthermore, it is stated that particularly the chemicals used to deice airport concrete pavements and based on alkali metal salts (potassium acetate-KAc, sodium acetate-NaAc, etc.) cause ASR. Rangaraju et al. (2006) determined the alkali silica reactivity of Spratt limestone aggregate in 50% by weight potassium acetate (KAc) solution and 1N sodium hydroxide (NaOH) solution. While the expansion for 14 days in potassium acetate solution is about 0.7%, it is 0.3% in NaOH solution, approximately. Also, the expansion of Ottawa aggregate with low alkaline reactivity in potassium acetate solution for 28 days increases up to about 0.1%. The indicated study shows that alkali metal salt-based deicers significantly increase the expansion of aggregates with high alkali reactivity and also trigger alkali silica reaction in aggregates with low alkali reactivity. In Figure 2.7, the photographs of ASR-induced damages on airport runways are given.

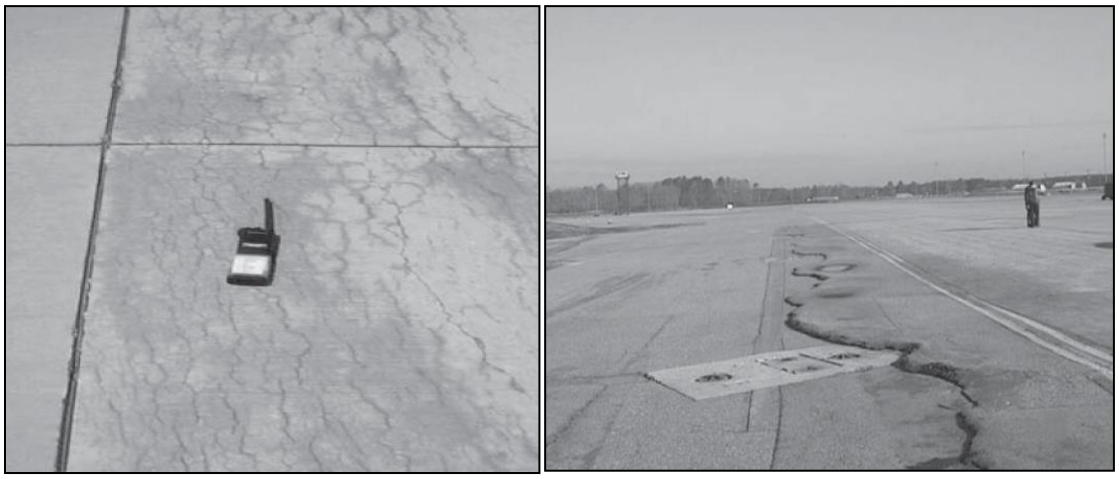

a.) b.)

Figure 2.7. Caused by ASR damage in airport rigid pavements; a) Cracking b) Expansion of concrete pavement adjacent to asphalt pavement (Shi, 2008)

2.1.2. Heated Pavement Systems

The use of heated pavement systems (electrical heating, hydraulic heating etc.) as an alternative to mechanical and chemical processes is still limited because of their expensive installation/maintenance requirements. These systems use electrical wires or hydraulic pipes to supply heat energy, which can be used to melt snow and ice. In electric cable heating systems, the electric current encounters resistance as it passes through the cables embedded in the pavement or the grid/strapped conductors. The heat energy produced is a function of the current flowing through the conductor and the composition of the conductor resisting the current. Hydraulic systems, on the other hand, are closed-circuit systems formed when the hot fluid in the hydraulic pipes (metal or polyethylene) embedded in the pavement releases the heat energy and then returns to the heat source. The fluid that generates heat is derived from a variety of energy sources, including fossil fuels, geothermal wells, and waste heat (Anand et al., 2014). On the other hand, there are conductive concrete heating systems, which are formed by connecting the pavement, whose electrical conductivity is increased thanks to conductive material addition, to a power source (Yehia and Tuan, 1998). Apart from this, there are also systems that provide heating with infrared lamps or microwaves installed outside the pavement (Zhang and Das, 2009). Heated systems eliminate the damage caused by chemical solvents to the environment and pavement, and help to shorten the cleaning time of snow/ice in critical areas in airports. However, the drawback of these systems is the complex installation

procedures and expensive installation/maintenance requirements. (Anand et al., 2014; Zhang and Das, 2009). According to the study of Lun (2005), the cost of installing a geothermal system with heating pipes in bridge decks ranges between $1075 and $1615 per m^2. It is mentioned that using this system only in critical sections of road, bridge and airport pavements provides economy and benefit (Lund, 2005). The high costs of some heating systems based on data from different studies are presented in Table 2.2.

Table 2.2. Costs and power consumptions of various heating systems (Seferoğlu, Seferoğlu and Akpınar, 2015; Yehia and Tuan, 1998).

Heating System	Installation Cost	Operating Cost	Power Consumption
Infrared Heating Lamp	$96/m^2	Not available	75 W/m^2
Electric Cable Heating	$54/m^2	$4.8/m^2	323-430 W/m^2
Hot Water Heating	$161/m^2	$2.5/m^2	473 W/m^2
Gas Heating	$378/m^2	$2.1/m^2	Not available
Heating with Conductive Concrete	$48/m^2	$5.4/m^2	516 W/m^2

2.1.3. Phase Change Materials

One of the most recent ways to remove ice/snow collected on roads and pavements is to use renewable energy sources. While non-renewable energy sources such as oil and coal are used and consumed once, renewable energy sources that serve sustainable development and the environment can be reused cyclically. Wind, solar, hydraulic, biomass and geothermal energy systems are considered among the main renewable energy sources (Karalı, 2017) and Phase Change Materials (PCM), which is based on solar heat as a renewable energy source (Aydın and Okutan, 2010). They have already been used for thermal purposes in many sectors thanks to their ability to store/release heat energy. For example, they can serve for cold storage of food products, transportation of medical materials such as drugs and blood source (Aydın and Okutan, 2010), insulation in construction structures (Kuznik et al., 2011; Ansuini et al., 2011; Weinläder, Klinker and Yasin, 2017) and de-icing applications (Farnam et al. 2017). They store energy during

the transition from the solid phase to the liquid phase and reduce the temperature rise of the system in which they are included. In contrast, they reduce the cooling rate of the system by releasing the thermal energy that they store by transitioning from the liquid phase to the solid phase (Fernandes et al., 2014) (Figure 2.8).

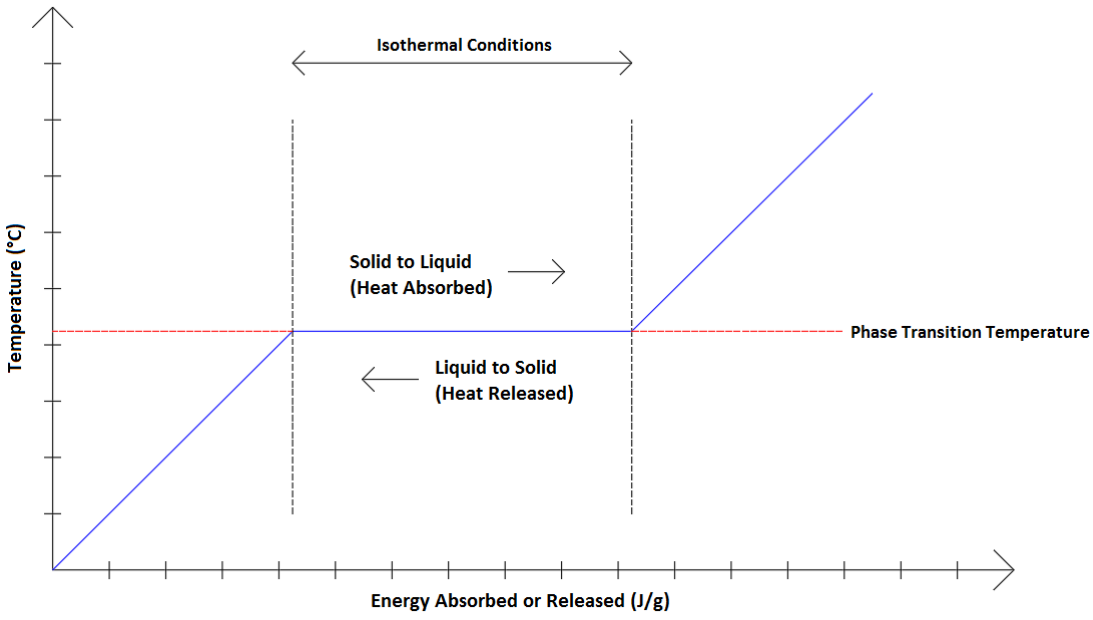

Figure 2.8. Energy-temperature relationship of PCMs (Fernandes et al., 2014)

PCMs play a significant role in keeping the system between the desired temperatures and they are considered as solution to reduce freeze-thaw effects, which concrete exposes (Manning et al., 2015; Savija, 2018; Yeon and Kim, 2018) (Figure 2.9). Bentz and Turpin (2007) studied the effect of the PCM on the deterioration resulted from the freeze-thaw cycles through numerical simulations. They inputted the actual number of freeze-thaw cycles experienced in 12 distinct locations annually in the United States as data and the PCM, having a latent heat of 250 J/g and a melting temperature of 30-40 °C, was used in concrete at the rate of 15% by weight in their simulation. It was found that in concrete containing PCM, the number of the freeze-thaw cycles and thus the frost action decreased by approximately 30 % on average for all locations compared to the control concrete without PCM. Sakulich and Bentz (2012) simulated a concrete having PCM (50 kg/m^3) suitable for various locations in the United States. It was concluded that in 104 of 237 locations, light aggregate-saturated different types of PCMs reduced the effects of freeze-

thaw and increased service life by at least one year. In another study, Yeon and Kim (2018) added microencapsulated organic paraffin-based n-tetradecane ($C_{14}H_{30}$) (latent heat value of 124.5 J/g and a phase change temperature of 4.5 °C) as PCM to the cement at rates of 10 % and 20 % by weight. They formed a sinusoidal freeze-thaw cycle with the maximum and minimum cabin temperature of 9 °C and -5 °C, respectively. The results revealed that the maximum and minimum temperatures measured from the specimen varied almost linearly with the PCM addition rate and the addition of 1% PCM reduced the temperature rise or fall by approximately 0.06 °C.

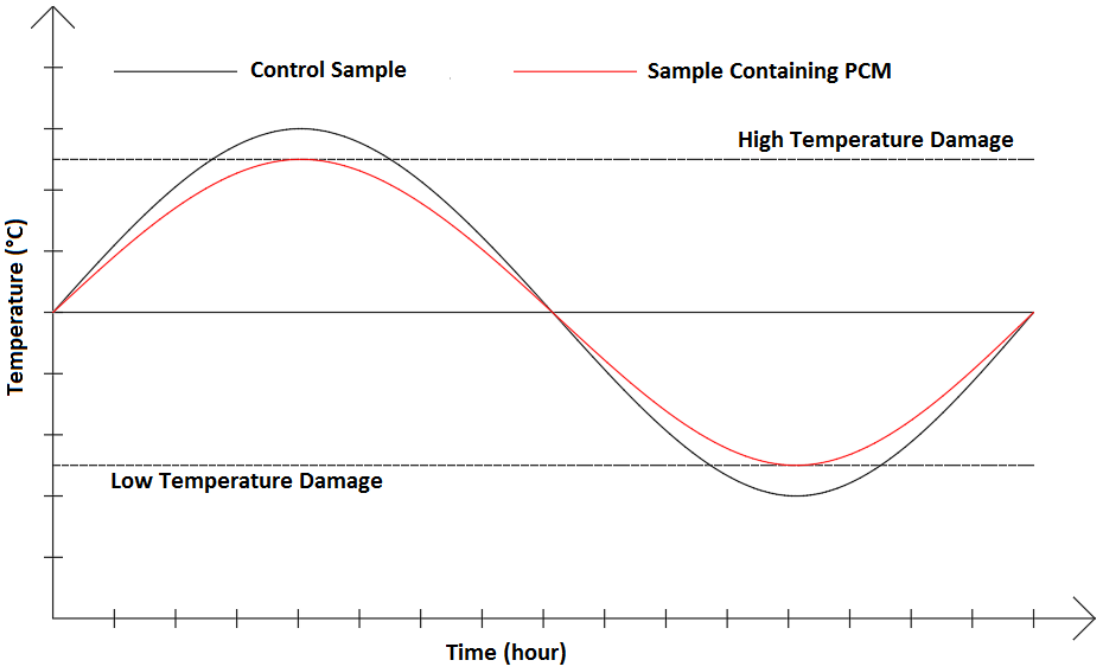

Figure 2.9. Effect of PCMs on temperature amplitudes in asphalt and concrete pavements (Manning et al., 2015)

The effectiveness of PCMs on roads, bridges and airports, reducing freeze-thaw damage and high performance in snow/ice melting depend on certain factors. First of all, one of these factors, the latent heat (ΔH) of PCMs, shows that the quantity of heat will be transferred to the pavement surface at the phase change temperature. Another factor is the phase change temperature. The phase change temperature of the PCM is the temperature that the structure will protect and resist falling, thanks to the heat energy released by the PCM as the ambient temperature decreases. Other factor is the thermal conductivity of the structure in which the PCM is included. Sakulich and Bentz (2012) investigated the

effects of increasing the thermal conductivity of bridge deck composites with different PCM types from 1.5 W/m.K to 3 W/m.K on the durability in freeze-thaw cycles for 237 locations in the USA in the numerical model they created. As seen in Table 2.3, adding PCMs with ideal phase change temperature range (according to the aforementioned publication, this range is 3.55°C and 6°C) to composites with a thermal conductivity of 3 W/m.K has been determined that the service life of the structure is extended according to composites with thermal conductivity of 1.5 W/m. The PCM contributed more to reduced freeze-thaw effect at ambient temperatures where its melting/freezing points and thermal differentials were low in their simulation. In such cases, the ambient temperature drops to the minimum temperature before the thermal energy of the PCM is depleted, and a high thermal conductivity prevents freezing on the surface, creating an even temperature distribution. When PCMs that do not have an ideal phase change temperature are used (for example, relatively high temperatures such as 7-8 °C and further than 0 °C) and the thermal differentials are high, the opposite effect occurs and the service life of composites with a thermal conductivity of 3 W/m.K is shortened. Before the ambient temperature drops to the minimum value that the energy released by the PCM is exhausted. Thus, heat from the interior of structure would be rapidly drawn to the surface and dissipated into the environment, resulting in rapid cooling of the entire body.

As shown in Table 2.4, the PCMs are chemically divided into three groups: organic, inorganic and eutectic. The organic PCMs are classified into paraffin (C_nH_{2n+2}) and non-paraffin. With the hydrocarbon chain length in paraffins, the phase change temperature increases. The organic PCMs have low thermal conductivity, are resistant to corrosion and can remain thermally and chemically stable for a long time without phase segregation. The non-paraffin PCMs are fatty acids, alcohols, esters and glycols. These PCMs have high latent heat energy, low thermal conductivity, moderately corrosive properties, toxicity, flammability and instability at high temperatures. Inorganic PCMs are salt hydrates and metallic PCMs. Although these materials have high latent heat energy, they have a highly corrosive effect. They also show supercooling properties. Eutectic PCMs have two or more components, which melt and freeze simultaneously without phase segregation. The percent mass of the components can be modified by adjusting (Anupam et al., 2020).

Table 2.3. Data on the number of locations predicted to extend the service life by at least 1 year as the thermal conductivity of bridge deck composites with different PCM types increases from 1.5 W/m.k to 3 W/m.k in the simulation model (Sakulich and Bentz, 2012)

Different PCM Types	**PCM Melting Tempereature (°C)**	**Number of locations whose service life is expected to be extended by at least 1 year**
1	0	-1
2	1.7	18
3	3.55	19
4	4	8
5	4	10
6	4.55	6
7	5	8
8	5.5	-1
9	6	-5
10	6.1	-3
11	7.8	-2
12	8	-2

Table 2.4. Classification and technical specifications of PCMs (Savija, 2018)

	Avantages	**Disadvantages**
Organic PCMs	-Has high latent heat energy -Does not show supercooling -Chemically stable and recyclable -Compatible with traditional building materials	-Has low thermal conductivity -More volume change compared to other types -Moderately flammable
Inorganic PCMs	-Has high latent heat energy -Has high thermal conductivity -Has low volume change -Has lower costs -Has sharp phase change -Not flammable	-Has a corrosive effect -Indicates supercooling
Eutectic PCMs (Combination of 2 or more PCMs)	-Has sharp melting point -Can be adjusted to meet specific needs -High volume heat storage	-High cost -Limited data on the thermo-physical properties of many PCM combinations

Thermally, physically and chemically suitable PCM should be used in concrete pavements and cementitious composites. In order to have a high snow and ice melting performance, the PCM should have a phase change temperature close to 0°C, a latent heat as high as possible (>150 J/g), high heat capacity and high thermal conductivity. In terms of physical properties, the PCM should show a small volume change during the phase change. It should melt and freeze harmoniously without phase segregation. Also, the PCM should be chemically non-flammable, compatible with the alkaline environment of the concrete material, non-corrosive and chemically stable. For their high efficiency, PCMs should not have overcooling problem caused by a high nucleation/crystallization rate (Hawes, Banu and Feldman, 1992; Farnam et al., 2015; Liston, 2015).

In addition to serving as an insulation materials, the PCMs also aid in lowering heat of hydration. Due to high hydration temperatures, mass concretes develop thermal cracks at an early age. The PCMs play a key role in reducing the difference in temperature gradients between the core and surface of mass concretes. Mihashi et al. (2004) added microencapsulated paraffins to the concrete mixture in their study and determined that the maximum hydration temperature reached decreased. Qian et al. (2010), on the other hand, added PCM in the embedded pipes at the rates of 0%, 3% and 6% of the cement weight. It was found that as the PCM ratio increased, the maximum hydration temperature decreased and delayed. Hunger et al. (2009) added microencapsulated PCM to the self-compacting concrete at the ratios of 0, 1, 3, and 5% of the concrete mass, and as seen in Figure 2.10, the maximum temperature decreased as the PCM ratio increased. It was determined that the addition of 5% PCM reduced the maximum hydration temperature by 28%.

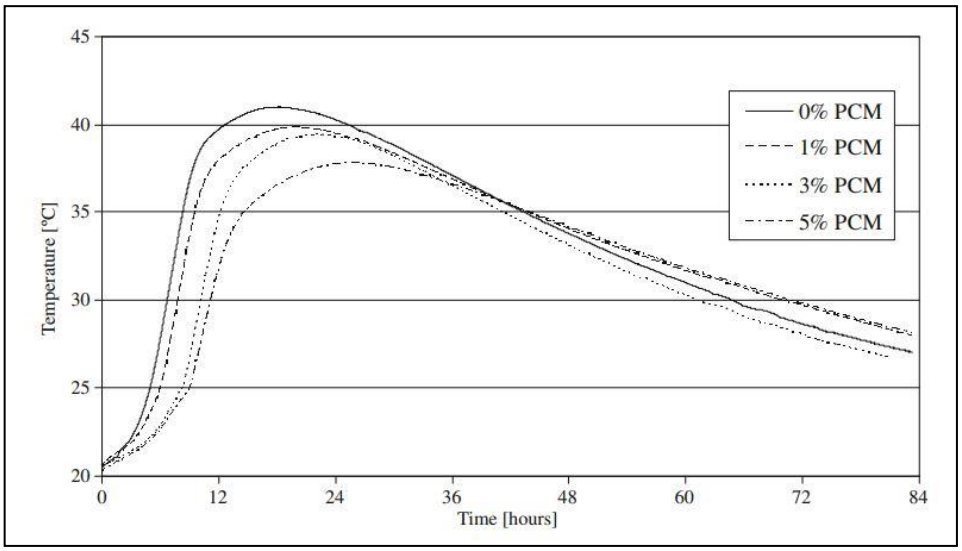

Figure 2.10. Effect of PCM on heat of hydration (Hunger et al., 2009)

Farnam et al. (2017) investigated at the time-dependent snow melting capability of paraffin oil, which has a latent heat of 157.8 J/g and a phase transition temperature of 5.7 °C. This PCM was added to the concrete by both the impregnation method with light aggregates (22.1 %, by volume) and the embedded pipe system method (14 %, by volume). They added 3000 g of handmade snow to the reference sample without PCM and the samples having PCM under a cycle created with a maximum temperature of 7 °C and a minimum of 2 °C in cabinet. The reference sample melted all the snow in 65 hours, whereas the ones having PCM did in 35 hours (Figure 2.11). In another study, a composite sample simulating a bridge deck with anti-freezing capabilities was produced by Gao et al. (2016). It had a phase change functional layer made up of embedded steel pipes filled with PCM to reduce the amount of ice and snow formed. 12.5 mm of ice was melted by providing 3775.9 kJ of energy in a steel pipe containing 15.7 kg of PCM in a layer at a depth of 50 mm. Their research supported the view that using PCM-filled pipes was an effective technique to prevent ice from forming on structures like bridge decks.

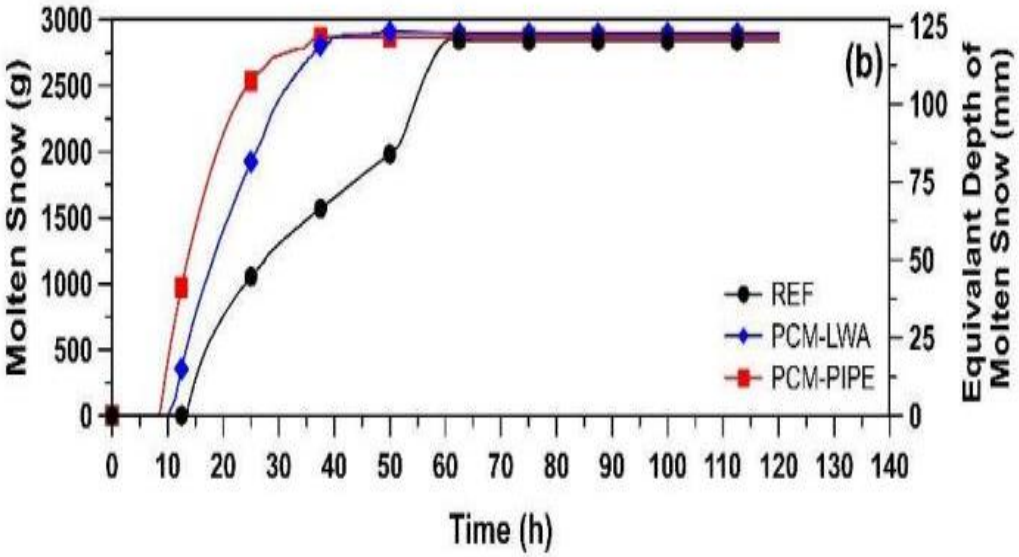

Figure 2.11. Effect of PCM in concrete on snow melting (Farnam et al., 2017)

In literature studies, some problems are encountered regarding the direct use of PCM in asphalt and concrete pavements. If PCM is used in hot bituminous mixtures, it is necessary to produce microencapsulated PCMs resistant to high temperatures (140-160°C) during the mixing, placing and compaction stages of these mixtures. Otherwise, it is expected that PCMs will leak from the microcapsules and lose their effectiveness and affect the physical and rheological properties of the asphalt mixture (Anupam, Sahoo and Rath, 2020). In case PCMs are used directly on concrete pavements, it is expected that the heat energy that will be released or absorbed at the phase change temperature will remain at low levels due to the insulating nature of the concrete material.

The methods of incorporation of PCM into concrete and cement-based composites are shown in Figure 2.12. Different incorporation methods have advantages and disadvantages compared to each other. Thanks to the embedded pipe method, the physical and chemical interaction of the PCM with the matrix is prevented (Figure 2.12 (a)). In addition, there is no PCM leakage into the matrix in this method. But the disadvantage of this system is that PCM is effective around the pipe. That is, the PCM effect does not occur at every point of the matrix but remains regional. As another method, homogeneous distribution can be achieved by using lightweight aggregates (through vacuum) impregnated with PCM (Figure 2.12 (b)). Thus, the heat effect of PCM can reach every area of the matrix. The drawback of this method is that PCM directly interacts with the

matrix and changes its chemical and physical characteristics (Savija, 2018). Microencapsulation method shown in the Figure 2.12 (c) is preferred cementitious composites containing self-healing agents (Lv et al., 2016) and corrosion inhibitors (Xiong et al., 2015). Its helps maintain PCM purity, provided optimized heat transfer with a high surface area, and offered flexibility for phase change (Norvell, Sailor and Dusicka, 2013; Anupam et al., 2020). The possibility of damage to the microcapsule and leakage of PCM during mixing and casting of concrete or cement-based composites is a disadvantage of this method.

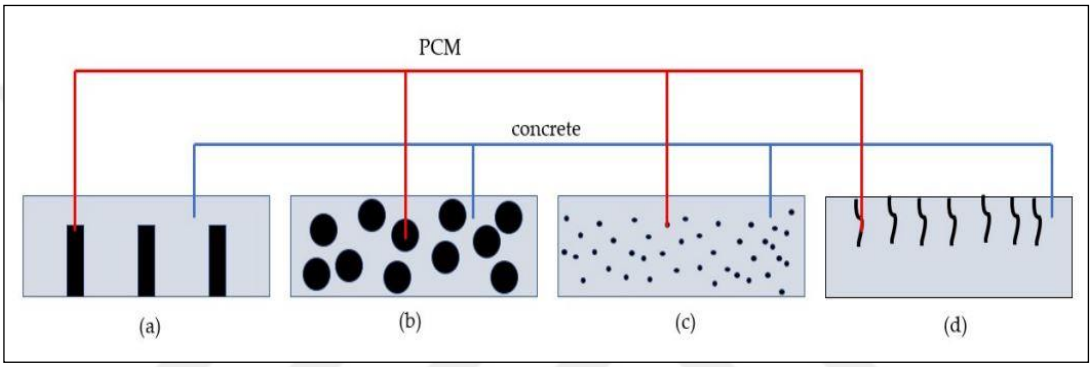

Figure 2.12. Methods of incorporation of PCM into concrete and cement-based composites; a) Using pipes filled with PCM b) Using lightweight aggregate particles saturated with PCM c) Using microcapsules containing PCM d) Filling surface voids with PCM absorption (Savija, 2018)

Studies have shown that the addition of PCM to concrete adversely affects the strength. In the use of lightweight aggregate saturated PCM, the bond between aggregate and cement paste is damaged when the PCM comes into contact with the matrix (Sharifi and Sakulich, 2015). In addition, PCM leaking from the lightweight aggregate chemically interacts with the hydration products, causing cracking and expansion (Farnam et al., 2015). Also, it was observed that the compressive and flexural strengths decreased as a result of the addition of microencapsulated PCM to the concrete. Yeon and Kim (2018) added microencapsulated PCM to concrete at 0%, 10% and 20% of the cement mass. The compressive and flexural strength results of the producing samples are given in Figure 2.13. It was determined that the compressive strength value decreased by approximately 50% with the addition of 20% PCM. On the other hand, there are few studies in the literature on the effects of the addition of PCM to concrete or cementitious composites

on durability. The drying shrinkage of PCM microencapsulated cement paste was found to be higher than cement paste containing the same volume of quartz sand, indicating that the addition of PCM causes shrinkage deformation. (Fernandes et al., 2014). This is because the microcapsule structure, which is softer than quartz sand, cannot limit the shrinkage of the cement paste.

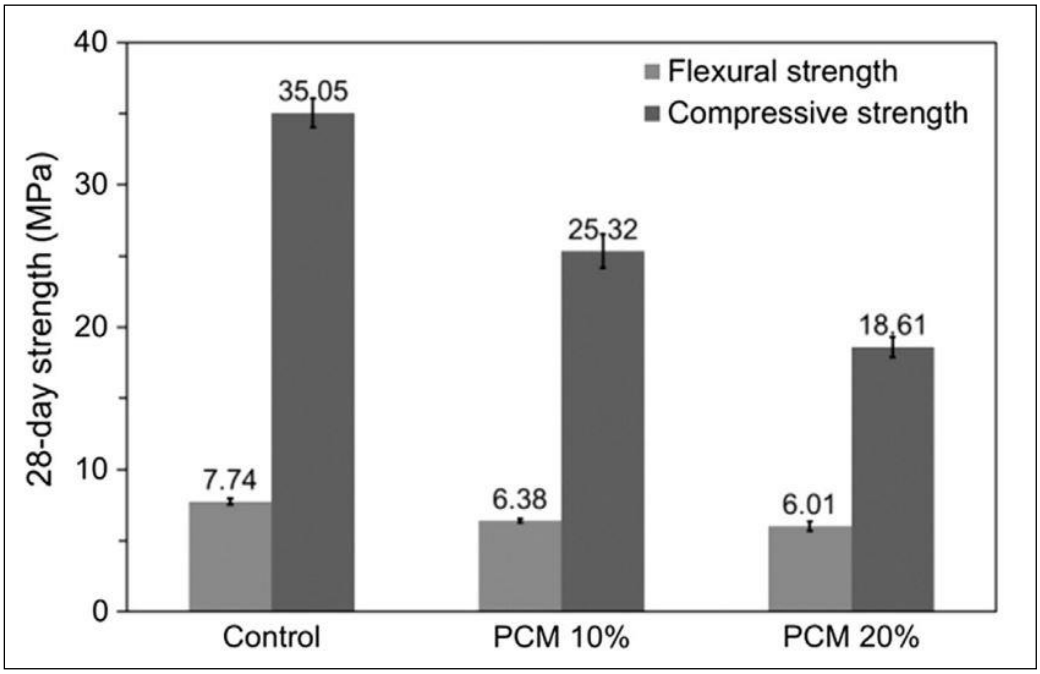

Figure 2.13. Effect of PCM on compressive and flexural strength of concrete (Yeon and Kim, 2018)

2.2. Multifunctional Cementitious Materials

Ordinary concrete materials are widely preferred in various applications of infrastructures and superstructures due to their advantages such as high compressive strength, affordable cost, and ease of production and application. However, such materials have a high brittleness, low toughness, and low tensile strength, also. Under the influence of tensile forces, cracks occur in these materials due to their low tensile strength, which adversely affects the mechanical and durability properties of the structures and shortens their service life (Yildirim et al., 2015). Recently, to eliminate the problems caused by the weakness of ordinary concrete materials, the composites have been introduced a new concept: Multifunctionality, meaning to use of the structural material itself to assess/use non-structural functions without the need for any external power source or device (Gomis et al., 2015). With the additional functions, it is aimed to develop multifunctional

cementitious composites providing satisfying structural performance, low energy consumption, high durability, sustainability, safety, and/or high efficiency. For this purpose, the cementitious composites having improved electrical, thermal, magnetic, and optical properties are produced for years (Yehia and Tuan, 2000). Besides these, the materials with self-sensing capability (Sun et al., 2014), self-healing capability (Wiktor and Jonkers, 2015), or high fracture toughness (Li and Kanda, 1998) are also available in the current literature. Examining studies on high fracture toughness reveals that cement-based composites with ductile characteristics and high performance can be made. Because of the fibers, these micromechanically engineered composites demonstrated strain hardening behaviour under direct tensile test. The cementitious composites with high strain-hardening rates exhibit a behavior similar to ductile metals. A cement-based mixture containing 2% Poly-vinyl-alcohol (PVA) fiber demonstrated strain hardening 300 to 500 times that of conventional concrete, with the formation of closely spaced microcracks following the first crack under axial stress (Şahmaran, Lachemi and Li, 2009). On the other hand, in a study on self-healing composites, which is another multifunctional feature, Wiktor and Jonkers (2015) used a bacteria-based repair solution to heal cracks. They sprayed the solution over cracks and also on concrete pavement in a parking lot measure frost and thaw spalling damage. The average scaling damage of the control samples was 3.6 ± 1.3 kg/m^2, while the value of this damage was 1.9 ± 0.3 kg/m^2 in the samples which sprayed with bacteria-based repair solution. While the control cracks in the parking lot leaked water to the lower floor, photographs demonstrated that cracks sprayed with bacteria-based repair solution did not leak water to the lower floor.

2.2.1. Electrical Conductive Cementitious Composites

The conductive cementitious composites can be considered as multifunctional cementitious materials since these are used for heating, anti-static and anti-corrosion purposes, and electromagnetic protection (Yehia and Tuan, 1998; Yehia and Tuan, 2000). The conductive property can be achieved incorporating different types of conductive materials, such as CF, carbon powders, carbon nanotubes, carbon nanofibers, carbon black, SF and steel powder to the cementitious materials.

CF has many advantages compared to other carbon-based materials. The CFs provide better electrical conductivity with lower production costs compared to carbon powders,

carbon nanotubes, and other carbon-based materials (Al-Dahawi et al., 2016). In addition, CFs have high specific strength (strength/weight), fatigue resistance, good conductivity and heat transfer, a small coefficient of thermal expansion, and satisfactory corrosion resistance (Wu, Liu and Yang, 2015). These fibers, which are chemically inert and provide an increase in the conductivity of the cementitious materials, provide some additional functions in favor of multifunctionality for the cementitious systems such as damage detection (Yildirim et al., 2018), electro-magnetic protection, piezo-electric resistance behavior, self-sensing capability (Reza, Yamamura and Batson, 2014; Al-Dahawi et al., 2016). In addition, CFs enhance some mechanical aspects of the cementitious composites including flexural strength, toughness, and ductility (Chung, 2000). TUBİTAK's "New Generation Cement-Based Composites with Electrostatic Discharge Capability" project, coordinated by Prof. Dr. Mustafa Şahmaran, developed a conductive cement-based floor covering material with anti-static properties, high compressive strength and self-leveling ability, and high resistant to chemicals. In this project, carbon nanotubes, CFs and SFs were used to create multifunctional conductive composites. At the 90th day, the electrical resistance of the reference mixture was 504500 Ω, but a composite with a CF ratio of 0.6% of the cement weight had an electrical resistance value of 182.5 Ω (Şahmaran, 2020). The cement-based multifunctional composites, the conductivity of which is improved by adding carbon and steel-based materials, are also produced for snow/ice melting applications. Wu et al. (2015) investigated the performance of the conductive SF, CF, and graphite powder to improve the snow/ice melting performance of the electrically heated concrete pavements. Although the mixtures in which only use of SF provided high strength values, it was observed that the SFs were corroded in the sample over time and blocked the conductivity. Graphite powder, on the other hand, is used with SFs because it causes serious decreases in strength while increasing conductivity at a high rate. After various preliminary trials, it was found that the triple mixture containing 1% (volume fraction) SF, 0.4% (volume fraction) CF, and 4% (mass fraction) graphite powder showed optimal performances. This mixture provided the lowest electrical resistivity (322 Ωcm) on the 28th day among all composites and had a satisfactory snow/ice melting potential. Since SFs have a corrosive behavior (Gomis et al., 2015), it is seen in the literature that carbon-based materials (CF, carbon nanofiber, carbon nanotube etc.) are more widely used in the creation of conductive composites (Faneca et al., 2018). Gomis et al. (2015) added CF, carbon nanofiber, CF powder, carbon nanotube, and graphite powder to the cementitious

composites and studied the deicing performance of electrically heated pavements. Ice layer with 0.5 cm thickness was placed on the samples with a surface area of 10×10 cm and a thickness of 1 cm. After applying electric current to the samples to provide an initial electrical power of about 30 W, the ice melting rates were measured. The samples containing carbon-based material melted 40 g of ice in about 1000 seconds, while the reference sample melted the same amount of ice in about 4500 seconds (Figure 2.14).

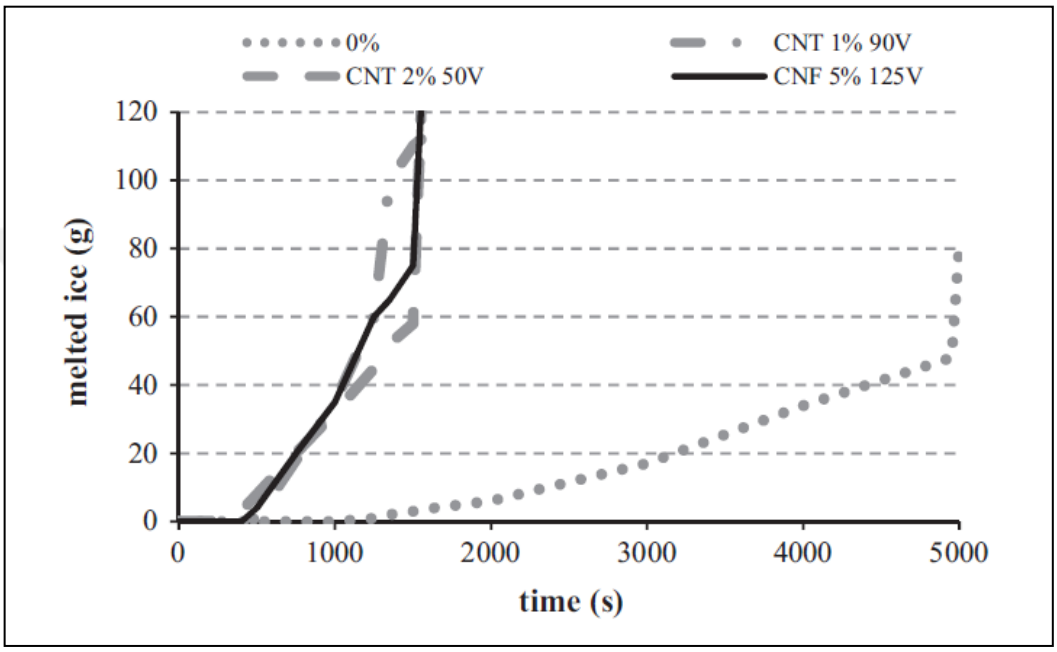

Figure 2.14. De-icing time of composites containing carbon nanotubes and carbon nanofibers (Gomis et al., 2015)

The distribution of fibers in cementitious systems is an important issue that should be considered since homogeneously dispersed – fibers throughout the cement-based composites are known to cause in increase both the conductivity and mechanical properties in comparison with the composites having non-uniform distribution of fibers. In order to obtain a conductive path, the fibers must come into contact with each other in the cementitious composite and form a conductive line by connecting to each other (percolation theory) (Devpura, Phelan and Ravi, 2001). At low fiber incorporation rates, the fibers limitedly available in the system are surrounded by the non-conductive cement paste and therefore the fiber-incorporated cementitious system cannot possess appreciable conductivity. Increasing the rate of homogeneously dispersed fibers in the matrix can enable more fibers to come into contact with each other, and thus, the number

of conductive lines and the conductivity of the composite increase (Figure 2.15). However, the incorporation ratio of fiber is usually selected close to the percolation threshold which is defined the minimum conductive material content at which sharp decreases in electrical resistance begin to be observed in order to reduce the costs due to conductive materials as much as possible (Al-Dahawi et al., 2016; Chuang et al., 2017). In this direction, the optimum fiber ratio should be determined in the production of cementitious composites considering their basic mechanical properties, conductivity- and cost-related aspects. In Figure 2.16, the electrical resistance values of the CF ratios added individually are given belong to study of Wu et al. (2015). The optimum value of CF is 0.4% and at values above this ratio, the electrical resistance increased because the CFs were not fully dispersed in the matrix. In their study, Sargam et al. (2020) found that the SF they used in 0.25% volume had no effect on the thermal conductivity value in concrete, but that when this fiber was used in 0.50% to 2% volume, the thermal conductivity increased by 10-15%. This shows that 0.50% is a threshold value and at values above this, the fibers form a transmission line.

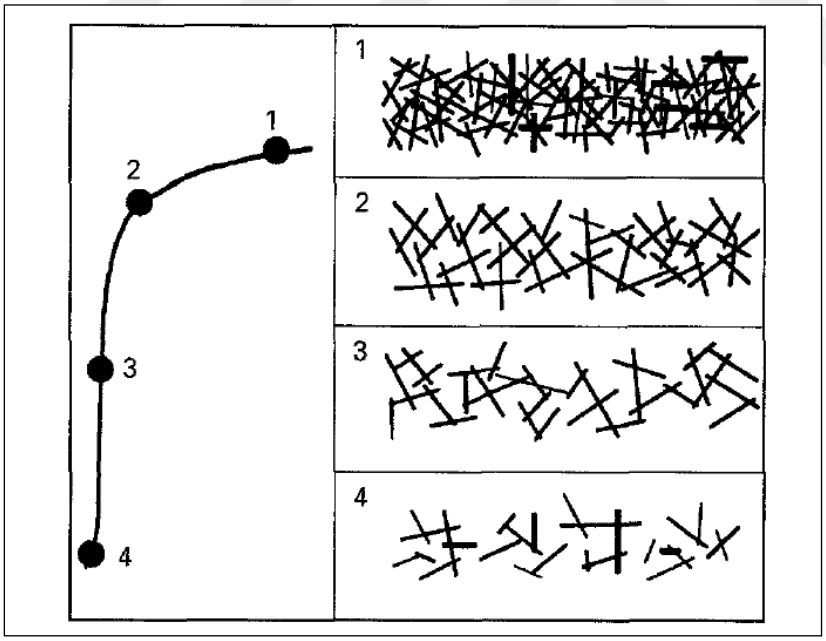

Figure 2.15. The relationship between conductivity and the rate of contact between fibers (Xie et al., 1996)

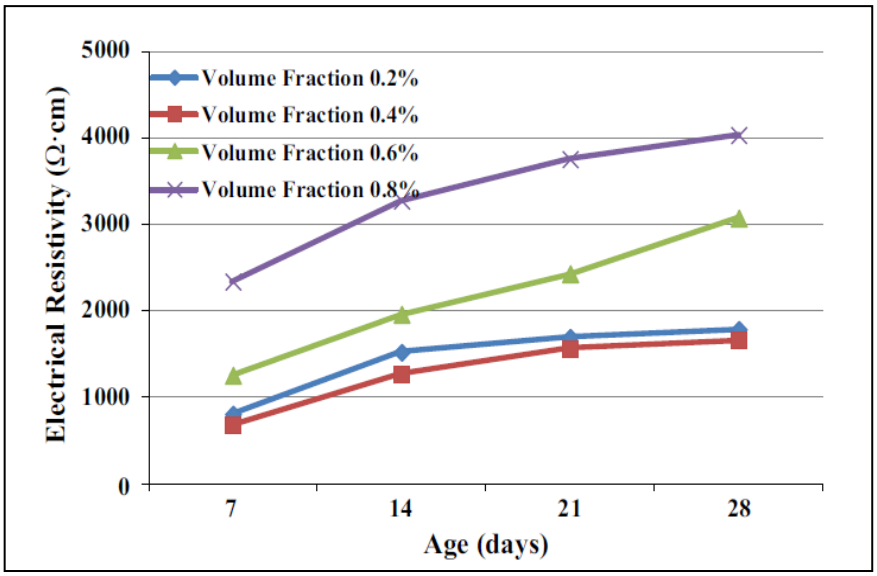

Figure 2.16. Electrical resistance values of conductive composites containing different volumes of CF depending on the hydration age (Wu, Liu and Yang, 2015).

If the fiber ratio is low and there is no contact between the fibers, the transmission takes place through another theory, the "tunnel effect". When the CF content is low, conductivity is mainly achieved in two ways: hydrated ions (such as OH^-, K^+, Na^+ and Ca^{+2}) that move freely in the inner pore water in the cement matrix, and current-carrying electrons that move in conductive CFs through the tunneling effect. The ionic conduction of the matrix under dry conditions is negligible. With the increase of the CF content, the conduction by the current carrier electrons through the tunnel effect and by superimposing the CFs becomes the main conductive mode. When the CF content exceeds the percolation threshold, that is, a fully conductive network is formed within the material, the resistivity does not change much with increasing CF content. There may be only slight variation and the resistance tends to be within a certain limit. In general, low CF ratio (usually close to the percolation threshold) is preferred because it provides low cost, high workability and high compressive strength (Chuang et al., 2017). On the other hand, curing age affects the conductivity of fibrous composites. With the development of hydration reactions, the free water in the composite turns into gel water and adsorption water. Thus, the fiber and matrix interface turns into solid-solid contact and gradually becomes thicker. As a result, the conductive path is blocked, the ion conductivity decreases, and it also becomes more difficult for electrons to jump through tunneling. However, composites with high fiber content are less affected by curing age. The reason

for this is that the fibers are very close to each other and contact makes it easier for the electrons to jump (Chuang et al., 2017).

CFs and SFs provide conductive properties to composites but diminish workability as usage rate and aspect ratio increase. Slump test is not sufficient to determine the consistency and rheological properties of fiber-containing composites This is because determining the optimal sand/gravel ratio for slump testing is problematic because significant amounts of slump in fibrous composites are difficult to measure (Martinie, Rossi and Roussel, 2010). Therefore, the Bingham model, which consists of two independent parameters, yield stress and plastic viscosity, is preferred. When the shear stress is higher than the yield value, the mixture flows and the flow resistance depends on the plastic viscosity (Wang et al., 2018). Bingham viscoplastic behavior is expressed by the following relation;

$$\tau = \tau_0 + \mu.\gamma \quad (1)$$

τ (Pa): shear stress

τ_0 (Pa): yield stress

μ (1/s): shear rate

γ (Pa.s): plastic viscosity

The reology of the matrix affect the distribution of fibers. In a fluid matrix, that is, a composite with a lower yield stress, the fibers have great mobility within the cement matrix. This situation causes the sedimentation of SFs, which have a higher specific gravity than the other components of the composite. On the other hand, in composites with high yield stress, the non-homogeneous distribution of the fibers occurs. Especially CFs in particular tend to cluster in bundles. In mixtures with low yield stress, the fibers are aligned perpendicular to the flow direction; but, at high yield stress, they display a random distribution and can even aggregate (Boulekbache et al., 2010; Wang et al., 2018).

While CFs used to increase the conductivity value have a flexible structure, SFs are classified as rigid fibers (Martinie, Rossi and Roussel, 2010). In the case of using relatively low proportions of rigid SF, the cement matrix dominates the rheology of the

composite. However, when SFs reach critical volume ratios, they become mechanically interlocked and dominate the flow behavior (Kuder et al., 2007). Also, the diameter of the fibers influences their distribution throughout the mixture (Chung, 2000). Even when used at lower volume fractions than SFs, which are employed at higher volume ratios, CFs provide a greater number of fiber in the mixtures due to their smaller diameter than SFs. Because of its flexible structure, small diameter and high availability in the mixture, CF can be easily dispersed throughout the cementitious composites. Beside this, SFs are surrounded by more cement matrix than CFs, even if they are used at high rates. Therefore, SF percolation is formed at a more limited rate compared to CF, and as the hydration age progresses, the effect of thickening of the hydration products around the fibers on the decrease in conductivity was observed more prominently in SF-containing mixtures compared to CF-containing mixtures. On the other hand, another advantage of CFs over SFs is that they do not undergo sedimentation thanks to their low specific gravity. However, CFs tend to cluster in bundles in mixtures that do not have sufficient consistency and mixing time. Especially in the use of CF at high rates, the fact that the fibers do not disperse homogeneously and remain in clusters does not affect the conductivity and even causes a decrease in conductivity. In the literature, silica fume or dispersant additives are used to ensure that CFs are easily dispersed (Wu, Liu and Yang, 2015).

2.2.2. Thermal Conductive Cementitious Composites

Thermal conductivity is defined as the ratio of heat flux to temperature gradient. This definition means uniform heat flow from one side of a material to the other. Heat flow occurs through conduction in cementitious composite materials with heterogeneous structure. The thermal conductivity value (k) is expressed by the following formula (Bhattacharjee and Krishnamoorthy, 2004; Shin and Kodide, 2012);

$$k = (\Delta Q.x)/(\Delta t.A.\Delta T) \quad (2)$$

ΔQ: heat energy exchange between two points

x: distance between two points

Δt: time change

A: sample area where the heat flow is measured

ΔT: temperature change

According to the application, it can also be aimed to decrease or increase the thermal conductivity (which is another type of conductivity) of cementitious composites providing another property in favor of multifunctionality. In general, the low thermal conductivity of cementitious systems provides better thermal insulation in living areas and reduces energy consumption and represents considerable savings in the service cost. In addition, the materials having low thermal conductivity are also used for the protection from radiation in nuclear power plants (Campbell-Allen and Thorne, 1963; Fu and Chung, 1997; Asadi et al., 2018). "Light concrete" and "foam concrete" materials are preferred for low thermal conductivity. Thus, the unit weight of cement-based materials is reduced and an air-void structure system is obtained. Uysal et al. (2004) obtained light-weight concrete by substituting pumice aggregate in certain proportions for normal weight concrete. The thermal conductivity value of the reference concrete with a unit weight of 2270 kg/m^3 without pumice aggregate is 1.458 W/m.k. While the unit weight of concrete was 1761 kg/m^3 and thermal conductivity was 1.70 W/m.k with 50% pumice aggregate substitution, unit weight was 1329 kg/m^3 and thermal conductivity was 0.776 W/m.k with 100% pumice aggregate replacement. With the increase of the pumice aggregate ratio, the lightweight concrete with lower thermal conductivity was obtained. On the other hand, increasing the thermal conductivity of the concrete used in the construction of dams, roads and large foundations that require massive concrete casting allows the heat of hydration to spread to the whole of the structure more quickly. Thus, the temperature difference between the outer surface of the structure and its core is reduced. Folliard et al. (2017) modelled a bridge foundation to investigate the effect of thermal conductivity on the heat of hydration at early age (Figure 2.17). It was determined that the hydration temperature in the core of the building decreased from 68 °C to 63 °C on the 3rd day when the thermal conductivity was increased from 0.4 W/m.K to 1.6 W/m.K. Moreover, according to the study of Bai et al. (2017), with the increase in thermal conductivity in heated pavement systems, the easily radiated heat energy could reach the road surface faster in favor of snow/ice melting.

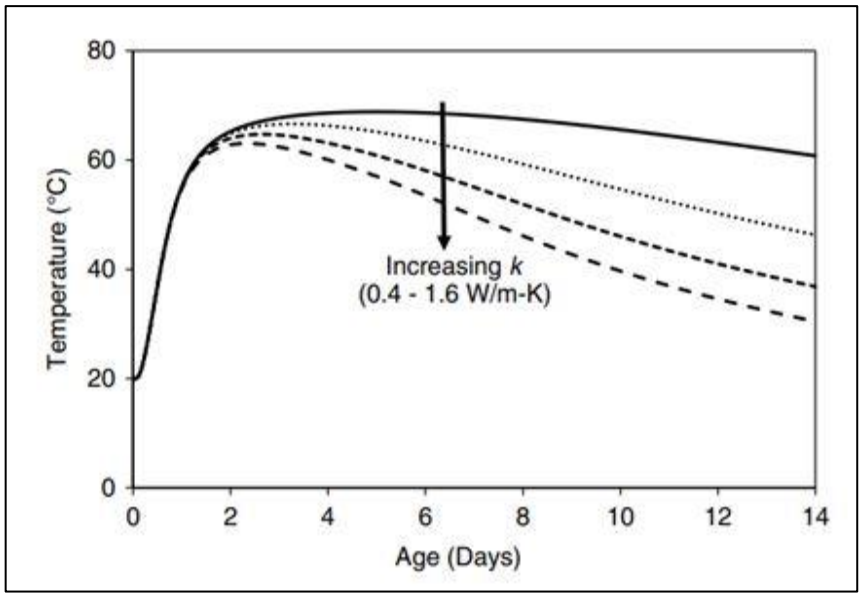

Figure 2.17. Temperature change in the center of mass concrete with increasing k value (Folliard et al., 2017)

Many factors affect the thermal conductivity of cement-based materials such as moisture and void amount, density, water/cement ratio, aggregate type, aggregate volume ratio, mineral additives, fibers etc. The changes in thermal conductivity occur with the change in density and, as the density decreases, the thermal conductivity of cement-based materials decreases (Uysal et al., 2004). The conductivity value drops as the water-to-cement ratio increases due to more voids in cementitious composites. However, since the thermal conductivity of water (0.60 $W \cdot m^{-1} \cdot K^{-1}$) is higher than that of air (0.026 $W \cdot m^{-1} \cdot K^{-1}$), moisture accumulation in the pores of cementitious composites increases the thermal conductivity (Zhang et al., 2015). Furthermore, since mineral additives have a lower density than cement, they reduce the density of cement composites and their thermal conductivity. The conductivity value of the rocks used as aggregate in normal concrete varies between 1.16 and 8.60 $W \cdot m^{-1} \cdot K^{-1}$ (Khan, 2002) and this value is higher than cement paste (Fu and Chung, 1997). Thus, as the overall aggregate ratio in the component increases relative to the cement paste ratio, the thermal conductivity value of cement-based materials increases. The effect of fibers on thermal conductivity has also been studied. SFs whose thermal conductivity is approximately 45.0 $W \cdot m^{-1} \cdot K^{-1}$ are effective in increasing the thermal conductivity of cement-based materials (Sargam, Wang and Alleman, 2020). Liu et al. (2017) found in their study that the thermal conductivity of concrete rised with the increase in the volumetric incorporation of SFs

into the concrete. While the thermal conductivity value of conventional concrete at a water/cement ratio of 0.40 is 1.95 $W \cdot m^{-1} \cdot K^{-1}$, the thermal conductivity reached up to 2.2 $W \cdot m^{-1} \cdot K^{-1}$ with the incorporation of SFs into the concrete at a volumetric ratio of 1.5%. By increasing the water/cement ratio to 0.55, the thermal conductivity reduces to the value of 2.05 W/m.K (Figure 2.18). As mentioned before, SFs are used to obtain conductive cementitious composites in snow/ice melting applications. However, due to the corrosive behavior of SFs, it is seen that carbon-based materials (CF, carbon nanofiber, carbon nanotube) are more commonly preferred in the creation of conductive composites. Carbon-based materials have a high thermal conductivity value, although not as high as metals. Also they are highly resistant to corrosion. All these properties make carbon-based materials good candidates for thermal applications in multifunctional cementitious composites, such as heating structures or de-icing roads (Galao et al., 2016). In snow/ice melting applications, the conductivity provided by carbon/steel based materials to composites was measured by in terms of electrical conductivity (Gomis et al., 2015; Wu, Liu and Yang, 2015) rather than thermal conductivity. This can be due to the fact that it is difficult to make accurate and precise measurements with existing thermal conductivity measurement methods for materials that do not comply with macro and micro-level homogeneity and isotropy in their internal structure (Yeşilata, Turgut and Işıker, 2007). However, it was stated that an improvement in thermal conductivity in heated pavement systems allows easily radiated heat energy to reach the road surface faster, promoting snow/ice melting in the study of Bai et al. (2017).

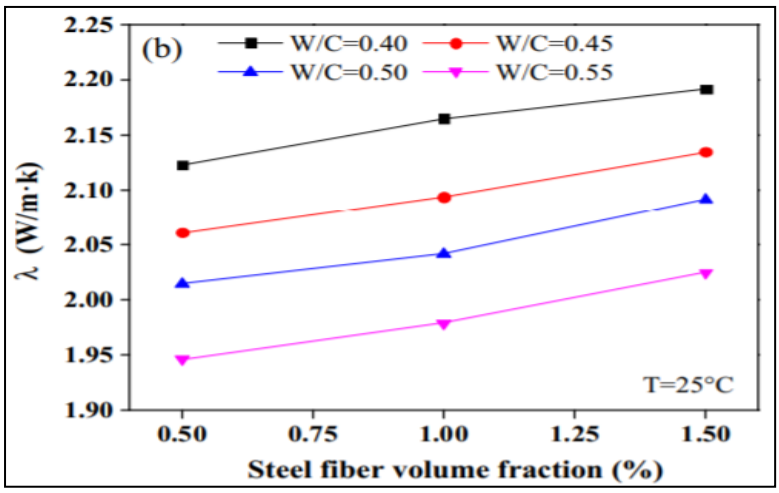

Figure 2.18. Effect of SF volume on the thermal conductivity of concrete (Liu et al., 2017)

3. EXPERIMENTAL STUDIES

3.1. Materials

The materials utilized in the experimental studies for the thesis are described in detail in this section, including their physical and chemical properties. CF and SF were used to provide conductive property to the cementitious composite overlay, and organic PCM, which can store and release solar energy, was used to provide snow/ice melting ability. Early high-strength cement was utilized to expedite the opening of the overlay to traffic, and a water-reducing additive was added to improve fresh state qualities of composite. To produce a strong matrix of quartz sand was used. Ground granulated blast furnace slag was added to the composites to lower the overlay cost.

3.1.1. Binder

A commercial CEM I 52.5 R White Portland Cement (PC), supplied from Çimsa Cement company and meeting the requirements specified in the EN-197-1 (2012) standard, was used as the binding component. This cement was chosen for the objective of producing an overlay with high early age strength since the overlay is expected to be used 24 hours after application. The chemical and physical properties of cement are given in Table 3.1.

3.1.2. Aggregates

In the study, quartz sand (QS) with the maximum particle size of 400 μm was used as an aggregate to generate a homogenous mixture, prevent fiber aggregation, and reduce matrix toughness. The QS was supplied by Pomza Export company (Figure 3.1). The chemical and physical properties of QS are given in Table 3.1.

Figure 3.1. Digital camera of QS

3.1.3. Mineral Additives

In the study, Ground Granulated Blast Furnace Slag (GGBFS), which is the by-product of Iskenderun Iron and Steel factory, was used as a mineral additive and provides economy (Şahmaran, Christianto and Yaman, 2006). In addition, it can have a bleeding-reducing effect during the application of the overlay to be produced. The properties of GGBFS are given in Table 3.1.

Table 3.1 Chemical and physical properties of PC, GGBFS, and QS

Chemical Composition	**PC**	**GGBFS**	**QS**
SiO_2 (%)	21.6	32.1	99.79
CaO (%)	65.7	36.1	0.02
Al_2O_3 (%)	4.05	11.2	0.06
Fe_2O_3 (%)	0.26	0.60	0.02
MgO (%)	1.30	5.60	0.01
SO_3 (%)	3.30	1.20	-
K_2O (%)	0.35	0.80	0.01
Na_2O (%)	0.30	0.30	0.02
Free CaO (%)	1.60	-	-
CO_2 (%)	-	9.10	-
Loss of Ignition (%)	3.20	2.80	0.07
Physical Properties			
Density (g/cm^3)	3.06	2.79	2.65
Specific Surface, Blaine (cm^2/g)	4600	4250	-

3.1.4. Chemical Additives

EBA 1447, a polymer-based high-range water reducing admixture (HRWRA) supplied by BASF, was used to produce mixtures having lower water-cement ratio and correspondingly, higher mechanical property. Table 3.2 gives the characteristics of the HRWRA additive.

Table 3.2. Technical characteristics of HRWRA

Chemical Structure	Drying Loss	Bulk Density	Density	Color
Polymer Based	Maks. %2	300-600 kg/m^3	1.184-1.244 kg/liter	Yellow

Considering the mixture components with different properties and also the inclusion of fibers in the mixtures, the rheological properties of the mortar become important. Fresh cement-based composites that behave like viscous liquids must have a flowing property in order to self-leveling. However, high fluidity reduces the yield stress and plastic viscosity of the mixtures. This results in the formation of mixes that are not homogeneous, exhibit segregation behavior, and have low cohesion (İşsever, 2002). It is known that especially SFs with high specific gravity tend to segregate in the middle and lower layers. In this regard, in order to determine the optimum fluidity and viscosity level during the studies, Viscosity Modifier (VM) additive was also used, while being sensitive to HRWRA ratios. As VM, Ashland's Culminal M2030 additive with water-retaining characteristics in powder form was used. The characteristics of the additive are given in Table 3.3.

Table 3.3. Properties of VM (Culminal)

Chemical Structure	Viscosity	Purity	Humidity	Density	Color
Cellulose Ether	17000-23000 Mpa.s	% 98	Max. %8	200 – 500 kg/m^3	Beyaz

3.1.5. Carbon Fiber

In the thesis research, carbon fiber (CF), which was provided by the ELG firm and whose technical details are listed in Table 3.4, was employed to increase conductivity. The photographs and SEM (Scanning Electron Microscope) images of CF are given in Figure 3.2.

Table 3.4. Physical properties of CF

Properties	**CF**
Diameter	7.5 µm
Length	12 mm
Aspect Ratio	1600
Elastic Modulus	240 GPa
Density	1.7 - 2.0 g/cm^3
Elongation Rate	%1.8

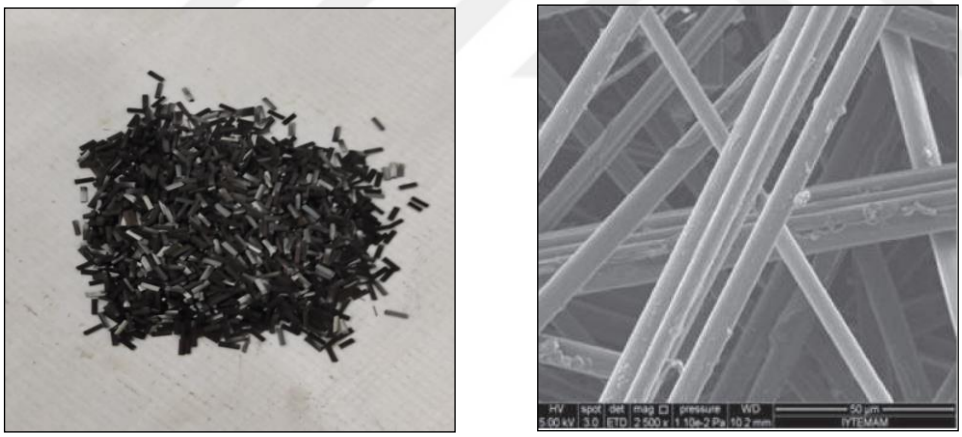

Figure 3.2. Digital camera photo and SEM analysis image of CF

3.1.6. Steel Fiber

In order to improve the conductive properties of composites in the study, Dramix OL 6/16 steel fiber (SF) supplied from Bekaert was used. The technical characteristics of the fiber are given in Table 3.5, and the digital camera image is shown in Figure 3.3.

Table 3.5. Physical properties of SF

Properties	SF
Diameter	0.16 mm
Length	6 mm
Aspect Ratio	37.5
Tensile Strength	3000 MPa
Density	7.17 g/cm^3
Young's Modulus	200.000 MPa

Figure 3.3. Digital camera image of SF

3.1.7. Phase Change Materials

The microencapsulated paraffin wax from MikroCaps Company, which has the chemical formula n-tetradecane ($C_{14}H_{30}$), was the organic type of PCM used in this study. The technical data for the microencapsulated PCM dispersion is shown in Table 3.6. This is made up of fluid with microcapsules that can store energy, and its fluid facilitates both addition of PCM to the composite and distribution of PCM in the composite, homogeneously (Kitchener, Wainwright and Parsons, 2017). The microencapsulation method used in cementitious composites containing self-healing agents (Lv et al. 2016) and corrosion inhibitors (Xiong et al. 2015) was preferred in this study to maintain PCM purity, provide optimized heat transfer with a high surface area, and offer flexibility for phase change (Anupam, Sahoo and Rath, 2020; Norvell, Sailor and Dusicka, 2013). The

digital camera image and SEM analysis of PCM are given in Figure 3.4 and Figure 3.5, respectively.

Table 3.6. Technical data of PCM dispersion

Properties	**PCM**
Classification	PCM-Microcapsule dispersion
Type of membrane	Melamine-formaldehyde
Type of PCM	Paraffin wax
PCM content in the dispersion (by weight)	% 25-30
Dry content in the dispersion (by weight)	% 35-38
Water content in the dispersion (by weight)	% 62-66
Ph	7.0-9.0
Density	900-970 g/L
Viscosity (at 25°C)	10-500 cPs
Appearance	White slurry

Figure 3.4. Digital camera view of PCM

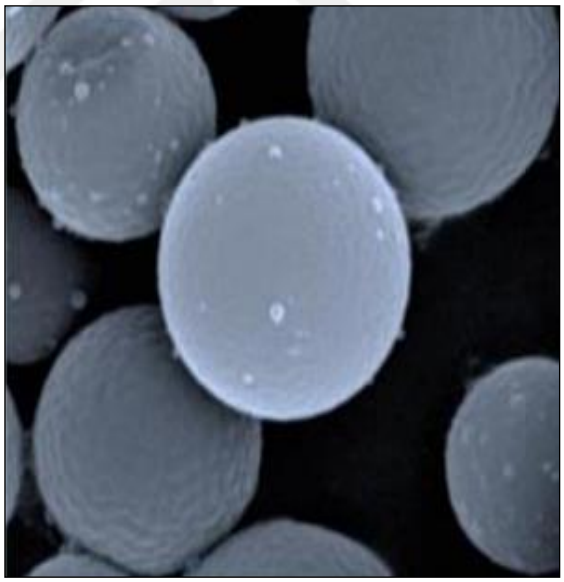

Figure 3.5. SEM analysis image of PCM

In order to determine its technical features in more detail, the PCM obtained from the company was examined in detail at the Chemistry Department of Tokat Gaziosmanpaşa University. Differential Scanning Calorimeter (DSC) was used to determine the physicochemical properties of PCMs in terms of thermal energy storage. As a matter of fact, in this method, very small samples can be heated/cooled at a constant rate. Therefore, the heat transfer rate related to the sample is not an issue. The heating rate gives the

material time to complete the physical transitions, and the possible low speed or low speed suitable for the analyzed sample is considered as the operating temperature. Organic PCMs can be analyzed at higher speeds since they do not show supercooling behavior. Since almost all known microencapsulated PCMs consist of organic polymer shell and core, they are analyzed at high speeds. Only polyethylene glycol polymers are considered as exceptions because of their supercooling behavior. The result of the DSC study utilized to ascertain the thermal characteristics of PCM is illustrated in Figure 3.6, and the heat storage characteristics based on DSC analysis data are given in Table 3.7. As can be seen from the DSC graph, the microencapsulated PCMs can take and return heat isothermally. In these materials, onset temperatures, that is, the temperatures at which the phase transition starts, are taken into account. Melting is indicated by the ascending endothermic peak. The exothermic transition peak is the downward peak. The shouldering of the downward peak means that the PCM used as the core material has the solid-solid phase transition usually seen in n-alkane derivatives just before melting. The solid-solid phase transition also has to be reversible, and it is evaluated that it is not clearly seen at the melting peak and is masked by overlapping with the melting transition. In summary, the actual melting temperature may be slightly higher. For the PCM used in this study, the starting and ending temperatures of the freezing point, which is the heat release region, were between 2°C and -14.0°C. It has been determined that the PCM has the capacity to deliver 155.5 J/g of energy in this range. The heat release of PCM, which begins near 0°C and continues below 0°C, is suitable range for snow/ice melting applications. Apart from the favorable phase transition temperatures, the enthalpies of microencapsulated PCMs are relatively high. Melamine formaldehyde is a very good material system compared to its peers in terms of stability, according to literature findings. On the other hand, the melting zone, which is the heat storage range of PCM, starts from 1.3 °C and continues up to 11.0 °C. The PCM, which has an energy storage capacity of 150.9 J/g in the melting region, provides benefits in reducing freeze-thaw temperature amplitudes and limiting temperature variations due to this heat storage range.

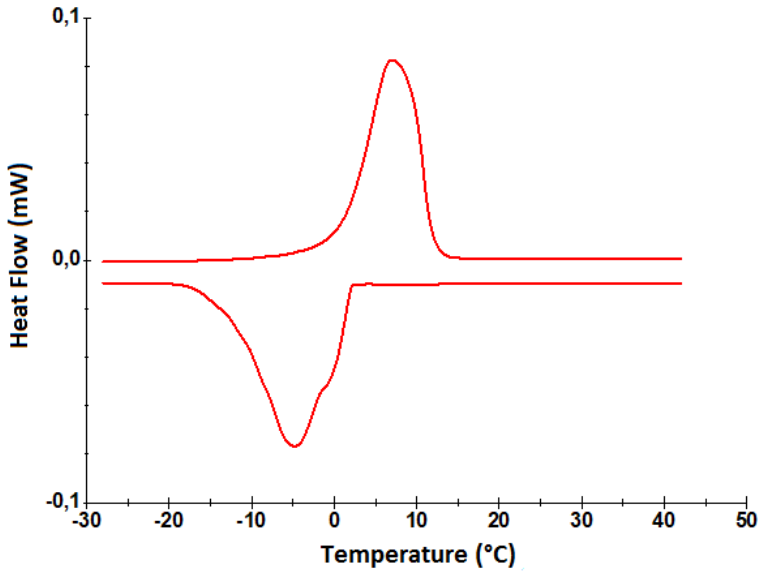

Figure 3.6. DSC analysis of PCM

Table 3.7. Heat properties of PCM

Melting Point Initial Temperature (°C)	**Melting Point Final Temperature (°C)**	**Melting Enthalpy (J/g)**
1.3	11.0	150.9
Freezing Point Initial Temperature (°C)	**Freezing Point Final Temperature (°C)**	**Freezing Enthalpy (J/g)**
2.0	-14.0	-155.5

Figure 3.7 was obtained by fluorescent microscopy. In the figure, total solid analysis was performed by means of particle imaging. The study revealed that the microcapsule particles were of varying sizes, with 49.4% of the total solid matter in the dispersion. The laser light scattering device was used to determine particle size distribution analysis, which produced the best results for similar investigations, and the particle size analysis of PCM is shown in Figure 3.8. The particle sizes ranged between 20 and 110 µm, and roughly 60% of the particle volume was between 80 and 120 µm, according to the analysis. The particle size of 100 µm had the greatest volume in the distribution, accounting for approximately 25% of the overall volume. Microcapsule particles 20 microns and larger are generally regarded as appropriate for the majority of applications. According to these values, 98% of the particles are smaller than 132 µm. Smaller microcapsule particles mean that PCM allows for faster reaction (Anupam, Sahoo and Rath, 2020; Norvell, Sailor and Dusicka, 2013) and better dispersion in the cement matrix

(Aguayo et al. 2016) compared to using large or agglomerated particles. Due to its polar and interactable features, it has been determined that the melamine-formaldehyde shell can be easily and efficiently employed in construction materials in terms of thermal conductivity.

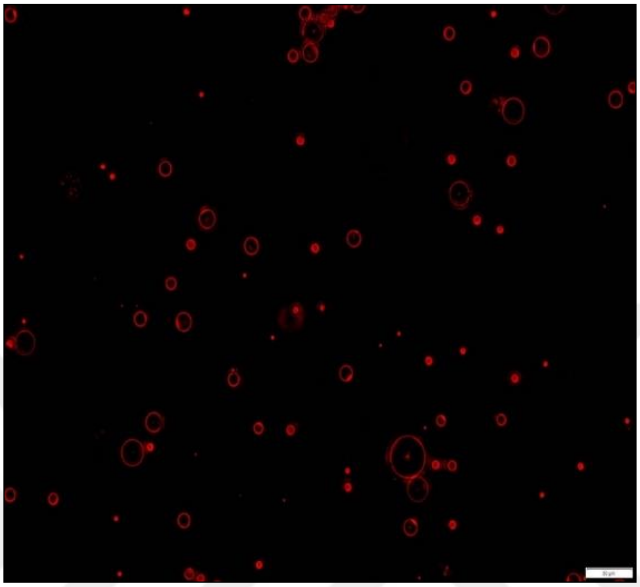

Figure 3.7. PCM particles in fluorescent microscopy

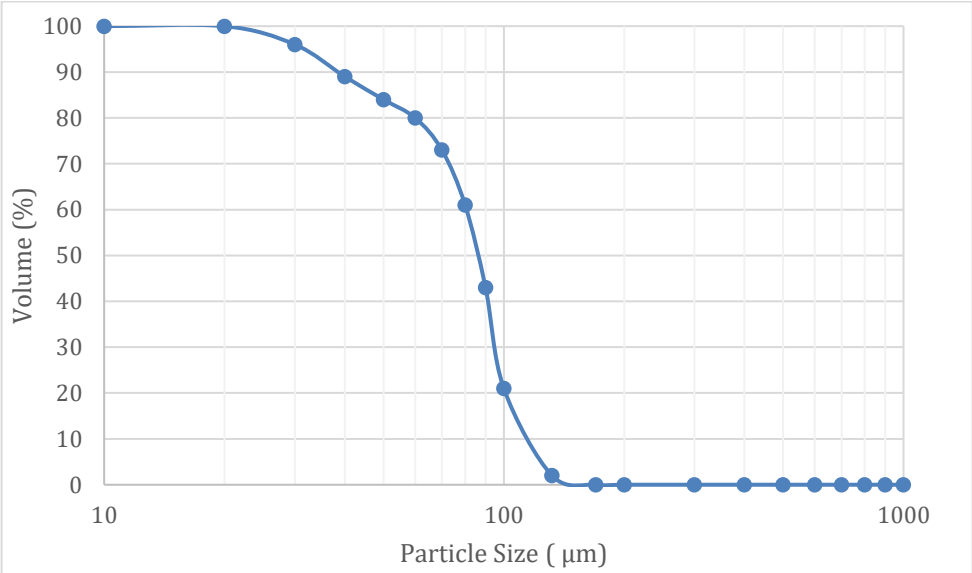

Figure 3.8. The cumulative particle size distribution of microencapsulated PCMs

Figure 3.9 shows the results of the Fourier Transform Infrared (FTIR) Spectroscopy investigation with peaks for organic PCM (n-Tetradecane-$C_{14}H_{30}$) and shell melamine-

fermaledehyde. The FTIR analysis of microcapsules was performed to explain the core structure. In melamine formaldehyde structures, the CH_2 groups are classically observed as a triple peak in the range of 2800-3000 cm^{-1}. The absorption peaks of pure n-Tetradecane occurred at values of 2850.27 cm^{-1}, 2919.7 cm^{-1}, 2956.34 cm^{-1}. The peak observed at 3500 cm^{-1} was caused by methylol OH. Although this broad peak is primarily derived from the OH or NH groups, it is part of a broad band formed by the accumulation of several identical peaks from groups that interact with one another due to the fact that these groups are appropriate for hydrogen bond interactions. The most important peaks observed on the right side of the spectrum is the shoulder-shaped NH peak on the left side of 1549 cm^{-1}. This peak is due to the melamine formaldehyde structure. Melamine formaldehyde polymers are polymer systems that have an irregular structure and are terminated with insoluble resins. The peaks of ether bonds remaining from methylol bridges are observed around 1450 cm^{-1}. The scheme for the synthesis of melamine formaldehyde resins is shown in Figure 3.10.

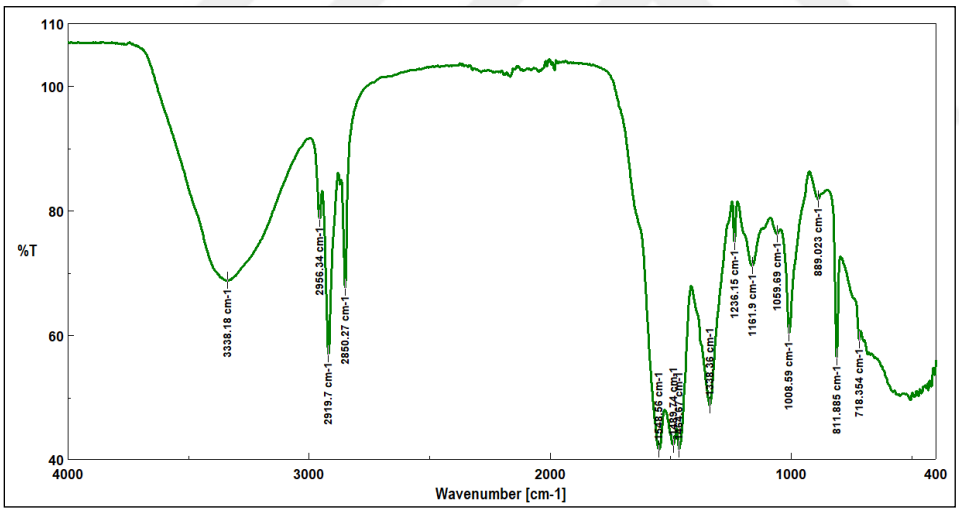

Figure 3.9. FTIR spectra of PCM

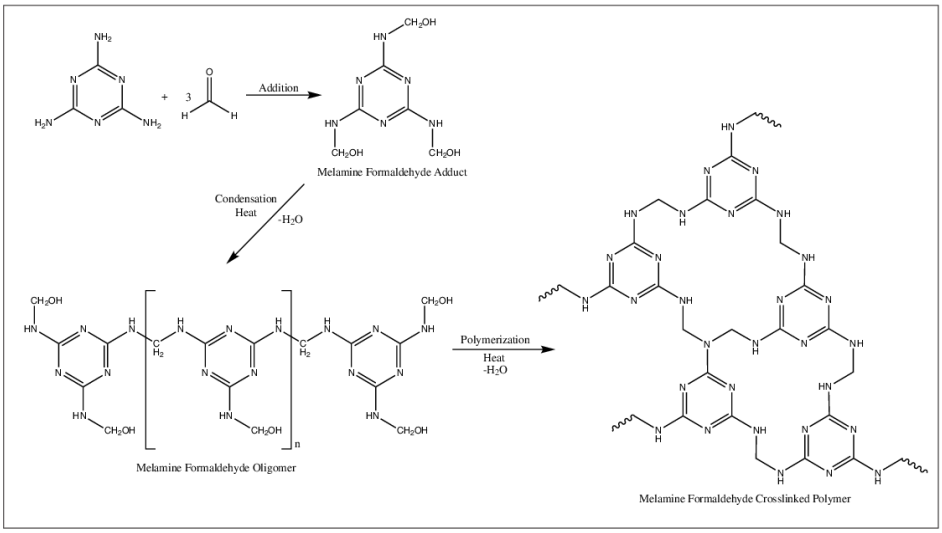

Figure 3.10. Scheme of synthesis of melamine formaldehyde resins

3.2. Methodology

This section presents experimental procedures in detail, including mixtures preparation, specimen preparation and curing, and testing procedures.

3.2.1. Production of Reference Composite

It is well known that PCMs dramatically decrease the compressive strength of cementitious composite. For this reason, the goal of this part is to maximize the strengths of the reference composite and fiber-reinforced conductive mixes created prior to the inclusion of PCM. So, to reduce the negative effects of PCM on compressive strength and to produce a self-levelling and high-strength reference matrix, the mixture contents in the TUBITAK project named “High Performance Fiber Reinforced Cementitious Composites For Rapid Repair Of Concrete Structures-Project Number:112M035” was taken as basis (Sahmaran, 2013). Accordingly, the water/binding material ratio was kept constant at 0.23, the water/cement ratio was 0.36, and the sand/cement ratio was 0.73, and CEM I 52.5 R Portland cement with high mechanical properties was used.

The dry ingredients (PC, QS, GGBFS, HRWRA, VM) were firstly introduced to mixing bowl and after the speed rate of the mixer was set at 150 rpm and the mixer was turned on. After 10 minutes, within 30 seconds, water was added to the mixture, and it was then

mixed at 150 rpm for an additional 4 minutes. At the end of this period, the speed of the mixer was set to 265 rpm and mixed for another 4 minutes and the mixer was stopped. The mixture with suitable strength and sufficient workability was determined as "Reference Composite" at the end of the 24th hour. The material content and amount of the reference mixture are given in Table 3.8.

Table 3.8. Weight ratios of compounds for the reference mixture composite

Water	PC	QS	GGBFS	HRWRA	VM
300	819	598	493	10	1

3.2.2. Production of Conductive Composites

In order to produce the conductive composites, the CF and SF were added to the reference mixture at the volume ratios specified in Table 3.9. During the studies, it was aimed to ensure the homogeneous distribution of the fibers in the mixture and to contact each other to obtain continuous conductive path.

Different mixing methods have been determined for mixtures containing CF and SF to distribute all the ingredients homogeneously. The mixing procedure of the composites is as follows: A mortar mixer was used to mix all the ingredients of the composites homogenously. For mixtures, powder ingredients were mixed at 150 rpm for 10 minutes. Then, water was added within 30 seconds and mixing was continued for additional 4 minutes at 150 rpm. At the end of this step, all ingredients were continued to be mixed for another 4 minutes at 265 rpm. CFs were added immediately before the high-speed mixing process since it was known that it provided a more homogeneous distribution and showed high conductivity performance compared to adding them to the dry mix (Sahmaran, 2020). However, SF was added to the mixture with the powder ingredients at the initial step, instead.

Table 3.9. Volumetric incorporation rates of fibers into referenc mixture

Mixture No	Code	CF (%) (relative to the volume of the reference mixture)	SF (%) (relative to the volume of the reference mixture)
1.Mixture	CF(0)-Reference	0.0	-
2.Mixture	CF(0.1)	0.1	-
3.Mixture	CF(0.2)	0.2	-
4.Mixture	CF(0.3)	0.3	-
5.Mixture	CF(0.4)	0.4	-
6.Mixture	CF(0.5)	0.5	-
7.Mixture	SF(1)	-	1.0
8.Mixture	SF(2)	-	2.0
9.Mixture	SF(3)	-	3.0
10.Mixture	SF(4)	-	4.0
11.Mixture	SF(5)	-	5.0

3.2.3. Production of Composites with Self-Melting Capability of Snow/Ice

The ultimate goal of the thesis research is to develop high thermal conductivity overlays that can melt snow/ice utilizing PCMs that take use of solar heat without the use of external energy sources. In this direction, CFs and SFs were used to increase the conductivity of the composites. However, during the thesis studies, it was determined that high-level thermal conductivity increased the amplitudes of the freeze-thaw cycles of the composites. Therefore, optimum fiber utilization rates have been determined, which have snow/ice melting capacity but will not adversely affect freeze-thaw amplitudes. It was discovered throughout the investigations that CFs offer many superior qualities to SFs. Based on the results in Section 4.1 and Section 4.3, SFs were eliminated and CFs were used in castings with PCM. On the other hand, when SFs are used to heat pavements, as was indicated in the literature review section, the steel is subjected to corrosion and the transmission line becomes blocked. However, CFs have a high level of corrosion resistance.

In order to produce conductive mixtures containing PCM, the dry ingredients (PC, QS, GGBFS, HRWRA, VM) were firstly introduced to mixing bowl and after the speed rate of the mixer was set at 150 rpm and the mixer was turned on. After 10 minutes, within 30 seconds, water was added to the mixture, and it was then mixed at 150 rpm for an additional 4 minutes. After the mixer was turned off, the conductive material were added. The PCM was added within 30 seconds after restarting (Figure 3.11) the mixer for 265 rpm and mixed for an additional 4 minutes. Also, to reduce the probability of damaging microcapsules, PCM was added as the final component (Jayalath et al. 2016, Hunger et al. 2009).

Figure 3.11. Addition of PCM dispersion to the mortar mix

In this study, CF was used in order to increase the conductivity, and the composites with low, moderate and high conductivity levels were produced based on the CF ratio. In this direction, the PCM was added to composites with three conductivity levels (low, moderate, and high) at a rate of 0, 2, 4, 6 and 8% of the cement weight, respectively. The PCM and CF ratios in all 15 mixtures that were produced in the study are shown in Table 3.10. Considering that PCM increases the fludity level of the mixture, the amount of HRWRA was used in mixtures containing PCM by reducing it to 3 kg/m^3. The PCM dispersion rate was arranged with respect to the required amount of PCM, assuming that the PCM content in dispersion was 27.5 % (it ranged from 25 to 30% by weight (Table 3.6)). The PCM dispersion rate and correspondingly, the w/c ratio of the mixtures are shown in Table 3.10.

Table 3.10. Conductive composites containing PCM and CF

Code	CF (%) (volume of mixture)	Conductivity Level	PCM (%) (weight of cement)	PCM dispersion rate (%) (weight of cement)	w/c
PCM(0)CF(0)	0	Low	0	0.0	0.36
PCM(2)CF(0)			2	7.4	0.41
PCM(4)CF(0)			4	14.8	0.45
PCM(6)CF(0)			6	22.2	0.50
PCM(8)CF(0)			8	29.6	0.55
PCM(0)CF(0.1)	0.1	Moderate	0	0.0	0.36
PCM(2)CF(0.1)			2	7.4	0.41
PCM(4)CF(0.1)			4	14.8	0.45
PCM(6)CF(0.1)			6	22.2	0.50
PCM(8)CF(0.1)			8	29.6	0.55
PCM(0)CF(0.3)	0.3	High	0	0.0	0.36
PCM(2)CF(0.3)			2	7.4	0.41
PCM(4)CF(0.3)			4	14.8	0.45
PCM(6)CF(0.3)			6	22.2	0.50
PCM(8)CF(0.3)			8	29.6	0.55

3.3. Testing

Figure 3.12 depicts a flow diagram of the tests performed on the mixtures developed for better understanding and follow-up.

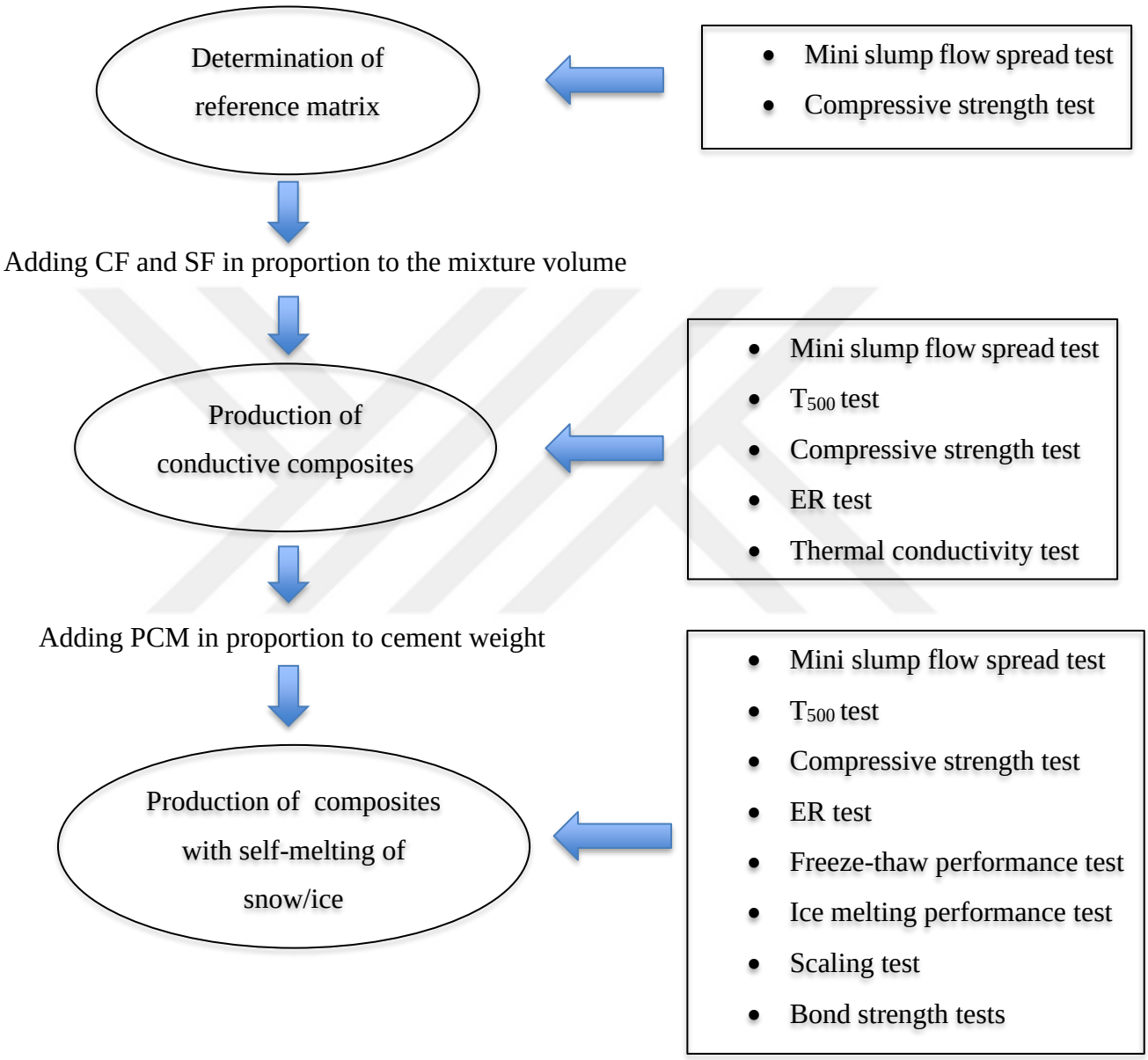

Figure 3.12. Flow diagram of tests applied to produced mixture

3.3.1. Mini Slump Flow Spread Test and T_{500} Tests

Mini slump flow spread test was conducted to determine the consistency properties of the mixtures. Test was performed on all fresh-state cement-based mixtures immediately after the mixing process. For this test, a metal mini slump cone with a height of 75.8 mm, a lower internal diameter of 92.1 mm and an upper internal diameter of 43.5 mm was used. The prepared mixture was filled into the mini-slump cone without applying any compaction and after finishing the mortar surface, the cone was slowly lifted vertically (Figure 3.13). When the spreading of the fresh-state material was completed, the diameter of the resulting circular shape was measured in two perpendicular directions and the average of these two measurements was regarded as the mini slump flow diameter value of the mixture. The T_{500} test, which is an indicator of viscosity in the case of self-compacting concrete (Satish, Kumar and Rai, 2017), was performed to evaluate the flow rate (Özerkan, 2009) of the designed composites. Without applying compression, the produced mixtures were filled into a cone with a height of 200 mm, a lower diameter of 200 mm, and an upper diameter of 130 mm. The cone was lifted 30 seconds after the material was placed in it, and the time when the material attained a diameter of 500 mm was recorded.

Figure 3.13. Determination of the consistency of mixtures with the mini slump flow spread test

3.3.2. Compressive Strength Test

The compressive strength of the mortars was also measured in accordance with the ASTM C109 standard. After the mixing procedure, 50 mm-cubic specimens (Figure 3.14) were kept at the laboratory environment with a relative humidity (RH) of 50±5% and a temperature of 23±2 °C for 24 hours. At the end of the initial 24 hours, the samples were removed from the molds and subjected to curing in a curing pool at the temperature of 23±2 °C until the testing time. The compressive strength tests were performed at a loading speed of 0.900 kN/s on the 1st, 3rd, 7th, 28th days using 6 cube samples for each mixture, and the results were averaged.

a) b)

Figure 3.14. a) Placing the mortar in the mold b) Subjecting the sample to the compressive strength test

3.3.3. Electrical Resistivity and Thermal Conductivity Tests

The improved conductivity properties of the composites produced by adding CF and SF were determined by electrical resistance and thermal conductivity tests at this stage. The consistency of the electrical resistance values taken from different regions of the same sample was analyzed to determine the homogenous distribution of the fibers. The electrical resistance was measured with the Electrical Resistance (ER) method. In this method specified in the study of Spragg et al. (2013), Ø100×200 mm samples were prepared for each mixture. Three Ø100×50 mm specimens removed from cylindrical specimens with Ø100×200 mm dimensions were used. A 2 cm part was cut from the mold

surface and the top of the Ø100×200 mm sample in contact with the air. The reason for this process is to eliminate the negative effect of the surfaces in contact with the air and mold on the conductivity properties. Wet sponges (10 mm in height, 150 mm in diameter) saturated with the same amount of water were placed between the plates of the device and the sample, and the results were recorded by the device. The ER measurements were performed on the ambient-cured specimens at the curing ages of 1, 3, 7, and 28 days, as shown in Figure 3.15. The ER measurement was made on three samples from each mixture and their average was reported. These were carried out with the RCON^{TM} device of the GIATEC brand. It has a uniaxial configuration and works with the AC impedance technique. This device, capable of measurements in less than 5 seconds, operates in the frequency range of 1 Hz-30 kHz and detects the phase angle between 0-180°. The operating frequency value was set at 1 kHz to nullify the polarization effect. The impedance and phase angle values, which can be converted to resistivity values using geometric factors, are given by the following equation:

$$\rho = Z \times \cos(\Theta) \times A/L$$

ρ: resistance (Ω.m)
Z: empedance(Ω)
Θ: phase angle (°)
A: cross section area (m^2)
L: length (m)

Figure 3.15. Resistivity meter with the test specimen

The thermal conductivity measurements were carried out with ambient-cured specimens on the 7th and 28th days. For the test, the samples were prepared by casting the mixtures into the Ø100×50 mm cylindrical molds. After curing, cutting, and etching processes, three Ø50×25 mm samples were obtained from the samples (Figure 3.16). In the thermal conductivity measurements, the Lasercomp Fox-50 Heat Flow Meter device (Figure 3.17), which can measure thermal conductivity between 0.1 W/mK and 10 W/mK and works with the steady-state method specified in ASTM C518 and ISO 8301 standards was used. The thermal conductivity measurement was made on three samples from each mixture in Table 3.9 and their average was reported.

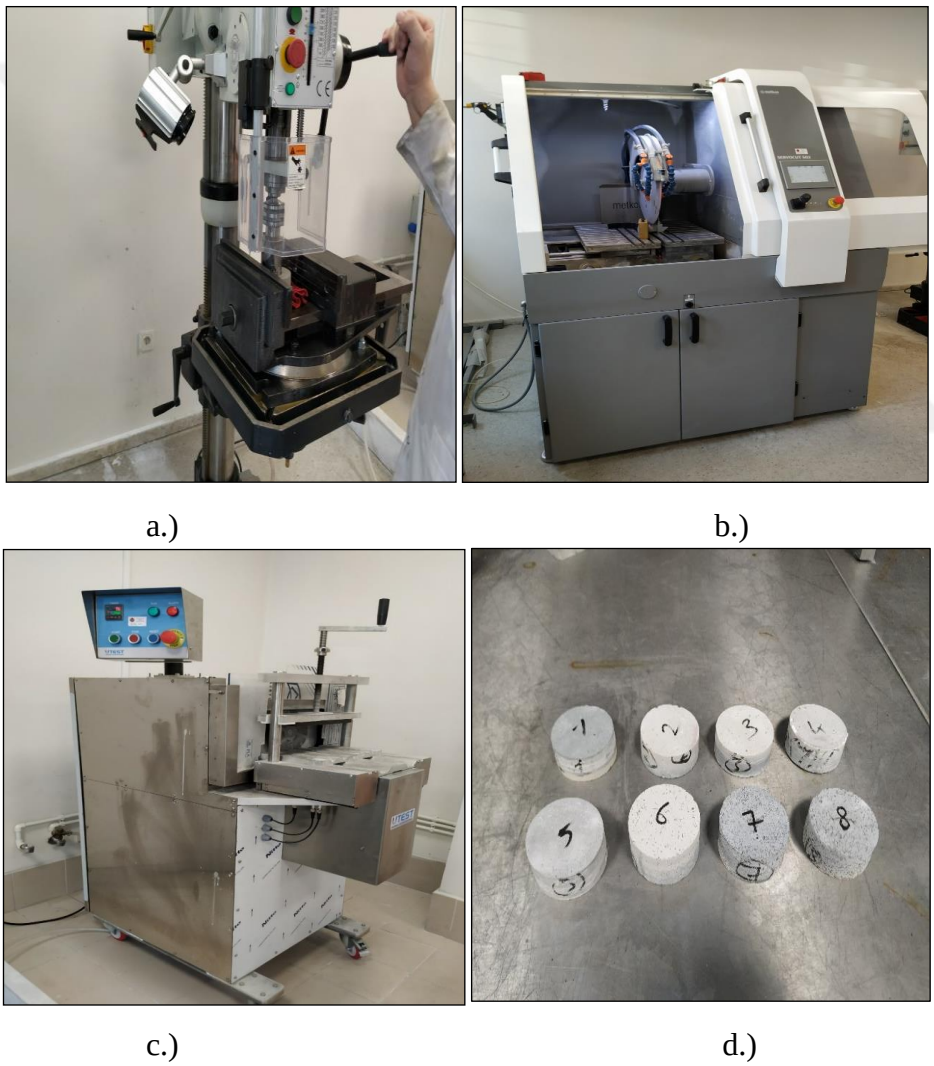

a.) b.)

c.) d.)

Figure 3.16. a.) Core drilling machine b.) Cutting machine c.) Abrasion machine d.) Thermal conductivity samples of Ø50×25 mm obtained after coring, cutting and abrasion processes (GDH-Concrete Laboratory)

Figure 3.17. Heat Flow Meter (Lasercomp Fox-50 device)

3.3.4. Freeze-Thaw Performance Test

The purpose of the freeze-thaw performance test is to examine the behavior of the PCM-added composites with the reference composite (PCM(0)CF(0) code composite for this test) under freeze-thaw cycles and to interpret the effect of the PCM on temperature amplitudes for Turkish cities. Therefore, two distinct regions having different weather conditions were selected from the Central Anatolia Region of Türkiye. The first region included the cities such as Konya, Aksaray and Kayseri, the maximum and minimum temperatures of which, went beyond the limits of the melting/freezing of PCM used in this study according to the meteorological data, during the 2021-2022 winter season. To mimic the weather conditions of the second group cities like Ankara, Çankırı and Çorum, the second simulation was also created. For these, the maximum and minimum temperatures were measured around the melting and freezing point of the PCM, respectively. In other words, for example, while temperature at Konya from the first group cities was a highest of 17 °C, it was a lowest of -22 °C and these temperatures exceeded the melting/freezing point limits of the PCM. However, for the second group cities, for instance, Çankırı, the temperature was +15 °C at most, it decreased to a minimum of -10 °C (see https://www.mgm.gov.tr/FILES/iklim/yillikiklim/2022/mevsimlik-sicaklikanalizi-2022-kis.pdf) and these temperatures were around the melting/freezing points of PCM. The simulations were created similar to studies of Yeon and Kim (2018) and Farnam et al. (2017). In the first simulation, the ambient temperature in the freeze-thaw cabinet was

adjusted to raise the reference sample to a maximum of +20 ºC and to reduce it to a minimum of -20 ºC (Figure 3.18). The rate of temperature drop from +20 to -20 °C and temperature rise from -20 to +20 °C was determined to be 4 °C/h. The test was performed in two cycles and calculations were based on the second cycle, which was thought to provide better thermal balance between the cabinet and the samples. In the second simulation with a maximum and minimum temperature of +10 and -10 ºC, respectively; the criteria of the cycle system specified for the first simulation were applied completely (Figure 3.18). The samples were kept at maximum and minimum temperatures for 4 hours in both simulations. Consequently, it was intended to follow the behavior of the PCM after the process of releasing/absorbing thermal energy was completed (the first simulation) and before it was completed (the second simulation). As the freeze-thaw cabinet, a Schleibinger Slabtester device with a digital display was used (Figure 3.19-e). The temperature of the cabinet was monitored from the computer connected to the device and could be adjusted in the range of -35 °C and +40 °C. Pt100 thermocouples, which have a data rate of 50 kpbs and can operate between -200°C and 600°C and are commonly used in low temperature settings and sensitive measurements were employed in the study. The test was carried out in two procedures, the descriptions of which are given below.

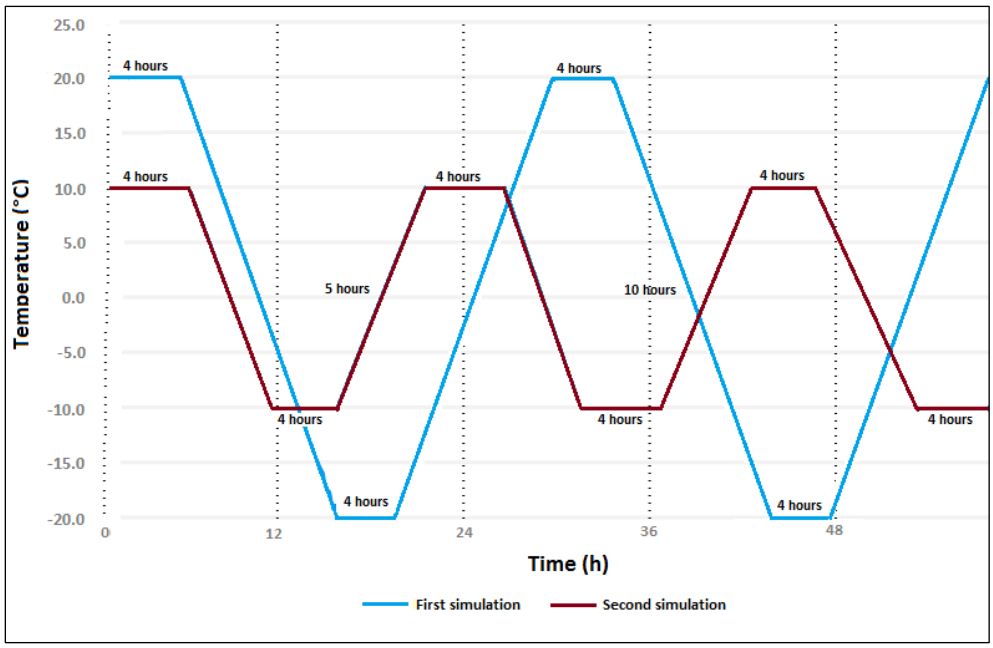

Figure 3.18. Graph of the cycle systems created on the reference sample

3.3.4.1. First Procedure-Different PCM Ratios by Cement Weight

The samples of the 15 mixtures specified in Table 3.10 were tested in this procedure. 150×150×40 mm freeze-thaw molds (Figure 3.19-a) filled with composites were kept at 95% humidity for 24 hours and then moved to laboratory conditions for 28 days. The edges of samples were sealed with silicone (Figure 3.19-b) and a-20-mm hole was drilled across its entire thickness to insert the thermocouples in the center of the samples (Figure 3.19-c). To reduce temperature fluctuations and ensure that every sample achieved the same temperature, the samples were stored in an isothermal cabinet for three days at a constant temperature of 20 °C. The samples were then placed in the freeze-thaw cabinet, and thermocouples were embedded in their centers to monitor their interior temperature (Figure 3.19-d). The test was performed separately on the samples having each PCM percentage.

3.3.4.2. Second Procedure-Composites of Different Thicknesses Containing 6% PCM of the Cement Weight

In the second procedure, PCM(0)CF(0) (Reference), PCM(6)CF(0) and PCM(6)CF(0.1) coded composites were used among 15 mixtures in order to perform the thickness tests. The purpose of this test is to determine the overlay thickness in the application. In this direction, freezing and thawing tests were carried out on the samples of the mixtures with a size of 150×150 mm and a thickness of 20, 30, 40 and 50 mm (Figure 3.20). 150×150×40 mm freeze-thaw molds (Figure 3.19-a) filled with composites were kept at 95% humidity for 24 hours and then moved to laboratory conditions for 28 days. The edges of samples were sealed with silicone (Figure 3.19-b) and hole was drilled through half the thickness to insert the thermocouples in the center of the samples (Figure 3.19-c). To reduce temperature fluctuations and ensure that every sample achieved the same temperature, the samples were stored in an isothermal cabinet for three days at a constant temperature of 20 °C. The samples were then placed in the freeze-thaw cabinet, and thermocouples were embedded in their centers to monitor their interior temperature (Figure 3.19-d). Each thickness group was tested separately.

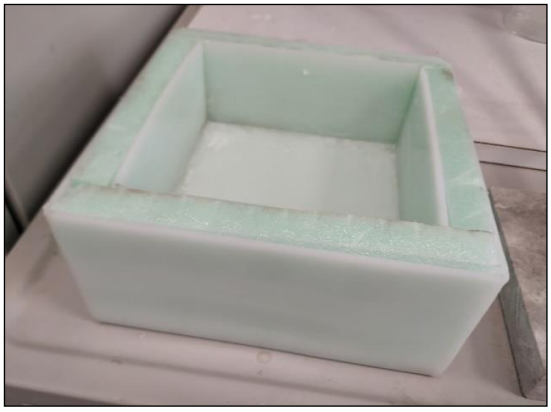

a)

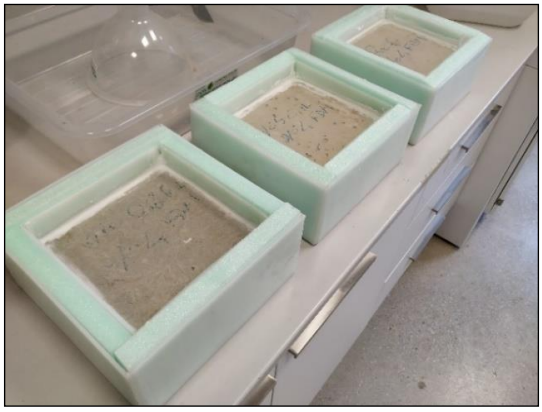

b)

c)

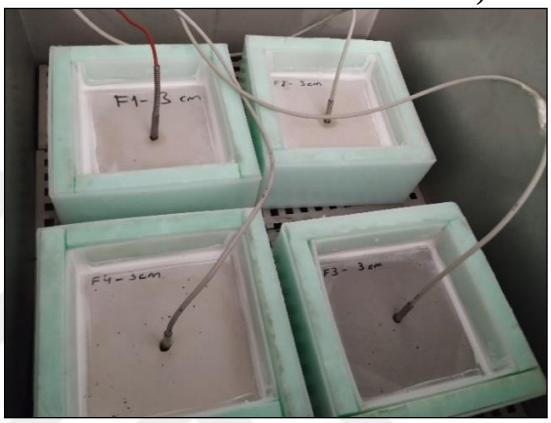

d)

e)

Figure 3.19. a) Ready-made freeze-thaw molds b) Samples placed in molds and siliconized on the edges c) Drilling process from the middle of the sample in the mold d) The samples placed in the cabinet with a thermocouple in their center e) Freeze-Thaw cabinet.

Figure 3.20. Samples with a thickness of 10, 20, 30, 40, 50 mm

3.3.5. Ice Melting Performance Test

3.3.5.1. First Procedure-Different PCM Ratios by Cement Weight

The Ice Melting Performance Test was applied to determine the effect of PCM and CF on the rate of ice melting in composites that were produced. 15 mixtures given in Table 3.10 were casted into molds measuring 150×150×40 mm. After the samples were cured in the environment having 95% relative humidity for 24 hours, they were demolded, and the curing was proceeded in laboratory conditions for 28 days. Then, they were placed in insulated ready-made freeze-thaw molds their edges were sealed for water with silicone. The samples were put in the freeze-thaw cabinet, and the cabinet was set to a constant temperature of 2.5 ^{o}C. After 24 hours, 100×100 mm in size and 15 mm thick ice was placed on the samples (Figure 3.21) and samples were tilted slightly in the cabinet, allowing the melted ice to collect at the edge of mold and be extracted with the injector. The mass of the water resulted from the melted ice was monitored for 72 hours with 8-hour intervals. The test was performed separately on the samples having each PCM percentage.

3.3.5.2. Second Procedure-Composites of Different Thicknesses Containing 6% PCM of the Cement Weight

In order to test the effect of sample thicknesses on ice melting, 6% PCM rate was taken as basis. In this regard, PCM(0)CF(0) (Reference), PCM(6)CF(0) and PCM(6)CF(0.1)

coded composites were used among 15 mixtures. Ice melting tests were performed on samples of the specified composites with a thickness of 10, 20, 30, 40 and 50 mm. The sample dimensions of 150×150 mm were chosen. The conditioning for this step is the same as for the first, but the cabin is set to a constant temperature of 1.5 °C. Thus, the behavior of the PCM below the phase change temperature was followed and the effect of the cabin temperature on ice melting reduced compared to 1st procedure. Each thickness group was tested separately.

Figure 3.21. The process of placing ice on the samples in the cabinet

3.3.6. Scaling Test

The experiment was carried out over 56 cycles in accordance with the "Slab Test Method" specified in the TS EN 12390-9 standard. The 15 mixtures specified in Table 3.10 were cast into molds with 150×150×40 mm dimensions. The samples, which were kept in the molds at 95% humidity after casting, were removed from the molds after 24 hours and placed in the curing pool. After 7 days, the samples removed from the curing pool were placed in the air-conditioning cabinet providing the humidity. The samples were moved to molds and their edges were sealed with silicone on the 31st day. After they were placed in a freeze-thaw cabinet. 67 mL of 3% NaCl solution was introduced to the sample. The depth of the solution on the specimen was arranged 3 mm. The cabinet was operated in

accordance with the cycles in Table 3.11. The values in the table are expressed by the scanned area in Figure 3.22.

Table 3.11. Spalling resistance test cycle intervals

Upper Limit		**Lower Limit**	
Time (hour)	Temperature (°C)	Time (hour)	Temperature (°C)
0	+24	0	+16
5	-3	3	-5
12	-15	12	-22
16	-18	16	-22
18	-1	20	-1
22	+24	24	+16

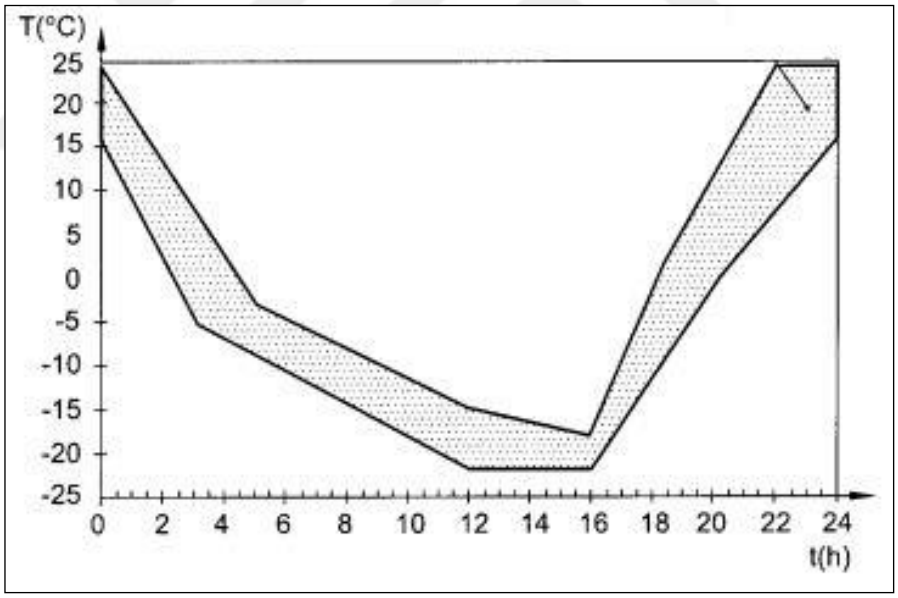

Figure 3.22. Scaling test cycle plot

3.3.7. Bond Strength Tests

The conductive cementitious composites with self-melting snow/ice melting capability are considered to be applied as an overlay between 1 and 5 cm on asphalt and concrete pavements. In order for the overlay to perform well, sufficient adherence must be formed

with the layer on which it is casted. In this context, Slant Shear Test and Pull-Off Test were performed to measure the adherence between two layers. Adhesion with the existing substrate concrete and the cementitious overlay produced depends on mechanical interlocking forces and negligible Van der Walls forces. Mechanical locking forces are produced by the C-S-H gel created in the penetration layer given by the cement-bonded composite cast on the substrate concrete and a little quantity of $(CaOH)_2$. On the other hand, the strong adhesion of asphalt creates the adherence between asphalt and cement-based composite. Adhesion forces of asphalt binder are realized by Van der Waals forces and some chemical bonds between polar molecules in asphalt and hydrates in concrete (Peng et al., 2019).

3.3.7.1. Slant Shear Test

In order to test the bond strength of the overlay produced to asphalt and concrete roads, slant shear test was carried out in accordance with ASTM C882 standard. This commonly used test is appropriate for circumstances in which the interface is subjected to both pressure and shear stresses (Harris, Sarkar and Ahlborn, 2011). In the scope of the test method, Ø10x20 cm concrete samples with C30/37 strength class were cast in accordance with the GDH Concrete Pavement Technical Specification. The samples were taken out from the molds after 24 hours and left to cure for 27 days in the curing pool before being kept in the curing room for 5 months at a temperature of 23±2 ^{o}C and a relative humidity of 50±5%. Following the curing procedure, the cylindrical samples were cut obliquely at an angle of 30°C to be half cylinders (Figure 3.23-a), and they were then put in 10x20 cm molds. The remaining parts of the molds were filled with the PCM(6)CF(0.1) mixture, which showed appropriate performance in other experiments, and the monolithic sample were removed from the molds after 24 hours (Figure 3.23-b). The samples that were taken out of the molds were maintained in the curing room until test day at a temperature of 23±2 ^{o}C and 95±5% relative humidity. On the other hand, the slant shear test of the generated overlay was performed with samples with asphalt road surface layer properties. Asphalt sample was casted in GDH Bituminous Mixtures Laboratory in accordance with the Highways Technical Specification (2013) in a Ø10x20 cm cylinder dimensions with a bitumen rate of 5.52%, void ratio of 4.17% and Marshall Stability of 920 kg. Cylindrical specimens were cut obliquely at an angle of 30°C to be half-cylindrical (Figure 3.24-a) and placed in molds of 10×20 cm. The remaining parts of the molds were filled with the

PCM(6)CF(0.1) mixture and the samples, which were made monolithic in the mold, were removed from the molds after 24 hours (Figure 3.24-b). The samples that were taken out of the molds were maintained in the curing room until test day at a temperature of 23±2 ^{o}C and 95±5% relative humidity. For all samples with asphalt and concrete substrates, compressive strength test was applied on the 3rd, 7th and 28th days in accordance with the loading rate (900-1800 N/s) in the ASTM C109 standard. Four samples were fractured for each of the three required ages, for a total of 12 samples. The bond strength values and fracture patterns of the samples were analyzed as a result of the compressive strength test. No additional bonding material was used between the two layers, and also such as roughening, sandblasting on the substrate process had not been performed.

a) b)

Figure 3.23. a) Substrate concrete samples cut at an angle of 30 °C b) Monolithic state of PCM(6)CF(0.1) mixture and substrate concrete sample

a) b)

Figure 3.24. a) Substrate asphalt samples cut at an angle of 30 °C b) Monolithic state of PCM(6)CF(0.1) mixture and substrate asphalt sample

3.3.7.2. Pull-Off Test

The Pull-Off test described in the ASTM D 4541 standard was performed to determine the adhesion between the overlay developed and the asphalt/concrete road. This method is one of the commonly used tensile testing methods to evaluate the adhesion between overlay/repair materials and the existing concrete substrate. On the other hand, unlike bond test methods, which have limited use in the laboratory, Pull-Off test can be easily used in the field evaluation of the bond strength between the overlay/repair material and the main concrete in a structure (Bonaldo, Barros and Lourenço, 2005). The parameters of the substrate concrete/asphalt were employed in this experiment as indicated in the Slant Shear Test. The dimensions of the substrate concrete/asphalt samples were determined as 320×260×50 mm, and PCM(6)CF(0.1) coded composite, which showed appropriate performance in other experiments, was casted on them separately, from 1 cm to 5 cm thick, at 1 cm intervals. The goal of evaluating PCM added composites of various thicknesses is to find the optimum overlay thickness while maintaining adequate bond strength values. The samples that were taken out of the molds were maintained in the curing room until test day at a temperature of 23±2 ^{o}C and 95±5% relative humidity. Then, cores with a diameter of 50 mm and a drilling depth of 15±5 mm substrate concrete/asphalt were taken. Considering that the vibrations of the core drilling device will affect the bond strength of samples, an equal and sufficient distances have been left between the samples. The metal rings to be used in the test were adhered to each core sample with epoxy. The direct pull-off test was performed on 1st, 7th and 28th days with three samples for each day. The test was carried out using the Proceq DY-225 device, as shown in Figure 3.25. Tensile force was applied at a constant rate speed until the rupture. The photographs of the casting of the substrate concrete are shown in Figure 3.26, whereas the image of the substrate concrete sample with the PCM(6)CF(0.1) combination, which was formed monolithic and the test process continues, is shown in Figure 3.27. In Figure 3.28-a, one cm thick PCM(6)CF(0.1) coded composite and the bottom layer asphalt sample image is given, while Figure 3.28-b shows the sample with a metal ring attached. No additional bonding material was used between the two layers, and also such as roughening, sandblasting on the substrate process had not been performed.

Figure 3.25. Pull-Off Test Device

Figure 3.26. Substrate concrete casting

Figure 3.27. Substrate concrete sample with 5 cm thickness PCM(6)CF(0.1) coded composite

a) b)

Figure 3.28. a) 1 cm thick PCM(6)CF(0.1) coded composite and substrate asphalt sample b) Core taked and metal ring attached sample

3.3.8. Microstructural Analysis

SEM, scanning electron microscope, was used for microstructural analysis in order to determine the morphologies and elemental compositions of cementitious composites with self-meltig snow/ice ability (Figure 3.29). Additionally, with this method, the homogeneous distribution of both fibers and microencapsulated PCM was investigated in order to function properly in the composite. Samples kept in cure for 28 days were used for analysis. The specimens tested surfaces were first sanded and cleaned. Following that, the specimen was split into small pieces, and samples were drawn at random from among the broken pieces. After being oven-dried overnight, these specimens were subjected to SEM analysis. SEM micrographs were taken, and the elemental compositions of the sections examined were determined using SEM mapping. SEM analyzes of the reference composite and CF(0.1), CF(0.3), PCM(0)CF(0), PCM(2)CF(0), PCM(4)CF(0), PCM(6)CF(0), PCM(8)CF(0), PCM(2)CF(0.1), PCM(4)CF(0.1), PCM(6)CF(0.1), PCM(8)CF(0.1) composites were performed in the HUNITEK Laboratory of Hacettepe University.

Figure 3.29. SEM analysis device

4. RESULTS AND DISCUSSION

4.1. Results of Mini Slump Flow Spread and T_{500} Tests

The goal of the thesis is to produce conductive cement-based composites with the capability to self-melt snow/ice as well as self-leveling property. Mini slump flow diameter (mm) and T_{500} (sec) tests were conducted in this direction to determine the consistency, fluidity, and workability characteristics of the produced composites. Slump flow spread is a more complicated function of both yield stress and plastic viscosity rather than being solely a function of yield stress. On the other hand, the T_{500} was associated equally with both yield stress and viscosity, however the slump flow spread is more closely related to yield stress than to viscosity, particularly at high viscosities (Esping, 2007). The results of the tests for cementitious composites are given in Table 4.1 and Figure 4.1. When the results are examined, it was determined high level of correlation between the T_{500} test and mini slump flow tests. Especially in CF mixtures, SF mixtures and high conductivity mixtures, R^2 coefficent values were 0.95, 0.91 and 0.95, respectively. This value was calculated as 0.76 and 0.74 for low conductivity and moderate conductivity, respectively.

The most important parameter determining the consistency properties of the composites was the polymer-based HRWRA additive used. It improved the fresh state features of the mixtures, increased the workability, and supplied the self-leveling feature. On the other hand, the effect of fibers on consistency was examined in the study. The distribution of fibers throughout the cementitious matrix can be significantly affected from its rheology. Although the risk of sedimentation of the CFs in the cementitious mixtures with low viscosity and more fluidity was low, it is known that they might not be dispersed homogeneously and they tended to agglomerate in composites with high yield stress (Gao et., 2017). To avoid the aforementioned issue, it was preferred to keep the composites mixing times in the mixer as long as possible (Section 3.2.2). It was determined CF had the significant impact on consistency. While the spreading diameter of CF(0.1) was 350 mm, this value decreased to 210 mm in CF(0.5) (Table 4.1). T_{500} duration for self-compacting concrete ranges from 2 to 7 seconds (Marina et al., 2010) and the mixture with the highest T_{500} value (4.9 seconds) was CF(0.5) in this study . It shows that all mixtures produced in this study have self-compacting properties.

Table 4.1. Consistency properties of cementitious composites

Mixture Type	**Mixture Code**	**Mini slump flow diameter (mm)**	**T_{500} (s)**	**Coefficient of determination (R^2) between T_{500} (s) and mini slump flow diameter (mm)**
Reference	CF (0)	360	2.9	-
CF Mixtures	CF (0.1)	350	3.0	0.95
	CF (0.2)	310	3.6	
	CF (0.3)	260	4.0	
	CF (0.4)	225	4.2	
	CF (0.5)	210	4.9	
SF Mixtures	SF (1)	320	3.1	0.91
	SF (2)	320	3.2	
	SF (3)	310	3.3	
	SF (4)	300	3.4	
	SF (5)	300	3.4	
Low Conductivity	PCM(0)CF(0)	285	3.8	0.76
	PCM(2)CF(0)	295	3.3	
	PCM(4)CF(0)	300	3.3	
	PCM(6)CF(0)	310	3.2	
	PCM(8)CF(0)	310	3.1	
Moderate Conductivity	PCM(0)CF(0.1)	285	3.6	0.74
	PCM(2)CF(0.1)	295	3.7	
	PCM(4)CF(0.1)	295	3.6	
	PCM(6)CF(0.1)	305	3.3	
	PCM(8)CF(0.1)	310	3.3	
High Conductivity	PCM(0)CF(0.3)	270	3.9	0.95
	PCM(2)CF(0.3)	270	3.8	
	PCM(4)CF(0.3)	275	3.7	
	PCM(6)CF(0.3)	285	3.5	
	PCM(8)CF(0.3)	285	3.5	

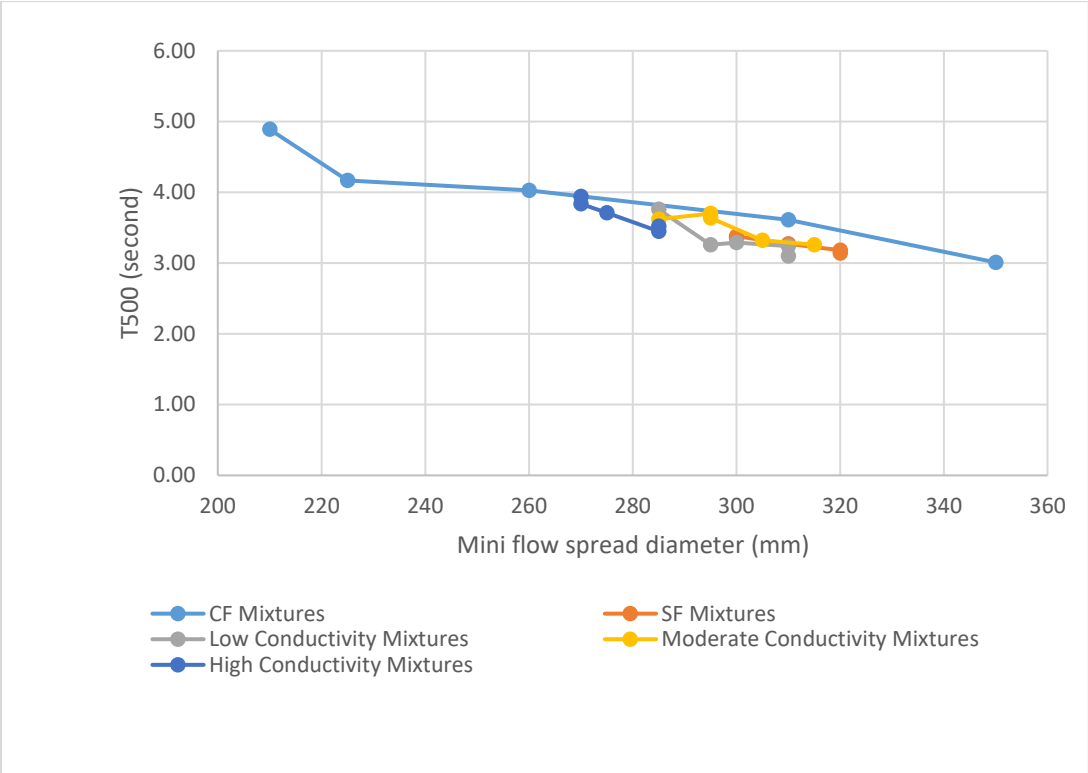

Figure 4.1. Results of mini slump flow spread and T_{500} test

On the other hand, in a matrix with relatively lower yield stress (more fluid matrix), the fibers have relatively greater mobility within the cement matrix. This situation causes the sedimentation of the SFs, which have a higher specific gravity than the other ingredients of the cementitious systems. In line of these statements, it has been experienced that SFs undergo segregation, especially in mixtures with a spreading diameter greater than 330 mm (Figure 4.2). In order to obtain consistent conductivity results, SF containing mixtures have been reported with a consistency in the range of 300-330 mm spreading diameters. As a matter of fact, the homogeneous distribution of the SF mixtures in this range was determined visually (Figure 4.3) and also the electrical resistance and thermal conductivity results were consistent (Table 4.3). Although the amount of plasticizer was kept constant in SF mixtures, the workability was slightly affected as the SF ratio increased. This is because the frictionless surface of the brass-coated SF compensates for the workability, which is negatively affected by the increased fiber ratio. The SF(1) and SF(2) have the same level of workability and a mini flow diameter of 320 mm. SF(3) the mini flow diameter was only 10 mm lower than SF(1) and SF(2). Besides, in SF (4) and SF (5), the SFs did not affect the workability much and the mini flow diameter was 300 mm for them.

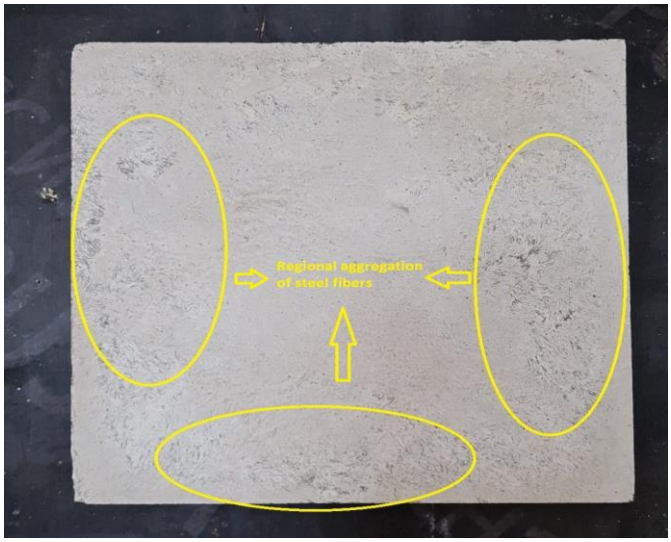

Figure 4.2. Clustering of SFs collapsing to the substrate in a mixture with a mini flow diameter of 360 mm

a.) b.)

Figure 4.3. Visual determination of the homogeneous distribution of SFs a.) Distribution of SFs in the mixture with code SF(5) broken with a hammer b.) Distribution of SFs in a sample cored for thermal conductivity test

In order for SFs to be distributed evenly, it is necessary to work at high viscosity and within a limited fluidity range. Although CFs do not collapse even in mixes with low viscosity and high workability, SFs have a tendency to segregate to a significant extent. Therefore, it was preferred to use CF in PCM castings. The results shows that while the PCM had consistency-enhancing effect in moderate and high conductivity composites,

the CFs had the reverse effect (Table 4.1). The mini-spread diameters of the PCM(4)CF(0), PCM(4)CF(0.1), PCM(4)CF(0.3) mixtures containing 4% PCM were 300, 295 and 275 mm, respectively. Nonetheless, the results of the mixtures at the moderate conductivity level being close to those of the mixtures at the low conductivity level without CF, demonstrate that the consistency was only slightly impacted by the 0.1% CF ratio. This can be seen from the mini-spread diameters of the PCM(0)CF(0) and PCM(0)CF(0.1) composites (285 mm), the PCM(2)CF(0) and PCM(2)CF(0.1) composites (295 mm) and the PCM(8)CF(0) and PCM(8)CF(0.1) composites (310 mm). However, it was observed that the T_{500} time was prolonged and the mini flow diameter was significantly reduced in the mixtures with high thermal conductivity containing 0.3% CF by volume. For example, the spreading diameter for the PCM(0)CF(0.3) composite was 15 mm lower than the PCM(0)CF(0.1) and PCM(0)CF(0) composites, that for PCM(2)CF(0.3) coded composite was 25 mm lower than the PCM(2)CF(0.1) and PCM(2)CF(0) composites, that for the PCM(8)CF(0.3) composite was 25 mm lower than these of the PCM(8)CF(0.1) and PCM(8)CF(0) composites. When CF-free PCM composites are examined, due to the PCM liquid dispersion, the mini flow diameter dropped and the T_{500} time shortened as the PCM percentage increased. Depending on the PCM ratio, the mini-spread diameter ranged from 285 mm (PCM(0)CF(0)) to 310 mm (PCM(8)CF(0)) for the composites with low conductivity level. 8% PCM ratio reduced the T_{500} time by 0.7 seconds for these composites (Table 4.1).

4.2. Results of Compressive Strength Test

The compressive strength results of all cement-based composites produced within the scope of the thesis were given in Table 4.2. Also, the graphs of the compressive strength results of conductive composites and composites with PCM in Figure 4.4 and Figure 4.5, respectively.

Table 4.2. Compressive strength of cementitious composites

	Compressive Strength Results (MPa)			
Sample Code	**1st day**	**3rd day**	**7th day**	**28th day**
CF(0)-Reference	42.8	53.7	62.8	72.2
CF(0.1)	38.2	51.5	57.3	62.0
CF(0.2)	37.1	47.9	52.8	56.2
CF(0.3)	32.4	42.8	45.5	53.8
CF(0.4)	38.4	40.1	47.1	51.5
CF(0.5)	33.5	36.5	42.9	48.5
SF(1)	43.7	58.6	63.7	68.6
SF(2)	42.2	60.0	66.4	70.2
SF(3)	47.0	60.1	70.1	76.7
SF(4)	47.3	64.1	70.9	78.5
SF(5)	45.9	66.0	72.8	85.6
PCM(0)CF(0)	44.5	54.2	63.1	74.4
PCM(2)CF(0)	33.8	46.7	52.2	64.3
PCM(4)CF(0)	34.5	40.1	42.8	57.2
PCM(6)CF(0)	29.3	37.2	43.7	56.2
PCM(8)CF(0)	24.1	30.2	37.9	45.4
PCM(0)CF(0.1)	41.0	48.6	57.5	65.5
PCM(2)CF(0.1)	34.3	39.4	46.8	58.3
PCM(4)CF(0.1)	35.1	36.2	47.1	54.7
PCM(6)CF(0.1)	28.0	34.7	42.8	53.3
PCM(8)CF(0.1)	21.2	29.4	34.8	46.6
PCM(0)CF(0.3)	35.6	40.2	49.3	54.9
PCM(2)CF(0.3)	34.6	39.5	43.2	52.5
PCM(4)CF(0.3)	24.4	28.5	37.8	46.7
PCM(6)CF(0.3)	23.4	30.7	36.1	43.8
PCM(8)CF(0.3)	23.5	29.1	33.1	39.2

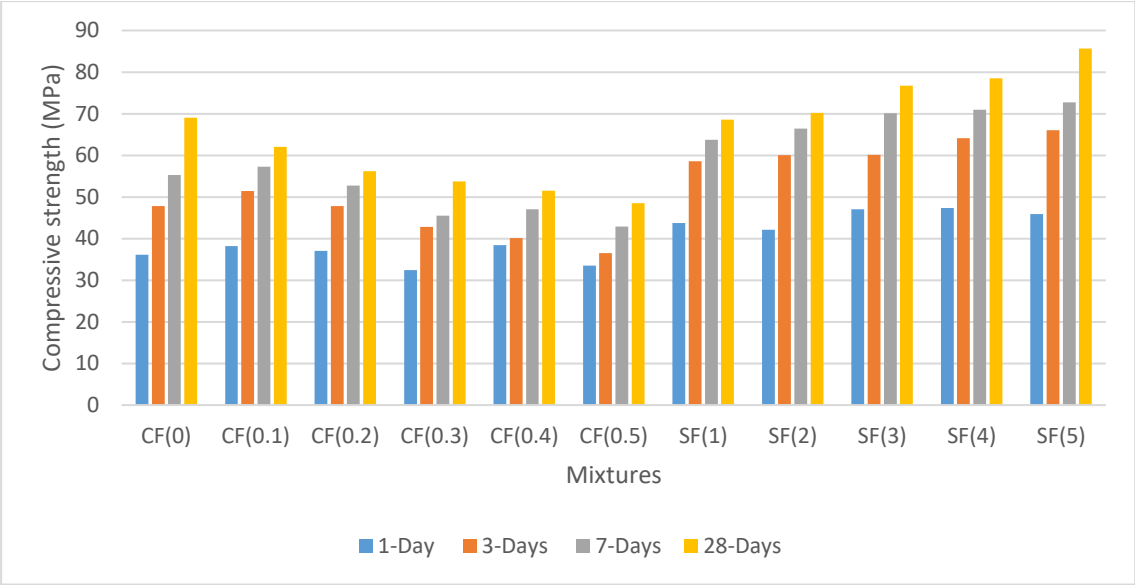

Figure 4.4. Compressive strength results of conductive composites

When the results were examined, it was determined that CFs had a negative effect on the compressive strength on all measurement day. It has been observed that as the CF ratio increases, the strength decreases, despite some outliers. The fact that the CF(0.1) coded composite providing similar results to the reference composite on the 1st, 3rd and 7th days is due to the use of low fiber content. The CF(0.2)-coded composite generated compressive strength values that were similar to those of the reference composite on 1st and 3rd, while producing a weaker strength value of about 16 MPa on 28th days. CF(0.3), CF(0.4) and CF(0.5) coded composites generally gave lower results on all measurement days compared to the reference composite. CF(0.3) coded composite, which gave a lower strength of 10.4 MPa on the 1st day compared to the reference composite, gave a lower strength of 18.4 MPa on the 28th day. Similarly, CF(0.4) coded composite, which gave lower strenght of 4.4 MPa on the 1st day compared to the reference composite, gave a lower strength value of 20.7 MPa on the 28th day. The strength performance of the CF(0.5) coded composite, which had a lower strength value of 9.3 MPa on the first day compared to the reference composite, was about 32% lower on the 28th day. This negative effect on compressive strength is due to the air voids formed by CFs (Chung, 2000; Wang et al., 2008; Chuang et al., 2017).

On the other hand, SF incorporation provided a positive (incremental) effect on the compressive strength test results. On all measurement days, a significant increase in

strength was observed from the mixtures containing SFs at the incorporation rates of 3%, 4% and 5% (SF(3), SF(4) and SF(5) mixtures). Compared to the reference composite, strength increased by 4.2 MPa on the 1st day, 6.4 MPa on the 3rd day and 7.3 MPa on the 7th day for the SF(3)-coded composite. Similarly, the composite coded SF(4) increased the strength by 4.5 MPa on the 1st day, 10.4 MPa on the 3rd day and 8.2 MPa on the 7th day. SF(3) with a strength value of 76.7 MPa (increased the strength by 6.2%) and SF(4) with a strength value of 78.5 Mpa (increased the strength by 8.7%) had higher strength results compared to reference on the 28th days. It was remarkable that the mixture coded SF(5) contributed to the strength above 10 MPa on all days except the 1st day. When the results on the 28th day were examined, the compressive strength of SF(5) (85.6 MPa) was approximately 20% higher than that of reference (72.2 MPa). However, the use of low proportions of SF did not have an incremental effect on the compressive strength and a slight reduction occurred in these composites (SF(1) and SF(2) mixtures) most probably due to the experimental variations on the 28th day. The mixture coded SF(1) decreased the strength by 4.9%, the mixture with the code SF(2) decreased by 2.7% compared to reference composite. The fact that the mixtures with the code SF(1) produces similar results to the mixture with the reference composite on all measurement days indicates that the addition of 1% SF has a negligible influence on compressive strength.

The compressive strength results of the mixtures including PCM were given in Figure 4.5. It is obvious that the presence of the PCM decreased their mechanical performance for various reasons. Firstly, the strength was negatively impacted by the increase in the water/cement ratio due to the PCM dispersion. Also, the soft microcapsule structure also had a strength-reducer effect, even if it was indicated that the microcapsules could act as nucleation zones for cement hydration products (Savija, 2018; Yeon and Kim, 2018). Moreover, the weak intermediate zone formed between the microcapsule (organic) and the matrix (inorganic), which had a detrimental effect on mechanical property, was also a factor reducing the compressive strength according to Cui et al. (2018). When the 28th day strength values at low conductivity level were examined, it was seen that the strength of the PCM(0)CF(0) composite was 74.4 MPa, while the PCM(8)CF(0) composite had a strength value of 45.4 MPa. The 8% addition of the PCM reduced the strength by around 40%. The strengths of other composites, the PCM(2)CF(0), PCM(4)CF(0), PCM(6)CF(0)

composites, having low conductivity levels were found to be 64.3, 57.2 and 56.2 MPa, respectively on the 28th day.

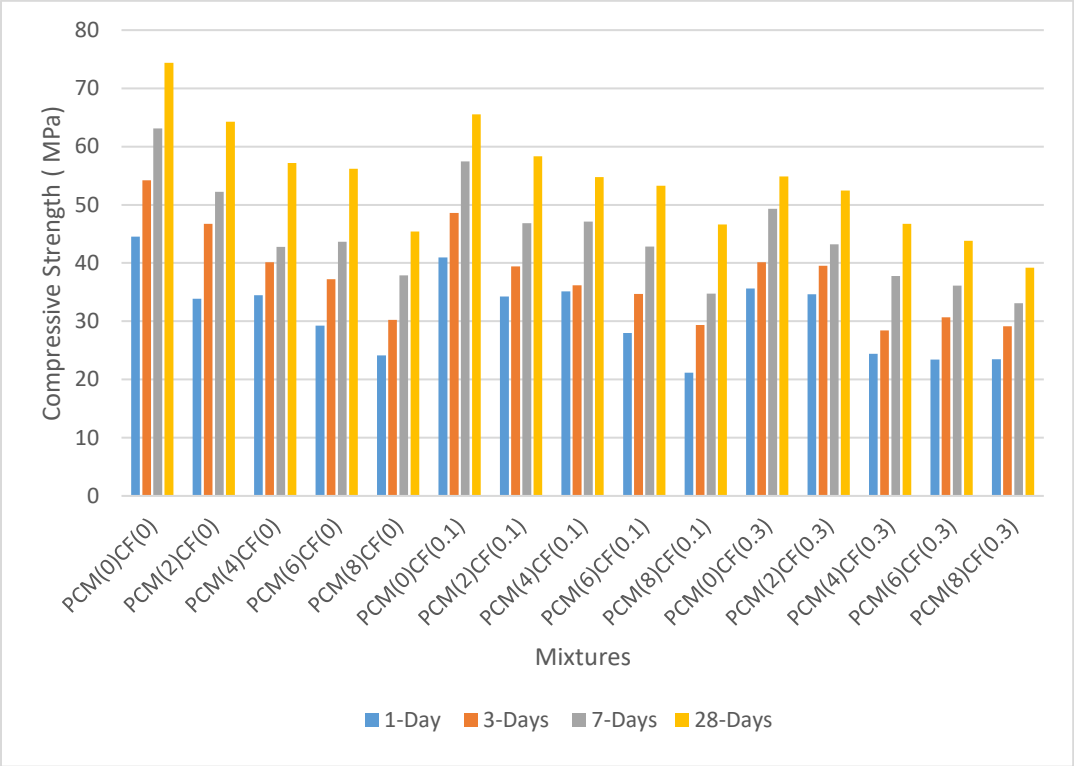

Figure 4.5. Compressive strength results of conductive composites containing PCM

The compressive strength of PCM composites containing 0.1% CF, by volume revealed a tendency toward decrease in strength when compared to PCM composites without fiber. On the 1st day, the strength values of the PCM composites with and without CF were close, but on the 3rd day, the PCM(0)CF(0.1) coded composite was from PCM(0)CF(0) coded composite, the PCM(2)CF(0.1) coded composite was from composite PCM(2)CF(0) coded composite, PCM(4)CF(0.1) coded was from PCM(4)CF(0) coded composite, PCM(6)CF(0.1) coded composite was from PCM(6)CF(0) coded composite, PCM(8)CF(0.1) coded composite was from PCM(8)CF(0) coded composite were lower 5.6 MPa, 7.3 MPa, 3.9 MPa, 2.5 MPa, 0.8 MPa, respectively. It was determined that especially addition of 0.3% CF ratio, by volume, resulted in significant strength loss. For example, the 28th day strengths of the PCM(6)CF(0), PCM(6)CF(0.1), PCM(0)CF(0.3) composites were found 56.2, 53.3 and 43.8 MPa, respectively. In other words, the 0.1% CF ratio caused about 5% strength loss, while 0.3% CF ratio decreased the strength by

22% for these composites. Similarly, the strengths of the PCM(4)CF(0), PCM(4)CF(0.1), PCM(4)CF(0.3) composites were 57.2, 54.7 and 46.7 MPa, respectively. Moreover, the PCM(8)CF(0.1) composite (46.6 MPa) provided close strength values with the PCM(8)CF(0) composite (45.4 MPa), while the strength of the PCM(8)CF(0.3) composite (39.2 MPa) was approximately 7 MPa lower. On all measurement days, the strength of the composite coded PCM(8)CF(0.3) was 20-35 MPa lower than that of the composite coded PCM(0)CF(0) due to PCM and CF.

4.3. Results of Electrical Resistivity and Thermal Conductivity Tests

The thermal conductivity and electrical resistance results of conductive cement based composites were given in Table 4.3. For a clearer understanding, the ER and thermal conductivity results are also shown in Figure 4.6 and Figure 4.7, respectively. Figure 4.6 has been arranged considering that almost all of the results are between 0-3000 Ω. Thus, low values are made more understandable in the graph.

Table 4.3 gives the average values of three samples whose electrical resistance and thermal conductivity were measured. Despite some variances, the electrical resistance results of all composites increased while the thermal conductivity values dropped as the hydration age proceeded. The inclusion of CF resulted in considerable reductions in electrical resistance. For the mixtures containing CF, due to the ongoing hydration reactions, free water in CF-incorporated cementitious composites turned into gel water and adsorption water. Thus, the fiber-to-matrix interface turned into solid-solid contact and gradually became thicker. As a result, the conductive path was blocked, the ion-related conductivity was reduced, and it was also more difficult for electrons to jump through tunneling (space) (Chuang, 2017). The results of this study were parallel to these statements however CF-incorporated cementitious composites with high fiber content were less affected by curing age. The ER value of CF(0.1), which was 305 Ω on the 1st day, reached 1670 Ω on the 28th day. However, while the ER value of CF(0.5) was 233 Ω on the 1st day, this value increased to 440 Ω on the 28th day. That is, the ER value of CF(0.1) increased by approximately 5.5 times, whereas the ER value of CF(0.5) increased by approximately 1.9 times with the curing age. This indicated that CF(0.5) containing higher amount of CF than CF(0.1) was affected less with the age of hydration. This was

because when the CF content reached the threshold value, the fiber transmission line became the main mode (not hydration products) and the effect of solid hydration products surrounding the fiber was reduced. In addition, with the increase in the CF content resulting shortening of the distance between the fibers, the current carrier electrons were also activated by the tunnel effect. The CF presence leaded to the change in the thermal conductivity, also. While the thermal conductivity value of CF(0.1) decreased by 164 mW/m.K from 7-day to 28-day, the thermal conductivity value of CF(0.5) was not influenced by the hydration age, which also supported the above-mentioned statements. Considering the ER results, it could be concluded that, in CF-incorporated mixtures, the threshold ratio for CF content was 0.3%. While mixtures with 0.3% and higher CF ratio showed a minimal increase on the 7th day compared to the 3rd day, mixtures with lower CF ratio increased 1.5 times. In addition, the ER values of the mixtures with 0.1% and 0.2% CF increased by approximately 2.5-3 times from the 7th day to the 28th day, while this increase was 1.5-2 times in the mixtures with 0.3%, 0.4%, and 0.5% CF.

Table 4.3. Electrical resistance and thermal conductivity avarage results of composites containing CF and SF

Code	**Electrical Resistance (Ω)**				**Thermal Conductivity (mW/m.K)**	
	Day 1	**Days 3**	**Days 7**	**Days 28**	**Days 7**	**Days 28**
CF(0)	1400	2500	4410	50250	1120	1090
CF(0.1)	305	360	544	1670	1150	986
CF(0.2)	233	297	461	1064	1210	1150
CF(0.3)	277	391	390	796	1150	1100
CF(0.4)	274	307	311	634	1070	981
CF(0.5)	233	271	291	440	1200	1210
SF(1)	355	656	1355	3230	928	974
SF(2)	322	587	1214	2450	907	883
SF(3)	229	502	990	2240	901	797
SF(4)	240	493	978	2010	1030	986
SF(5)	210	428	855	1670	1160	1090

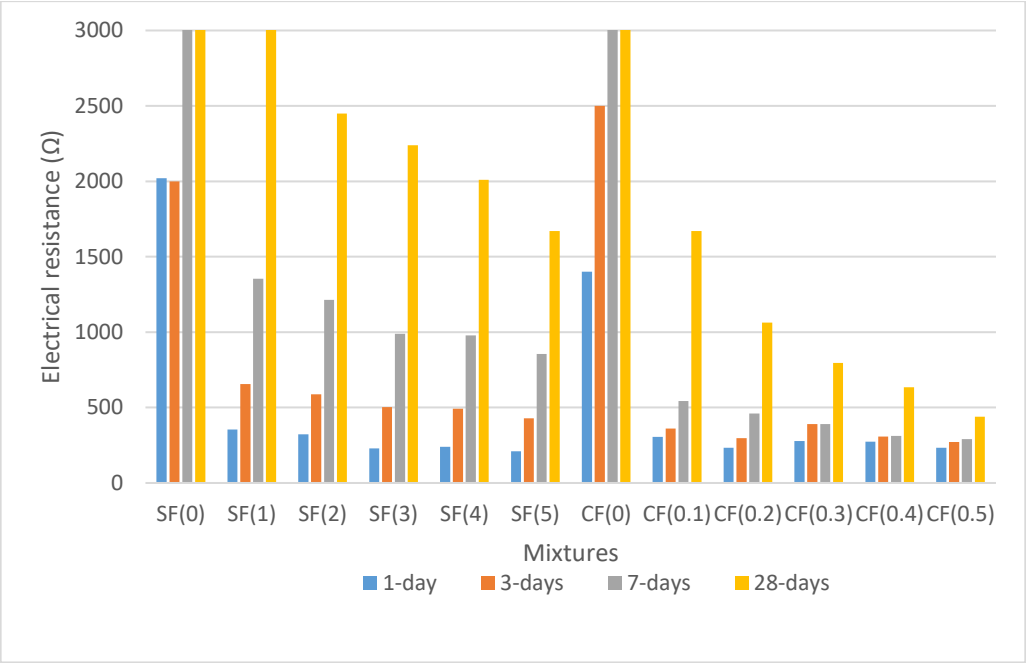

Figure 4.6. Electrical resistance values of composites containing CF and SF

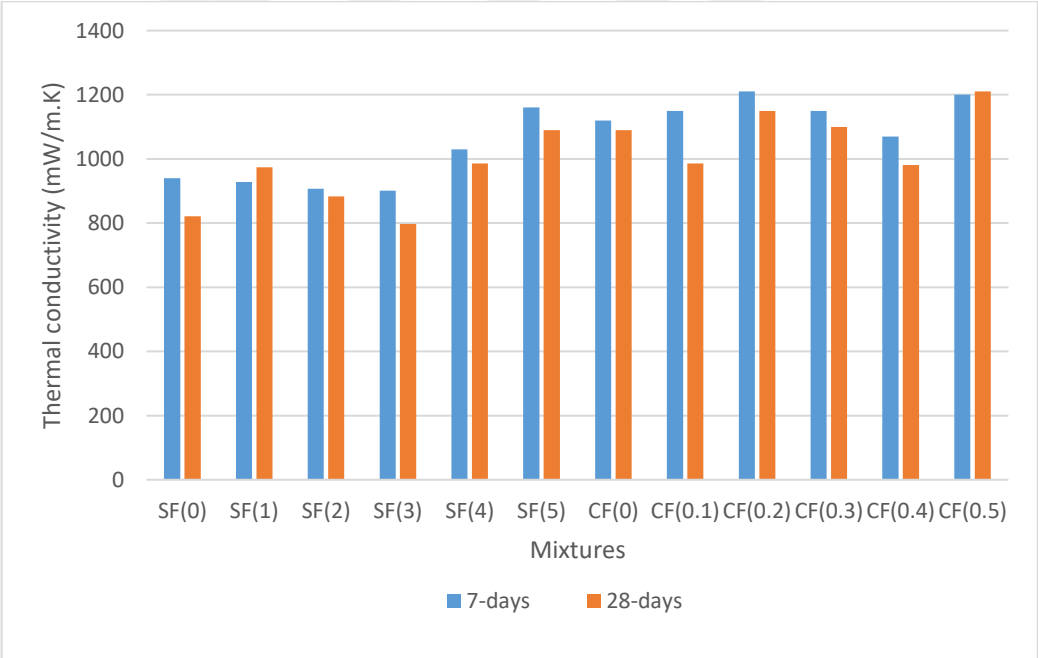

Figure 4.7. Electrical Thermal conductivity values of composites containing CF and SF

It was seen that the ER values of the mixtures containing SF reduced as the fiber content increased on all measurement days. However, as in other conductive composites, hydration products formed rised the ER values of SF-containing mixtures. On the other hand, the hydration age was more effective on the SF-incorporated mixtures compared to

the CF-incorporated ones. Although the 1-day ER values of the mixtures containing two different kinds of fiber (CF or SF) were close to each other, the ER values of the 7-day-old SF-incorporated mixtures were around 1000 Ω while they were 300-500 Ω for the CF-incorporated mixtures at the same age. This result can be attributed to several possible reasons. First, the diameter of the fibers influences their distribution throughout the mixture (Chung, 2000). The CF used in the current study had a diameter of 7.5 µm, while the SF had a diameter of 0.16 mm. This fact provides a greater number of CFs in the mixtures even if the CF is used at lower volume ratios compared to SFs used at higher volume ratios, resulting in lower resistivity. On the other hand, while CFs are classified in flexible fibers, SFs are classified in rigid ones (Martinie, Rossi and Roussel, 2010). Because of its flexible structure, small diameter, and higher availability in the mixture, the CF can be easily dispersed throughout the cementitious composites compared to SF. Consequently, the SFs are surrounded by more cement matrix than the CFs, even if they are used at high rates. Therefore, SF percolation is formed at a more limited rate compared to CF. As the hydration age progresses, the effect of thickening of the hydration products around the fibers on the decrease in conductivity was observed more prominently in SF-containing mixtures. In another study, it was also determined that the electrical resistance of mixtures containing SF raised at a higher rate as the curing age progressed compared to mixtures containing CF (Belli et al., 2020). The results of this study coincides with the findings.

When the thermal conductivity results of CF mixtures were examined, the effect of hydration age on reducing conductivity can be seen. On the 28th day compared to the 7th day, the composites coded CF(0), CF(0.1), CF(0.2), CF(0.3), CF(0.4) decreased by 30 mW/m.K, 164 mW/m.K, 60 mW/m.K, 50 mW/m.K, 89 mW/m.K, respectively and CF(0.5) coded composite increased by 10 mW/m.K. Generally, the thermal conductivity differential between the two testing days reduced as the CF ratio increased. The composites were less affected by the hydration age as the fiber ratio increased due to the high rate of percolation. On the other hand, on the 28th day compared to the 7th day, the composites coded SF(2), SF(3), SF(4), SF(5) decreased by 24 mW/m.K, 4 mW/m.K, 44 mW/m.K, 70 mW/m.K, respectively and SF(1) coded composite increased by 46 mW/m.K. The unexpected result of SF(1) is the may be related to experimental variations such as test device, casting, compacting etc.

Figure 4.8 and 4.9 show the relation between the thermal conductivity and ER results for 7-day-old and 28-day-old samples, respectively. The 7-day values of SF-incorporated mixtures provided the highest correlation (R^2=0,5413) among the mixtures, this correlation decreased to the lowest level (R^2=0,1496) on the 28th day. As the cure age progresses, the hydration products surrounding the fibers in mixtures containing SF affect the thermal conductivity and electrical conductivity differently, causing a weak correlation on the 28th day compared to the 7th day. Moreover, with the addition of conductive-based materials, both the electrical and thermal conductivity of the composites increased, but it was found that a high level of correlation between the two types of conductivity could not be established. The literature indicates that there are several reasons for these results. Firstly, it could be difficult to make accurate and precise measurements via existing thermal conductivity measurement methods for materials that did not comply with the homogeneity and isotropy in their internal structure at the macro and micro levels (Yeşilata, Turgut and Işıker, 2007). In this study, the use of the steady-state method based on uniaxial heat flow, which was among the existing thermal conductivity measurement methods, was estimated to be one of the reasons stated. Other reason can be the amount of the air voids entrapped inside the composite. The ER and thermal conductivity test samples were taken from the same mixture and the same level of compaction was applied when placing the mixtures into the molds. However, it was not possible to completely remove the air voids in the samples no matter how compaction was made. Although the ER values were affected by the pore structure, it basically depended on the contact of the fibers (percolation) and current carrier electrons (tunnel effect) (Chuang et al., 2017). However, the thermal conductivity results were heavily dependent on the pore structure, and since the measurement method was based on the uniaxial heat flow, the voids in the sample could seriously affect the results (Koru, 2016)

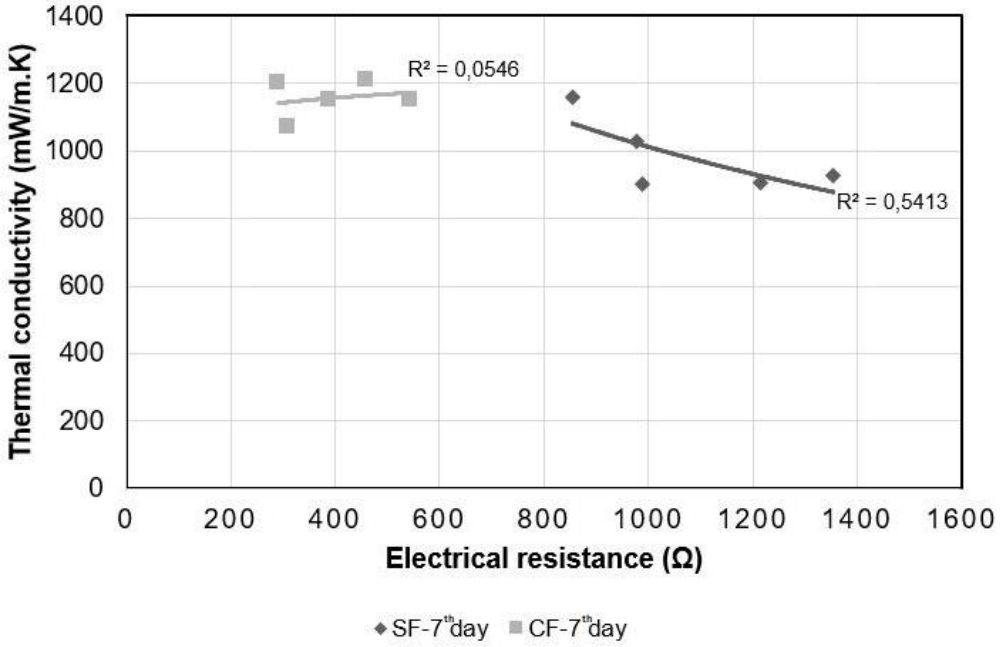

Figure 4.8. Relationship between ER and thermal conductivity for 7th day

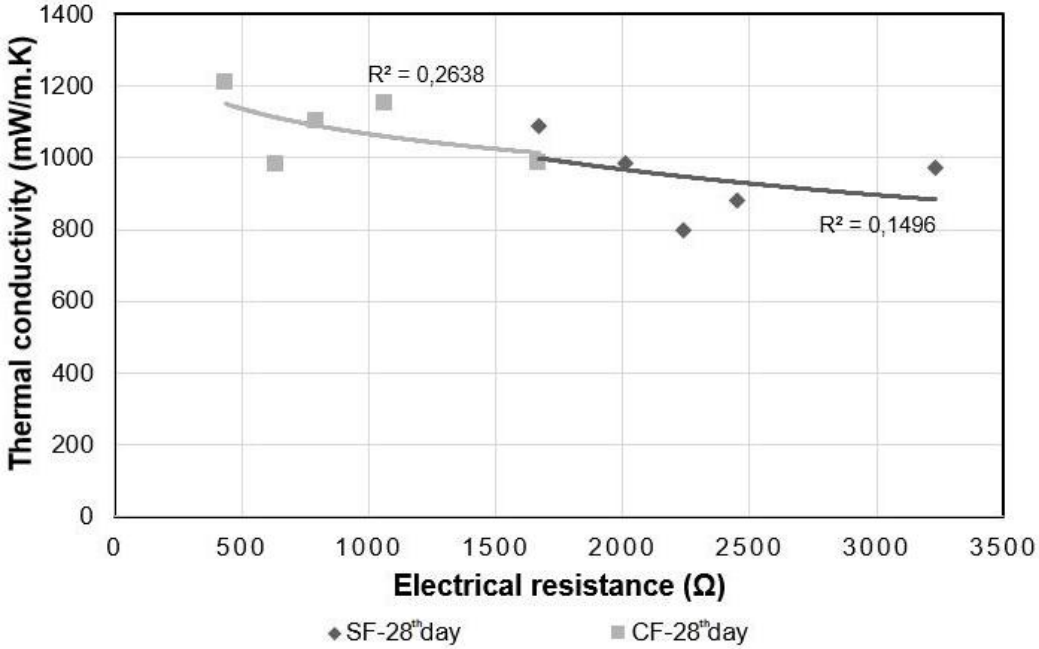

Figure 4.9. Relationship between ER and thermal conductivity for 28th day

Another reason for the elimination of SFs in mixtures containing PCM is that hydration age affects composites with CFs less. Table 4.4 shows the electrical resistance results of composites containing PCM. Figure 4.10 depicts the graph created using the data from

Table 4.4. Figure 4.10 has been arranged considering that almost all of the results are between 0-5000 Ω. Thus, low values are made more understandable in the graph. It was seen that the hydration products formed reduced the conductivity of all composites. The maximum resistance values were found in PCM composites without CF, as expected. On the other hand, as the amount of the PCM in these composites increased, the electrical resistance values increased as well. The ER of the PCM(0)CF(0) coded composite, which was 2020 Ω on the 1st day, increased to 46900 Ω on the 28th day. The PCM(2)CF(0)-coded composite with 2% PCM ratio had a value of 2892 Ω on the 1st day, while this value was 48033 Ω on the 28th day. PCM(4)CF(0)-coded composite had a value of 3842 Ω on the 1st day, while this value became 52598 Ω on the 28th day. Higher resistance values occured in PCM(6)CF(0) and PCM(8)CF(0) coded composites compared to PCM(0)CF(0), PCM(2)CF(0), PCM(4)CF(0). The explanation for this was thought to be that the microcapsule nucleation areas enhanced resistances. However, PCM had no resistance-enhancing impact in composites containing 0.1% and 0.3% CF by volume. The fiber conduction becomes the main mode in these composites and prevents this effect of PCM. The resistance values of the composites containing 0.1% CF by volume with PCM were close to each other on the same measurement days. On the other hand, composites containing 0.3% CF and PCM showed the lowest resistance values on all measurement days. Composites containing 0.1% CF with PCM increased 6 to 7 times compared to the 1st day in the 28th day measurements. However, composites containing 0.3% CF and PCM increased 1 to 3 times. This shows that the fiber transmission line is highly effective and less affected by hydration products in composites containing 0.3% CF.

Table 4.4. Electrical resistance avarage results of PCM containing composites

Code	Electrical resistance (Ω)			
	1-day	3-days	7-days	28-days
PCM(0)CF(0)	2020	2000	6100	46900
PCM(2)CF(0)	2892	4050	7657	48033
PCM(4)CF(0)	3842	4713	6302	52598
PCM(6)CF(0)	3180	4847	8173	58182
PCM(8)CF(0)	3890	5842	8145	49708
PCM(0)CF(0.1)	305	360	544	1670
PCM(2)CF(0.1)	367	421	773	1770
PCM(4)CF(0.1)	337	440	837	1765
PCM(6)CF(0.1)	388	572	1065	1983
PCM(8)CF(0.1)	346	518	992	1810
PCM(0)CF(0.3)	277	391	390	796
PCM(2)CF(0.3)	259	266	337	462
PCM(4)CF(0.3)	312	388	433	499
PCM(6)CF(0.3)	305	330	388	548
PCM(8)CF(0.3)	339	394	441	526

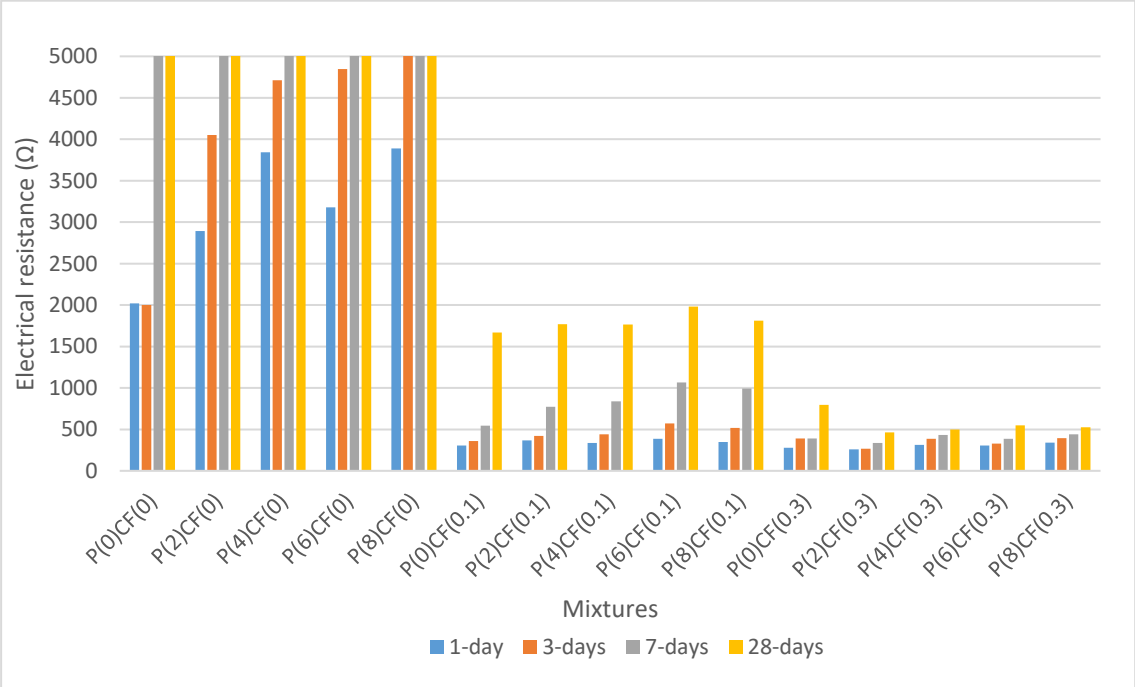

Figure 4.10. Electrical resistance values of composites containing PCM

4.4. Results of Freeze-Thaw Performance Test

4.4.1. First Procedure-Different PCM Ratios by Cement Weight

As was indicated in the Literature Review section, PCM is known to have the ability to melt snow and ice and can also lessen damage by lowering the amplitudes of freeze-thaw cycles. This type of overlay, which is thought to be used in our country, is aimed to be effective in reducing these damages in regions where freeze-thaw damages are high, together with its snow/ice melting feature.

4.4.1.1. Samples Containing 8% PCM By Weight of Cement

In order to make the freeze-thaw test system carried in the thesis studies more understandable, the graphics of the samples containing 8% PCM by cement weight are explained in detail in this section. In the first simulation, a cycle system was developed to increase the temperature of the reference sample to +20 °C and decrease it to -20 °C. Figure 4.11 illustrates the cabin temperature with the temperature which was measured by the thermocouples embedded to the reference sample. In Figure 4.12, the temperature – time curves of the reference sample and the PCM(8)CF(0) composite, and the shoulders formed in the graph due to the release and absorption of the heat energy by the PCM were shown. From the shoulders numbered with ‘1’ and ‘3’, it is understood that the PCM froze, released the heat energy and the temperature of the composite raised. For the shoulders numbered with ‘2’ and ‘4’, it is seen that the PCM melted, absorbed the heat energy and the temperature of the composite decreased. Therefore, it is concluded that PCM provided an effective thermal activation in the composite. Moreover, it was visually observed that the temperature amplitudes were close together in the regions numbered with ‘5’ and ‘7’, while the composite containing 8% PCM in the region numbered with ‘6’ reduced the amplitude thanks to the ability of the PCM to restrict the temperature variations by absorbing/releasing heat energy.

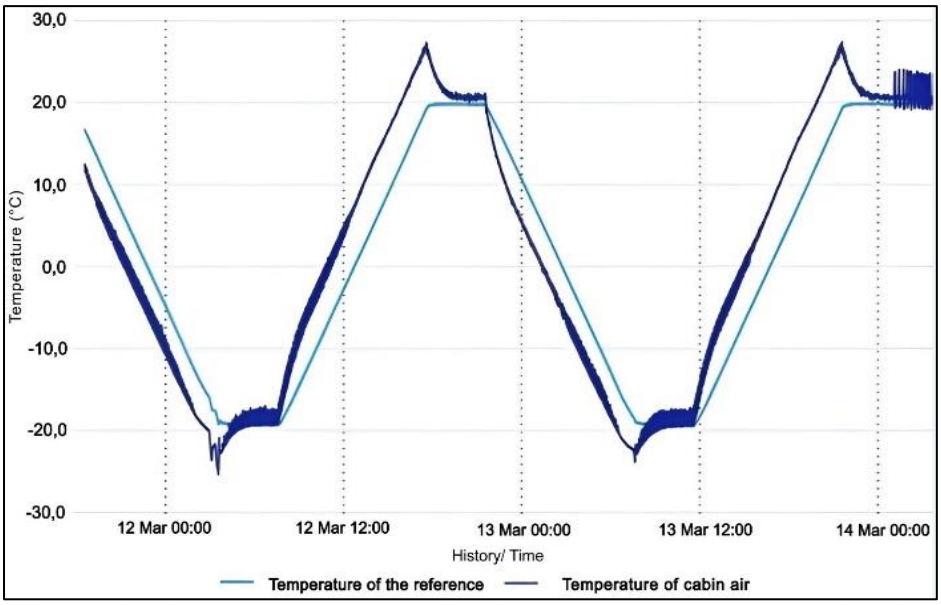

Figure 4.11. +20/-20 ^{o}C temperature cycle for the reference composite

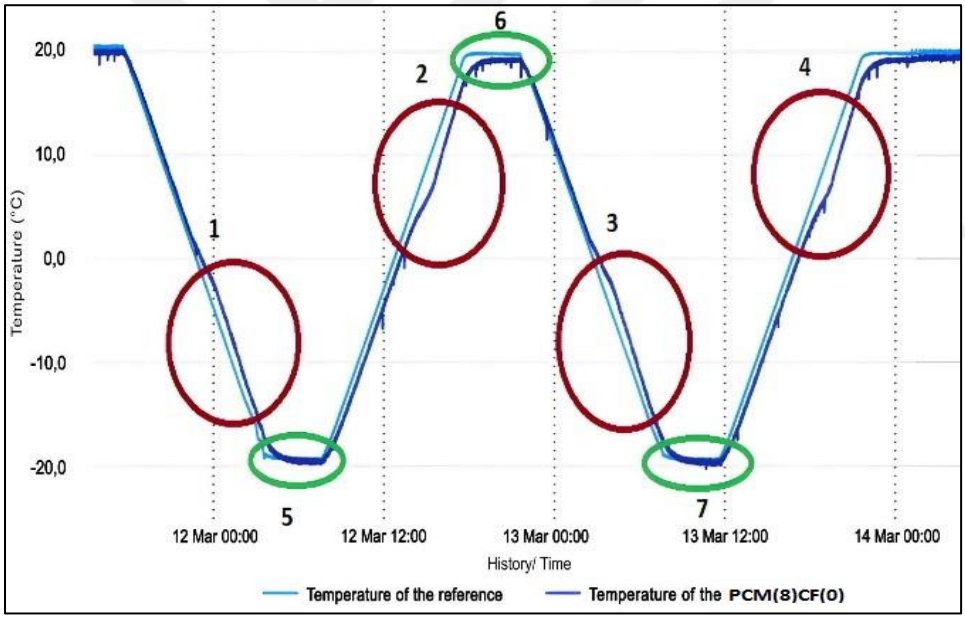

Figure 4.12. The shoulders formed in the PCM(8)CF(0) composite

In Figure 4.13, temperature graphs of PCM(0)CF(0) and PCM (8)CF(0.1) coded composites were given in the first simulation. In Figure 4.14, the regions where the PCM emits heat energy are enclosed in rings 1 and 3, while the regions that absorb heat energy of PCM are enclosed in rings 2 and 4. It was observed that the temperature graph of the PCM(8)CF(0.1) had shoulders in the regions within the rings. Similarly, the temperature amplitudes increased in the PCM(8)CF(0.1) coded composite in the 5th, 6th, and 7th rings

when compared to the PCM (0)CF(0) coded reference composite. This is because CFs have a tendency to make composite materials more thermally conductive. Comparatively to samples without CF, samples containing CF cool faster as the cabinet temperature drops and heat up faster as the cabinet temperature rises. Due to this tendency, the CF composites maintain a higher temperature than the reference composite at maximum temperature and a lower temperature at minimum temperature. In Figure 4.15, temperature graphs of the reference sample coded PCM(0)CF(0) and the sample coded PCM(8)CF(0.3) were given. It was determined visually that the temperature amplitudes increased in the sample coded PCM(8)CF(0.3). In the above paragraphs, the graphs of the PCM(8)CF(0), PCM(8)CF(0.1), and PCM(8)CF(0.3) coded samples and the PCM(8)CF(0) coded sample (reference sample) was examined separately and in detail. In Figure 4.16, these composites are collected in a single graphic. In Figure 4.17, the 4-hour sections at +20 ^{o}C and -20 ^{o}C, where temperature data are taken, are enclosed in green circles in the same graph.

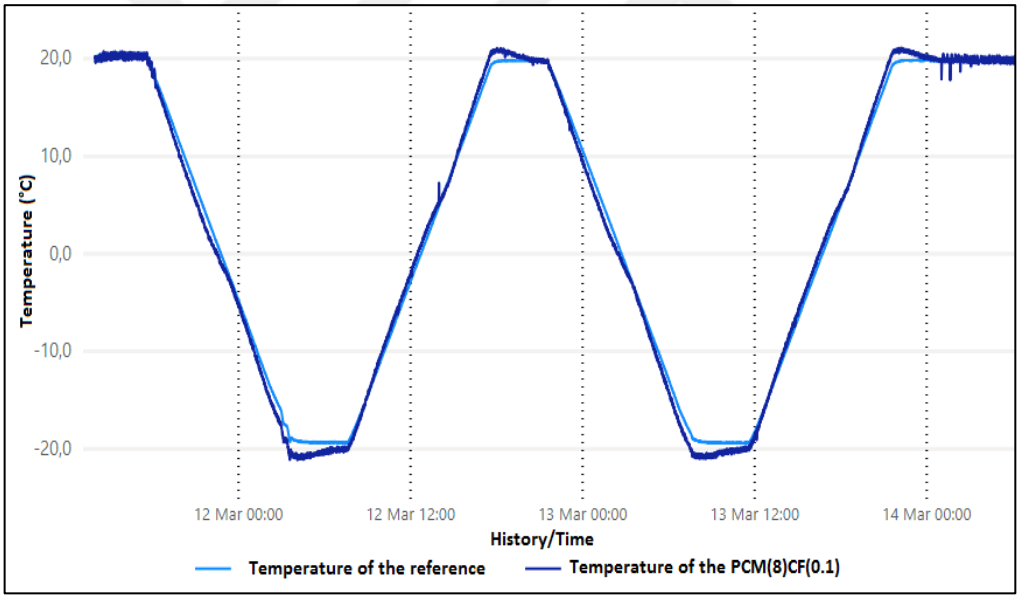

Figure 4.13. PCM(0)CF(0) and PCM(8)CF(0.1) in the first simulation

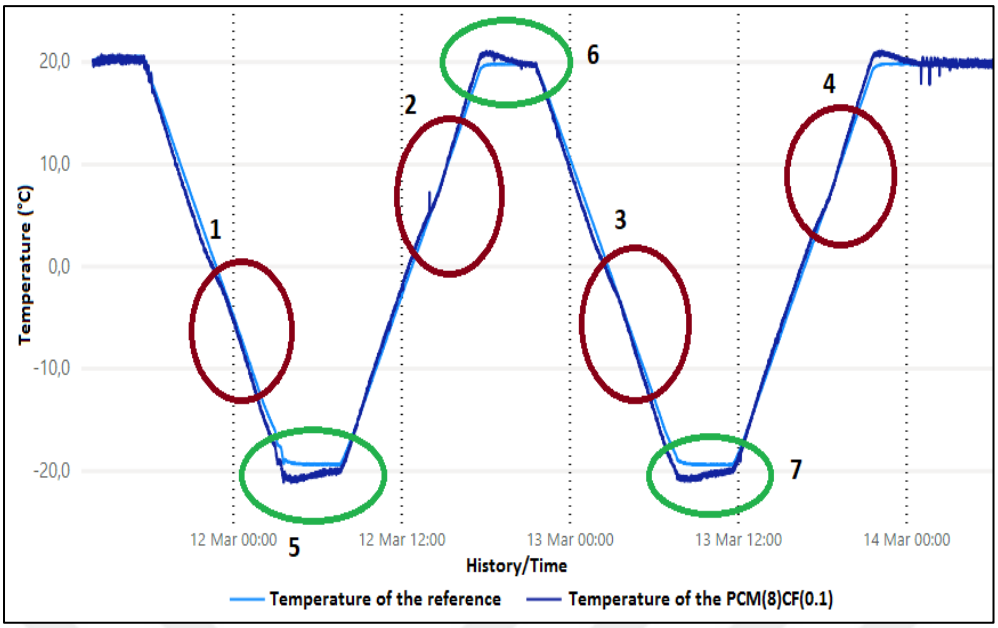

Figure 4.14. Determining the regions where the PCM emits and absorbs heat energy and the effect of the PCM on the temperature amplitudes for first simulation

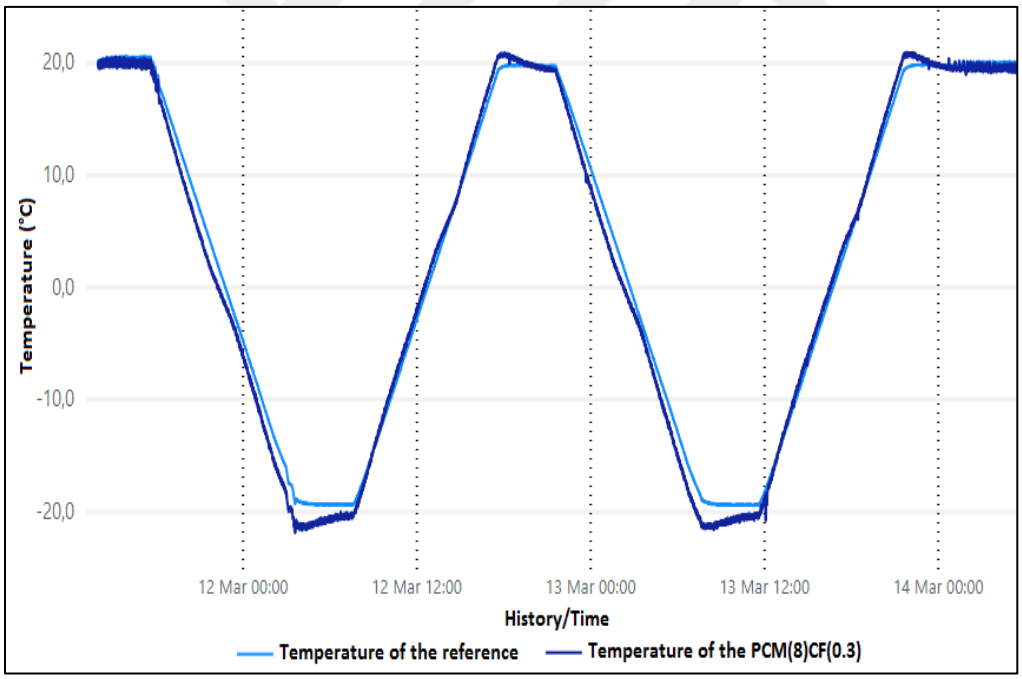

Figure 4.15. PCM(0)CF(0) and PCM(8)CF(0.3) in the first simulation

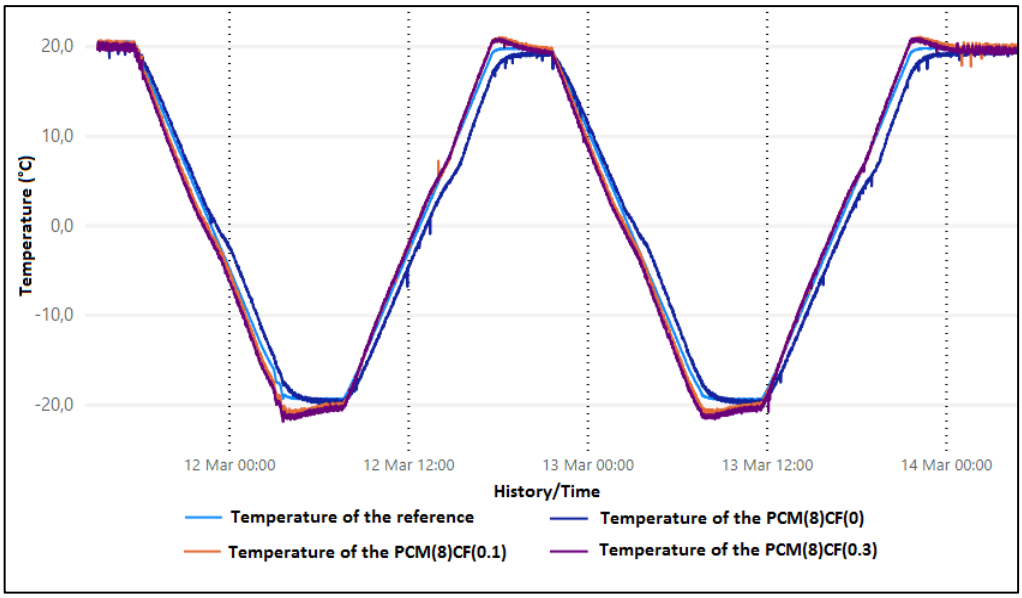

Figure 4.16. PCM(0)CF(0), PCM(8)CF(0), PCM(8)CF(0.1) and PCM(8)CF(0.1) in the first simulation

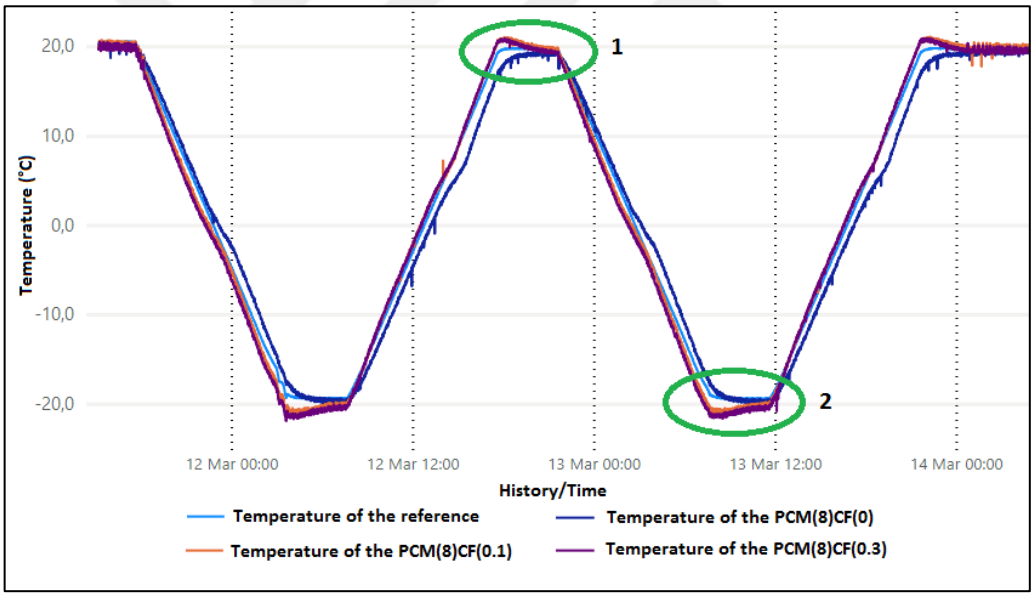

Figure 4.17. Zones 1 and 2 where temperature data are taken for the first simulation

The results of the calculations based on the parameters obtained from the simulations for the composites containing 8 % PCM were given in Tables 4.5, respectively. The maximum and minimum temperature periods included in the calculations are circled in green on graphs and the average temperatures are given in the related tables. At +20 °C, the "Temperature difference compared to reference sample" was calculated by subtracting the corresponding sample's average temperature from the reference sample's average temperature. At -20 °C, this was calculated by subtracting the reference sample's average

temperature from the corresponding sample's average temperature. The summation of "Temperature difference compared to reference sample" for +20 °C and -20 °C in the table gives "Total temperature difference compared to reference sample". Similar comparison and calculating steps were performed for the second simulation as well.

Table 4.5. Freeze-thaw performance test results of composites which containing 8% PCM by weight of cement

First simulation		**Reference**	**PCM(8)CF(0)**	**PCM(8)CF(0.1)**	**PCM(8)CF(0.3)**
+ 20 ºC	Temperature average	19.75	18.88	20.24	19.96
	Temperature difference compared to reference sample	0	-0.87	0.49	0.21
- 20 ºC	Temperature average	-19.33	-19.31	-20.46	-20.71
	Temperature difference compared to reference sample	0	-0.02	1.13	1.38
	Total temperature difference compared to reference sample	**0**	**-0.89**	**1.62**	**1.59**
Second simulation		**Reference**	**PCM(8)CF(0)**	**PCM(8)CF(0.1)**	**PCM(8)CF(0.3)**
+ 10 ºC	Temperature average	10.20	8.65	10.16	9.89
	Temperature difference compared to reference sample	0	-1.55	-0.04	-0.31
- 10 ºC	Temperature average	-9.33	-8.85	-10.19	-10.61
	Temperature difference compared to reference sample	0	-0.48	0.86	1.28
	Total temperature difference compared to reference sample	**0**	**-2.03**	**0.82**	**0.97**

The temperature amplitudes of the PCM(8)CF(0) coded sample dropped by 0.89 ° C compared to the reference sample as a result of the above analyses, and this mixture has the potential to deliver benefits in freeze-thaw locations. However, the opposite effect occurred in the sample coded PCM(8)CF(0.1), and the temperature amplitudes increased

by 1.62 °C compared to the reference sample. As a result, it has been established that this mixture will have a negative impact on freeze-thaw damage. Similarly, as compared to the reference sample, the temperature amplitudes of the sample with the code PCM(8)CF(0.3) increased by 1.59 ^{o}C. In the PCM(8)CF(0) coded sample containing only PCM and no CF, PCM limited the temperature variations/amplitudes by releasing and absorbing heat energy. However, in PCM(8)CF(0.1) coded and PCM(8)CF(0.3) coded samples containing PCM and CF, although it is thought that PCM has a decreasing effect on temperature amplitudes but it is insufficient against CFs amplitude increasing effect.

On the other hand, a temperature cycle of a second simulation was used to evaluate the behavior of the same samples. Figure 4.18 shows the temperature graphs for the samples during this cycle, and Table 4.5 contains the data derived from these graphs. The temperature amplitudes in the sample coded PCM(8)CF(0) fell by 2.03 ^{o}C when compared to the reference sample, while its increased in the samples coded PCM(8)CF(0.1) and PCM(8)CF(0.3) by 0.82°C and 0.97°C, respectively. 8 % PCM addition decreased the temperature amplitudes by 0.89 and 2.03 °C for the first and second simulations, compared to the reference, respectively. This means that 1.14 °C more amplitude restricted in the second simulation than the first simulation. Likewise, the temperature amplitudes of PCM(8)CF(0.1) and PCM(8)CF(0.3) coded samples increased 0.80 ^{o}C and 0.62 ^{o}C less in this simulation compared to the first simulation, respectively. According to the results, it was determined that the temperature amplitude was decreased at a higher rate in all composites containing PCM in the second simulation than in the first simulation. This is because the heat energy released by the composites containing PCM in the + 10/-10 °C temperature cycle was not depleted to -10 °C, and heat energy absorbed at +10°C was not yet complete. The freezing zone (heat energy release zone) of the PCM was found to be in the range of +2°C and -14°C, and the melting zone (heat energy absorption zone) was between +1.3°C and +11°C in the DSC analysis shown in Table 3.7. However, in the first simulation, when +20 °C or -20 °C was achieved, the effect of the heat energy released/absorbed on the temperature amplitudes was less since the efficiency process was already completed.

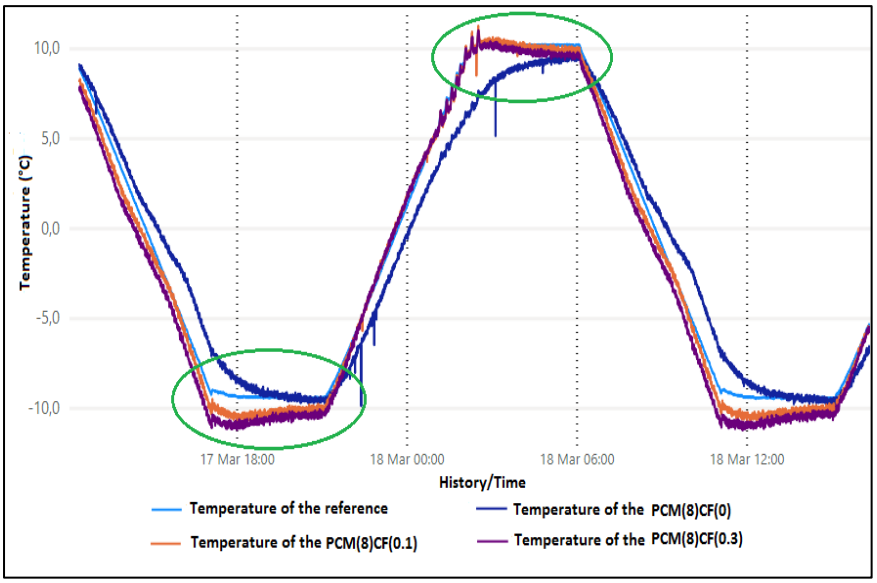

Figure 4.18. Second simulation for composites which containing 8% PCM by weight of cement.

4.4.1.2. Samples Containing 6% PCM By Weight of Cement

PCM(0)CF(0), PCM(6)CF(0), PCM(6)CF(0.1) and PCM(6)CF(0.3) coded composites under first and second simulations were given in Figure 4.19 and Figure 4.20, respectively. With the data obtained from these graphs, the temperature differences between the PCM(6)CF(0), PCM(6)CF(0.1) and PCM(6)CF(0.3) coded composites compared to the reference composite were shown in Table 4.6. When the table was examined, the amplitude in the PCM(6)CF(0) coded composite decreased by 0.71 ^{o}C in the first simulation and by 1.07 ^{o}C in the second simulation. The temperature restriction measured for the PCM(6)CF(0), containing 2 % less PCM than the PCM(8)CF(0) composite, was 0.18 °C lower than that for the PCM(8)CF(0) composite, for the first simulation. However, amplitude constraint difference between PCM(8)CF(0) and PCM(6)CF(0), became 0.96 °C for the second simulation. On the other hand, the amplitude increase in the PCM(6)CF(0.1) composite in the first simulation was 0.13 °C, the PCM (6)CF(0.3) composite was 0.36 °C, and in the second simulation, the PCM(6)CF(0.1) composite was 1.13 °C and the PCM (6)CF(0.3) composite was 0.88 °C.

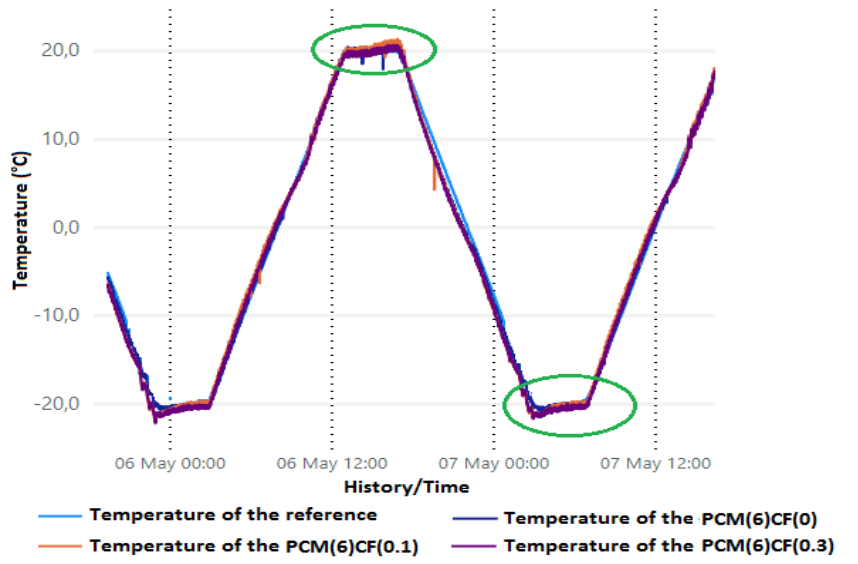

Figure 4.19. First simulation for composites which containing 6% PCM by weight of cement

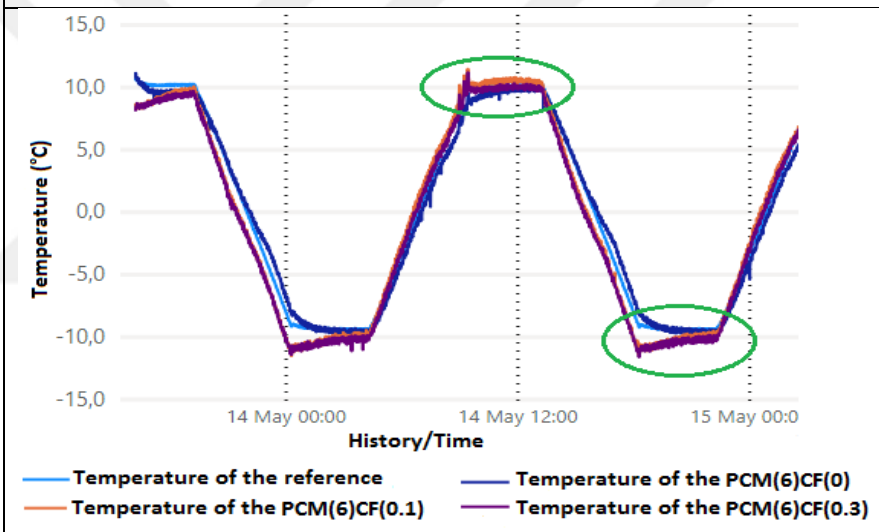

Figure 4.20. Second simulation for composites which containing 6% PCM by weight of cement

Table 4.6. Freeze-thaw performance test results of composites which containing 6% PCM by weight of cement

First simulation		**Reference**	**PCM(6)CF(0)**	**PCM(6)CF(0.1)**	**PCM(6)CF(0.3)**
+ 20 ºC	Temperature average	20.18	20.01	19.89	20.36
	Temperature difference compared to reference sample	0	-0.17	-0.29	0.18
- 20 ºC	Temperature average	-20.20	-19.66	-20.62	-20.38
	Temperature difference compared to reference sample	0	-0.54	0.42	0.18
	Total temperature difference compared to reference sample	**0**	**-0.71**	**0.13**	**0.36**
Second simulation		**Reference**	**PCM(6)CF(0)**	**PCM(6)CF(0.1)**	**PCM(6)CF(0.3)**
+ 10 ºC	Temperature average	10.07	9.21	10.23	9.81
	Temperature difference compared to reference sample	0	-0.86	0.16	-0.26
- 10 ºC	Temperature average	-9.31	-9.09	-10.28	-10.45
	Temperature difference compared to reference sample	0	-0.21	0.97	1.14
	Total temperature difference compared to reference sample	**0**	**-1.07**	**1.13**	**0.88**

4.4.1.3. Samples Containing 4% PCM By Weight of Cement

PCM(0)CF(0), PCM(4)CF(0), PCM(4)CF(0.1) and PCM(4)CF(0.3) coded composites under first and second simulations were given in Figure 4.21 and Figure 4.22, respectively. With the data obtained from these graphs, the temperature differences between the PCM(4)CF(0), PCM(4)CF(0.1) and PCM(4)CF(0.3) coded composites compared to the reference composite were shown in Table 4.7. When the table was examined, the amplitude in the PCM(4)CF(0) coded composite decreased by 0.32 ºC in the first simulation and by 1.02 ºC in the second simulation. The temperature restriction

measured for the PCM(4)CF(0) was 0.57 °C lower than that for the PCM(8)CF(0) composite, for the first simulation. However, amplitude constraint difference between PCM(8)CF(0) and PCM(4)CF(0), became 1.01 °C for the second simulation. On the other hand, the amplitude increase in the PCM(4)CF(0.1) composite in the first simulation was 0.77 °C, the PCM (4)CF(0.3) composite was 0.83 °C, and in the second simulation, the PCM(4)CF(0.1) composite was 0.25 °C and the PCM (4)CF(0.3) composite was 0.48 °C.

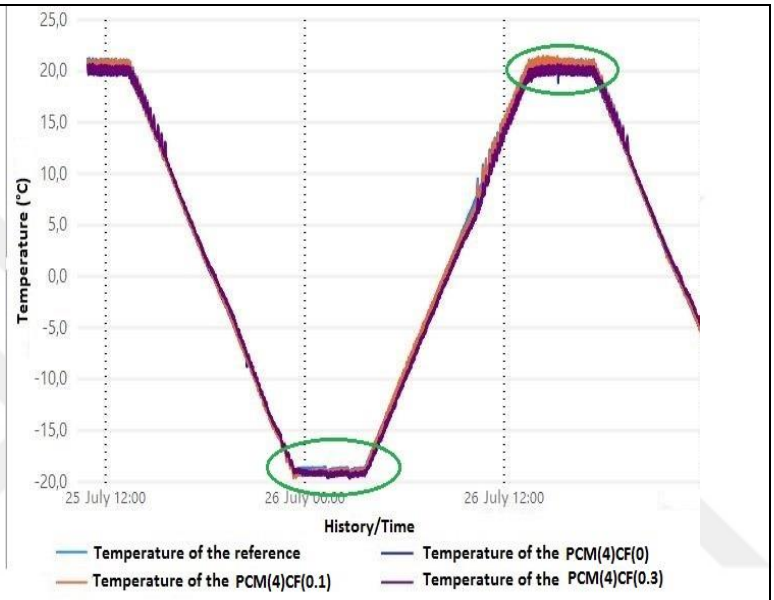

Figure 4.21. First simulation for composites which containing 4% PCM by weight of cement

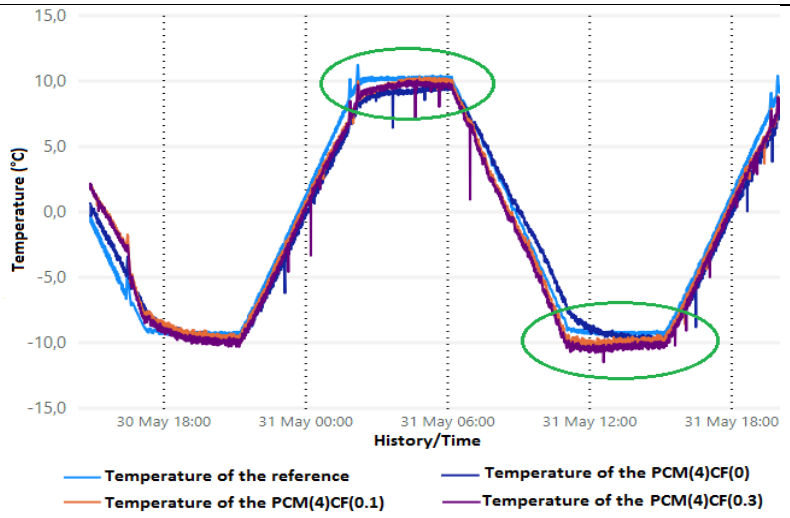

Figure 4.22. Second simulation for composites which containing 4% PCM by weight of cement.

Table 4.7. Freeze-thaw performance test results of composites which containing 4% PCM by weight of cement

First simulation		**Reference**	**PCM(4)CF(0)**	**PCM(4)CF(0.1)**	**PCM(4)CF(0.3)**
+ 20 ºC	Temperature average	20.61	20.06	20.65	21.02
	Temperature difference compared to reference sample	0	-0.55	0.04	0.41
- 20 ºC	Temperature average	-18.68	-18.91	-19.41	-19.10
	Temperature difference compared to reference sample	0	0.23	0.73	0.42
	Total temperature difference compared to reference sample	**0**	**-0.32**	**0.77**	**0.83**
Second simulation		**Reference**	**PCM(4)CF(0)**	**PCM(4)CF(0.1)**	**PCM(4)CF(0.3)**
+ 10 ºC	Temperature average	10.21	9.15	9.77	9.58
	Temperature difference compared to reference sample	0	-1.06	-0.44	-0.63
- 10 ºC	Temperature average	-9.21	-9.25	-9.90	-10.32
	Temperature difference compared to reference sample	0	0.04	0.69	1.11
	Total temperature difference compared to reference sample	**0**	**-1.02**	**0.25**	**0.48**

4.4.1.4. Samples Containing 2% PCM By Weight of Cement

PCM(0)CF(0), PCM(2)CF(0), PCM(2)CF(0.1) and PCM(2)CF(0.3) coded composites under first and second simulations were given in Figure 4.23 and Figure 4.24, respectively. With the data obtained from these graphs, the temperature differences between the PCM(2)CF(0), PCM(2)CF(0.1) and PCM(2)CF(0.3) coded composites compared to the reference composite were shown in Table 4.8. PCM(2)CF(0) composite had a minimal effect on the amplitude restriction (0.05 °C) in the first simulation, whereas

it was more effective in the second simulation by providing 0.42 °C temperature restriction. In the first simulation, the amplitude increased by 1.20 °C in the PCM(2)CF(0.1) composite and by 1.50 °C in the PCM (2)CF(0.3) composite compared to the reference sample. In the second simulation, the amplitude increased by 0.78 °C in the PCM(2)CF(0.1) composite and by 1.03 °C in the PCM(2)CF(0.3) composite. CFs raised their temperature amplitudes greater in composites with 2% PCM ratio compared to other composites with 8, 6 and 4% PCM ratios. This demonstrated that the effect of the 2% PCM ratio on lowering temperature amplitudes is minimal.

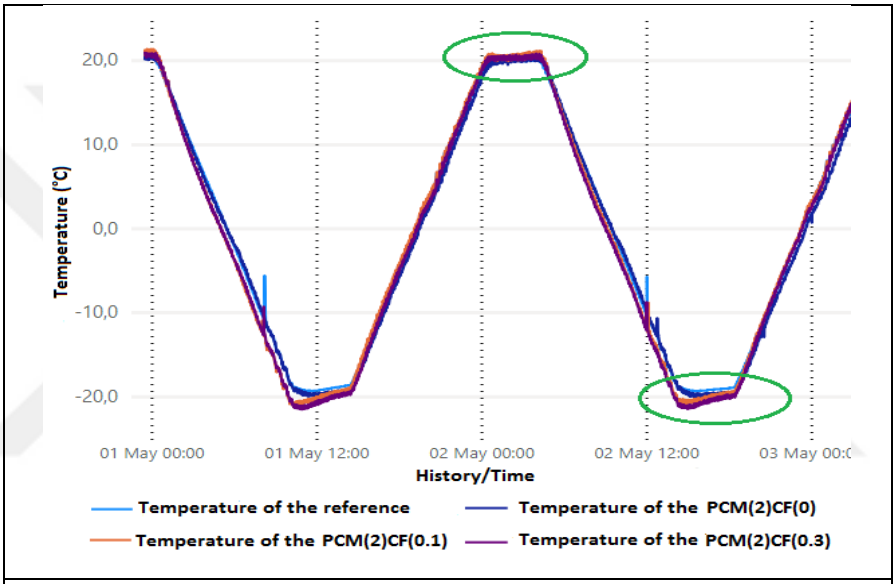

Figure 4.23. First simulation for composites which containing 2% PCM by weight of cement

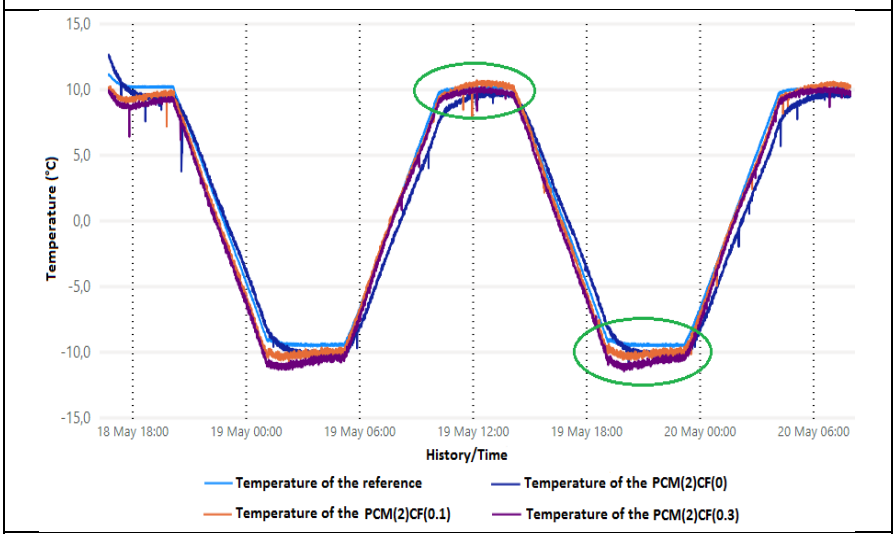

Figure 4.24. Second simulation for composites which containing 2% PCM by weight of cement.

Table 4.8. Freeze-thaw performance test results of composites which containing 2% PCM by weight of cement

First simulation		Reference	PCM(2)CF(0)	PCM(2)CF(0.1)	PCM(2)CF(0.3)
+ 20 ºC	Temperature average	20.18	19.74	20.37	20.20
	Temperature difference compared to reference sample	0	-0.44	0.19	0.02
- 20 ºC	Temperature average	-19.29	-19.68	-20.30	-20.77
	Temperature difference compared to reference sample	0	0.39	1.01	1.48
	Total temperature difference compared to reference sample	**0**	**-0.05**	**1.20**	**1.50**
Second simulation		**Reference**	**PCM(2)CF(0)**	**PCM(2)CF(0.1)**	**PCM(2)CF(0.3)**
+ 10 ºC	Temperature average	10.09	9.27	10.18	9.75
	Temperature difference compared to reference sample	0	-0.82	0.09	-0.34
- 10 ºC	Temperature average	-9.39	-9.79	-10.08	-10.76
	Temperature difference compared to reference sample	0	0.40	0.69	1.37
	Total temperature difference compared to reference sample	**0**	**-0.42**	**0.78**	**1.03**

4.4.1.5. PCM-Free Samples

PCM(0)CF(0), PCM(0)CF(0.1) and PCM(0)CF(0.3) coded composites under first and second simulations were given in Figure 4.25 and Figure 4.26, respectively. With the data obtained from these graphs, the temperature differences between the PCM(0)CF(0.1) and PCM(0)CF(0.3) coded composites compared to the reference composite were shown in Table 4.9. When results of PCM-free composites examined, in the PCM(0)CF(0.1) composite, the temperature amplitude increased by 0.80 °C compared to the reference sample in the first simulation, and by 1.30 °C in the second simulation. This increase was

1.71 °C in the first simulation and 1.33 °C in the second simulation for the PCM(0)CF(0.3) composite. It was clearly seen that CFs had an effect on increasing the temperature amplitudes. The reason for this is that the composites showed rapid heating and cooling behavior (Sakulich and Bentz 2012) as a result of the increased conductivity due to the presence of the CFs. Since the specified composites do not contain PCM, there were no heat released/absorbed regions and shoulders formed by these regions in the graphics. Furthermore, there was no factor restricting the temperature amplitudes in these samples, such as PCM, and the increase in temperature amplitudes was high in composites containing CF.

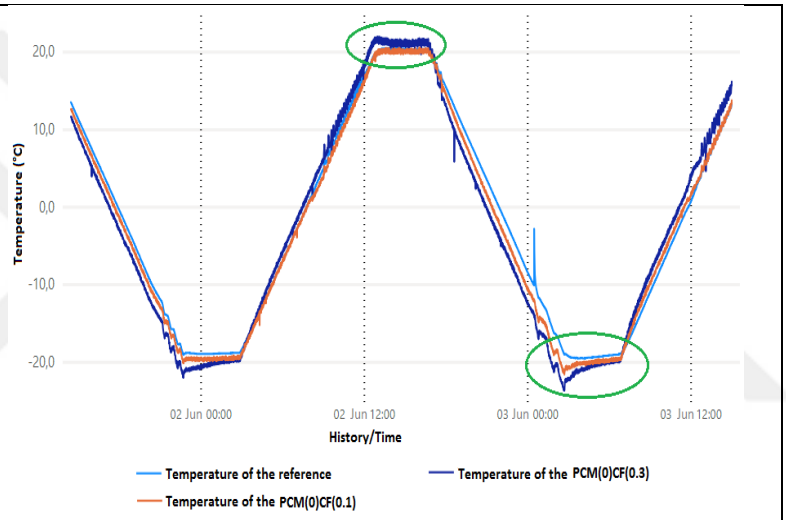

Figure 4.25. First simulation for composites which containing 0% PCM by weight of cement

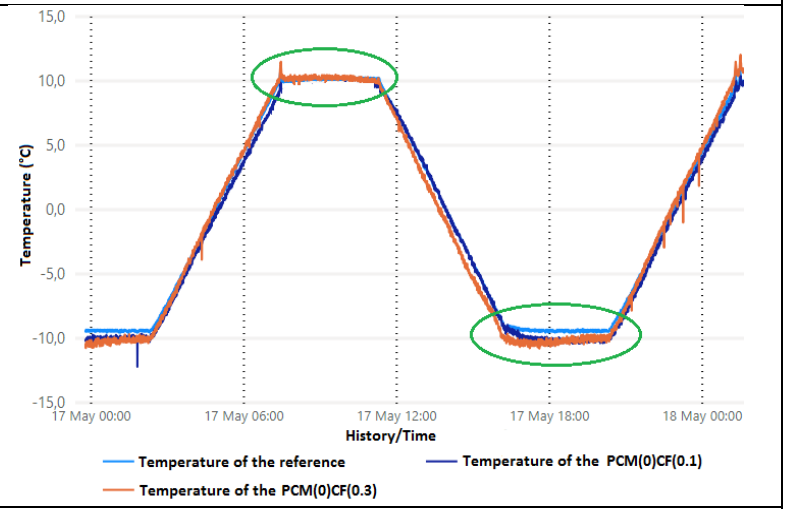

Figure 4.26. Second simulation for composites which containing 0% PCM by weight of cement

Table 4.9. Freeze-thaw performance test results of composites which containing 0% PCM by weight of cement

First simulation		**Reference**	**PCM(0)CF(0.1)**	**PCM(0)CF(0.3)**
+ 20 ºC	Temperature average	20.26	20.37	20.74
	Temperature difference compared to reference sample	0	0.11	0.48
- 20 ºC	Temperature average	-18.87	-19.56	-20.10
	Temperature difference compared to reference sample	0	0.69	1.23
	Total temperature difference compared to reference sample	**0**	**0.80**	**1.71**
Second simulation		**Reference**	**PCM(0)CF(0.1)**	**PCM(0)CF(0.3)**
+ 10 ºC	Temperature average	9.53	10.13	10.19
	Temperature difference compared to reference sample	0	0.60	0.66
- 10 ºC	Temperature average	-9.41	-10.11	-10.08
	Temperature difference compared to reference sample	0	0.70	0.67
	Total temperature difference compared to reference sample	**0**	**1.30**	**1.33**

In order to make the data in the tables more understandable, the temperature differences compared to the reference sample were given in Figure 4.27. As the PCM ratio rises, it was clear from the figure that the temperature amplitudes of the samples with PCM but no CF decrease. Under the second simulation, PCMs were even more successful at lowering temperature amplitudes. The temperature amplitude of the PCM(8)CF(0) coded sample decreased by 2.03 ºC at an 8% PCM ratio in the second simulation. However, even if the CF samples included PCM, these PCMs were unable to prevent the amplitude increase. It is worth noting that samples containing 0.3% CF by volume raise temperature amplitudes more than samples containing 0.1% CF in the majority of the composites evaluated. The reason for this is that as the CF ratio increases, the conductivity increases and these samples absorb the cabin heat/cool energy faster. Except PCM(0)CF(0.1), PCM(6)CF(0.1) and PCM(6)CF(0.3) coded samples, amplitude according first simulation under second simulation increase was less. There may be various reasons why this situation did not occur as expected in all three samples. The reasons for this deviation are considered to be the experimental variations such as sudden and irregular temperature

changes in the cabinet, different temperatures of the environment in which the cabinet was located on different days and inhomogeneous PCM distribution in the matrix. On the other hand, as expected, the highest temperature amplitude increases in both cycle types occurred in the PCM(0)CF(0.3) coded sample, which did not contain PCM and had a CF content of 0.3% by volume. In this sample, the temperature difference was 1.71 ºC in the first simulation and 1.33 ºC in the second simulation.

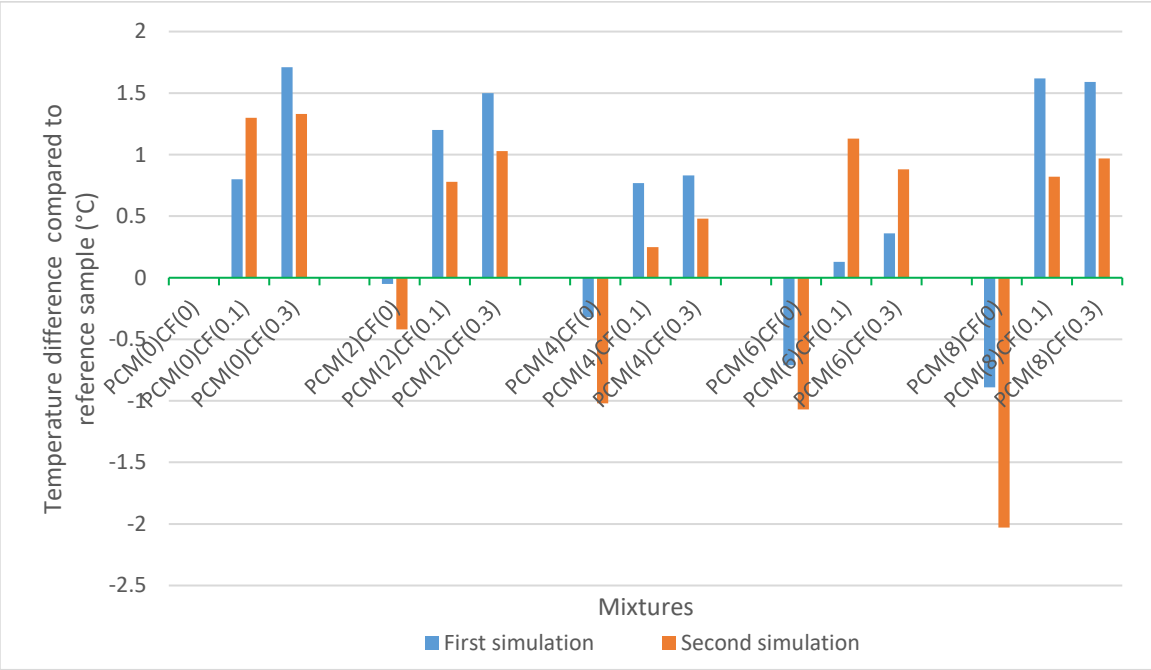

Figure 4.27. Temperature differences compared to the reference sample

4.4.2. Second Procedure-Composites of Different Thicknesses Containing 6% PCM of the Cement Weight

While the effect of composites with different PCM ratios on freeze-thaw amplitudes was examined in the previous section, different thicknesses of composites with fixed PCM ratios were tested in this section. The purpose of this test is to give an idea of the pavement thickness to be used in the application. In this direction, composites with sample dimensions of 150×150×20 mm, 150×150×30 mm, 150×150×40 mm, 150×150×50 mm were produced. These composites were drilled from the middle to the center in order to place the sensors and placed in ready-made molds. Since it was not physically possible to drill a 10 mm thick sample and place a sensor, this thickness has been eliminated. On the other hand, tests were performed at a constant 6% PCM rate by cement weight.

4.4.2.1. Samples with 50 mm Thickness

In this section, 150×150×50 mm samples of PCM(0)CF(0) coded reference composite and PCM(6)CF(0) and PCM(6)CF(0.1) coded composites were subjected to freeze-thaw tests. The graph formed by these composites in the first simulation was given in Figure 4.28, and the graph formed in the second simulation was given in Figure 4.29. The temperature differences compared to the reference sample were presented in Table 4.10 based on the data obtained from the graphs. In the PCM(6)CF(0) coded composite, the temperature amplitudes decreased by 0.25 ^{o}C in the first simulation and 0.31 ^{o}C in the second simulation. In the PCM(6)CF(0.1) coded composite, the temperature amplitudes increased by 0.50 ^{o}C in the first simulation and decreased by 0.15 ^{o}C in the second simulation. 50 mm thick PCM provided small and close temperature differences in both simulation types of the PCM(6)CF(0) coded composite. However, PCM provided a high performance by creating 0.15 ^{o}C amplitude decrease in the PCM(6)CF(0.1) coded composite, especially in the second simulation, despite the CF.

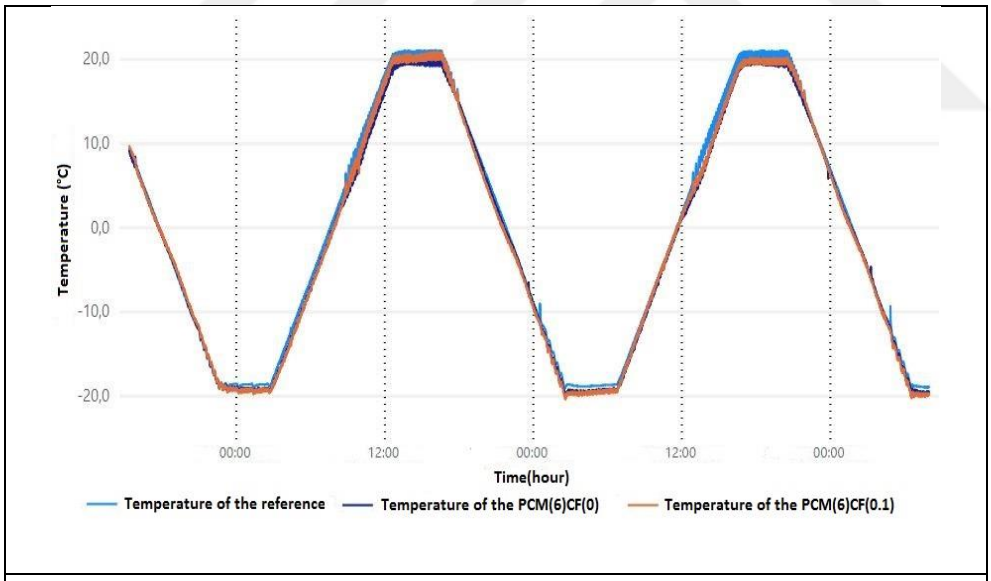

Figure 4.28. Sample thickness of 50 mm in first simulation

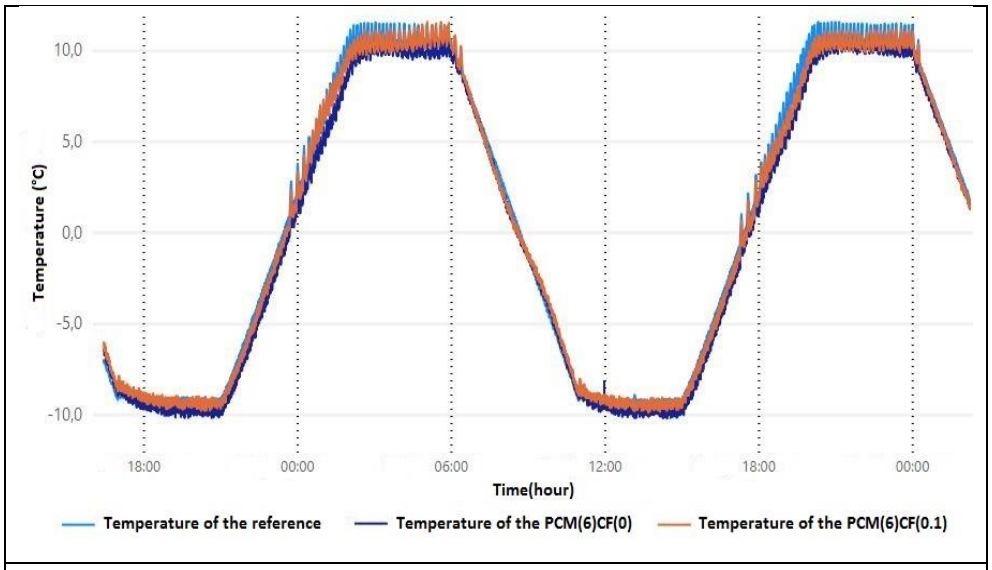

Figure 4.29. Sample thickness of 50 mm in second simulation

Table 4.10. The difference in temperature amplitudes at 50 mm sample thickness

First simulation		**Reference**	**PCM(6)CF(0)**	**PCM(6)CF(0.1)**
+ 20 ºC	Temperature average	20.55	19.58	20.20
	Temperature difference compared to reference sample	0	-0.97	-0.35
- 20 ºC	Temperature average	-18.76	-19.48	-19.61
	Temperature difference compared to reference sample	0	0.72	0.85
	Total temperature difference compared to reference sample	**0**	**-0.25**	**0.50**
Second simulation		**Reference**	**PCM(6)CF(0)**	**PCM(6)CF(0.1)**
+ 10 ºC	Temperature average	10.72	9.97	10.51
	Temperature difference compared to reference sample	0	-0.75	-0.21
- 10 ºC	Temperature average	-9.18	-9.62	-9.24
	Temperature difference compared to reference sample	0	-0.44	0.06
	Total temperature difference compared to reference sample	**0**	**-0.31**	**-0.15**

4.4.2.2. Samples with 40 mm Thickness

In this section, 150×150×40 mm samples of PCM(0)CF(0) coded reference composite and PCM(6)CF(0) and PCM(6)CF(0.1) coded composites were subjected to freeze-thaw tests. The graph formed by these composites in the first simulation was given in Figure

4.30, and the graph formed in the second simulation was given in Figure 4.31. The temperature differences compared to the reference sample were presented in Table 4.11 based on the data obtained from the graphs. In the PCM(6)CF(0) coded composite, the temperature amplitudes decreased by 0.71 ^{o}C in the first simulation and 1.07 ^{o}C in the second simulation. In the PCM(6)CF(0.1) coded composite, the temperature amplitudes increased by 0.13 ^{o}C in the first simulation and 1.13 ^{o}C in the second simulation with the effect of CF.

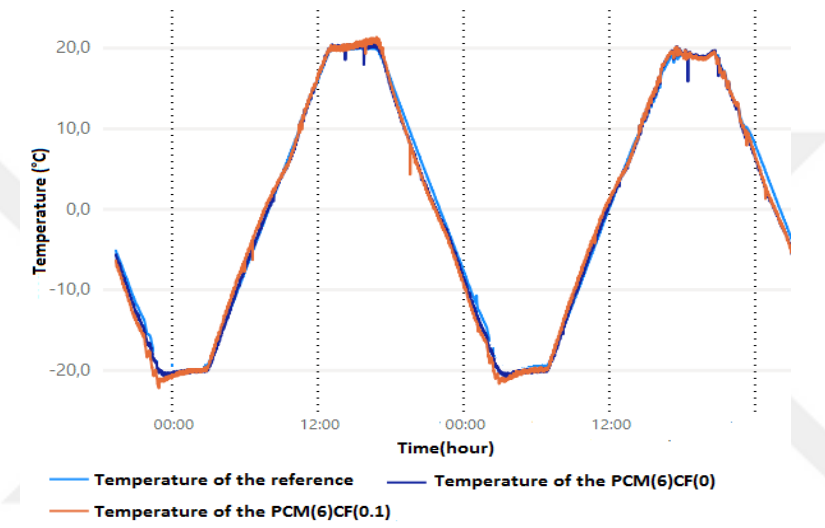

Figure 4.30. Sample thickness of 40 mm in first simulation

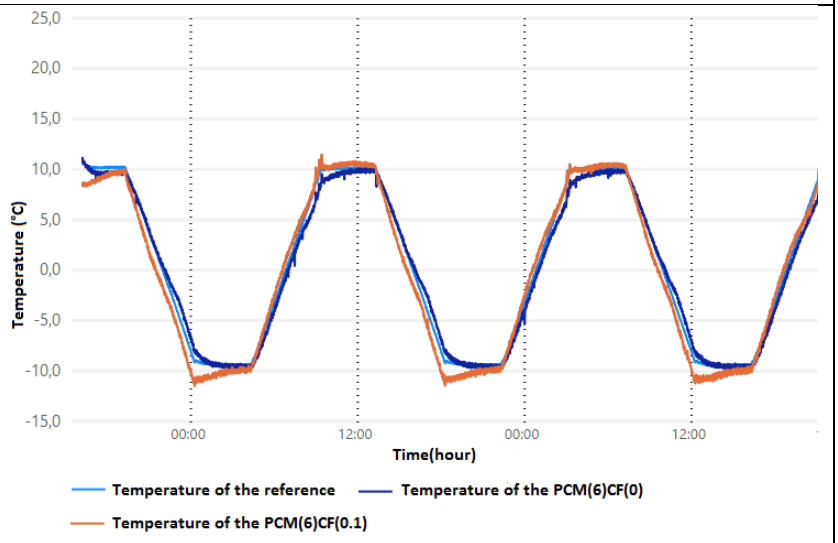

Figure 4.31. Sample thickness of 40 mm in second simulation

Table 4.11. The difference in temperature amplitudes at 40 mm sample thickness

First simulation		**Reference**	**PCM(6)CF(0)**	**PCM(6)CF(0.1)**
+ 20 ºC	Temperature average	20.18	20.01	19.89
	Temperature difference compared to reference sample	0	-0.17	-0.29
- 20 ºC	Temperature average	-20.20	-19.66	-20.62
	Temperature difference compared to reference sample	0	-0.54	0.42
	Total temperature difference compared to reference sample	**0**	**-0.71**	**0.13**
Second simulation		**Reference**	**PCM(6)CF(0)**	**PCM(6)CF(0.1)**
+ 10 ºC	Temperature average	10.07	9.21	10.23
	Temperature difference compared to reference sample	0	-0.86	0.16
- 10 ºC	Temperature average	-9.31	-9.09	-10.28
	Temperature difference compared to reference sample	0	-0.21	0.97
	Total temperature difference compared to reference sample	**0**	**-1.07**	**1.13**

4.4.2.3. Samples with 30 mm Thickness

In this section, 150×150×30 mm samples of PCM(0)CF(0) coded reference composite and PCM(6)CF(0) and PCM(6)CF(0.1) coded composites were subjected to freeze-thaw tests. The graph formed by these composites in the first simulation was given in Figure 4.32, and the graph formed in the second simulation was given in Figure 4.33. The temperature differences compared to the reference sample were presented in Table 4.12 based on the data obtained from the graphs. In the PCM(6)CF(0) coded composite, the temperature amplitudes decreased by 0.11 ºC in the first simulation and 0.39 ºC in the second simulation. In the PCM(6)CF(0.1) coded composite, the temperature amplitudes increased by 1.38 ºC in the first simulation and 0.42 ºC in the second simulation with the effect of CF. In PCM(6)CF(0.1) coded composite decreased by approximately amplitude of 1 ºC at second simulation compared to first simulation.

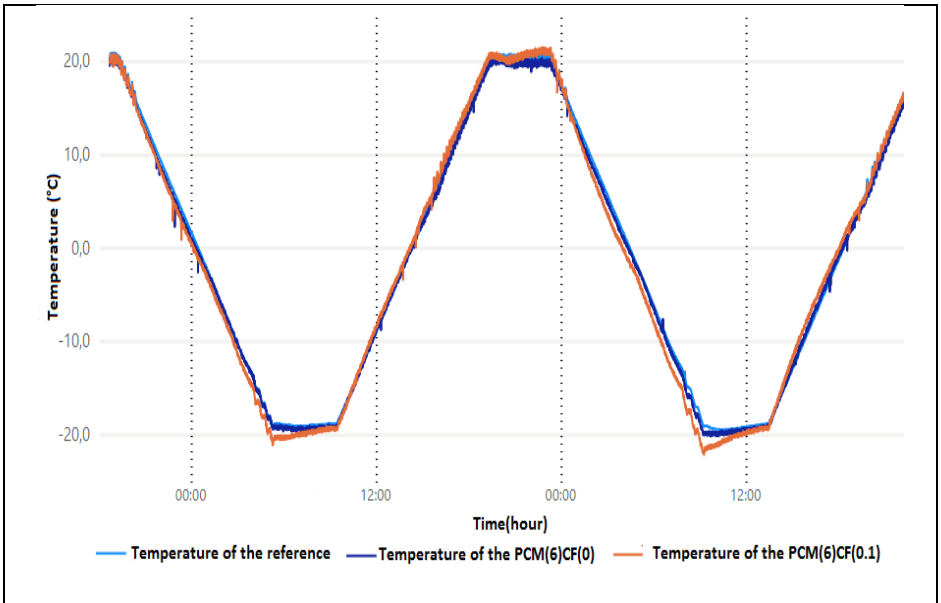

Figure 4.32. Sample thickness of 30 mm in first simulation

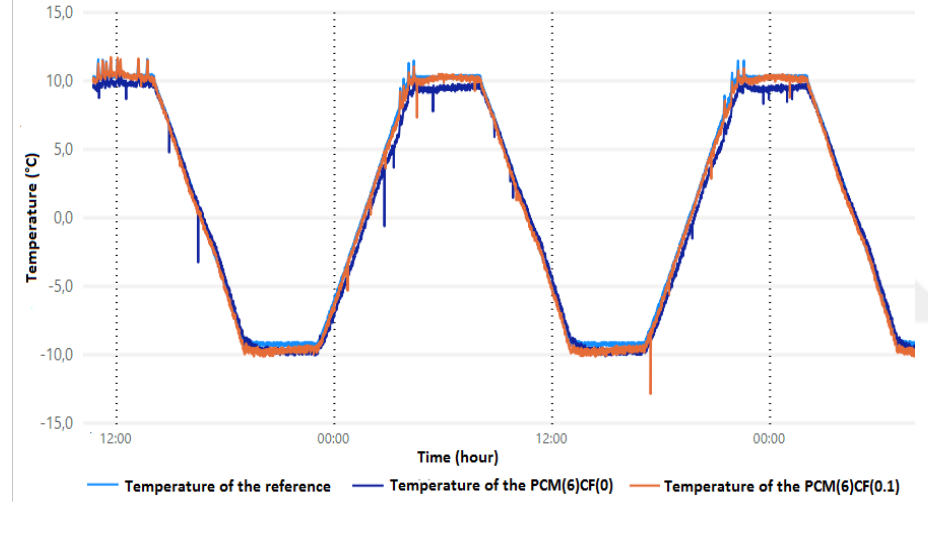

Figure 4.33. Sample thickness of 30 mm in second simulation

Table 4.12. The difference in temperature amplitudes at 30 mm sample thickness

First simulation		**Reference**	**PCM(6)CF(0)**	**PCM(6)CF(0.1)**
+ 20 ºC	Temperature average	20.41	19.88	20.68
	Temperature difference compared to reference sample	0	-0.53	0.27
- 20 ºC	Temperature average	-19.19	-19.61	-20.30
	Temperature difference compared to reference sample	0	0.42	1.11
	Total temperature difference compared to reference sample	**0**	**-0.11**	**1.38**
Second simulation		**Reference**	**PCM(6)CF(0)**	**PCM(6)CF(0.1)**
+ 10 ºC	Temperature average	10.27	9.48	10.16
	Temperature difference compared to reference sample	0	-0.87	-0.09
- 10 ºC	Temperature average	-9.18	-9.66	-9.69
	Temperature difference compared to reference sample	0	0.48	0.51
	Total temperature difference compared to reference sample	**0**	**-0.39**	**0.42**

4.4.2.4. Samples with 20 mm Thickness

In this section, 150×150×20 mm samples of PCM(0)CF(0) coded reference composite and PCM(6)CF(0) and PCM(6)CF(0.1) coded composites were subjected to freeze-thaw tests. The graph formed by these composites in the first simulation was given in Figure 4.34, and the graph formed in the second simulation was given in Figure 4.35. The temperature differences compared to the reference sample were presented in Table 4.13 based on the data obtained from the graphs. Although it is observed in the graphs that the PCM makes shoulders, the temperature amplitudes of the PCM(6)CF(0) coded sample can be observed both in first simulation and second simulation did not show any benefit in reducing. In the PCM(6)CF(0.1) coded composite, the temperature amplitudes increased by 0.53 ºC in the first simulation and 0.35 ºC in the second simulation with the effect of CF. The reason for the less amplitude increase in the second simulation indicates that the PCM is somewhat more effective in this cycle.

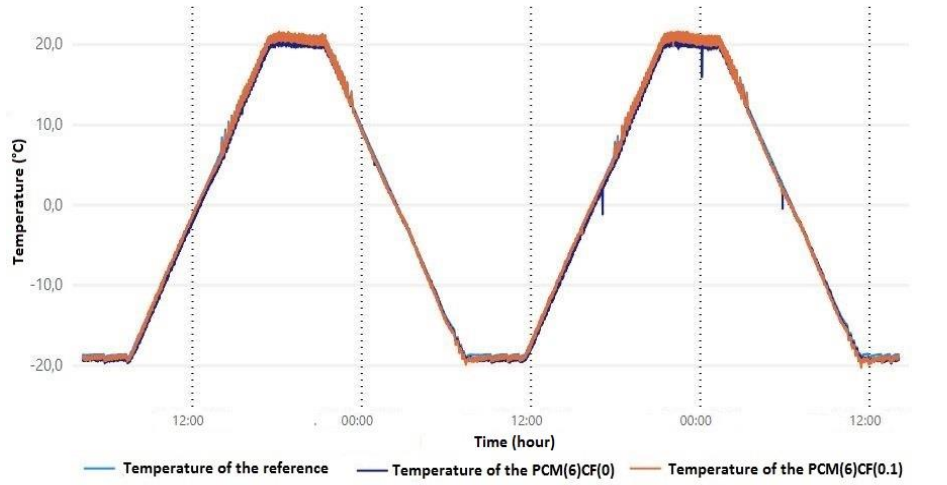

Figure 4.34. Sample thickness of 20 mm in first simulation

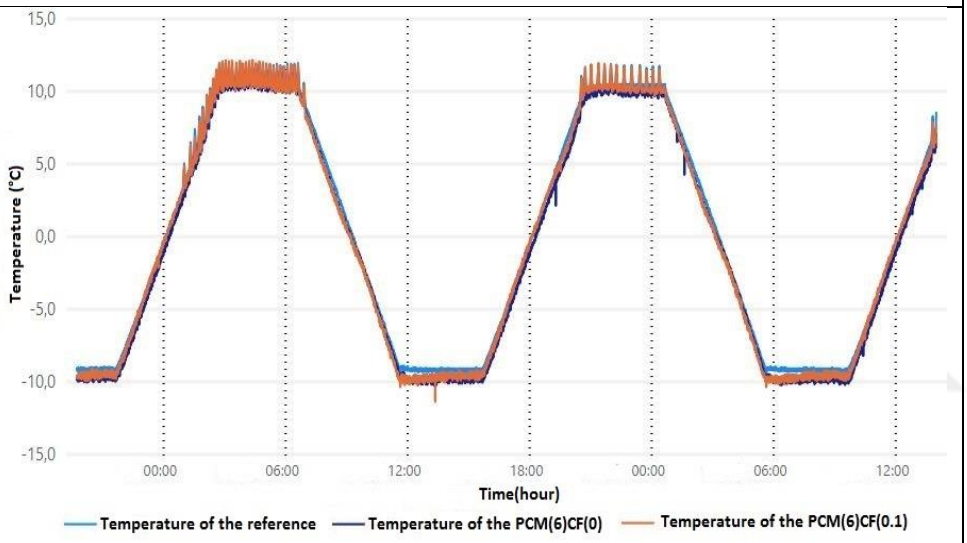

Figure 4.35. Sample thickness of 20 mm in second simulation

Table 4.13. The difference in temperature amplitudes at 20 mm sample thickness

First simulation		**Reference**	**PCM(6)CF(0)**	**PCM(6)CF(0.1)**
+ 20 ºC	Temperature average	20.61	20.13	20.73
	Temperature difference compared to reference sample	0	-0.48	0.12
- 20 ºC	Temperature average	-18.71	-19.24	-19.12
	Temperature difference compared to reference sample	0	0.53	0.41
	Total temperature difference compared to reference sample	**0**	**0.05**	**0.53**
Second simulation		**Reference**	**PCM(6)CF(0)**	**PCM(6)CF(0.1)**
+ 10 ºC	Temperature average	10.61	10.06	10.43
	Temperature difference compared to reference sample	0	-0.55	-0.18
- 10 ºC	Temperature average	-9.15	-9.84	-9.68
	Temperature difference compared to reference sample	0	0.69	0.53
	Total temperature difference compared to reference sample	**0**	**0.14**	**0.35**

In Figure 4.36, based on the data in the tables, the graph showing the variation of the temperature differences with respect to the reference sample according to the sample thicknesses is given. Except for 20 mm thickness, temperature amplitudes in other thickness types decreased in both cycle types in the sample coded PCM(6)CF(0), which contains only PCM without CF. It was observed that this decrease in amplitudes was higher in the second simulation compared to the first simulation. The reason for this is that the energy released/absorbed by the PCM continues to be effective at maximum and minimum temperature points. In the 40 mm thick sample, coded PCM(6)CF(0), showing the best performance compared to other thickness types, the temperature amplitudes decreased by 0.71 ºC in the first simulation and by 1.07 ºC in the second simulation. Excluding the 50 mm thickness type, it was determined that the temperature amplitudes decreased more in PCM(6)CF(0) coded composites as the thickness increased. It is estimated that this is related to the increase in the amount of PCM in the sample as the thickness increases. However, the fact that this performance cannot be achieved in the 50 mm thickness type suggests that the thickness has an optimum value. In other words, as the thickness increases, the amount of PCM increases, but the cross-section size that the

PCM needs to heat also increases. In PCM(6)CF(0.1) coded samples, temperature amplitudes increased despite PCM in other cycle and thickness types except for the second simulation of 50 mm thickness type. Especially, the composite coded PCM(6)CF(0.1) showed the most unfavorable performance, in which the amplitude increased by 1.38 °C in the first simulation in the 30 mm thickness type and by 1.13 °C in the second simulation in the 40 mm thickness type. Except for the 40 mm thickness type, PCM was more effective in the second simulation and kept the amplitude increase at lower levels compared to the first simulation in other thickness types. In particular, in the second simulation of the 50 mm thickness type, 0.15 °C amplitude decrease was observed instead of amplitude increase.

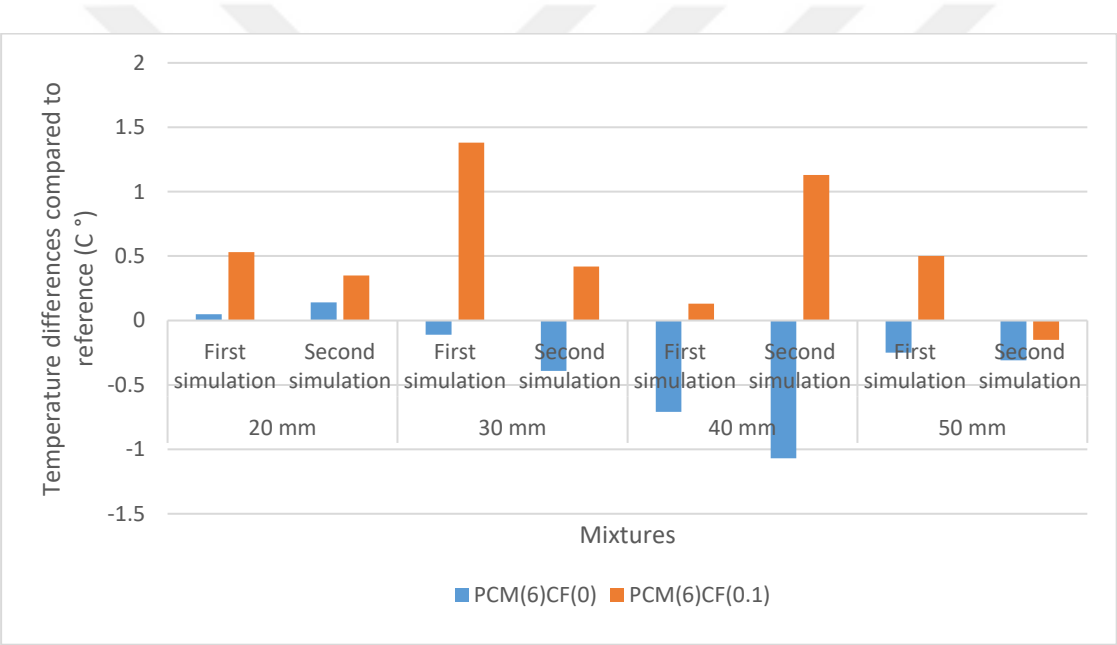

Figure 4.36. Variation of temperature differences compared to the reference sample according to sample thicknesses

4.5. Results of Ice Melting Performance Test

4.5.1. First Procedure-Different PCM Ratios by Cement Weight

The aim of the ice melting performance test was to determine the contribution of PCM to the ice melting rate in low, moderate and high conductive levels. It was intended that composites with increased thermal conductivity with CFs will transfer the heat energy released by the PCM to the surface faster. Even in samples with low PCM content, it was

predicted that the ice would melt faster than the reference sample thanks to fast heat transfer.

4.5.1.1. Samples Containing 8% PCM By Weight of Cement

In Table 4.14, the cumulative amount of ice melted by the conductive samples containing 8% of the cement weight PCM together with the reference sample within 72 hours was given. Based on the data obtained from the table, the line graph formed by the amount of ice melted by the composites was shown in Figure 4.37. Among all composites, the best performance was achieved by the PCM(8)CF(0.1) composite, which had the highest PCM ratio and was moderately conductive. This composite had an average ice melting rate of 1.04 g/h and melted a total of 75.06 grams of ice. The reason why PCM(8)CF(0.3) melts less ice than PCM(8)CF(0) can be that the relatively high homogeneous distribution of carbon fibers causes it to cool faster (Sakulich and Bentz 2012). The ice melting rates of the PCM(8)CF(0) and PCM(8)CF(0.3) composites were 0.39 g/h and 0.22 g/h, respectively (Figure 4.44). Due to the CFs, the PCM(8)CF(0.1) composite performed better than the PCM(8)CF(0) composite by melting 46.7 grams more ice.

Table 4.14. Time-dependent cumulative ice melting of conductive samples containing 8% of the cement weight of PCM and the reference sample

	Amount of melting ice (g)								
	8 hours	**16 hours**	**24 hours**	**32 hours**	**40 hours**	**48 hours**	**56 hours**	**64 hours**	**72 hours**
PCM(0)CF(0)	1.35	3.42	5.17	8.11	10.32	14.56	18.44	23.17	25.81
PCM(8)CF(0)	2.38	5.39	8.00	10.22	12.90	17.21	22.65	25.49	28.34
PCM(8)CF(0.1)	9.67	22.30	32.98	39.82	45.63	52.03	59.55	67.30	75.06
PCM(8)CF(0.3)	1.28	4.70	6.98	7.41	7.88	9.39	12.09	13.83	15.58

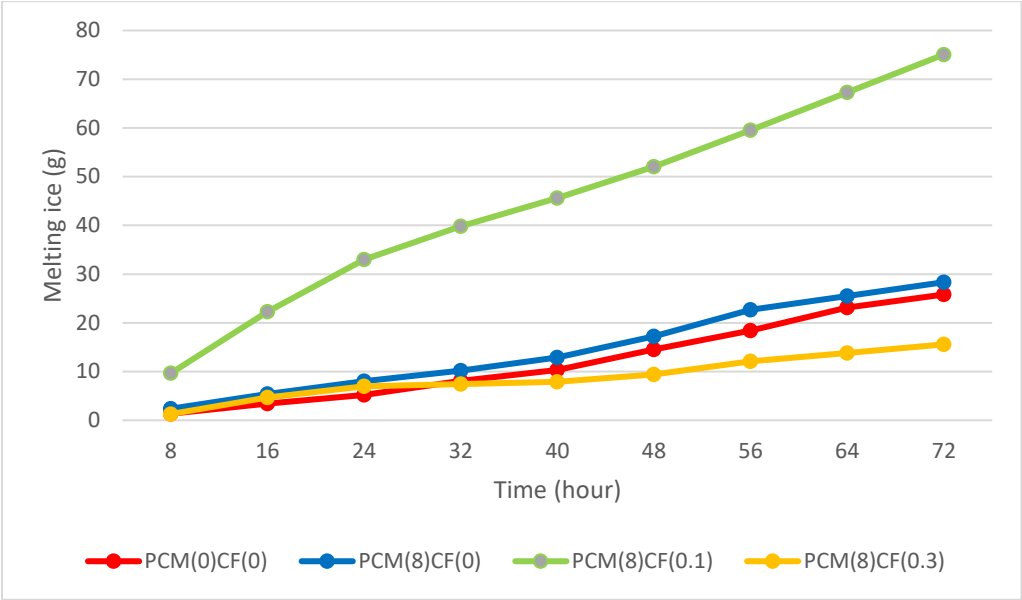

Figure 4.37. Melting Ice Amounts In The Samples Containing 8% PCM Relative to Cement Weight

4.5.1.2. Samples Containing 6% PCM By Weight of Cement

In Table 4.15, the cumulative amount of ice melted by the conductive samples containing 6% of the cement weight PCM together with the reference sample within 72 hours was given. Based on the data obtained from the table, the line graph formed by the amount of ice melted by the composites was shown in Figure 4.38. The best performance was achieved by the PCM(6)CF(0.1) composite, which had the highest PCM ratio and was moderately conductive. The average ice melting rate of the PCM(6)CF(0.1) composite, which melted a total of 69.84 grams of ice for 72 hours, was 0.97 g/h, while the rate for the PCM(6)CF(0) composite was 0.42 g/h and that for the PCM(6)CF(0.3) composite was 0.76 g/h (Figure 4.44). The PCM(6)CF(0.1) composite having moderate conductivity melted 39.4 grams more ice than the PCM(6)CF(0) composite having low conductivity, providing a superior performance. However, within 72 hours, the composite coded PCM(6)CF(0.1) melted 5.22 grams less snow than the composite coded PCM(8)CF(0.1), and the average snow melting rate was 0.07 g/h lower remained. The sample coded PCM(6)CF(0.3), on the other hand, showed a more effective performance than the reference and PCM(6)CF(0) coded sample with 54.68 grams of ice melting amount. On the other hand, the reference sample and the PCM(6)CF(0) coded sample provided close results. The sample coded PCM(6)CF(0) melted 4.61 grams more ice in 72 hours compared to the reference sample and the ice melting rate was 0.07 g/h higher. In the

PCM(6)CF(0) composite, since the energy transmission is not fast, the efficiency of PCM remained low and therefore, compared to the reference sample, it created a small difference in mass of the ice melted. On the other hand, the digital image showing the form of the melting ice layers was taken during measuring the amount of ice melting in the 24th hour in Figure 4.39. On the image, the ice layers existing are shown by a solid line. The ice layers on the PCM(6)CF(0) and PCM(6)CF(0.3) composites maintained their square form, but this was not the case for the PCM(6)CF(0.1) composite because of more melting.

Table 4.15. Time-dependent cumulative ice melting of conductive samples containing 6% of the cement weight of PCM and the reference sample

	Amount of melting ice (g)								
	8 hours	**16 hours**	**24 hours**	**32 hours**	**40 hours**	**48 hours**	**56 hours**	**64 hours**	**72 hours**
PCM(0)CF(0)	1.35	3.42	5.17	8.11	10.32	14.56	18.44	23.17	25.81
PCM(6)CF(0)	2.56	5.17	8.43	11.36	13.81	18.11	22.35	25.83	30.42
PCM(6)CF(0.1)	7.26	16.00	25.25	32.33	40.18	47.23	53.89	61.13	69.84
PCM(6)CF(0.3)	4.18	10.16	16.41	21.54	27.37	33.86	40.84	46.89	54.68

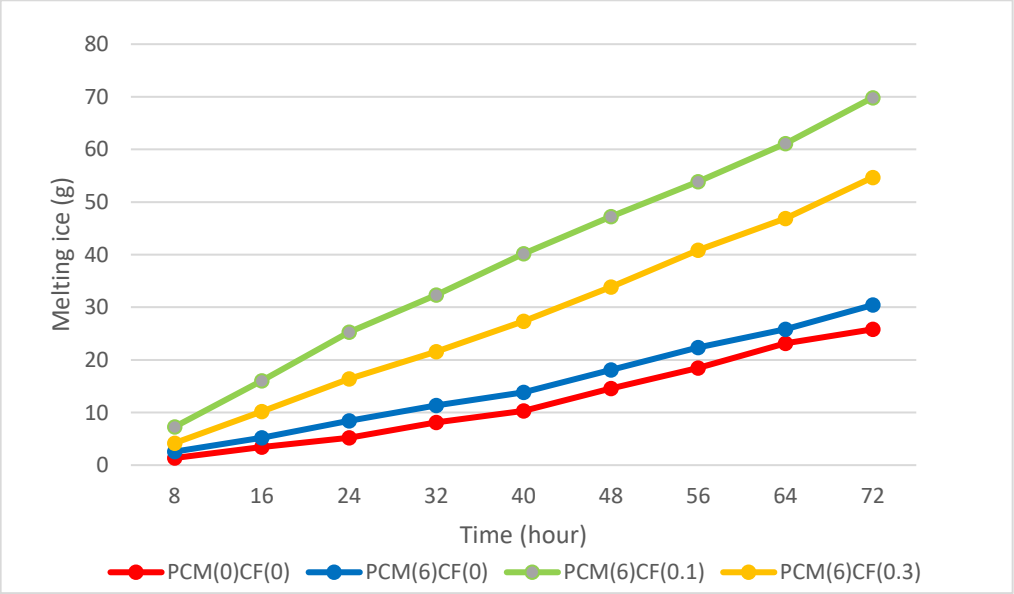

Figure 4.38. Melting Ice Amounts In The Samples Containing 6% PCM Relative to Cement Weight

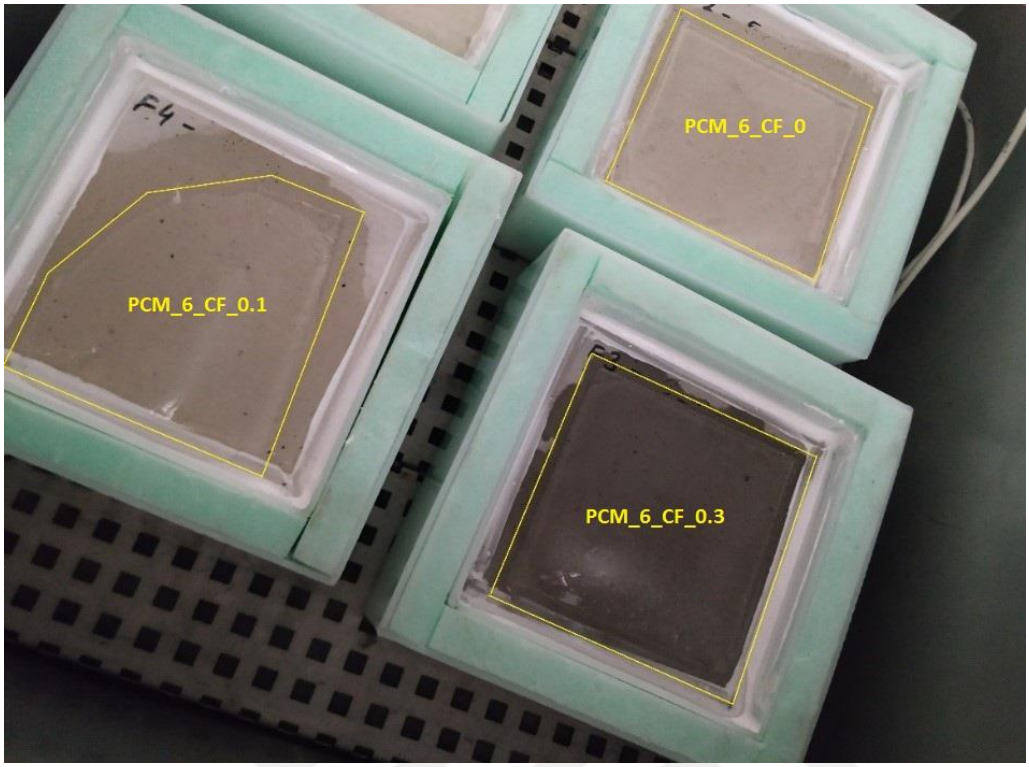

Figure 4.39. Condition of the ice layers on the samples at the 24th hour of the test

4.5.1.3. Samples Containing 4% PCM By Weight of Cement

In Table 4.16, the cumulative amount of ice melted by the conductive samples containing 4% of the cement weight PCM together with the reference sample within 72 hours was given. Based on the data obtained from the table, the line graph formed by the amount of ice melted by the composites was shown in Figure 4.40. 33.3 g, 56.2 g and 37.5 g of ice melted on the PCM(4)CF(0), PCM(4)CF(0.1), PCM(4)CF(0.3) composites, respectively. The PCM(4)CF(0.1) composite with a moderate conductivity level demonstrated the best ice melting performance. The ice melting rate of the PCM(4)CF(0) coded composite containing 4% PCM addition and not containing CF was 0.46 g/h, while the PCM(4)CF(0.3) coded composite was 0.52 g/h (Figure 4.44). PCM(4)CF(0.1) melted 13.6 grams less snow than the composite coded PCM(6)CF(0.1), and the average snow melting rate was 0.19 g/h lower remained. Reference composite with 0.35 g/h melting rate showed the lowest performance (Figure 4.44). On the other hand, the non-conductive reference sample and the PCM(4)CF(0) coded sample provided close results. The ice melting rate for the PCM(4)CF(0) composite was 0.11 g/h higher than that for the

reference. In the this composite, since the energy transmission is not fast, the efficiency of PCM remained low and therefore, compared to the reference sample, it created a small difference in mass of the ice melted.

Table 4.16. Time-dependent cumulative ice melting of conductive samples containing 4% of the cement weight of PCM and the reference sample

	Amount of melting ice (g)								
	8 hours	**16 hours**	**24 hours**	**32 hours**	**40 hours**	**48 hours**	**56 hours**	**64 hours**	**72 hours**
PCM(0)CF(0)	1.35	3.42	5.17	8.11	10.32	14.56	18.44	23.17	25.81
PCM(4)CF(0)	2.25	6.15	10.11	12.37	15.64	20.03	25.41	30.14	33.25
PCM(4)CF(0.1)	5.32	14.24	21.77	26.84	31.23	36.52	45.56	51.28	56.24
PCM(4)CF(0.3)	2.01	7.18	10.59	14.15	17.84	22.34	27.84	32.45	37.49

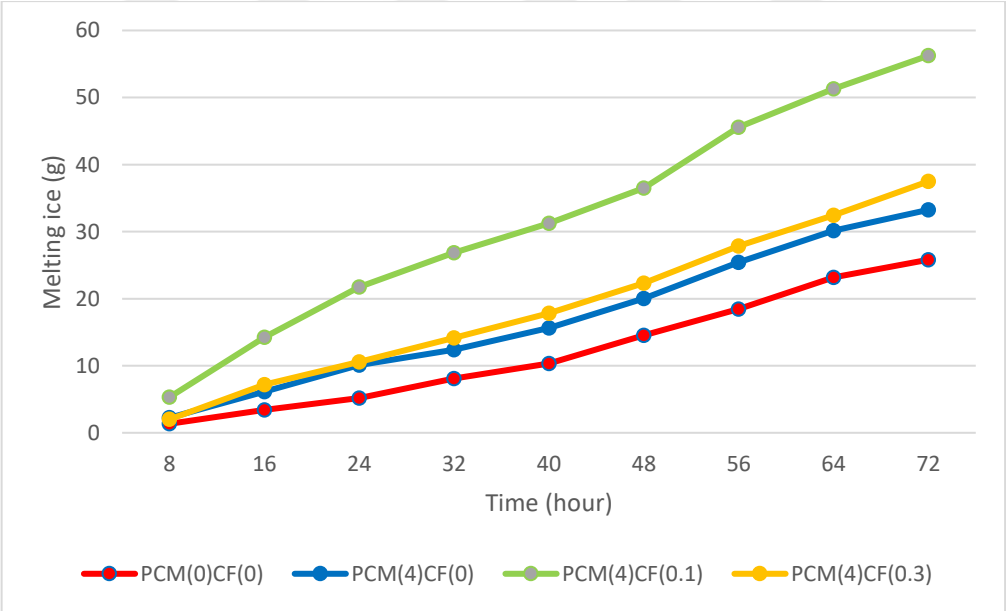

Figure 4.40. Melting Ice Amounts In The Samples Containing 4% PCM Relative to Cement Weight

4.5.1.4. Samples Containing 2% PCM By Weight of Cement

In Table 4.17, the cumulative amount of ice melted by the conductive samples containing 2% of the cement weight PCM together with the reference sample within 72 hours was

given. Based on the data obtained from the table, the line graph formed by the amount of ice melted by the composites was shown in Figure 4.41. The PCM(2)CF(0.1) composite had an average ice melting rate of 0.66 g/h and total of 47.6 grams of ice melted. The ice melting rate of the PCM(2)CF(0) composite was 0.42 g/h, and that of the PCM(2)CF(0.3) composite was 0.44 g/h. Considering the results, the amount of ice melted for the PCM(2)CF(0.1) composite was significantly higher than those for the PCM(2)CF(0) and PCM(2)CF(0.3) composites. However, within 72 hours, the composite coded PCM(2)CF(0.1) melted 8.68 grams less ice than the composite coded PCM(4)CF(0.1), and the average snow melting rate was 0.19 g/h lower remained. The sample coded PCM(2)CF(0.1) showed a superior performance by melting 17.39 grams more ice in 72 hours compared to the sample coded PCM(2)CF(0). On the other hand, the non-conductive reference sample and the PCM(2)CF(0) coded sample provided close results. The sample coded PCM(2)CF(0) melted 4.36 grams more ice in 72 hours compared to the reference sample and the ice melting rate was 0.07 g/h higher. In this composite, since the thermal energy from the ice is not transmitted quickly, the PCM efficiency remained low and it was observed that the cabin temperature was effective in melting ice. The sample coded PCM(2)CF(0.3), on the other hand, showed a performance close to the two non-conductive composites with a melting amount of 32.02 grams and a melting rate of 0.44 g/h.

Table 4.17. Time-dependent cumulative ice melting of conductive samples containing 2% of the cement weight of PCM and the reference sample

	Amount of melting ice (g)								
	8 hours	**16 hours**	**24 hours**	**32 hours**	**40 hours**	**48 hours**	**56 hours**	**64 hours**	**72 hours**
PCM(0)CF(0)	1.35	3.42	5.17	8.11	10.32	14.56	18.44	23.17	25.81
PCM(2)CF(0)	1.93	4.98	7.84	10.22	13.08	17.32	23.37	27.25	30.17
PCM(2)CF(0.1)	4.84	12.48	19.62	22.82	23.44	29.85	40.89	44.27	47.56
PCM(2)CF(0.3)	1.72	4.80	7.79	10.50	13.65	18.79	25.51	28.76	32.02

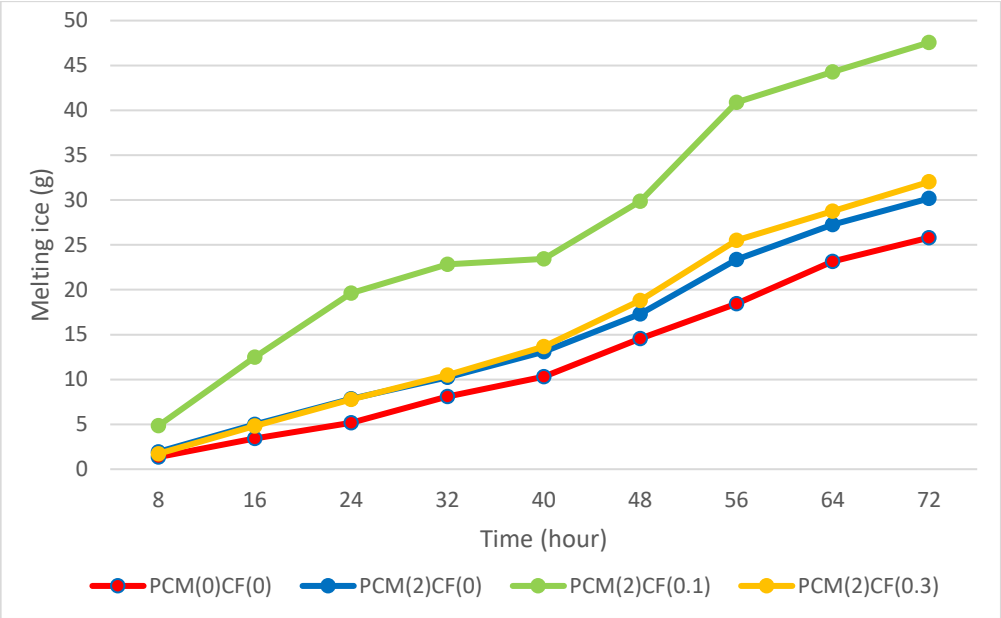

Figure 4.41. Melting Ice Amounts In The Samples Containing 2% PCM Relative to Cement Weight

4.5.1.5. PCM-Free Samples

In Table 4.18, the cumulative amounts of ice melted by the PCM-free conductive samples and the reference sample within 72 hours were given. Based on the data obtained from the table, the line graph formed by the amount of ice melted by the composites was shown in Figure 4.42. Since there was no PCM providing heat energy for the samples, melting of the ice layer on the surface of the samples was only due to the cabin temperature, therefore the composites showed similar performances. 25.8 g, 26.5 g and 24.3 g of ice melted on the PCM(0)CF(0), PCM(0)CF(0.1), PCM(0)CF(0.3) composites, respectively. The average ice melting rate for the PCM(0)CF(0) composite was 0.35 g/h, while the rates for the PCM(0)CF(0.1) and PCM(0)CF(0.3) composites were 0.36 g/h and 0.33 g/h, respectively (Figure 4.44).

Table 4.18. Time-dependent cumulative ice melting of conductive samples containing 0% of the cement weight of PCM and the reference sample

	Amount of melting ice (g)								
	8 hours	**16 hours**	**24 hours**	**32 hours**	**40 hours**	**48 hours**	**56 hours**	**64 hours**	**72 hours**
PCM(0)CF(0)	1.35	3.42	5.17	8.11	10.32	14.56	18.44	23.17	25.81
PCM(2)CF(0.1)	2.60	4.55	5.94	8.12	10.14	15.17	19.23	24.00	26.51
PCM(2)CF(0.3)	1.73	2.81	4.45	8.25	9.11	15.73	18.81	23.66	24.29

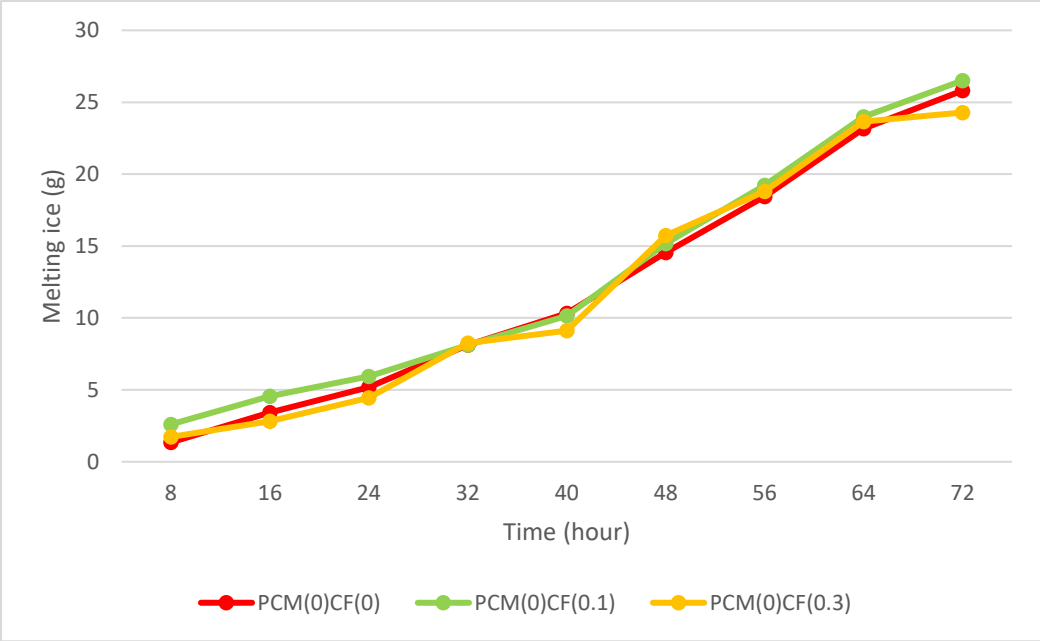

Figure 4.42. Melting Ice Amounts In The Samples Containing 0% PCM Relative to Cement Weight

In Figure 4.43, ice melting rates of all mixtures were given with bar graph. In the experiments performed on all PCM groups, the composites containing 0.1% by volume CF having moderate conductivity level showed the best performance. In these samples, the thermal energy present in the ice layer was rapidly transmitted from the sample surface to the entire sample caused faster cooling thanks to the CFs. Thus, the temperature of the samples reached the temperature limits of the heat energy release zone of the PCM (between 2 ^{o}C and -14 ^{o}C) more quickly. In this case, the PCM in the microcapsules frozen and released heat energy faster than the composites containing no CFs. The heat

energy produced by the PCM in the samples, reached the surface quickly due to the presence of CFs and melted the ice faster. However, the mentioned situation was not detected in the ice melting rate for the composites produced having high conductivity level. This is thought to be because thermal energy of the ice reduces the high conductivity samples to lower temperatures compared to the moderate conductivity samples. It was also mentioned in previous studies that high conductivity led to rapid cooling (Sakulich and Bentz, 2012). As a result, although the composites having high conductivity levels released the heat energy of the PCM earlier, this heat energy was not sufficient to heat the composites due to their lower temperature. For example, the PCM(8)CF(0.3) composite performed even worse than the PCM(0)CF(0) and PCM(8)CF(0) composites. This showed that an optimum CF content should be present in snow/ice melting applications.

As the PCM ratio decreased in the samples containing 0.1% CF by volume, the melting rate of the ice layers of the samples also decreased. On the other hand, samples containing PCM and not containing CF provided melting rate values close to the reference composite since they were not conductive. Reference composite , PCM(2)CF(0) coded composite, PCM(4)CF(0) coded composite, PCM(6)CF(0) coded composite and PCM(8)CF(0) coded composite had a melting rate of 0.35 g/h, 0.42 g/h, 0.46 g/h, 0.42 g/h and 0.39 g/h, respectively. On the other hand, samples containing 0.3% CF and PCM with high conductivity exceeded the optimum fiber ratio and their performance remained lower than samples containing 0.1% CF and PCM. PCM(2)CF(0.3) coded composite, PCM(4)CF(0.3) coded composite, PCM(6)CF(0.3) coded composite and PCM(8)CF(0.3) coded composite had a melting rate of 0.44 g/h, 0.52 g/h, 0.76 g/h and 0.22 g/h, respectively.

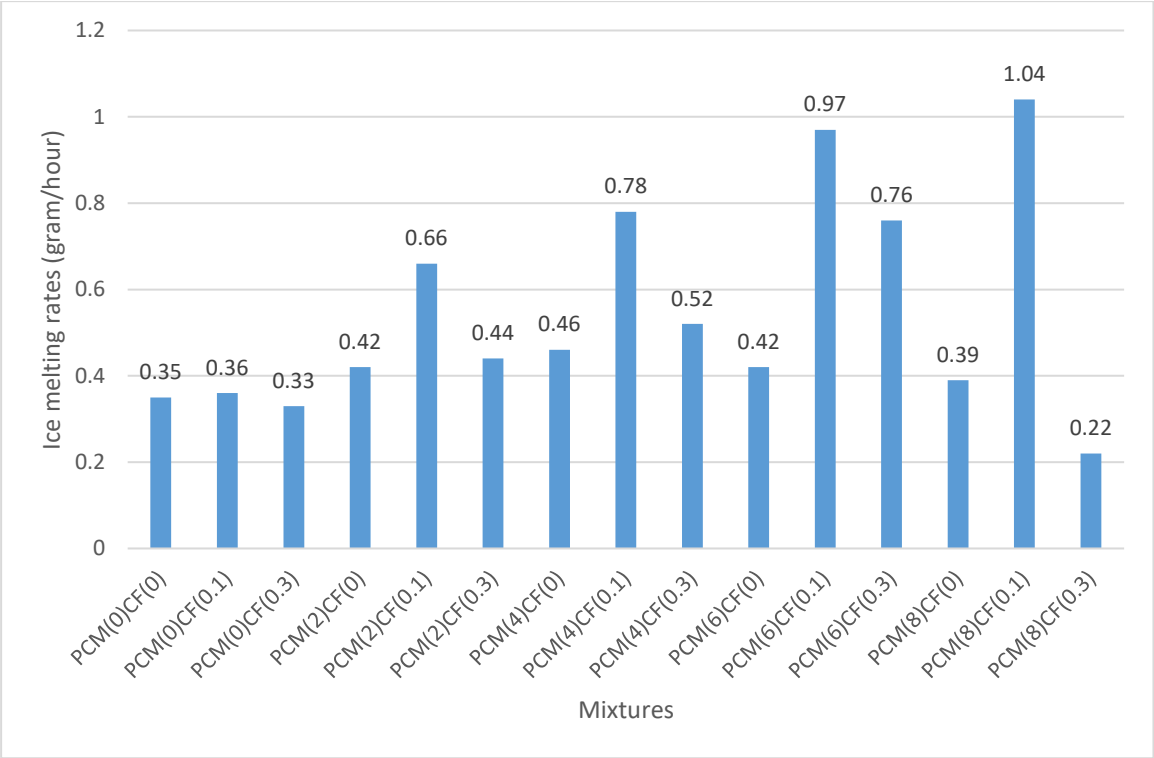

Figure 4.43. Ice melting rates of composites

4.5.2. Second Procedure-Composites of Different Thicknesses Containing 6% PCM of the Cement Weight

In the previous section, the contribution of composites with different PCM ratio content to the ice melting rate for different conductive level. In this section, the test of different thicknesses of composites with 6% PCM ratio was carried out. The purpose of this test is to give an idea about the pavement thickness to be used in the application. Unlike the previous section, the cabin temperature is set to 1.5 °C in order to determine the effect of PCM when it is in the phase change temperature range (between 2°C and -14°C).

4.5.2.1. Samples with 50 mm Thickness

Composites coded PCM(0)CF(0), PCM(6)CF(0) and PCM(6)CF(0.1) with a thickness of 50 mm were tested at a cabin temperature of 1.5 ^{o}C. In Table 4.19, the cumulative amount of ice melted by composites within 72 hours was given. Based on the data obtained from the table, the line graph formed by the amount of ice melted by the composites was shown in Figure 4.44. Among the composites, the PCM(6)CF(0.1) coded composite, which melted 34.57 grams of ice for 72 hours and had a melting rate of 0.48 g/h (Figure 4.49),

showed the best performance. The lowest performance was shown by the reference sample, which melted 12.95 grams of ice for 72 hours and had a melting rate of 0.18 g/h. PCM(6)CF(0) coded composite melted 9.11 grams more ice than the reference composite with the effect of PCM and had a 0.31 g/h ice melting rate (Figure 4.49).

Table 4.19. Cumulative ice melting amounts of samples with a thickness of 50 mm depending on time

	Amount of melting ice (g)								
	8 hours	**16 hours**	**24 hours**	**32 hours**	**40 hours**	**48 hours**	**56 hours**	**64 hours**	**72 hours**
PCM(0)CF(0)	1.38	2.49	4.37	5.48	7.07	8.49	9.54	11.21	12.95
PCM(6)CF(0)	2.50	5.33	7.64	9.62	12.07	14.60	16.35	19.58	22.06
PCM(6)CF(0.1)	3.81	8.27	12.98	17.07	21.62	24.52	28.66	31.90	34.57

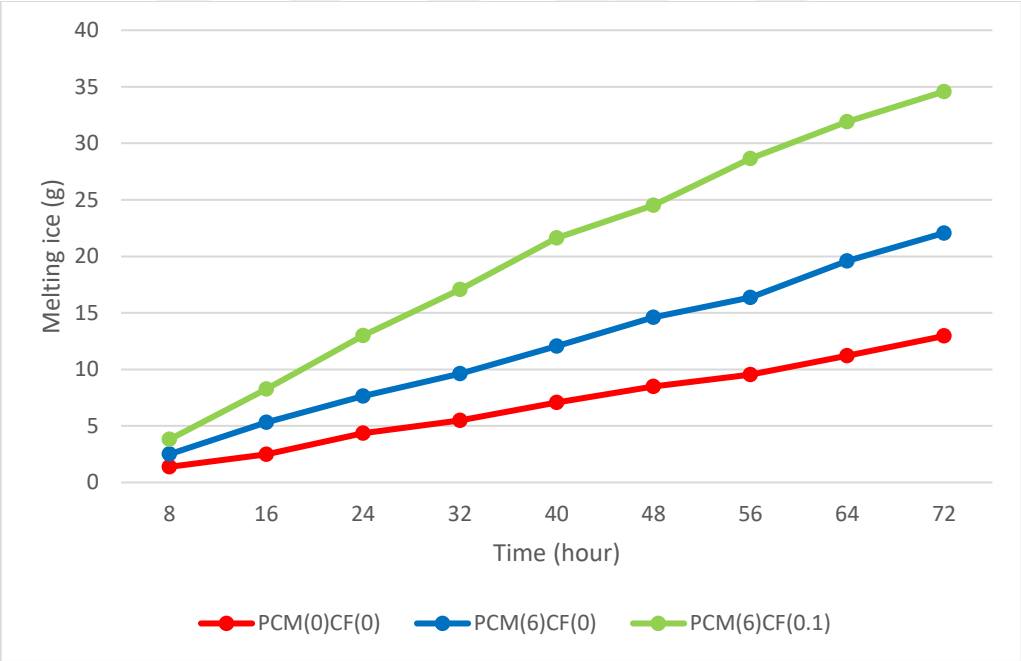

Figure 4.44. Melting Ice Amounts in Samples with a Thickness of 50 mm

4.5.2.2. Samples with 40 mm Thickness

Composites coded PCM(0)CF(0), PCM(6)CF(0) and PCM(6)CF(0.1) with a thickness of 40 mm were tested at a cabin temperature of 1.5 °C. In Table 4.20, the cumulative amount

of ice melted by composites within 72 hours was given. Based on the data obtained from the table, the line graph formed by the amount of ice melted by the composites was given in Figure 4.45. Among the composites, the PCM(6)CF(0.1) coded composite, which melted 35.48 grams of ice for 72 hours and had a melting rate of 0.49 g/h (Figure 4.49), showed the best performance. The lowest performance was shown by the reference sample, which melted 18.47 grams of ice for 72 hours and had a melting rate of 0.26 g/h. PCM(6)CF(0) coded composite melted 5.22 grams more ice than the reference composite with the effect of PCM and had a 0.32 g/h ice melting rate (Figure 4.49). When the results were examined, the 50 mm and 40 mm thicknesses of the PCM(6)CF(0.1) coded composite provided a very close performance.

Table 4.20. Cumulative ice melting amounts of samples with a thickness of 40 mm depending on time

	Amount of melting ice (g)								
	8 hours	**16 hours**	**24 hours**	**32 hours**	**40 hours**	**48 hours**	**56 hours**	**64 hours**	**72 hours**
PCM(0)CF(0)	1.42	2.35	5.41	7.89	9.69	11.74	14.05	16.78	18.47
PCM(6)CF(0)	2.56	6.47	9.81	11.22	13.98	16.77	19.84	22.50	23.69
PCM(6)CF(0.1)	4.87	7.65	11.23	16.87	21.65	25.47	29.65	32.44	35.48

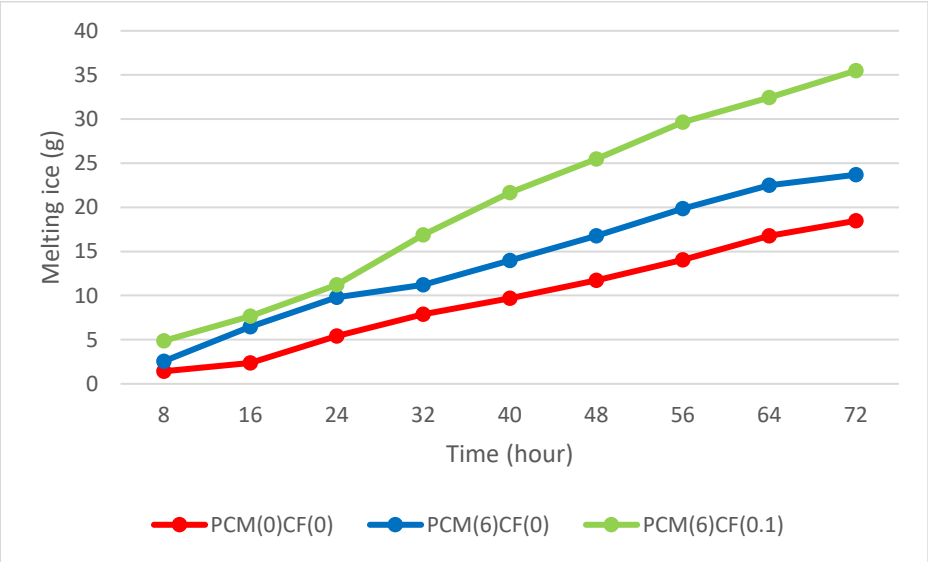

Figure 4.45. Melting Ice Amounts in Samples with a Thickness of 40 mm

4.5.2.3. Samples with 30 mm Thickness

Composites coded PCM(0)CF(0), PCM(6)CF(0) and PCM(6)CF(0.1) with a thickness of 30 mm were tested at a cabin temperature of 1.5 ^{o}C. In Table 4.21, the cumulative amount of ice melted by composites within 72 hours was given. Based on the data obtained from the table, the line graph formed by the amount of ice melted by the composites was shown in Figure 4.46. Among the composites, the PCM(6)CF(0.1) coded composite, which melted 40.29 grams of ice for 72 hours and had a melting rate of 0.56 g/h (Figure 4.49), showed the best performance. The lowest performance was shown by the reference sample, which melted 16.37 grams of ice for 72 hours and had a melting rate of 0.26 g/h. PCM(6)CF(0) coded composite melted 7.88 grams more ice than the reference composite with the effect of PCM and had a 0.23 g/h ice melting rate (Figure 4.49). When the results were examined, the 30 mm thickness of the PCM(6)CF(0.1) coded composite provided a more efficient performance compared to the 40 mm and 50 mm thicknesses.

Table 4.21. Cumulative ice melting amounts of samples with a thickness of 30 mm depending on time

	Amount of melting ice (g)								
	8 hours	**16 hours**	**24 hours**	**32 hours**	**40 hours**	**48 hours**	**56 hours**	**64 hours**	**72 hours**
PCM(0)CF(0)	1.23	2.83	4.28	5.91	8.09	10.79	12.89	14.59	16.37
PCM(6)CF(0)	2.36	5.39	7.97	10.00	13.82	17.24	19.38	21.49	24.25
PCM(6)CF(0.1)	5.43	10.49	16.35	21.07	25.85	29.76	32.94	36.96	40.29

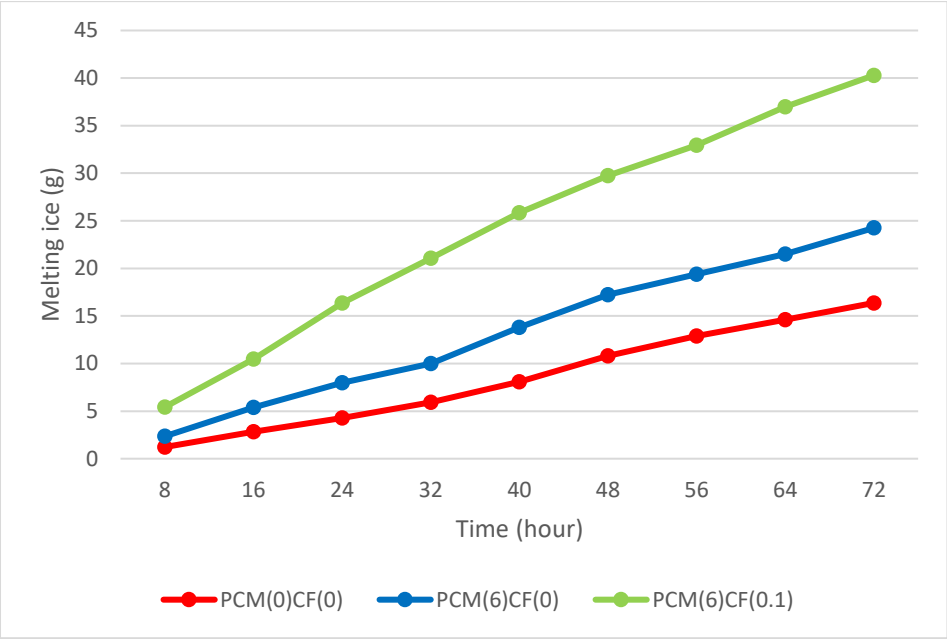

Figure 4.46. Melting Ice Amounts in Samples with a Thickness of 30 mm

4.5.2.4. Samples with 20 mm Thickness

Composites coded PCM(0)CF(0), PCM(6)CF(0) and PCM(6)CF(0.1) with a thickness of 20 mm were tested at a cabin temperature of 1.5 ºC. In Table 4.22, the cumulative amount of ice melted by composites within 72 hours was given. Based on the data obtained from the table, the line graph formed by the amount of ice melted by the composites was shown in Figure 4.47. Among the composites, the PCM(6)CF(0.1) coded composite, which melted 34.18 grams of ice for 72 hours and had a melting rate of 0.47 g/h (Figure 4.49), showed the best performance. The lowest performance was shown by the reference sample, which melted 10.10 grams of ice for 72 hours and had a melting rate of 0.14 g/h. PCM(6)CF(0) coded composite melted 10.67 grams more ice than the reference composite with the effect of PCM and had a 0.29 g/h ice melting rate (Figure 4.49). When the results were examined, the 20 mm thickness of the PCM(6)CF(0.1) coded composite provided an ice melting performance very close to the 40 mm and 50 mm thicknesses.

Table 4.22. Cumulative ice melting amounts of samples with a thickness of 20 mm depending on time

	Amount of melting ice (g)								
	8 hours	**16 hours**	**24 hours**	**32 hours**	**40 hours**	**48 hours**	**56 hours**	**64 hours**	**72 hours**
PCM(0)CF(0)	0.93	2.33	3.52	4.68	5.43	6.63	7.45	8.82	10.10
PCM(6)CF(0)	1.52	2.55	4.88	7.47	9.85	11.91	14.32	17.00	20.77
PCM(6)CF(0.1)	4.29	7.79	12.48	16.55	21.33	24.81	28.07	31.10	34.18

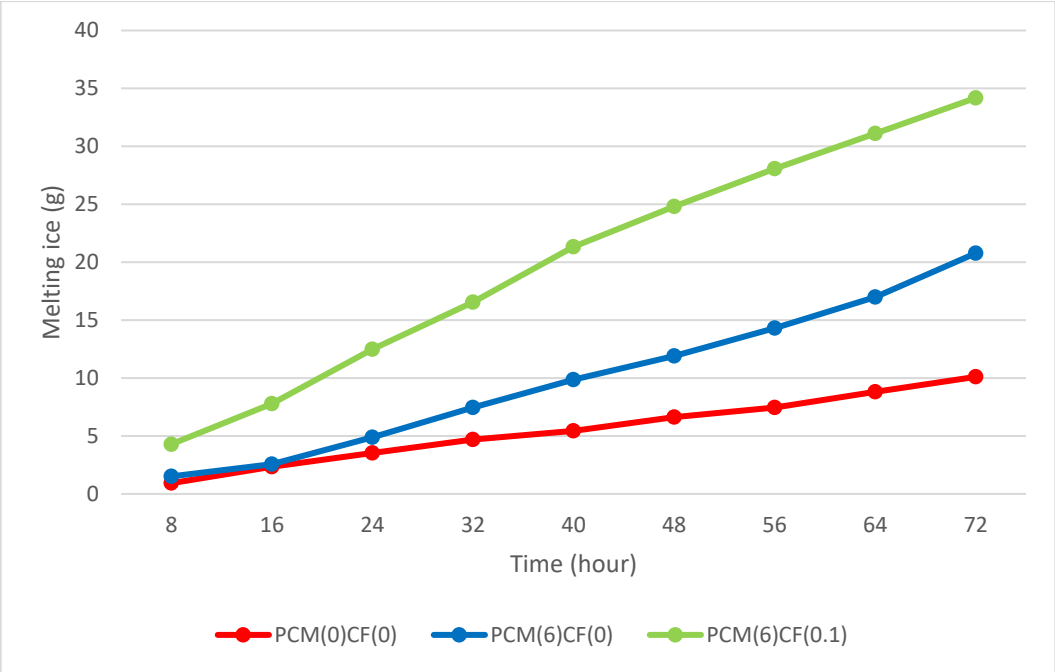

Figure 4.47. Melting Ice Amounts in Samples with a Thickness of 20 mm

4.5.2.5. Samples with 10 mm Thickness

Composites coded PCM(0)CF(0), PCM(6)CF(0) and PCM(6)CF(0.1) with a thickness of 10 mm were tested at a cabin temperature of 1.5 ^{o}C. In Table 4.23, the cumulative amount of ice melted by composites within 72 hours is given. Based on the data obtained from the table, the line graph formed by the amount of ice melted by the composites was shown in Figure 4.48. Among the composites, the PCM(6)CF(0.1) coded composite, which melted 35.14 grams of ice for 72 hours and had a melting rate of 0.49 g/h (Figure 4.49), showed the best performance. The lowest performance was shown by the reference

sample, which melted 15.54 grams of ice for 72 hours and had a melting rate of 0.22 g/h. PCM(6)CF(0) coded composite melted 6.52 grams more ice than the reference composite with the effect of PCM and had a 0.31 g/h ice melting rate (Figure 4.49). When the results were examined, the 10 mm thickness of the PCM(6)CF(0.1) coded composite provided a very close ice melting performance to the 20 mm, 40 mm and 50 mm thicknesses.

Table 4.23. Cumulative ice melting amounts of samples with a thickness of 10 mm depending on time

	Amount of melting ice (g)								
	8 hours	**16 hours**	**24 hours**	**32 hours**	**40 hours**	**48 hours**	**56 hours**	**64 hours**	**72 hours**
PCM(0)CF(0)	1.47	3.65	5.24	7.04	9.45	11.63	12.71	14.67	15.54
PCM(6)CF(0)	1.51	3.25	6.73	8.24	10.64	12.24	15.98	18.59	22.06
PCM(6)CF(0.1)	4.05	7.68	12.35	16.88	21.65	24.48	28.05	31.24	35.14

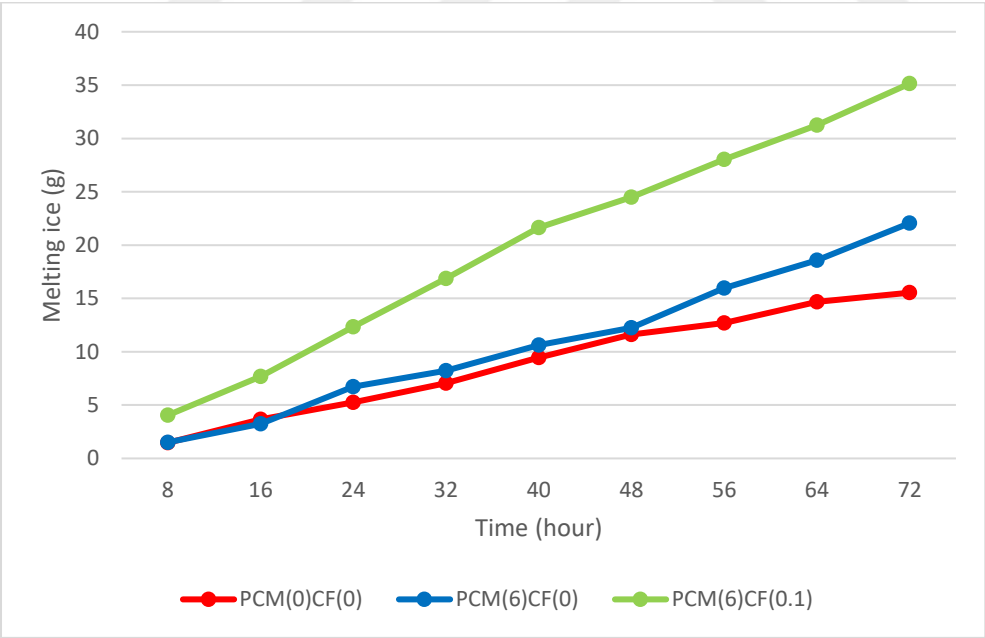

Figure 4.48. Melting Ice Amounts in Samples with a Thickness of 10 mm

In Figure 4.49, the ice melting rates of samples with different thicknesses were shown with a bar graph. PCM(6)CF(0.1) coded samples with moderate conductivity showed the most efficient performances. The ice melting rates of the 10, 20, 40, 50 mm thicknesses

of the PCM(6)CF(0.1) coded composite were close. The 30 mm thickness, with the highest ice melting speed at 0.56 g/h, provided the highest performance. It is thought that the reason why the composite with a thickness of 30 mm shows this performance is to provide a more effective percolation between the fibers compared to other composites. On the other hand, the samples with the slowest melting speed were PCM(0)CF(0) coded composites without PCM and CF. Since the ice layer on these composites melted due to the cabin temperature, the differences between them were due to minimal temperature variations in the cabin and the thickness values did not affect the performance of these composites. On the other hand, although PCM(6)CF(0) coded composites containing 6% PCM were not conductive, they performed better than PCM(0)CF(0) coded composites with PCM effect. This composite had an ice melting rate of about 0.30 g/h at all thickness values. Different thickness values did not significantly affect the ice melting rate of this composite. As the thickness increases, the PCM in the composite increases. However, since the cross-section size that this PCM needs to heat also increased, there was no huge difference in the ice melting speed.

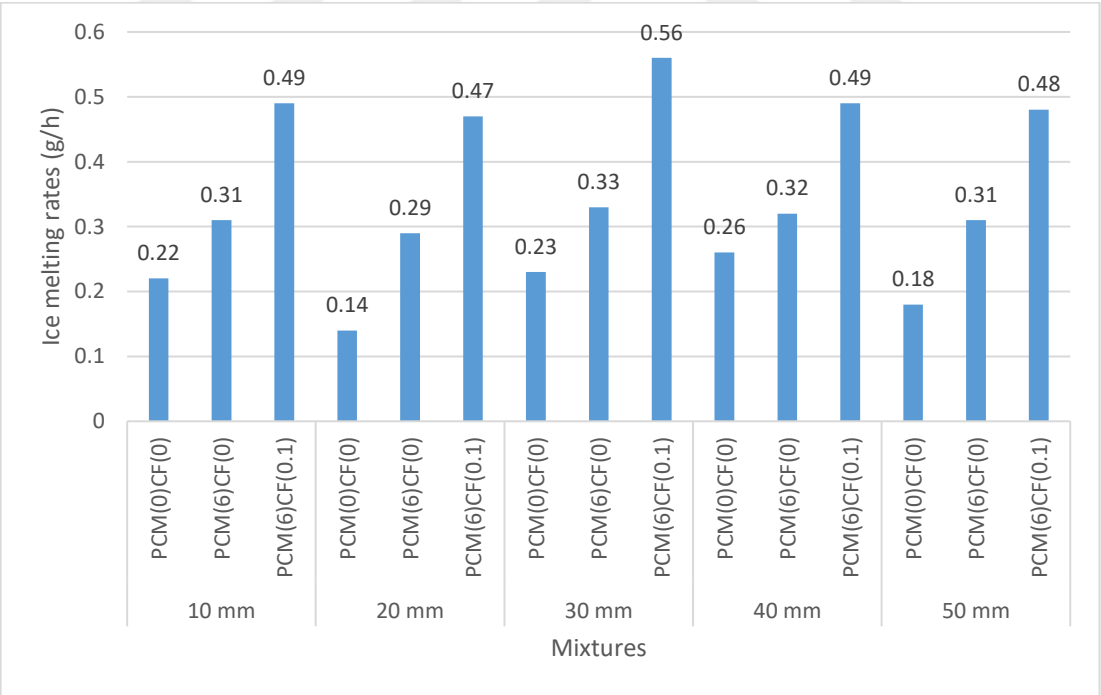

Figure 4.49. Ice melting rates of samples with different thickness

4.6. Results of Scaling Test

The test was carried out over 56 cycles in accordance with the "Slab Test Method" specified in the TS EN 12390-9 standard. The part of the sample that came into contact with the solution and scaling occurred was the trowelled surface. Since the part that will be exposed to climatic conditions in field applications is the trowel surface, such a preference was made within the scope of the experiment. As a result of the experiment, the amount of spalling material expressed in “grams” was divided by the 150×150 mm surface area that the solution came into contact with and converted to kg/m^2. The values resulting from the specified calculations were given in Table 4.24. In order to make the resulting values more understandable, the results were expressed in bar graphs in Figure 4.50.

Table 4.24. The amount of material that scaling as a result of the test cycles

Mixtures	**Amount of scaling material**	
	(g)	**(kg/m^2)**
PCM(0)CF(0)	1.54	0.068
PCM(0)CF(0.1)	16.37	0.728
PCM(0)CF(0.3)	18.45	0.820
PCM(2)CF(0)	0.40	0.018
PCM(2)CF(0.1)	8.50	0.378
PCM(2)CF(0.3)	14.35	0.638
PCM(4)CF(0)	3.23	0.144
PCM(4)CF(0.1)	16.32	0.725
PCM(4)CF(0.3)	17.82	0.792
PCM(6)CF(0)	1.33	0.059
PCM(6)CF(0.1)	17.45	0.776
PCM(6)CF(0.3)	20.76	0.923
PCM(8)CF(0)	1.22	0.054
PCM(8)CF(0.1)	19.32	0.859
PCM(8)CF(0.3)	7.11	0.316

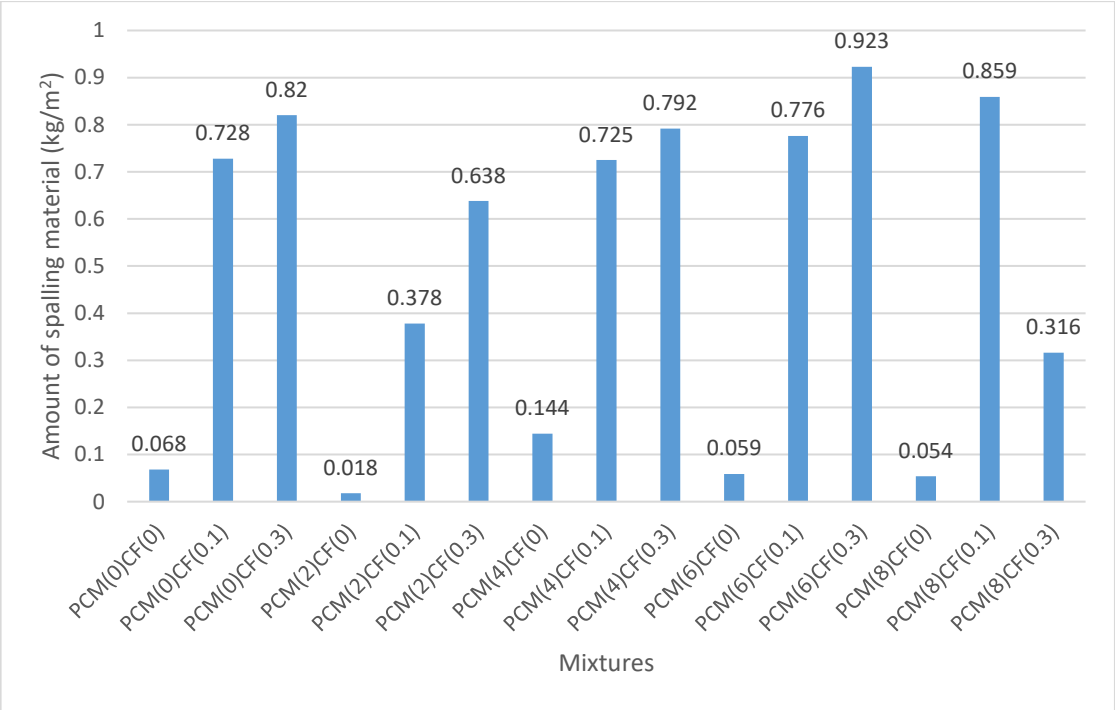

Figure 4.50. Results of scaling test

When the results were evaluated in general, composites containing CF showed the most unfavorable performance. Material losses of PCM(6)CF(0.3), PCM(0)CF(0.3), PCM(4)CF(0.3), PCM(2)CF(0.3) composites was 0.923 kg/m^2, 0.820 kg/m^2, 0.792 kg/m^2, 0.638 kg/m^2, respectively. In the Figure 4.51, spalling material occurring in the PCM(6)CF(0.3) coded composite, which indicated the lowest performance among all samples, is shown. In addition, material losses of PCM(8)CF(0.1), PCM(6)CF(0.1), PCM(4)CF(0.1), PCM(0)CF(0.3) composites was 0.859 kg/m^2, 0.776 kg/m^2, 0.725 kg/m^2, 0.728 kg/m^2, respectively. On the other hand, low rate of material losses occurred in composites that do not contain CF and that with/without PCM. The quantity of spalling that occurred in the PCM(4)CF(0) coded composite, which had the most material loss in composites which did not contain CF, was 0.144 kg/m^2. But this value remained at a very low level compared to the amount of spalling that occurred in the samples containing CF. It is known that CFs create an air void and negatively affect the compressive strength (Chung, 2000; Wang et al., 2008; Chuang, 2017). As a matter of fact, serious decreases occurred in the compressive strength of the samples containing CF within the scope of the study. The high amount of material that spalling in the samples containing CF in this section is also due to the air void created by the fibers. The air voids formed by the fibers absorbed the solution on the trowelled surface of the samples. The absorbed NaCl solution

caused spalling in the samples as a result of freeze-thaw cycles. Since the solution on the samples containing CF was absorbed by the sample, it was refreshed at regular intervals. However, since the void ratio was low in the other samples that did not contain fibers, the solution was not absorbed, remained on the surface all the time, and small amount of spalling occurred. Due to the formation of more air voids in composites containing 0.3% CF, more spalling compared to composites containing 0.1% CF, supporting the stated view. On the other hand, no significant effect of PCM on reducing scaling damage was detected in CF samples. According to the GDH Concrete Pavement Technical Specification, the mass loss as a result of scaling must be less than 1.5 kg/m^2 in places with freeze-thaw effects and where de-icing agents are used. It is observed that even the PCM(6)CF(0.3) coded sample, which has the highest damage and a material loss value of 0.923 kg/m^2, remains below the specification limit. In field applications, it is planned to use air-entraining additives in order to prevent spalling damage caused by CFs.

Figure 4.51. The spalling material from the PCM(6)CF(0.3) coded composite

4.7. Results of Bond Strength Tests

4.7.1. Slant Shear Test

The stages of the slant shear test are given in Figure 4.52. Table 4.25 shows the slant shear test findings and rupture patterns between PCM-added composites of varying thicknesses and the substrate asphalt/concrete. The results were given in the table were

taken as the average of four values. The test results were obtained by dividing the maximum load at the moment of rupture, which is caused by the pressure loading, by the elliptical interfacial area. In both the asphalt substrate and the concrete substrate, all of the rupture patterns on the 28th day occurred from the substrate. On the other hand, regardless of the substrate type, the shear strength value tended to increase as the hydration age progressed. The reason for this in the asphalt substrate is that the self-compacting and fluid consistency PCM-added composite fills the surface voids of the asphalt sample at a high rate and provides adequate adherence, which then increases due to the development of hydration products (C-S-H gel and $Ca(OH)_2$). In the concrete substrate, the reason for this situation is the mechanical locking forces provided by the hydration products in the cold joint zone (Peng et al., 2019). In the asphalt substrate, the value of 3.5 MPa on day 1st increased to 11.7 MPa 7th day. In the concrete substrate, the value of 2.3 MPa on the 1st day increased to 12.7 MPa on the 7th day. Especially when the test results on the 28th day were examined, in both substrates was provided strength values above 13.8 MPa (Chynoweth et al., 1996).

Table 4.25. Results of slant shear strength test

Substrate Type	**Slant Shear Strength (MPa)**			**Rupture Pattern**
	Day 1	**Days 7**	**Days 28**	**Days 28**
Asphalt Substrate	3.5	11.7	15.5	All from the substrate
Concrete Substrate	2.3	12.7	15.7	All from the substrate

Figure 4.52. Stages of slant shear test

4.7.2. Pull-Off Test

The direct tensile bond strength test results and rupture patterns between the PCM added composites with different thicknesses and the substrate asphalt were given in Table 4.26. Direct pull-off test was performed on the 1st, 7th, and 28th days with three samples. The results were given in the table were taken as the average of three values. While it was expected that the bond strength would rise with increasing composite thickness due to an increase in composite weight, this did not occur. On all test days, findings from different composite thicknesses were close. The bond strength values at the 7th and 28th days increased by about 50% in all of the composites as compared to the first day. The reason for this is that the hydration products of the PCM added composite in fluid consistency penetrating the porous surface structure of the asphalt, are improving day by day to increase the adherence.

Table 4.26. Results of pull-off test for asphalt substrate

Thickness	Bond Strength (MPa)			Rupture Pattern
	Day 1	Days 7	Days 28	Days 28
1 cm	0.99	1.45	1.54	All from the substrate
2 cm	0.96	1.40	1.44	Two from the substrate One from the interface
3 cm	0.97	1.54	1.52	All from the substrate
4 cm	0.94	1.47	1.42	Two from the substrate One from the interface
5 cm	0.91	1.39	1.41	All from the interface

When the 1st day test results are evaluated, it was seen that different thicknesses give close results (between 0.9 and 1 MPa). Similarly, on day 7, all composites gave similar results which between 1.39 and 1.54 MPa, and on day 28, between 1.41 and 1.54 MPa. On the 1st day, the 1 cm thick sample, on the 7th day the 3 cm thick sample, and on the 28th day, the 1 cm thick sample showed the best performance. On the other hand, the 5 cm thick sample showed the worst performance on all test days and the entire ruptures occurred at the interface. When the rupture patterns were examined, all of the 1 cm and 3 cm thick samples broke off from the substrate, while two of the 2 cm and 4 cm thick samples broke off from the substrate and one was from the interface. In Figure 4.53, the rupture patterns of the samples with a thickness of 4 cm were given.

Figure 4.53. The rupture patterns formed on the 28th day in the 4 cm-thick sample

The direct tensile bond strength test results and rupture patterns between the PCM added composites with different thicknesses and the substrate concrete were given in Table 4.27. Direct pull-off test was performed on the 1st, 7th, and 28th days with three samples. The results were given in the table were taken as the average of three values. While it was expected that the bond strength would increase due to the increase in the weight of the composite with the increase of the composite thickness, this situation did not occur. In all composites with different thicknesses, C-S-H products and $Ca(OH)_2$, which developed more as the hydration age progressed, increased the adherence in the cold joint region between the two layers. When the test results on the 1st day were examined, the best performance was shown by the 1 cm thick sample with a bond strength value of 1.37 MPa. At day 7, all thickness values gave close results which between 1.38 and 1.46 MPa. On the 28th day, 1 cm and 3 cm thick specimens provided bond strength values of 1.55 and 1.57 MPa, respectively, while all ruptures occurred from the substrate. The most unfavorable performance was observed in the 5 cm thick sample with a bond strength of 1.33 MPa, where one rupture occurred from the substrate and two rupture from the interface. In Figure 4.54, the rupture patterns of the samples with a thickness of 1 cm and 5 cm were given, and in Figure 4.55, the rupture patterns of the samples with a thickness of 2 cm were given on the 28th day. On the 28th day, the bond strength values exceeded the minimum value of 1.4 MPa determined in the study of Sprinkel and Özyıldırım (2000) between all thicknesses of the PCM added composite and the asphalt substrate sample,

and also between thicknesses of the PCM added composite (except 5 cm thickness) and the concrete substrate.

Table 4.27. Results of pull-off test for concrete substrate

Thickness	**Bond Strength (MPa)**			**Rupture Pattern**
	Day 1	**Days 7**	**Days 28**	**Days 28**
1 cm	1.37	1.45	1.55	All from the substrate
2 cm	0.92	1.46	1.52	Two from the substrate, One from the interface
3 cm	0.86	1.43	1.57	All from the substrate
4 cm	1.07	1.34	1.47	Two from the substrate One from the interface
5 cm	1.18	1.38	1.33	One from the substrate Two from the interface

Figure 4.54. The rupture patterns formed on the 28th day in 1 cm and 5 cm samples

Figure 4.55. Samples that broke off as a result of the test on the 28th day in the sample with a thickness of 2 cm

4.8. Microstructural Analysis Results of Cementitious Composites

SEM analysis was carried out in order to evaluate the conductive CF samples and the samples containing PCM in terms of microstructural properties. Since the size of the SFs was larger than the sample taken for analysis, it could not be detected in the SEM analysis, while the homogeneity of the distribution of these fibers was evaluated visually (Figure 4.3). In Figure 4.56, Figure 4.57 and Figure 4.58, images of the reference sample (CF(0) coded composite) taken from different regions under SEM analysis were given. In Figure 4.56 and Figure 4.57, it was seen that the C-S-H gel is predominantly present with a low percentage of ettringite crystals. On the other hand, especially in Figure 4.56 and Figure 4.58, it was seen the regions where the CH plates formed as a result of hydration reactions are dense.

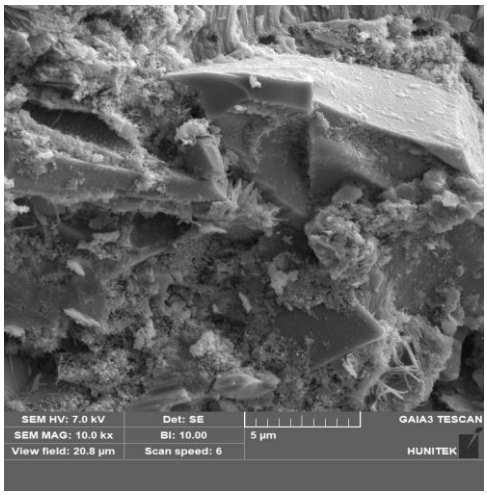

Figure 4.56. First image of reference sample with 10000x magnification

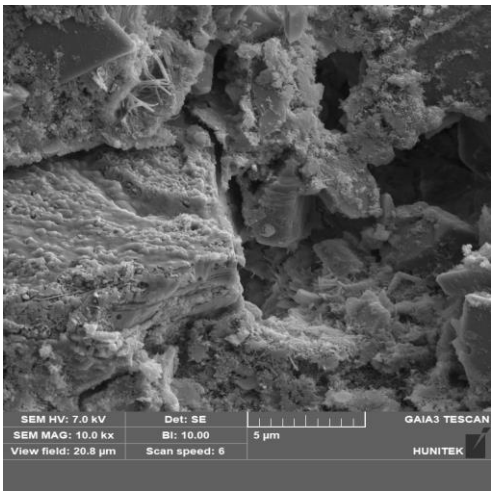

Figure 4.57. Second image of reference sample with 10000x magnification

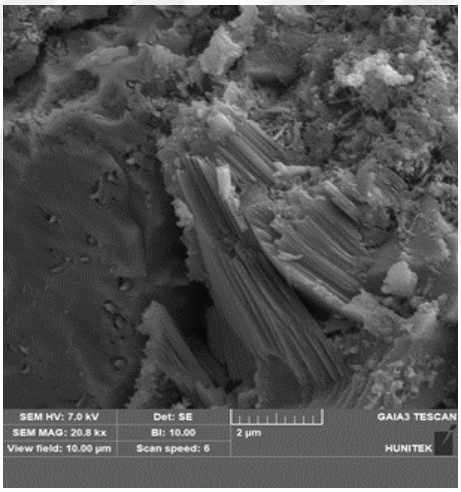

Figure 4.58. Third image of reference sample with 10000x magnification

On the other hand, SEM analysis was also carried out on the CF(0.1), CF(0.3) and also CF(0.5) with the highest probability of not dispersing homogeneously and bunching. SEM analysis image of the CF(0.1) was given in Figure 4.59. In the image, it was seen that the fibers had different directions and no clustering was observed. Figure 4.60 shows the SEM analysis of the CF(0.3). In this sample, the fibers were in close proximity to each other due to fiber ratio increasing compared to the CF(0.1) composite. However, there was no clustering tendency. However, fibers appearing shorter in the image and thought to be broken were also encountered. It is thought that the break in the fiber is not during mixing in the mixer, but during sampling for SEM analysis. On the other hand,

150x magnification SEM analysis image of the CF(0.5) composite which the highest carbon ratio was used in the study is given in Figure 4.61. The image shows the distribution of CFs with hydration products. It was seen that the fibers are not close to each other and have different directions at certain intervals. The absence of any bunching or clumping in this sample indicates that the mixtures with sufficient viscosity were mixed at the appropriate speed and for a sufficient time.

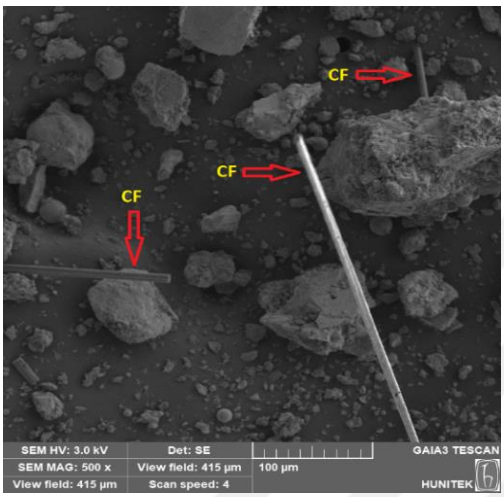

Figure 4.59. 500x magnification image of CF(0.1) composite

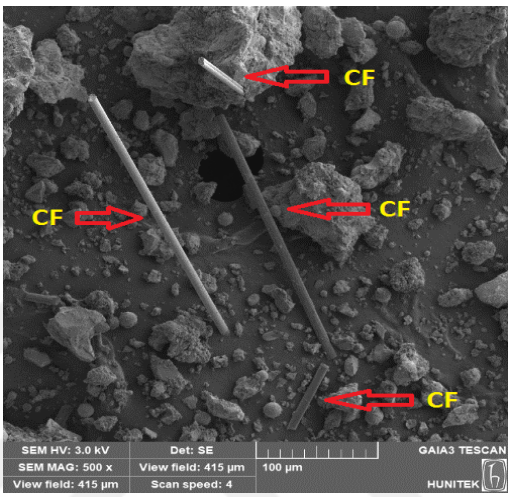

Figure 4.60. 500x magnification image of CF(0.3) composite

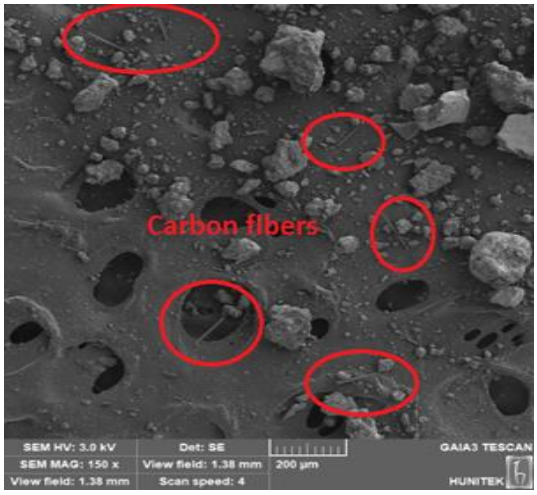

Figure 4.61. 150x magnification image of CF(0.5) composite

On the other hand, it is important that the microcapsules are distributed and not damaged in order for the PCM to be effective in the composite. It was determined from the SEM images that the microcapsules did not take any damage in general, even though a few were seen to be harmed for the PCM(2)CF(0) and PCM(4)CF(0) composites in Figure 4.62 and Figure 4.63, respectively. It was understood that the damaged PCMs explode and the PCM inside is discharged. However, it was seen that the other microcapsules in the images continue their effectiveness without being damaged. The PCM(6)CF(0) composite images were shown in Figure 4.64, Figure 4.65, Figure 4.66 and Figure 4.67. In the Figure 4.64, ettringite fibers were visible around the microcapsules in the PCM(6)CF(0) composite, but it was seen that this formation did not cause any damage. Figure 4.65 shows that the microencapsulated PCMs were dispersed and undamaged with no aggregation trend. However, in the Figure 4.66, it was seen that although the microcapsules could not maintain their spherical form, they did not explode. As in the studies conducted, the shell structure could be so flexible that it provided stability to the microcapsules against external effects such as formation of C-S-H gels or thermal expansion (Aguayo et al. 2016, Xiong, Shah and Kua, 2021). However, the crack line formed in the cement paste was observed to merge with the intermediate region of the PCM-cement paste, which was the one of the reasons for the strength reduction detected for the PCM-incorporated composites. Cui et al. (2018) also stated that due to the incompatibility between the microcapsule (organic) and the matrix (inorganic), a weak intermediate zone was formed between the two, which negatively affected the mechanical property (Figure 4.66 and Figure 4.67). The SEM images obtained for the PCM(8)CF(0) composite with different magnification factors were shown in Figure 4.68. Although the microencapsulated PCMs were concentrated in some areas of the composite, in general, it is considered that their distribution was homogeneous. No damaged or ruptured microcapsule was determined. The images show that the bond between the microcapsules and the cement paste seemed to be quite good and contained low void ratio. In addition, it was found that the microencapsulated PCMs became embedded in hydration products (C-S-H gels and CH plates).

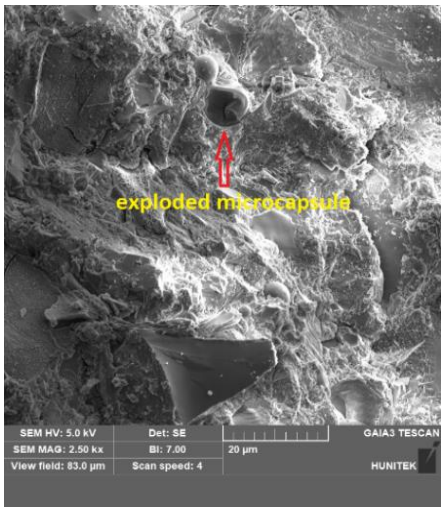

Figure 4.62. 2500x magnification image of PCM(2)CF(0) composite

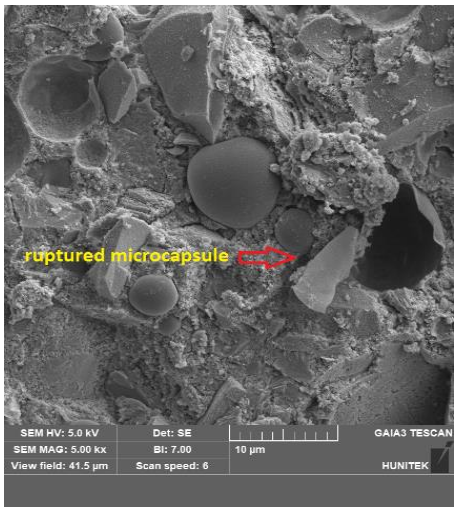

Figure 4.63. 5000x magnification image of PCM(4)CF(0) composite

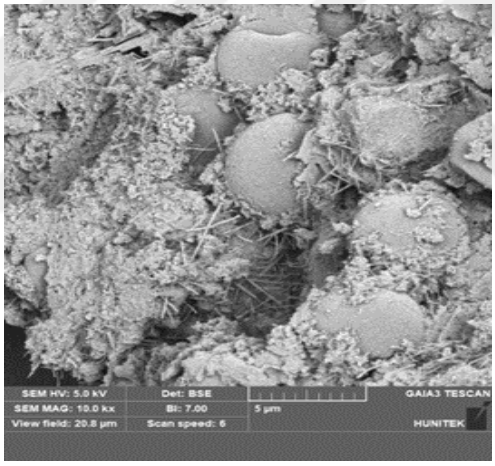

Figure 4.64. Ettringite formation around microcapsules for PCM(6)CF(0)

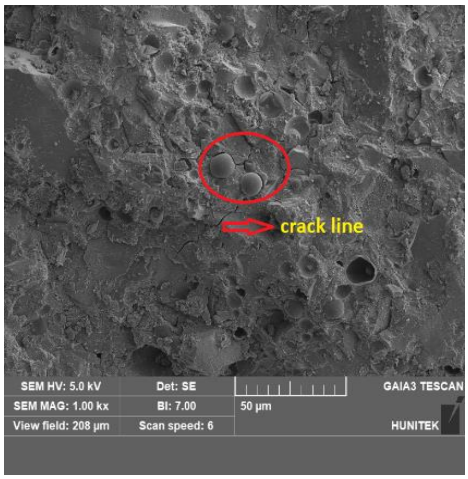

Figure 4.65. Distribution of PCM microcapsules for the PCM(6)CF(0) composite

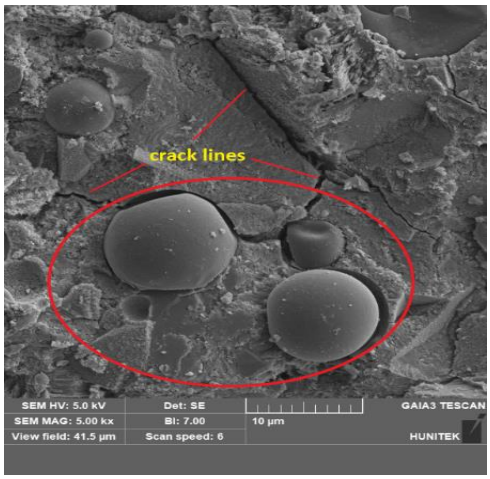

Figure 4.66. Flexible structure of microcapsules for the PCM(6)CF(0) composite

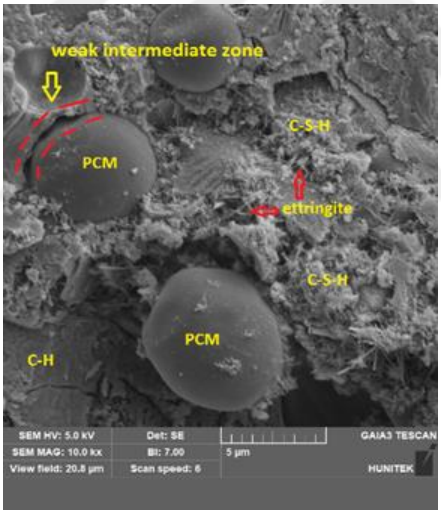

Figure 4.67. 10000x magnification image of PCM(6)CF(0) composite

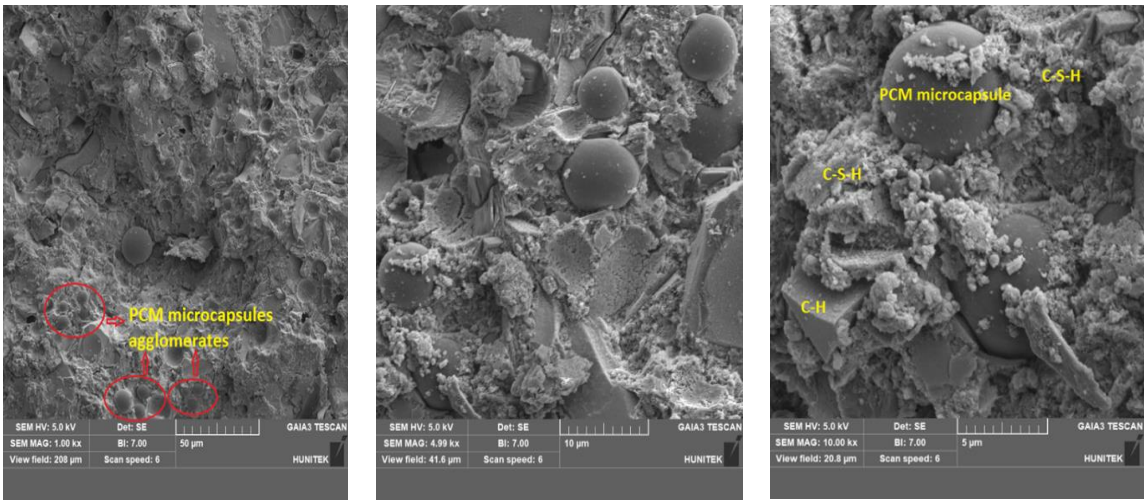

Figure 4.68. SEM image of the PCM(8)CF(0) composite at different magnification factors

SEM analysis was performed on the composites containing 0.1% CF by volume and 2, 4, 6 and 8 % PCM by weight of cement, which showed optimum performance in the tests of the project studies. In Figure 4.69, an SEM image of the PCM(2)CF(0.1) coded composite with 2500x magnification was given. In the analysis, it was observed that the PCMs around the CF were dispersed in the matrix without any agglomeration and remained embedded among the hydration products. Various microcapsule sizes found in the cumulative particle size (Figure 3.9) analysis were visually detected in this SEM analysis, also. It is known that the fine particle size makes the heat transfer more effective as it increases the surface area. In Figure 4.70, the 5000x magnification image of the PCM(4)CF(0.1) coded composite was given. In the figure, a microcapsule could not maintain its spherical form between the CH plates. However, due to its flexible structure, the microcapsule did not explode and proceeded its activity. In the SEM analysis of PCM(6)CF(0.1) composite, it was determined that one microcapsule exploded (Figure 4.71). The 1000x magnification SEM image of the sample coded PCM(8)CF(0.1), which was one of the mixtures in which the PCM ratio is used the highest, was given in Figure 4.72. When the figure was examined, it was understood that the microcapsules among the hydration products are dispersed to every point without being damaged. Due to its high usage rate, it was seen in the figure that there are more microcapsules than other mixtures.

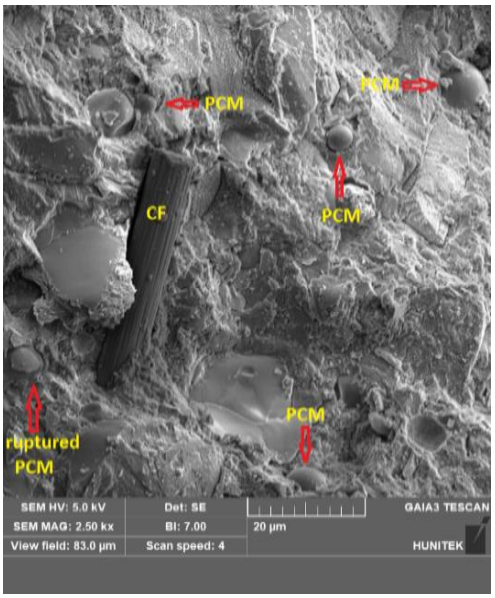

Figure 4.69. 2500x magnification image of PCM(2)CF(0.1) composite

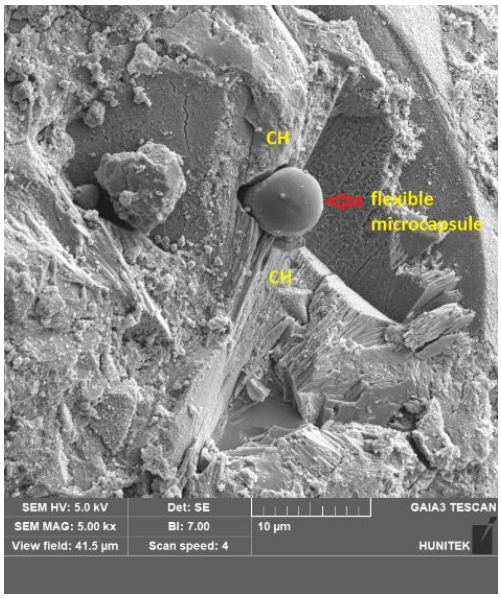

Figure 4.70. 5000x magnification image of PCM(4)CF(0.1) composite

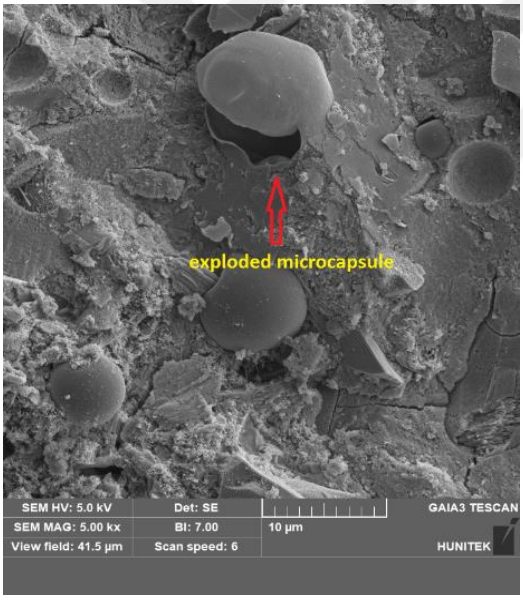

Figure 4.71. 5000x magnification image of PCM(6)CF(0.1) composite

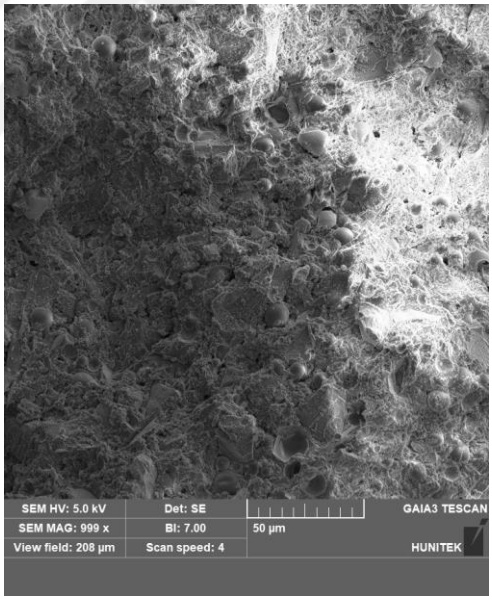

Figure 4.72. 1000x magnification image of PCM(8)CF(0.1)

5. CONCLUSION

The aim of the thesis is to contribute to overcoming the transportation problems caused by snow and ice in important infrastructures such as roads, airports and bridges by utilizing the heat energy that PCMs will release/absorb at phase change temperatures. In addition, thanks to PCM, it is intended to reduce freeze-thaw and de-icing salt damages and to reduce mechanical method, de-icing salt and maintenance and repair costs. With this thesis, multifonctional cementitious composites with self-melting snow/ice ability that can be applied as overlay on asphalt and concrete pavements have been developed.

With the thesis studies, the following results were obtained, respectively;

- With the application of composites with self-melting snow/ice capabilities in significant superstructures like highways, bridges, and airports and also it is intended to go into operation early so that it does not adversely affect road and airway traffic. In this direction, CEM I 52.5 R cement was used in order to establish early strength in the composites and the water/cement ratio was kept at 0.36. In the studies carried out to determine the reference composite without fiber and PCM, 42.8 MPa was reached in 24 hours. The reference composite also provided 72.2 MPa at day 28. On the other hand, SFs used to improve conductivity increased the compressive strength, while CFs adversely affected the strength. While the SF(5) reached 85.6 MPa strength on 28th day, the CF(0.5) remained at 48.5 MPa. On the other hand, it was determined that the compressive strength was negatively affected as the PCM ratio increased in the mixtures containing PCM. However, the mixture with the code PCM(6)CF(0.1), which is to be proposed within the scope of the thesis studies, showed a sufficient performance by providing a compressive strength value of 28.0 MPa on the 1st day and by providing a strength value of 53.3 MPa on the 28th day.

- Among the objectives of the thesis is to show the self-levelling feature of the composites. In this context, mini slump flow diameter (mm) and T_{500} (sec) tests were carried out in order to determine the consistency and workability properties of the composites formed. Studies have shown that CFs reduce the workability of

composites. While the mini slump flow diameter of the CF(0) coded mixture was 360 mm and the T_{500} time was 2.9 seconds, the mini slump flow diameter of the CF(0.5) coded mixture was 210 mm and the T_{500} time was 4.9 seconds. SFs, on the other hand, did not adversely affect workability as much as CFs. The mini slump flow diameter of the mixture coded SF(5) was 300 mm and the T_{500} time was 3.4 seconds. When the mixtures containing PCM were examined, it was observed that the mini slump flow diameter decreased and the T_{500} time shortened with the increase of the PCM ratio. Liquid dispersion containing PCM increased the workability of the mixtures. The mixture coded PCM(6)CF(0.1), which is considered to be proposed within the scope of the project studies, had a mini slump flow diameter of 305 mm and a T_{500} time of 3.3 seconds.

- In the scope of the study, conductivity properties of cement-based composites were developed thanks to CFs and SFs. Regardless of the fiber type and ratio, it was observed that the hydration products formed in all composites tend to decrease the electrical and thermal conductivity as the hydration age progresses. The electrical resistance of the CF(0.5) coded composite, which showed the highest conductivity performance among CF composites, was 233 Ω on the 1st day, while this value was 440 Ω on the 28th day. CF(0.5) coded composite was the sample that was least affected by the hydration age thanks to its high CF content. In addition, the thermal conductivity value of this composite on the 28th day was 1210 mW/m.K, and the highest thermal conductivity among the composites was obtained. The electrical resistance of the SF(5) coded composite, which showed the highest performance among SF composites, was 210 Ω on the 1st day, while this value was 1670 Ω on the 28th day. The advancement of hydration age increased the resistance of SF composites more than CF composites. On the other hand, SF(5) coded composite showed the best performance among the thermal conductivity values in the samples containing SF. The thermal conductivity value of this composite, which was 1160 mW/m.K on the 7th day, decreased to 1090 mW/m.K on the 28th day. Correlation relationships between electrical resistance and thermal conductivity on the 7th and 28th days were also examined in the study. While it was observed that there was no correlation relationship in the mixtures containing CF on the 7th day, a moderate correlation (R^2=0.5413) was detected in

the mixtures containing SF. On the 28th day, while no correlation was found in mixtures containing SF, a low level of correlation (R^2=0.2638) was observed in mixtures containing CF. The absence of high correlation coefficients between the two conductivity types was associated with the operation of conductivity measurement methods with different techniques.

- In the later parts of the project, PCM was added to the composites with improved conductivity in order to provide snow/ice melting capability. It is known to reduce temperature variations in systems where PCM is involved. In this context, samples with low, medium and high thermal conductivity containing 2, 4, 6 and 8 % PCM in proportion to cement weight were produced in the project. Freeze/thaw simulations with two different temperature systems, +20/-20 °C and +10/-10 °C, were applied to these samples. Freeze-thaw temperature amplitudes decreased at the highest level in PCM(8)CF(0) coded composite. While the temperature amplitudes of this composite decreased by 0.89 °C in the first simulation, it decreased by 2.03 °C in the second simulation. However, studies have shown that CFs added to composites at the rate of 0.1% and 0.3% by volume increase the freeze-thaw temperature amplitudes and the included PCM partially reduces this amplitude increase. The highest temperature amplitude increase was experienced in the PCM(0)CF(0.3) coded composite without PCM. While this composite increased the temperature amplitudes by 1.71 °C in the first simulation, it increased by 1.33 °C in the second simulation. However, within the scope of the thesis studies, it was determined that the contribution of the samples containing PCM to reduce the temperature amplitudes in the second simulation is higher than in the first simulation. For example, in PCM(4)CF(0.1) coded composite, the temperature amplitudes decreased by 0.32 °C in the first simulation, while they decreased by 1.02 °C in the second simulation. The reason for this situation is that the energy released or absorbed by the PCM at the maximum and minimum temperature values of the +10/-10 °C cycle has not been exhausted yet.

- Freeze-thaw cycles made by adding 2, 4, 6 and 8 % PCM to samples with low, medium and high thermal conductivity were applied at fixed sample sizes. In

order to get an idea about the overlay thickness to be applied in the field, freeze-thaw cycles were also tested in different composite thicknesses. In this direction, the PCM(0)CF(0) coded reference sample, PCM(6)CF(0) coded sample and PCM(6)CF(0.1) coded sample, which showed optimum performance in the previous section, were used. PCM(6)CF(0.1) coded composite, which is planned to be proposed as a result of the project studies, has the most positive performance by increasing the amplitude by 0.13 °C in 40 mm thickness (in the first simulation) and decreasing the amplitude by 0.15 °C in 50 mm thickness (second simulation).

- Ice melting performance test was conducted to measure the snow/ice melting potential of the producing composites. Samples containing 0.1% by volume CF with moderate thermal conductivity showed the best melting performance. It was determined that as the PCM ratio increased in these samples, the ice melting rate increased. On the other hand, the ice melting performances of the reference sample and the CF-free samples were close. PCM(8)CF(0.1) coded composite with 1.04 g/h ice melting speed showed the best performance among the composites. In addition, samples of different thicknesses of the PCM(6)CF(0.1) coded composite were also subjected to the ice melting performance test at a constant temperature of 1.5 °C. Among the different thicknesses of the PCM(6)CF(0.1) coded composite, the 30 mm thick composite with 0.56 g/h ice melting speed showed the best performance.

- The Test of Scaling Resistance was carried out over 56 cycles in accordance with the " Slab Test Method" specified in the TS EN 12390-9 standard. Very low spalling damage occurred in all CF-free and PCM containing/non-PCM samples. However, in the samples containing CF, the air voids formed by the fibers increased the scaling damage and caused material loss. It was observed that PCM(6)CF(0.3) coded composite, which has the highest scaling damage, 0.923 kg/m^2 material loss among the samples, is below the 1.5 kg/m^2 limit determined by the GDH Concrete Pavements Technical Specification. However, no significant effect of PCM on reducing scaling damage was detected in CF-

containing samples. In field applications, it is planned to use air-entraining additives in order to prevent scaling damage caused by CFs.

- Within the scope of the project works, it was planned to use the composites with self-melting ability snow/ice as a overlay on asphalt and concrete pavements in a way that will create sufficient adherence. In this direction, Slant Shear and Pull Off tests were carried out to measure the bond strength between two layers. According to the slant shear test results, the PCM(6)CF(0.1) composite provided by strength values of 15.47 MPa on the 28th day with the asphalt substrate and 15.65 MPa on the 28th day with the concrete substrate. However, in the pull-off test measured between cement-based composites and the concrete substrate, the best performance was demonstrated by the 1 cm thickness with 1.55 MPa strength value and the 3 cm thick sample with 1.57 MPa strength value at 28th day. At these thickness values that showed the best performance, the entire rupture pattern was from the substrate.

- In the SEM analysis, it was determined that the CFs were dispersed without showing a clustering tendency. On the other hand, it was understood that the microcapsules containing PCM were not damaged to a great extent and had a sufficient and homogeneous distribution in the composite in general.

- As a result of the thesis studies, the mixture, which finally showed optimum performance and was planned to be recommended in applications, was a 30 mm thick PCM(6)CF(0.1) coded composite. The properties of this composite are presented below;
  - The composite has a mini-spread diameter of 305 mm, a T_{500} time of 3.3 s, and is self-levelling feature.
  - The composite reached compressive strength values of 28.0 MPa on the 1st day, 34.7 MPa on the 3rd day, 42.8 MPa on the 7th day and 53.3 MPa on the 28th day.

- The electrical resistance of the CF(0.1) coded sample, which has the same CF ratio as the PCM(6)CF(0.1) composite, was 305 Ω on the 1st day and 1670 Ω on the 28th day. The thermal conductivity value of CF(0.1) was 1150 mW/m.K on the 1st day and 986 mW/m.K on the 28th day. The electrical resistance of the composite itself was 388 Ω on day 1 and 1983 Ω on day 28.
- In this composite, the temperature amplitudes increased by 1.38 °C in the first simulation, and increased by 0.42 °C in the second simulation.
- This composite had an ice melting rate of 0.56 g/h in a cabinet with a constant temperature of 1.5 °C in a laboratory environment. This speed is 143% higher than the ice melting speed of the reference sample and 70% higher than the speed of the PCM(6)CF(0) coded sample without CF.
- The composite lost 0.776 kg/m^3 of material as a result of the scaling test.
- Composite yielded slant shear strenght value of 15.47 MPa on day 28 with asphalt substrate and 15.65 MPa on day 28 with concrete substrate, and all fracture patterns occurred in the substrate.
- The direct tensile bond strength was 1.52 MPa with between the composite and substrate asphalt and 1.57 MPa with between the composite and the substrate concrete. And also, all of the rupture patterns occurred in the substrate.

6. REFERENCES

Abdulla H., Design, construction, and performance of heated concrete pavements system, Graduate Thesis, Iowa State University, **2018.**

Acıkök, F., Mineral Katkılar İçeren Beton Yol Karışımlarının Mekanik ve Durabilite Özelliklerinin İncelenmesi, Yüksek Lisans Tezi, Yıldız Teknik Üniversitesi, İstanbul, **2019.**

Aguayo, M., Das, S., Maroli, A., Kabay, N., Mertens, J.C.E, Rajan, S.D., Sant, G., Chawla, N. and Neithalath, N., The influence of microencapsulated phase change material (PCM) characteristics on the microstructure and strength of cementitious composites: Experiments and finite element simulations, Cement and Concrete Composites, 73 **(2016)** 29–41.

Al-Dahawi, A., Sarwary, M.H., Öztürk, O., Yıldırım, G., Akın, A., Şahmaran, M. and Lachemi, M., Electrical percolation threshold of cementitious composites possessing selfsensing functionality incorporating different carbon-based materials, Smart Materials and Structures, 25 **(2016)** 10.

Al-Dahawi, A., Öztürk, O., Emami, F., Yıldırım, G. and Şahmaran, M., Effect of mixing methods on the electrical properties of cementitious composites incorporating different carbon-based materials, Construction and Building Materials, 104() **(2016)** 160–168.

Anand, P., Ceylan, H., Taylor, P. and Pyrialakou, V.D., Cost comparison of alternative airfield snow removal methodologies, Civil, Construction and Environmental Engineering, Iowa State University, **2014.**

Ansuini, R., Larghetti, R., Giretti, A. and Lemma, M., Radiant floors integrated with PCM for indoor temperature control, Energy and Buildings, 43(11) **(2011)** 3019–3026.

Anupam, B.R., Sahoo, U.C. and Rath, P., Phase change materials for pavement applications: A review, Construction and Building Materials, 247 **(2020)** 118553.

Asadi, I., Shafigh, P., Hassan Z.F.B.A. and Mahyuddin N.B., Thermal conductivity of concrete - A review, Journal of Building Engineering, 20 **(2018)** 81-93.

Aydın, A.A. and Okutan H., Faz Değişim Malzemeleri ve Isı Enerjisinin Depolanması, İstanbul Sanayi Odası - İstanbul Teknik Üniversitesi Doktora / Yüksek Lisans Tezlerine Sanayi Desteği Projesi, **2010**.

Bai, Y.H., Chen, W., Chen, B. and Tu, R., Research on electrically conductive concrete with double-layered stainless SFs for pavement deicing, ACI Materials Journal, 114(6) **(2017)** 935–43.

Belli, A., Mobili, A., Bellezze, T. and Tittarelli, F., Commercial and recycled carbon/steel fibers for fiber-reinforced cement mortars with high electrical conductivity. Cement and Concrete Composites, 109 **(2020)** 103569.

Bentz, D.P. and Turpin, R., Potential applications of phase change materials in concrete technology, Cement and Concrete Composites, 29 (7) **(2007)** 527– 532.

Berberoğlu, Ş., Beton yollarda buz çözücü tuz etkisine su-çimento oranının etkileri, Yüksek Lisans Tezi, Sakarya Üniversitesi, Sakarya, **2011**.

Bhattacharjee, B. and Krishnamoorthy, S., Permeable porosity and thermal conductivity of construction materials, Journal of Materials in Civil Engineering, 16(4) **(2004)** 322-330.

Bonaldo, E., Barros, J.A.O. and Lourenço P.B., Bond characterization between concrete substrate and repairing SFRC using pull-off testing, International Journal of Adhesion and Adhesives, 25(6) **(2005)** 463–474.

Boulekbache, B., Hamrat, M., Chemrouk, M. and Amziane, S., Flowability of fibre-reinforced concrete and its effect on the mechanical properties of the material, Construction and Building Materials, 24(9) **(2010)**1664–1671.

Campbell-Allen, D. and Thorne, C.P., The thermal conductivity of concrete, Magazine of Concrete Research, 15(43) **(1963)** 39–48.

Casanova, P., Rossi, P. and Schaller, I., Can SFs replace transverse reinforcement in reinforced concrete beams?, ACI Materials Journal, 94(5) **(1997)** 341–54.

Chuang, W., Geng-sheng, J., Bing-liang, L., Lei, P., Ying, F., Ni, G. and Ke-zhi, L., Dispersion of CFs and conductivity of CF-reinforced cement-based composites, Ceramics International, () **(2017)** S027288421731739X–.

Chung, D.D.L., Cement reinforced with short CFs: a multifunctional material, Composites Part B: Engineering, 31(6-7) **(2000)** 511–526.

Chynoweth, G., Stankie, RR., Allen, WL., Anderson, RR., Babcock, WN. and Barlow, P., Concrete repair Guide, ACI Committee, Concrete Repair Manual, 546 **(1996)** 287-327.

Cui, H., Feng, T., Yang, H., Bao, X., Tang, W. and Fu J., Experimental study of CF reinforced alkali-activated slag composites with micro-encapsulated PCM for energy storage, Construction and Building Materials, 161 **(2018)** 442–451.

Devpura, A., Phelan, P. E. and Ravi, S., Size effects on the thermal conductivity of polymers laden with highly conductive filler particles, Microscale Thermophysical Engineering, 5(3) **(2001)** 177–189.

Ding, S., Dong, S., Wang, X., Ding, S., Han, B. and Ou, J., Self-heating ultra-high performance concrete with stainless steel wires for active deicing and snow-

melting of transportation infrastructures, Cement and Concrete Composites, 138 **(2023)** 105005.

Du L., and Folliard K.J., Mechanisms of air entrainment in concrete, Cement and Concrete Research, 35(8) **(2005)** 1463–1471.

Esping, O., Early age properties of self-compacting concrete, Ph.D. Thesis, Chalmers University of Technology, Göteborg, Sweden, **2007.**

Faneca, G., Segura, I., Torrents, J.M. and Aguado, A., Development of conductive cementitious materials using recycled carbon fibres, Cement and Concrete Composites, 92 **(2018)** 135–144.

Farnam, Y., Krafcik, M., Liston, L., Washington, T., Erk, K., Tao, B. and Weiss, J., Evaluating the Use of Phase Change Materials in Concrete Pavement to Melt Ice and Snow, Journal of Materials in Civil Engineering, 28 **(2015)** 04015161–.

Farnam, Y., Esmaeeli, H., Zavattieri, P., Haddock, J. and Weiss, J., Incorporating Phase Change Materials in Concrete Pavement to Melt Snow and Ice, Cement and Concrete Composites, 84 **(2017)** 134-145.

Fay, L., Volkening, K., Gallaway, C. and Shi, X., Performance and Impacts of Current Deicing and Anti-Icing Products: User Perspective versus Experimental Data, Transportation Research Board 87th Annual Meeting, Washington DC, United States, **2008**.

Fernandes, F., Manari, S., Aguayo, M., Santos, K., Oey, T., Wei, Z., Falzone, G., Neithalath, N. and Sant, G., On the feasibility of using phase change materials (PCMs) to mitigate thermal cracking in cementitious materials, Cement and Concrete Composites, 51 **(2014)** 14-26.

Folliard, K., Riding, K., Schindler, A., Pesek, P. and Drimalas, T., Concrete works V3 training/user manual concreteworks software (P2). Austin, TX: Univ. of Texas at Austin, **2017**.

Fu, X. and Chung D.D.L., Effects of silica fume, latex, methylcellulose, and CFs on the thermal conductivity and specific heat of cement paste, Cement and Concrete Research, 27(12) **(1997)** 1799–1804.

Galao, O., Bañón, L., Baeza, F., Carmona, J. and Garcés, P., Highly Conductive CF Reinforced Concrete for Icing Prevention and Curing, Materials, 9(4) **(2016)** 281-.

Gao, J., Wang, Z., Zhang, T. and Zhou, L., Dispersion of CFs in cement-based composites with different mixing methods, Construction and Building Materials, 134() **(2017)** 220–227.

Gomis, J., Galao, O., Gomis, V., Zornoza, E. and Garcés, P., Self-heating and deicing conductive cement, Experimental study and modeling, Construction and Building Materials, 75 **(2015)** 442–449.

Günal, N., Türkiye'de Kar Yağışı, Karın Yerde Kalma Süresi ve Daimi Kar Sınırı, Çevrimiçi Tematik Türkoloji Dergisi, 1**(2013).**

Harris, D., Sarkar, J. and Ahlborn, T., Characterization of Interface Bond of Ultra-High-Performance Concrete Bridge Deck Overlays, Transportation Research Record: Journal of the Transportation Research Board, 2240() **(2011)** 40–49.

Hassan, Y., Abd El Halim, A.O., Razaqpur, A. G., Bekheet, W. and Farha M.H., Effects of Runway Deicers on Pavement Materials and Mixes: Comparison with Road Salt, Journal of Transportation Engineering, 128(4) **(2002)** 385-391.

Hawes, D.W., Banu, D. and Feldman D., The stability of phase change materials in concrete, Solar Energy Materials and Solar Cells, 27(2) **(1992)** 103–118.

Hunger, M., Entrop, A.G., Mandilaras, I., Brouwers, H.J.H. and Founti, M., The behavior of self-compacting concrete containing micro-encapsulated phase change materials, Cement and Concrete Composites, 31(10) **(2009)** 731-743.

İsmail, K.A.R., Salinas, C.T. and Henriquez, J.R., Comparison between PCM filled glass windows and absorbing gas filled windows, Energy and Buildings, 40 (5) **(2008)** 710–719.

İşsever, F., Süperakışkanlaştırıcılı Ve Mineral Katkılı Taze Çimento Hamuru Ve Harçların Reolojisi, Yüksek Lisans Tezi, İstanbul Teknik Üniversitesi, Fen Bilimleri Enstitüsü, **2002**.

Jayalath, A.R., Nicolas, S., Sofi, M., Shanks, R., Ngo, T., Aye, L. and Mendis P., Properties of cementitious mortar and concrete containing micro-encapsulated phase change materials, Construction and Building Materials, 120 **(2016)** 408–417.

Karalı, Ş., Yenilenebilir Enerji Kaynaklarının Türkiye ve Dünya Ekonomisine Katkısı, Yüksek Lisans Tezi, Bahçeşehir Üniversitesi, İstanbul, **2017**.

Karayolları Genel Müdürlüğü Tesisler ve Bakım Dairesi Başkanlığı, Kar ve Buzla Mücadele Rehberi, Ankara, **2018**.

Karayolları Genel Müdürlüğü, 2020 Yılı Devlet ve İl Yolları Bakım-İşletme Maliyetleri, **2021.** https://www.kgm.gov.tr/SiteCollectionDocuments/KGMdocuments/Istatistikler/YapimBakimIsletmeMaliyet/2020BakimisletmeMaliyetKitabi.pdf

Khan, M.I., Factors affecting the thermal properties of concrete and applicability of its prediction models, Building and Environment, 37(6) **(2002)** 607–614.

Kim, K.H., Jeon, S.E., Kim J.K. and Yang, S., An experimental study on thermal conductivity of concrete, Cement and Concrete Research, 33(3) **(2003)** 363–371.

Kitchener, B.G., Wainwright, J., Parsons, A.J., A review of the principles of turbidity measurement, Progress in Physical Geography: Earth and Environment, 41(5) **(2017)** 620–642.

Koru, M., Determination of Thermal Conductivity of Closed-Cell Insulation Materials That Depend on Temperature and Density, Arabian Journal for Science and Engineering, 41**(2016)** 4337–4346.

Kuder, K.G.,Ozyurt, N., Mu, E.B. and Shah, S.P., Rheology of fiber-reinforced cementitious materials, Cement and Concrete Research, 37(2) **(2007)** 191–199.

Kuznik, F., David, D., Johannes, K. and Roux, J.J., A review on phase change materials integrated in building walls, Renewable and Sustainable Energy Reviews, 15 (1) **(2011)** 379-391.

Li, V.C. and Kanda T., Engineered cementitious composites for structural applications, ASCE J. Mater. Civil Eng.10(2) **(1998)** 66–9.

Liston, L., Using mixtures of fatty acid methyl esters as phase change materials for concrete, Purdue University, **2015**.

Liu, K., Lu, L., Wang, F. and Liang W., Theoretical and experimental study on multi-phase model of thermal conductivity for fiber reinforced concrete, Construction and Building Materials, 148 **(2017)** 465-475.

Lund, J.W., Pavement Snow Melting, Geo-Heat Center, Oregon Institute of Technology, Klamath Falls, OR, **2015**.

Lv, L., Yang, Z., Chen, G., Zhu, G., Han, N., Schlangen, E. and Xing, F., Synthesis and characterization of a new polymeric microcapsule and feasibility investigation in self-healing cementitious materials, Construction and Building Materials, 105 **(2016)** 487–495

Manning, B.J., Bender, P.R., Cote, S.A., Lewis, R.A., Sakulich, A.R. and Mallick, R.B., Assessing the feasibility of incorporating phase change material in hot mix asphalt, Sustainable Cities and Society, 19 **(2015)** 11–16.

Martinie, L., Rossi, P. and Roussel, N., Rheology of fiber reinforced cementitious materials: classification and prediction, Cement and Concrete Research, 40(2) **(2010)** 226–234.

Mehta, P.K. and Monterio, P.J.M., Concrete: Microstructure, Properties, and Materials, Third Edition, The McGraw-Hill Companies, New York, **2011**.

Meteoroloji Genel Müdürlüğü, 2019-2020 Yılları Kış Mevsimi Sıcaklıklarının Değerlendirilmesi, **2020**.
https://www.mgm.gov.tr/veridegerlendirme/sicaklik-analizi.aspx?ay=subat

Meteoroloji Genel Müdürlüğü. (2021). 2020-2021 Yılları Kış Mevsimi Sıcaklıklarının Değerlendirilmesi, **2021**. https://www.mgm.gov.tr/FILES/iklim/yillikiklim/mevsimlik-sicaklikanalizi-2020-kis.pdf

Mihashi, H., Nishiyama, N., Kobayashi, T. and Hanada, M., Development of a smart material to mitigate thermal stress in early age concret, Taylor & Francis: Abingdon, UK, 385–392, **2004.**

Neophytou, M. K. A., Pourgouri, S., Kanellopoulos, A. D., Petrou, M. F., Ioannou, I., Georgiou, G., and Alexandrou, A., Determination of the rheological parameters of self-compacting concrete matrix using slump flow test, Applied Rheology, 20(6) **(2010)** 62402.

Neville, A.M., Properties of Concrete. Fifth Edition, London, **2011.**

Norvell, C., Sailor, D. J. and Dusicka, P., The effect of microencapsulated phase-change material on the compressive strength of structural concrete, Journal of Green Building, 8(3) **(2013)** 116-124.

Özerkan, N.G., Evaluation of Air Void Parameters of Fly Ash Incorporated Self Consolidating Concrete by Image Processing, PhD. Thesis, Department of Civil Engineering, METU, Ankara, Türkiye, **2009.**

Peng, H., Zhang, Y., Wang, J., Liu, Y. and Gao, L., Interfacial Bonding Strength between Cement Asphalt Mortar and Concrete in Slab Track, Journal of Materials in Civil Engineering, 31(7) **(2019)** 04019107–.

Polat, R., The effect of antifreeze additives on fresh concrete subjected to freezing and thawing cycles, Cold Regions Science and Technology, 127 **(2016)** 10–17.

Powers, T.C. and Helmuth, R.A., Theory of volume changes in hardened Portland cement paste during freezing, Highway Research Board proceedings, 32 **(1953)** 285–297.

Qian, C., Gao, G., Zhu, C. and Guo, Z., Influence of phase change materials on temperature rise caused by hydration heat evolution of cement-based materials, Magazine of Concrete Research, 62(11) **(2010)** 789–794.

Rangaraju, P. R., Sompura, K., Desai, J. and Olek, J., Potential of Potassium Acetate Deicer to Induce ASR in Concrete, and Its Mitigation, American Society of Civil Engineers Airfield and Highway Pavements Specialty Conference, Atlanta, Georgia, United States, () **(2006)** 683–694.

Reza, F., Yamamuro, J. and Batson, G., Electrical resistance change in compact tension specimens of CF cement composites, Cement and Concrete Composites, 26(7) **(2004)** 873–881.

Sakulich, A.R. and Bentz, D.P., Incorporation of phase change materials in cementitious systems via fine lightweight aggregate, Construction Buildings Materials, 35 **(2012)** 483–490.

Sakulich, A. R. and Bentz, D. P., Increasing the Service Life of Bridge Decks by Incorporating Phase-Change Materials to Reduce Freeze-Thaw Cycles, Journal of Materials in Civil Engineering, 24(8) **(2012)** 1034–1042.

Sargam, Y., Wang, K. and Alleman, J.E., Effects of Modern Concrete Materials on Thermal Conductivity, Journal of Materials in Civil Engineering, ASCE Library, 32(4) **(2020)** 04020058.

Satish, K., Kumar, S., and Rai, B., Self compacting concrete using fly ash and silica fumes as pozzolanic material, Journal of Engineering Technology (ISSN: 0747-9964), 6(2) **(2017)** 394-407.

Savija, B., Smart Crack Control in Concrete through Use of Phase Change Materials (PCMs): A Review, Materials, 11(5) **(2018)** 654.

Seferoğlu, A., Seferoğlu, M. and Akpınar, V., Karayolu ve Havayolu Kaplamalarında Kullanılan Kar ve Buzla Mücadele Yöntemlerinin Mali Analizi, Gazi Üniversitesi Fen Bilimleri Dergisi Part C: Tasarım ve Teknoloji, 3(1) **(2015)** 407 – 416.

Sharifi, N.P. and Sakulich, A., Application of phase change materials to improve the thermal performance of cementitious material, Energy and Buildings, 103**(2015)** 83–95.

Shi, X., Impact of Airport Pavement Deicing Products on Aircraft and Airfield Infrastructure, Transportation Research Board, Washington, D.C, **2008.**

Shi, X., Akin, M., Pan, T. and Fay, L., Deicer Impacts on Pavement Materials: Introduction and Recent Developments, The Open Civil Engineering Journal, 3 **(2009)** 16-27.

Shin, A.H. and Kodide U. Thermal conductivity of ternary mixtures for concrete pavements, Cement and Concrete Composites, 34(4) **(2012)** 575–582.

Spragg, R., Bu, Y., Snyder, K, Bentz, D and Weiss, J., Electrical testing of cement-based materials: role of testing techniques, sample conditioning, and accelerated curing, Publication FHWA/IN/JTRP-2013/28, Joint Transportation Research Program, Indiana Department of Transportation and Purdue University, West Lafayette, Indiana, **2013**.

Sprinkel, M. and Ozyildirim, C., Evaluation of high performance concrete overlays placed on Route 60 over Lynnhaven Inlet in Virginia, Final report, Virginia Transportation, **2000.**

Sun, M., Liew, R.J.Y., Zhang, M.H. and Li, W., Development of cement-based strain sensor for health monitoring of ultra-high strength concrete, Construction and Building Materials, 65 **(2014)** 630–637.

Şahin, Y., Gündüz, Y. and Taşkan E., Çelik Tel Donatılı Betonların Kırılma Parametrelerinin Yapay Sinir Ağları ile Modellenmesi, Uluslararası Mühendislik Araştırma ve Geliştirme Dergisi, 12(2) **(2020)** 454-463.

Şahmaran, M., Christianto, H.A., and Yaman, İ.Ö., The effect of chemical admixtures and mineral additives on the properties of self-compacting mortars, Cement and Concrete Composites, 28(5) **(2006)** 432–440.

Şahmaran, M., Lachemi, M., and Li, V.C., Assessing the durability of engineered cementitious composites under freezing and thawing cycles, Concrete, **(2010)** 85.

Şahmaran, M., Beton Yapıların Hızlı Onarımı İçin Yüksek Performanslı Lif Donatılı Çimento Bağlayıcılı Kompozitler, TÜBİTAK Projesi, 112M035 Numaralı Proje, Ankara, **2013.**

Şahmaran, M., Elektrostatik Yük Boşaltma Kabiliyetine Sahip Yeni Nesil Çimento Bağlayıcılı Kompozitler, TÜBİTAK 1002-Hızlı Destek Programı, 119M175 Numaralı Proje, Ankara, **2020**.

Taylor, P.C., Kosmatka, S.H. and Voigt, G.F., Intagrated Materials and Construction Practies For Concrete Pavement. Iowa State University, U.S. Department of Transportation Federal Highway Administration, **2007.**

Uysal, H., Demirboğa, R., Şahin, R. and Gül, R., The effects of different cement dosages, slumps, and pumice aggregate ratios on the thermal conductivity and density of concrete, Cement and Concrete Research, 34(5) **(2004)** 845– 8.

Wang, C., Li, K.Z., Li, H-J., Jiao, G.S., Lu, J. and Hou, D.S., Effect of CF dispersion on the mechanical properties of CF-reinforced cement-based composites, Materials Science and Engineering: A, 487(1-2) **(2008)** 52–57.

Wang, R., Gao, X., Zhang, J. and Han, G., Spatial distribution of SFs and air bubbles in UHPC cylinder determined by X-ray CT method, Construction and Building Materials, 160() **(2018)** 39–47.

Weinläder, H., Klinker, F. and Yasin, M., PCM cooling ceilings in the Energy Efficiency Center – regeneration behaviour of two different system designs, Energy and Buildings, 156 **(2017)** 70–77.

Whiting, D., Deicer-scaling resistance of lean concrete containing fly ash, in: Proceedings of the Third International Conference on Fly Ash, Silica Fume, Slag, and Natural Pozzolans in Concrete, ACI Special Publication SP-123. **(1989)** 349–372.

Wiktor, V. and Jonkers, H.M., Field performance of bacteria-based repair system: Pilot study in a parking garage, Case Studies in Construction Materials, 2 **(2015)** 11–17.

Wu, J., Liu, J. and Yang, F., Three-phase composite conductive concrete for pavement deicing, Construction and Building Materials, 75 **(2015)** 129–135.

Xie P., Gu P. and Beaudoin J.J., Electrical percolation phenomena in cement composites containing conductive fibres, Journal of Materials Science, 31(15) **(1996)** 4093–4097.

Xiong W., Tang J., Zhu G., Han N., Schlangen E., Dong B., Wang X. and Xing F., A novel capsule-based self-recovery system with a chloride ion trigger, Scientific Reports, 5(1) **(2015)**

Xiong, T., Shah, K.W. and Kua, H.W., Thermal performance enhancement of cementitious composite containing polystyrene/n-octadecane microcapsules: An experimental and numerical study, Renewable Energy, 169 **(2021)** 335–357.

Yehia, S. and Tuan, C., Bridge Deck Deicing, 1998 Transportation Conference Proceedings, University of Nebreska Omaha, Deparment of Civil Engineering, **1998.**

Yehia, S. and Tuan, C., Thin Conductive Concrete Overlay for Bridge Deck Deicing and Anti-Icing, Transportation Research Record: Journal of the Transportation Research Board, 1698 **(2000)** 45–53.

Yeon, J. and Kim, K., Potential applications of phase change materials to mitigate freeze-thaw deteriorations in concrete pavement, Construction and Building Materials, 177 **(2018)** 202-209.

Yeşilata, B., Turgut, P. and Işıker, Y., Kompozit Yapı Malzemelerinde Isıl Özellik Ölçümü-1: Mevcut Ölçüm Tekniklerin İrdelenmesi, Mühendis ve Makina, 48 **(2007)** (564).

Yıldırım, G., Aras, G.H., Banyhussan, Q.S., Şahmaran, M. and Lachemi, M. Estimating the self-healing capability of cementitious composites through non-destructive electrical-based monitoring, NDT & E International, 76 **(2015)** 26–37.

Yıldırım, G., Sarwary, M.H., Al-Dahawi, A., Öztürk, O., Anıl, Ö. and Şahmaran, M. Piezoresistive behavior of CF- and CNT-based reinforced concrete beams subjected to static flexural loading: Shear failure investigation, Construction and Building Materials, 168() **(2018)** 266–279.

Zhang, J. and Das, D.K., Selection of Effective and Efficient Snow Removal and Ice Control Technologies for Cold-Region Bridges. Journal of Civil, Environmental and Architectural Engineering, 3 **(2009)**

Zhang, W., Min, H., Gu, X., Xi, Y. and Xing, Y., Mesoscale model for thermal conductivity of concrete, Construction and Building Materials, 98 **(2015)** 8–16.

APPENDICES

APPENDIX 1 – Published articles from thesis work

International Journal of Pavement Engineering

ISSN: (Print) (Online) Journal homepage: https://www.tandfonline.com/loi/gpav20

Multi-functional conductive cementitious composites including phase change materials (PCM) with snow/ice melting capability

Fatih Acıkök, Utku Belendir, M. Kemal Ardoğa & Mustafa Şahmaran

To cite this article: Fatih Acıkök, Utku Belendir, M. Kemal Ardoğa & Mustafa Şahmaran (2023) Multi-functional conductive cementitious composites including phase change materials (PCM) with snow/ice melting capability, International Journal of Pavement Engineering, 24:1, 2248347, DOI: 10.1080/10298436.2023.2248347

To link to this article: https://doi.org/10.1080/10298436.2023.2248347

Published online: 22 Aug 2023.

Submit your article to this journal

View related articles

View Crossmark data

Full Terms & Conditions of access and use can be found at
https://www.tandfonline.com/action/journalInformation?journalCode=gpav20

INTERNATIONAL JOURNAL OF PAVEMENT ENGINEERING
2023, VOL. 24, NO. 1, 2248347
https://doi.org/10.1080/10298436.2023.2248347

Taylor & Francis
Taylor & Francis Group

Check for updates

Multi-functional conductive cementitious composites including phase change materials (PCM) with snow/ice melting capability

Fatih Acıkök[a], Utku Belendir[a], M. Kemal Ardoğa[b] and Mustafa Şahmaran[b]

[a]Institute of Science, Hacettepe University, Ankara, Türkiye; [b]Department of Civil Engineering, Hacettepe University, Ankara, Türkiye

ABSTRACT
To remove snow/ice collected on surface of pavements is a must to prevent not only significant structural damages of infrastructures but also traffic accidents, however, today's methods require higher labour and maintenance costs. Producing phase change materials (PCM)- and carbon fibre (CF)-incorporated multifunctional composites with melting snow/ice capability can be a cost effective alternative compared to mechanical methods and heating systems. In this study, the cementitious composites were produced adding 0, 2, 4, 6 and 8% PCM, by weight of the cement and 0.0, 0.1, 0.3% CF, by volume of the mixture. The composites were compared in means of ice melting performance and the damage resulted from freezing and thawing, applying two different simulations in a freeze–thaw cabinet: −10/+10°C and −20/+20°C. In addition, their compressive strength and consistency results were considered with their SEM analysis. As a result of the studies, the optimum CF ratio, which contributes the most to the melting ice performance of PCM-containing composites, was found to be 0.1% by volume. However, in freeze–thaw simulations, CFs increased the temperature amplitudes and PCMs were able to partially prevent this increase. While PCMs increased the workability of the composites and decreased their strength, CFs adversely affected both their workability and strength.

ARTICLE HISTORY
Received 12 May 2023
Accepted 9 August 2023

KEYWORDS
Multi-functional; cementitious composites; self-melting; phase change materials; electrical resistivity

1. Introduction

The icing, which is originated from the collected snow on roadways, with weather conditions causes traffic accidents which result in fatalities and property damage in winter seasons (Ding *et al.* 2023). To remove snow and ice on roads, de-icing salts are used in conjunction with costly and labour-intensive mechanical methods (Farnam *et al.* 2017, Ding *et al.* 2023). De-icing salts, however, damage metal components, the environment, plants (Seferoğlu *et al.* 2015, Karayolları Genel Müdürlüğü 2018) and also cause spalling and disintegration in concrete pavements with freeze–thaw cycles, and over time, they leach into the pavement, rusting reinforcement, if any (Abdulla 2018). Furthermore, particularly the deicers used to deice airport concrete pavements and based on alkali metal salts (potassium acetate-KAc, sodium acetate-NaAc, etc.) cause alkali-silica reactions (ASR) (Rangaraju *et al.* 2006). The heated pavement systems (electrical heating, hydraulic heating, etc.) can be an alternative to mechanical and chemical processes, but it is still limited because of their expensive installation/maintenance requirements. It was stated that in a pavement with an electric heating system with a power consumption of 323–430 W/m^2, the installation and maintenance costs were approximately \$54/m^2, \$4.8/m^2, respectively (Zhang and Das 2009, Anand *et al.* 2014). On the other hand, in recent years, phase change materials (PCM), which are used for thermal purposes in many industries and have the ability to store and release the solar energy depending on weather conditions, have been studied for their potential to melt snow/ice. PCMs tend to reduce the temperature variations of the system they were involved in, by releasing and absorbing heat energy at the phase change temperature and thus minimising freeze–thaw damage in concrete structures (Manning *et al.* 2015, Fernandes *et al.* 2014, Gao *et al.* 2016, Savija 2018). Farnam *et al.* (2017) investigated the time-dependent snow melting capability of paraffin oil, which has a latent heat of 157.8 J/g and a phase transition temperature of 5.7°C. This PCM was added to the concrete by both the impregnation method with light aggregates (22.1% by volume) and the embedded pipe system method (14% by volume). They added 3000 g of handmade snow to the reference sample without PCM and the samples with PCM under a cycle created with a maximum temperature of 7°C and a minimum of 2°C in cabinet. The reference sample melted all the snow in 65 h, whereas the ones having PCM did in 35 h. In another study, a composite bridge deck sample with anti-freezing capabilities was produced by Gao *et al.* (2016). It had a phase change functional layer made up of embedded steel pipes filled with PCM to reduce the amount of ice and snow formed. Their research supported the view that using PCM-filled pipes was an effective technique to prevent ice from forming on structures like bridge decks. In another study, through numerical models, Bentz and Turpin (2007) found that the incorporation of PCM lessened the impacts of freeze–thaw on concrete bridge decks. The PCM

CONTACT Mustafa Şahmaran sahmaran@hacettepe.edu.tr
© 2023 Informa UK Limited, trading as Taylor & Francis Group

having a latent heat of 250 J/g and a melting temperature of 30–40°C, was added to the concrete at a rate of 15% by weight. The data used to create this model included the actual number of freeze–thaw cycles experienced in 12 different locations annually throughout the United States. It was found that, when compared to the control concrete without PCM, the quantity of freeze–thaw cycles and, consequently, the frost action, decreased by around 30% on average for all places in the concrete containing PCM.

The cement-based multifunctional composites, the conductivity of which is improved by adding carbon and steel-based materials, are also produced for snow/ice melting applications. In order to increase the ability of electrically heated concrete pavements to melt snow and ice, Wu *et al.* (2015) studied the efficacy of conductive steel fibres, carbon fibre (CF) and graphite powder to conductivity of composites. Following numerous tests, it was found that the triple mixture containing 1% (volume fraction) steel fibres, 0.4% (volume fraction) CF and 4% (mass fraction) graphite powder performed the best. On the 28th day, this mixture had the lowest electrical resistivity (322 Ω.cm) among all the experimental matrices and hence the highest potential to melt snow and ice. In another investigation, Gomis *et al.* (2015) investigated the effectiveness of deicing electrically heated pavements by modifying cementitious composites with CF, carbon nanofibre, carbon nanotube and graphite powder. The samples were covered with an ice having the thickness of 0.5 cm and had a surface area of 10 cm by 10 cm. The applied voltages were selected to produce an initial electric power of approximately 30 W. The reference sample (mortar consisting only of water and cement) melted 40 g of ice in roughly 4500 s, but the samples containing carbon-based material melted the same quantity of ice in about 1000 s.

The aim of this study is to create multifunctional cement-based composites with increased electrical conductivity through carbon fibres, containing microencapsulated PCM (n-tetradecane-$C_{14}H_{30}$), and capable of self-melting snow/ice without the use of an external power source. The goal of enhancing conductivity is to create pavements that rapidly transmit heat energy of the PCM to the surface where the snow/ice is situated. To obtain a conductive composite, instead of steel fibre, which can have a corrosive behaviour, carbon-based materials, that were more widely used in previous studies were preferred (Gomis *et al.* 2015, Faneca *et al.* 2018). For this reason, CF was used to increase conductivity in the study and composites with low, moderate and high conductivity levels were produced based on electrical resistivity (ER) method, which is frequently used in snow/ice melting applications (Wu *et al.* 2015, Gomis *et al.* 2015) . In this direction, the PCM was added to composites with three conductivity levels (low, moderate and high) at a rate of % 0, 2, 4, 6 and 8 of the cement weight, respectively. In order to determine the snow/ice melting performance of the produced composites, the melting amount of the ice placed on the samples in the freeze–thaw cabinet at constant temperature was measured (Ice Melting Performance Test). Furthermore, their behaviour under two distinct freeze–thaw simulations were determined to investigate the effect of PCM and CF on freeze–thaw damage (Freeze–Thaw Performance Test). The temperatures for one of the cycles are set to a maximum of +20°C and a minimum of −20°C (first simulation), while the temperatures for the other are set to a maximum of +10°C and a minimum of −10°C (second simulation). Thus, it was possible to monitor the behaviour of the PCM both after the heat energy release/absorption process (the first simulation) and before it was completed (the second simulation). Moreover, DSC analysis of PCM was performed and the consistencies/mechanical properties of the composites were tested. The distribution of conductive materials throughout the matrix was assessed using scanning electron microscopy (SEM) analysis. In addition, a cost analysis comparing the use of different ice-melting technologies was done. The findings of this study are expected to contribute to the development of snow/ice melting capability pavements without the use of mechanical methods or heating systems.

Table 1. Chemical and physical properties of PC, GGBFS and QS.

Chemical Composition	PC	GGBFS	QS
SiO_2 (%)	21.6	32.1	99.79
CaO (%)	65.7	36.1	0.02
Al_2O_3 (%)	4.05	11.2	0.06
Fe_2O_3 (%)	0.26	0.60	0.02
MgO (%)	1.30	5.60	0.01
SO_3 (%)	3.30	1.20	–
K_2O (%)	0.35	0.80	0.01
Na_2O (%)	0.30	0.30	0.02
Free CaO (%)	1.60	–	–
CO_2 (%)	–	9.10	–
Loss of Ignition (%)	3.20	2.80	0.07
Physical Properties			
Density (g/cm^3)	3.06	2.79	2.65
Specific Surface, Blaine (cm^2/g)	4600	4250	–

2. Materials and test details

2.1. Materials

The chemical and physical properties of CEM I 52.5 R White Portland Cement (PC) (provided from Çimsa Cement factory) are listed in Table 1. In the same table, the properties of other ingredients, Ground Granulated Blast-Furnace Slag (GGBFS) and Quartz Sand (QS), are also shown. QS (D_{max} = 400 µm), was supplied by the Pomza Export. The GGBFS, a by-product of Iskenderun Iron and Steel Factory, was used as mineral additive to increase the durability of the exposed structures and provide economy (Sahmaran *et al.* 2016). EBA 1447, a polymer-based high-range water (HRWRA) reducing admixture supplied by BASF, was used in the mixtures for the mixtures having lower water–cement ratio and correspondingly, higher mechanical property. To prevent fibre agglomeration

Table 2. Physical properties of CF.

	CF
Diameter	7.5 µm
Length	12 mm
Aspect Ratio	1600
Elastic Modulus	240 GPa
Density	1.7–2.0 g/cm^3
Elongation Rate	%1.8
Carbon Content	% 95
Electric Resistivity (Ω.cm)	1.0E + 00

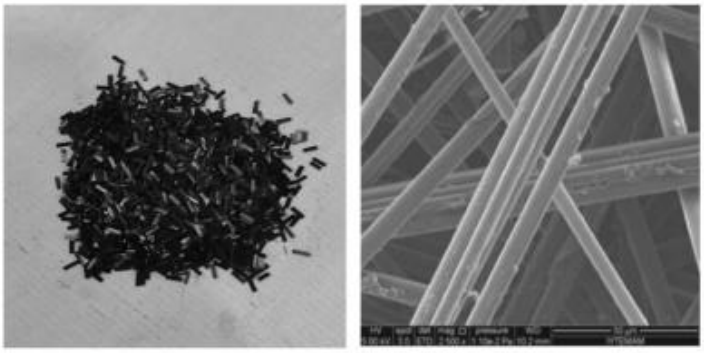

Figure 1. Digital camera and SEM images of the CF.

and adjust the viscosity of the produced mixtures, the Culminal M2030 was chosen as a viscosity modifier (VM). The physical properties of the CF obtained from ELG, which was used to increase conductivity are shown in Table 2. Since relatively longer fibres increase electrical conductivity more than short fibres (such as 6 mm), a 12 mm CF was preferred (Al-Dahawi *et al.* 2016). The digital camera and SEM images of the CF are shown in Figure 1.

The microencapsulated paraffin wax from MikroCaps Company, which has the chemical formula n-tetradecane ($C_{14}H_{30}$), was the organic type PCM employed in this study. The technical data for the microencapsulated PCM dispersion is shown in Table 3. This is made up of fluid with microcapsules that can store energy, and its fluid facilitates both addition of PCM to the composite and distribution of PCM in the composite, homogeneously (Kitchener *et al.* 2017). The microencapsulation method used in cementitious composites containing self-healing agents (Lv *et al.* 2016) and corrosion inhibitors (Xiong *et al.* 2015) was preferred in this study to maintain PCM purity, provide optimised heat transfer with a high surface area, and offer flexibility for phase change (Anupam *et al.* 2020, Norvell *et al.* 2013). The result of the Differential Scanning Calorimetry (DSC) study utilised to ascertain the thermal characteristics of PCM is illustrated in Figure 2, and the heat storage characteristics based on DSC analysis data are given in Table 4. In the DSC analysis, it has been determined that PCM has the capacity to deliver 155.5 J/g of energy between the freezing point start and end temperatures (2°C and −14.0°), which is the heat release region. The heat release of PCM, which starts close to 0°C and continues below 0°C, constitutes an ideal range for snow/ice melting applications. On the other hand, the melting zone, which is the heat storage range of PCM, starts from 1.3°C and continues up to 11.0°C. PCM, which has an energy storage capacity of 150.9 J/g in the melting region, provides benefits in reducing freeze–thaw temperature amplitudes and limiting temperature variations thanks to this heat storage range.

The digital camera image of the PCM dispersion is given in Figure 3 and total solid analysis carried out utilising fluorescent microscopic particle imaging is shown in Figure 4. Total solids analysis revealed that the microcapsule particles were of various sizes. Different sizes were also found in the cumulative particle size analysis in Figure 5, and 98% of the particles in the analysis were smaller than 132 micrometers. Smaller microcapsule particles mean that PCM allows for faster reaction (Anupam *et al.* 2020, Norvell *et al.* 2013) and better dispersion in the cement matrix (Aguayo *et al.* 2016) compared to using large or agglomerated particles.

Table 3. Technical data of PCM dispersion.

Classification	PCM-Microcapsule dispersion
Type of membrane	Melamine-formaldehyde
Type of PCM	Paraffin wax
PCM content in the dispersion (by weight)	% 25–30
Dry content in the dispersion (by weight)	% 35–38
Water content in the dispersion (by weight)	% 62–66
Ph	7.0–9.0
Density	900–970 g/L
Viscosity (at 25°C)	10–500 cPs
Appearance	White slurry

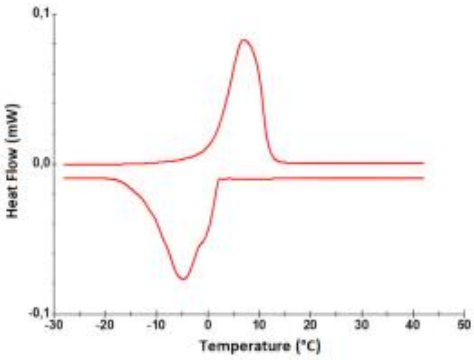

Figure 2. DSC analysis of PCM.

Table 4. Heat properties of PCM.

Melting Point Initial Temperature (°C)	Melting Point Final Temperature (°C)	Melting Enthalpy (J/g)
1.3	11.0	150.9
Freezing Point Initial Temperature (°C)	**Freezing Point Final Temperature (°C)**	**Freezing Enthalpy (J/g)**
2.0	−14.0	−155.5

2.2. Production of mixtures

The dry ingredients (PC, QS, GGBFS, HRWRA, VM) were firstly introduced to mixing bowl and after the speed rate of the mixer was set at 150 rpm and the mixer was turned on. After 10 min, within 30 s, water was added to the mixture, and it was then mixed at 150 rpm for an additional 4 min. After the mixer was turned off, the CFs were added. The CFs were added to wet mortar immediately before the high-speed mixing process, thus a more homogeneous distribution and correspondingly, higher conductivity performance were obtained (Sahmaran 2020). The PCM was added within 30 s after restarting the mixer for 265 rpm and mixed for an additional 4 min. Also, to reduce the probability of damaging microcapsules, PCM was added as the final component (Jayalath *et al.* 2016, Hunger *et al.* 2009).

The weight ratios of the reference mixture constituents were given in Table 5. The PCM and CF ratios in all 15 mixtures that were produced in the study are shown in Table 6. The PCM_0_CF_0 composite without the PCM and CF was determined as the reference composite. The conductivity level in Table 6 is based on the average 28th-day ER (Ω) values. On the other hand, the PCM dispersion rate was arranged with respect to the required amount of PCM, assuming that the PCM content in dispersion was 27.5% (it ranged from 25% to 30% by weight (Table 3)). The PCM dispersion rate and correspondingly, the w/c ratio of the mixtures are shown in Table 6.

Figure 3. Digital camera view of PCM.

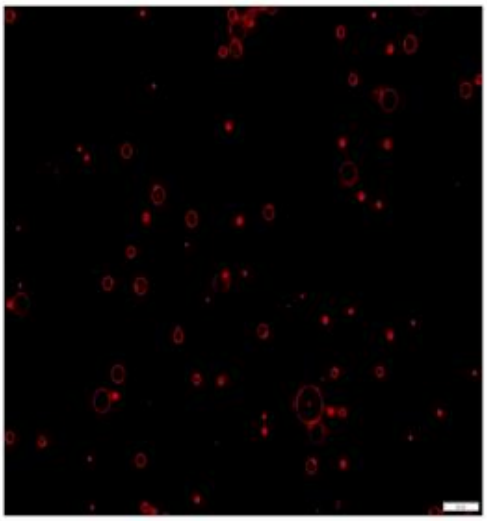

Figure 4. PCM particles in fluorescent microscopy.

3. Sample preparation and experimental procedure

3.1. Determination of consistency, mechanical properties and SEM analysis

All fresh-state cement-based mixtures were tested for consistency immediately after mixing. Mini-slump test were performed in accordance with the techniques of Kantro (1980). The test was conducted using a metal mini-slump cone with a height of 75.8 mm, lower and upper interior diameters of 92.1 and 43.5 mm, respectively. Without using any compaction, the produced mixture was casted into the mini-slump cone, and after the mortar surface was finished, the cone was slowly lifted vertically. The resulting circle's diameter was measured along two perpendicular axes, and the average of the results was assumed as the mini-spread diameter. The compressive strengths of the mortars were also measured in accordance with ASTM C109 standard. Following the mixing process, 50 mm-cube samples were left at a temperature of 23 ± 2°C and relative humidity of 50 ± 5% for 24 h. The samples were taken out from the moulds and allowed to cure in a curing pool until the testing period at a temperature of 23 ± 2°C. On the 28th day, compressive strength tests were performed with six cube samples at a loading rate of 900 N/s, and the average of the results was reported. In addition, scanning electron microscopy (SEM) was used to examine the samples to determine the microstructure of the composites and distribution of PCM, CF for 28th day.

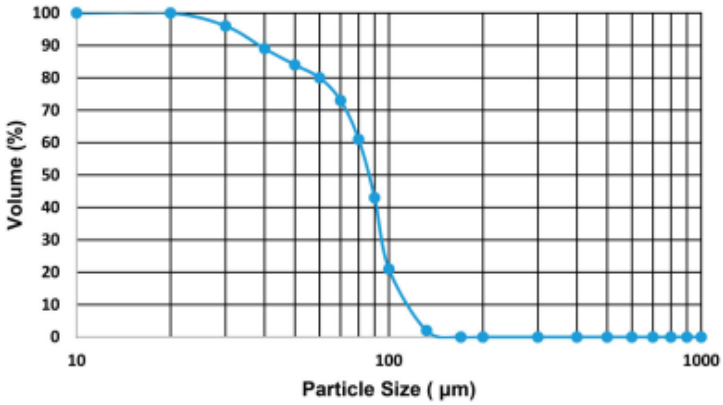

Figure 5. The cumulative particle size distribution of microencapsulated PCMs.

Table 5. Weight ratios of reference mixture (PCM_0_CF_0).

Materials	PC	Water	QS	GGBFS	HRWRA	VM
Weight ratios	100	36	73	60	3	1

3.2. Freeze–thaw performance test

The purpose of freeze–thaw performance test is to determine how PCM and CF affected the temperature amplitudes, which the composites were exposed to. In this direction, two distinct types of freeze–thaw simulations were developed. In the first simulation, the ambient temperature in the freeze–thaw cabinet was adjusted to raise the reference sample to a maximum of + 20°C and to reduce it to a minimum of −20°C (Figure 6). The rate of temperature drop from +20 to −20°C and temperature rise from −20 to +20°C was determined to be 4°C/h. The test was performed in two cycles and calculations were based on the second cycle, which was considered to provide better thermal balance between the cabinet and the samples. In the second simulation with a maximum and minimum temperature of +10 and −10°C, respectively, the criteria of the cycle system specified for the first simulation were applied completely (Figure 6). The reference sample was kept at maximum and minimum temperatures for 4 h in both simulations. Consequently, it was intended to follow the behaviour of the PCM after the process of releasing/absorbing thermal energy was completed (the first simulation) and before it was completed (the second simulation). This made it possible to investigate the behaviour of the composites in first and second simulations representing the climates with higher and lower temperature differences, respectively. 150 × 150 × 40 mm freeze–thaw moulds (Figure 7-a) filled with composites were kept at 95% humidity for 24 h and then kept in laboratory conditions for 28 days. The edges of samples were sealed with silicone (Figure 7-b) and a-20-mm hole was drilled across its entire thickness to insert the thermocouples in the centre of the samples (Figure 7-c). To reduce temperature fluctuations and ensure that every sample achieved the same temperature, the samples were stored in an isothermal cabinet for three days at a constant temperature of 20°C. The samples were then placed in the freeze–thaw cabinet, and thermocouples were embedded in their centres to monitor their interior temperature (Figure 7-d). As the freeze–thaw cabinet, a Schleibinger Slabtester device with a digital display was used (Figure 7-e). The temperature of

Table 6. The mixtures produced.

CF (%) (volume of mixture)	Conductivity Level	PCM (%) (weight of cement)	PCM dispersion rate (%) (weight of cement)	w/c	Code	Average 28th day ER (Ω)
0	Low	0	0.0	0.36	PCM_0_CF_0	51084
		2	7.4	0.41	PCM_2_CF_0	
		4	14.8	0.45	PCM_4_CF_0	
		6	22.2	0.50	PCM_6_CF_0	
		8	29.6	0.55	PCM_8_CF_0	
0.1	Moderate	0	0.0	0.36	PCM_0_CF_0.1	1800
		2	7.4	0.41	PCM_2_CF_0.1	
		4	14.8	0.45	PCM_4_CF_0.1	
		6	22.2	0.50	PCM_6_CF_0.1	
		8	29.6	0.55	PCM_8_CF_0.1	
0.3	High	0	0.0	0.36	PCM_0_CF_0.3	566
		2	7.4	0.41	PCM_2_CF_0.3	
		4	14.8	0.45	PCM_4_CF_0.3	
		6	22.2	0.50	PCM_6_CF_0.3	
		8	29.6	0.55	PCM_8_CF_0.3	

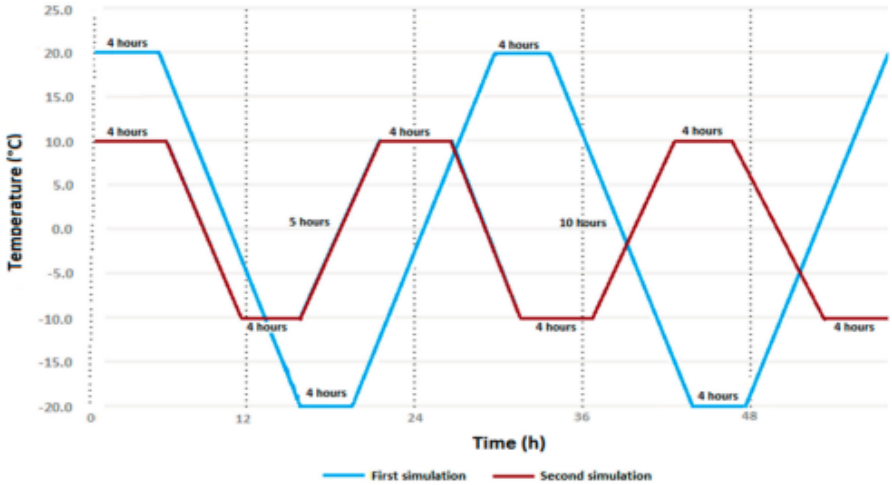

Figure 6. Graph of the cycle systems created on the reference sample.

the cabinet was monitored from the computer connected to the device and could be adjusted in the range of −35°C and +40°C. Pt100 thermocouples, which have a data rate of 50 kpbs and can operate between −200°C and 600°C and are commonly used in low temperatures and sensitive measurements were employed in the study. The tests were performed separately on samples for each pre-determined PCM percentage.

3.3. Ice Melting Performance Test

The Ice Melting Performance Test was applied to determine the effect of PCM and CF on the rate of ice melting in composites that were produced. 15 mixtures given in Table 6 were casted into moulds measuring 150 × 150 × 40 mm^3. After the samples were cured in the environment having 95% humidity for 24 h, they were demoulded and the curing was proceeded in laboratory conditions for 28 days. Then, they were placed in insulated ready-made freeze–thaw moulds their edges were sealed for water with silicone. The samples were put in the freeze–thaw cabinet, and the cabinet was set to a constant temperature of 2.5°C. In order for the samples to reach the equivalent temperature in the cabinet, the samples were kept at this temperature for 24 h. Then, 100 × 100 mm in size and 15 mm thick ice was placed on the samples (Figure 8) and samples were tilted slightly in the cabinet, allowing the melted ice to collect at the edge of mould and be extracted with the injector. The mass of the water resulted from the melted ice was monitored for 72 h with 8-hour intervals. To avoid the PCM from losing efficiency during the 24-hour period without ice, the cabinet temperature (2.5°C) was chosen above the PCM's heat energy release range (2°C and −14°C) rather than within it. The test was performed separately on the samples having each PCM percentage.

4. Results and discussion

4.1. Mini slump, compressive strength tests and SEM analysis

The mini-slump test results obtained from the fresh cementitious mixtures are given in Figure 9. Due to the PCM dispersion consisting of 62–66% water by weight, the mini-spread diameter increased as the PCM ratio rose. When the composites with low conductivity level are examined, depending on the PCM ratio, the mini-spread diameter ranged from 285 mm (PCM_0_CF_0) to 310 mm (PCM_8_CF_0). While the PCM had consistency-enhancing effect, the CFs had the reverse effect. Nonetheless, the results of the mixtures at the moderate conductivity level being close to those of the mixtures at the low conductivity level without CF, demonstrate that the consistency was only slightly impacted by the 0.1% CF ratio. Even, the mini-spread diameters of the PCM_0_CF_0 and PCM_0_CF_0.1 composites (285 mm), the PCM_2_CF_0 and PCM_2_CF_0.1 composites (295 mm) and the PCM_8_CF_0 and PCM_8_CF_0.1 composites (310 mm) were equal. However, in high conductivity composites containing 0.3% CF by volume, there was a significant decrease in mini-spreading diameters due to the increase in CF ratio. This resulted from the formation of high amount of CF lumps (Abbas *et al.* 2022). For example, the spreading diameter for the PCM_0_CF_0.3 composite was 15 mm lower than the PCM_0_CF_0.1 and PCM_0_CF_0 composites, that for PCM_2_CF_0.3 coded composite was 25 mm lower than the PCM_2_CF_0.1 and PCM_2_CF_0 composites, that for the PCM_8_CF_0.3 composite was 25 mm lower than these of the PCM_8_CF_0.1 and PCM_8_CF_0 composites.

The compressive strength results of the mixtures are given in Figure 10. It is obvious that the presence of the PCM decreased their mechanical performance for various reasons.

Figure 7. (a) Ready-made freeze–thaw moulds (b) Samples placed in moulds and siliconised on the edges (c) Drilling process from the middle of the sample in the mould (d) The samples placed in the cabinet with thermocouple in their centre (e) Freeze–Thaw cabinet.

Firstly, the strength was negatively impacted by the increase in the water/cement ratio due to the PCM dispersion. Also, the soft microcapsule structure also had a strength-reducer effect, even if it was indicated that the microcapsules could act as nucleation zones for cement hydration products (Savija 2018, Yeon and Kim 2018). Moreover, the weak intermediate zone formed between the microcapsule (organic) and the matrix (inorganic), which had a detrimental effect on mechanical property, was also a factor reducing the compressive strength according to Cui *et al.* (2018). Evidentially, a void was detected in the region between the microcapsule and the matrix in the PCM_6_CF_0 composite in Figure 11. When the samples with low conductivity level were examined, it is seen that the strength of the PCM_0_CF_0 composite was 74.4 MPa, while the PCM_8_CF_0 composite had a strength value of 45.4 MPa. The 8% addition of the PCM reduced the strength by around 40%. The strengths of other composites, the PCM_2_CF_0, PCM_4_CF_0, PCM_6_CF_0 composites, having low conductivity levels were found to be 64.3, 67.2 and 56.2 MPa, respectively. From the point of view of the presence of CF, it was frequently stated that CFs created air voids, which reduced mechanical performance (Chung 2000, Wang *et al.* 2008, Chuang *et al.* 2017). When the results were examined, it was determined that especially addition of 0.3% CF

Figure 8. The process of placing ice on the samples in the cabinet.

ratio, by volume, resulted in significant strength loss. For example, the strengths of the PCM_6_CF_0, PCM_6_CF_0.1, PCM_6_CF_0.3 composites were found 56.2, 53.3 and 43.8 MPa, respectively. In other words, the 0.1% CF ratio caused about 5% strength loss, while 0.3% CF ratio decreased the strength by 22% for these composites. Similarly, the strengths of the PCM_4_CF_0, PCM_4_CF_0.1, PCM_4_CF_0.3 composites were 57.2, 54.7 and 46.7 MPa, respectively. Moreover, the PCM_8_CF_0.1 composite (46.6 MPa) provided close strength values with the PCM_8_CF_0 composite (45.4 MPa), while the strength of the PCM_8_CF_0.3 composite (39.2 MPa) was approximately 7 MPa lower.

In SEM analysis, weak intermediate zone between PCM and matrix as well as hydration products (C–S–H gels, C–H plates and ettringite) were detected in Figure 11 for the PCM_6_CF_0 composite. Figure 12 shows the SEM analysis on the PCM_2_CF_0.1 composite. In the analysis, it was observed that the PCMs around the CF were dispersed in the matrix without any agglomeration and remained embedded among the hydration products. Various microcapsule sizes found in the cumulative particle size analysis were visually detected in this SEM analysis, also. In the SEM analysis of the PCM_4_CF_0.1 composite, Figure 13, a microcapsule could not maintain its spherical form between the CH plates. However, due to its flexible structure, the microcapsule did not explode and proceeded its activity. As demonstrated in previous studies, its shell structure could be so flexible that it provided the stability to the microcapsules against the external effects such as C–S–H gel formation or thermal expansion (Aguayo *et al.* 2016, Xiong *et al.* 2021). The SEM images showed that the microcapsules were not damaged in general, despite the fact that a few were seen to be harmed in Figures 12 and 14. The distribution of CFs in the PCM_0_CF_0.3 composite given was examined in Figure 15. In the analysis, it was observed that the CFs were homogeneously distributed without any clumping.

4.2. Freeze–thaw performance test

Figures 16 and 17 show the behaviour of the composites having no PCM in case of varying ambient temperatures in simulations. Figures 18 and 19 show the behaviour of the composites containing 2% PCM; Figures 20 and 21 show the behaviour of the composites containing 4% PCM; Figures 22 and 23 show the behaviour of the composites containing 6% PCM; and Figures 24 and 25 show the behaviour of the

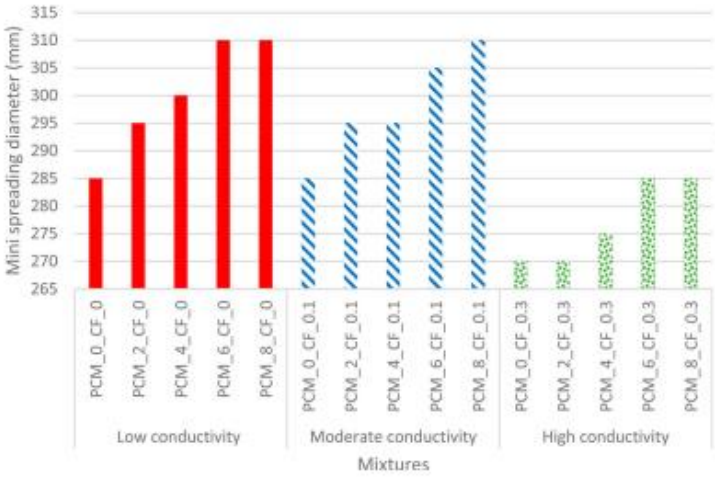

Figure 9. Mini-slump test results of produced cementitious composites.

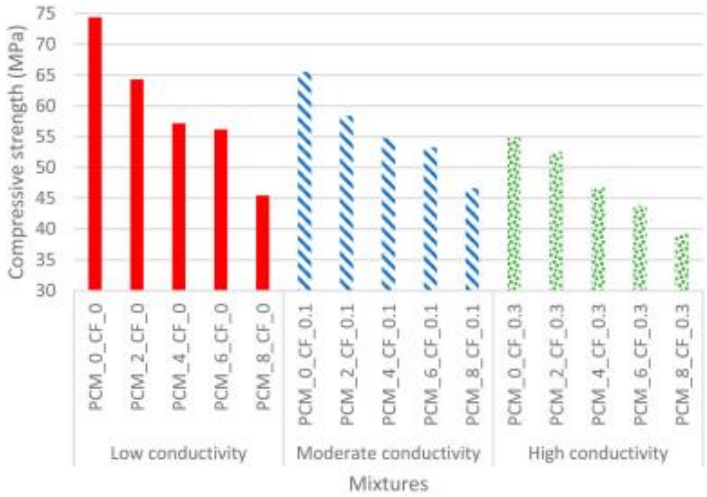

Figure 10. Compressive strength results of produced cementitious composites.

composites containing 8% PCM. The results of the calculations based on the parameters obtained from the simulations for the composites containing 0, 2, 4, 6, 8% PCM are given in Tables 7–11, respectively. The maximum and minimum temperature periods included in the calculations are circled in green on graphs and the average temperatures are given in the related tables. At +20°C, the 'Temperature difference compared to reference sample' was calculated by subtracting the corresponding sample's average temperature from the reference sample's average temperature. At −20°C, this was calculated by subtracting the reference sample's average temperature from the corresponding sample's average temperature. The summation of 'Temperature difference compared to reference sample' for +20°C and −20°C in the table gives 'Total temperature difference compared to reference sample'. Similar comparison and calculating steps were performed for the second simulation as well.

When results of PCM-free composites examined, in the PCM_0_CF_0.1 composite, the temperature amplitude increased by 0.80°C compared to the reference sample in the first simulation, and by 1.30°C in the second simulation. This increase was 1.71°C in the first simulation and 1.33°C in the second simulation for the PCM_0_CF_0.3 composite (Table 7). It was clearly seen that CFs had an effect on increasing the temperature amplitudes. The reason for this is that the composites showed rapid heating and cooling behaviour

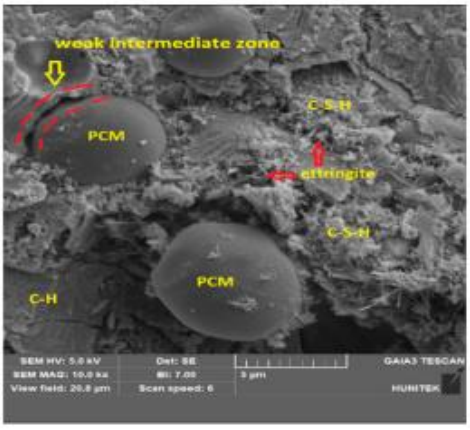

Figure 11. SEM image of the PCM_6_CF_0 composite.

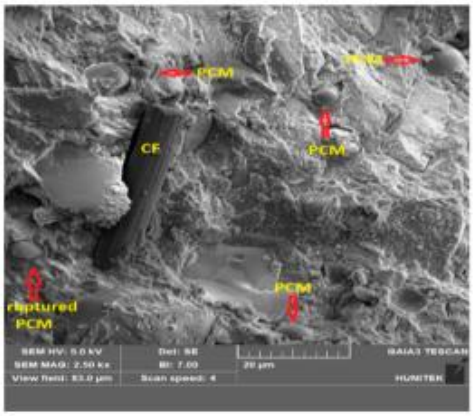

Figure 12. SEM image of the PCM_2_CF_0.1 composite.

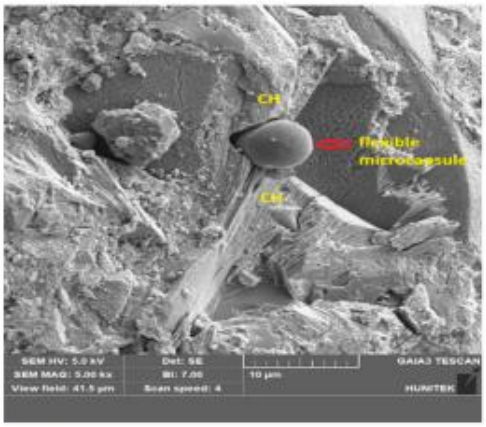

Figure 13. SEM image of the PCM_4_CF_0.1 composite.

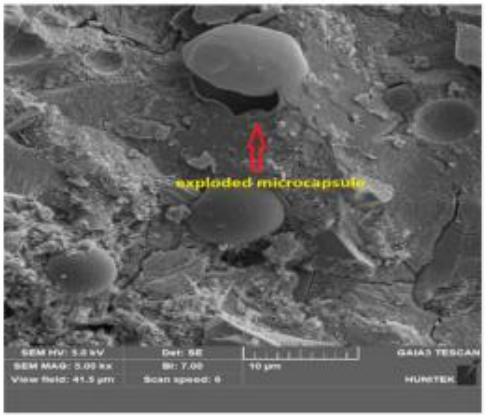

Figure 14. SEM image of the PCM_6_CF_0.1 composite.

(Sakulich and Bentz 2012) as a result of the increased conductivity due to the presence of the CFs. Temperature differences were higher in almost all composites tested in samples with high conductivity compared to the samples with moderate and low conductivity levels (Tables 7–11). This showed that the presence of CFs would result in more freeze–thaw damage to concrete. In contrast, temperature amplitudes decreased in both cycles as the PCM ratio increased in the CF-free mixtures. In the PCM_2_CF_0, PCM_4_CF_0, PCM_6_CF_0, PCM_8_CF_0 composites, the temperature amplitude decreased by 0.05°C, 0.32°C, 0.71°C and 0.89°C in the first simulation, while these values were 0.42°C, 1.02°C, 1.07°C and 2.03°C in the second simulation, respectively (Tables 8–11). The results also showed that the temperature amplitude was decreased for the majority of PCM-containing composites in the second simulation at higher rate than in the first simulation. This is because the heat energy released by the composites containing PCM in the +10/−10°C temperature cycle was not depleted to −10°C, and heat energy absorbed at +10°C was not yet complete. According to the DSC analysis reported in Table 4, the freezing zone (heat energy release zone) and melting zone of PCM (heat energy absorption zone) was determined to be between +2°C and −14°C, and between +1.3°C and +11°C, respectively. However, in the first simulation, when the peak temperatures were (+20°C / −20°C) were reached, the effect of the heat energy released/absorbed on the temperature amplitudes was less since the efficiency process was already completed. Sakulich and Bentz demonstrated that PCM contributed more to reduced freeze–thaw effect at ambient temperatures where its melting/freezing points and thermal differentials were low in their simulation. Also, they stated that if the conductivity was high, heat from the interior of structure would be rapidly drawn to the surface and dissipated into the environment, resulting in rapid cooling of the entire body (Sakulich and Bentz 2012).

When the results of the composites containing the PCM at the rate of 2% of the cement weight in Table 8 are examined, the PCM presence in the PCM_2_CF_0.1 and PCM_2_CF_0.3 composites could not prevent the CF-induced temperature amplitude increase. In the first simulation, the amplitude increased by 1.20°C in the PCM_2_CF_0.1

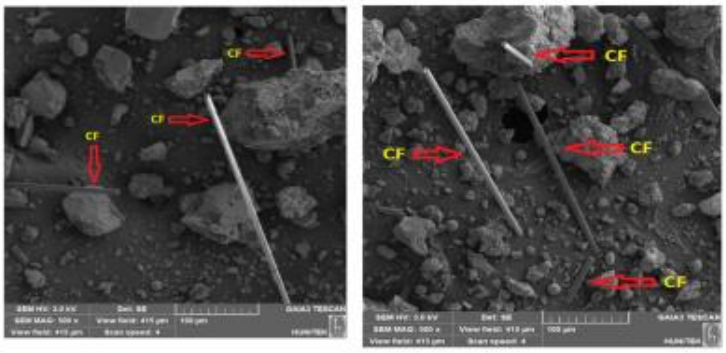

Figure 15. SEM images of the PCM_0_CF_0.3 composite.

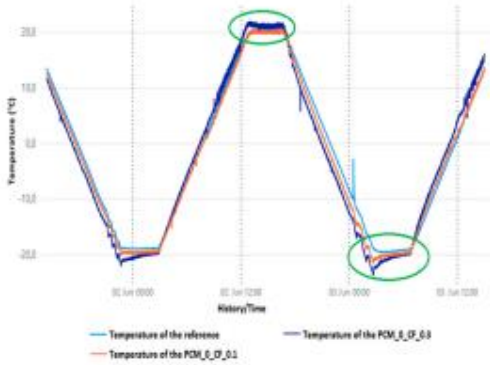

Figure 16. First simulation for composites which containing 0% PCM by weight of cement.

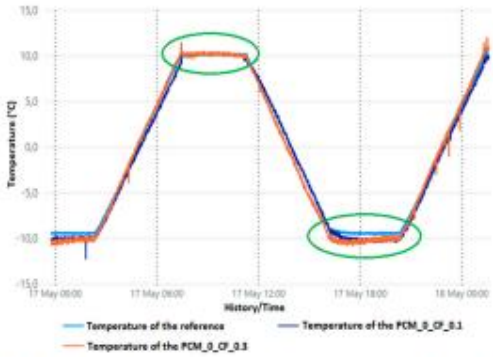

Figure 17. Second simulation for composites which containing 0% PCM by weight of cement.

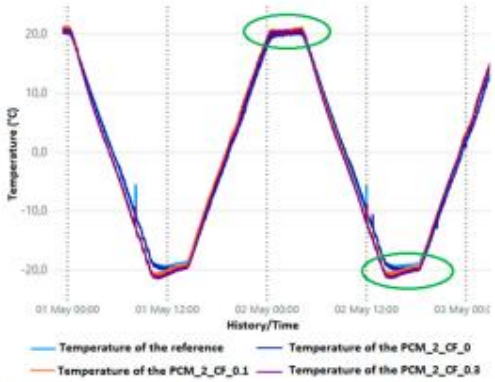

Figure 18. First simulation for composites which containing 2% PCM by weight of cement.

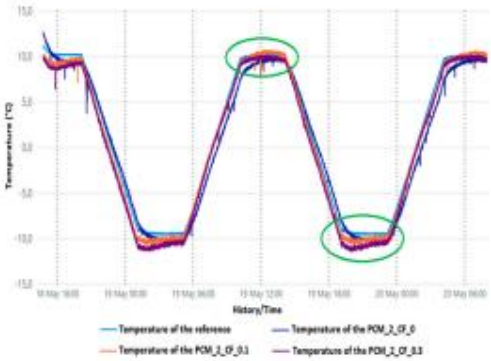

Figure 19. Second simulation for composites which containing 2% PCM by weight of cement.

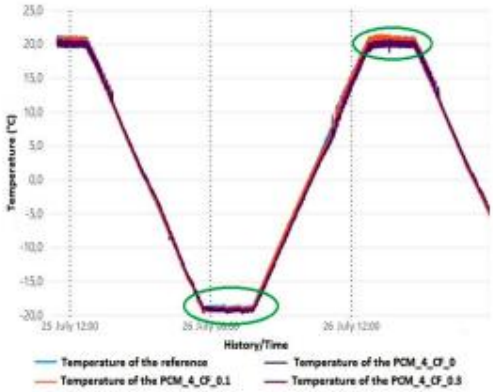

Figure 20. First simulation for composites which containing 4% PCM by weight of cement.

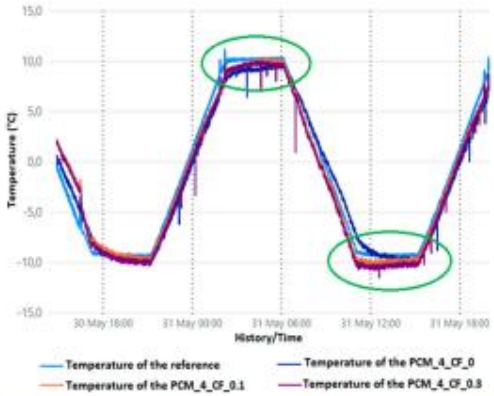

Figure 21. Second simulation for composites which containing 4% PCM by weight of cement.

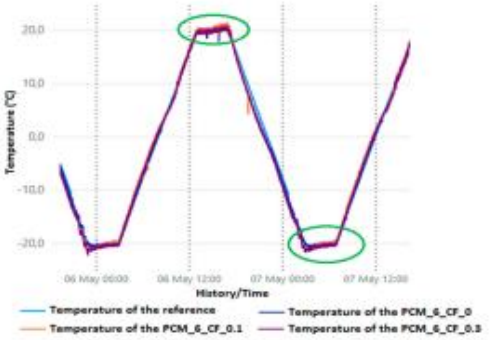

Figure 22. First simulation for composites which containing 6% PCM by weight of cement.

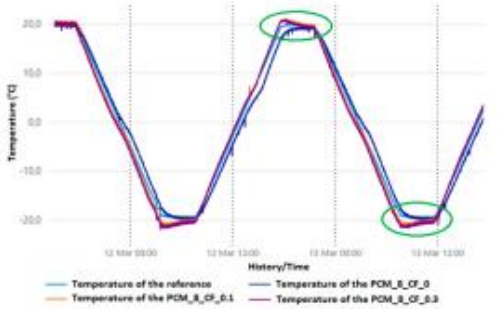

Figure 24. First simulation for composites which containing 8% PCM by weight of cement.

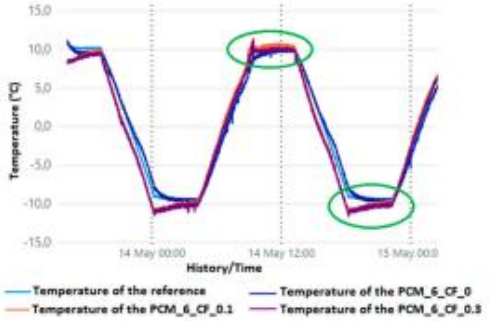

Figure 23. Second simulation for composites which containing 6% PCM by weight of cement.

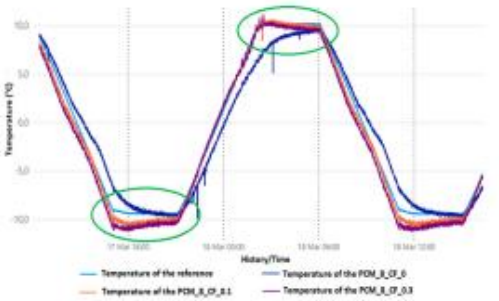

Figure 25. Second simulation for composites which containing 8% PCM by weight of cement.

Table 7. Freeze–thaw performance test results of composites which containing 0% PCM by weight of cement.

First simulation		Reference	PCM_0_CF_0.1	PCM_0_CF_0.3
+ 20 °C	Temperature average	20.26	20.37	20.74
	Temperature difference compared to reference sample	0	0.11	0.48
- 20 °C	Temperature average	−18.87	−19.56	−20.10
	Temperature difference compared to reference sample	0	0.69	1.23
	Total temperature difference compared to reference sample	**0**	**0.80**	**1.71**
Second simulation		**Reference**	**PCM_0_CF_0.1**	**PCM_0_CF_0.3**
+ 10 °C	Temperature average	9.53	10.13	10.19
	Temperature difference compared to reference sample	0	0.60	0.66
- 10 °C	Temperature average	−9.41	−10.11	−10.08
	Temperature difference compared to reference sample	0	0.70	0.67
	Total temperature difference compared to reference sample	**0**	**1.30**	**1.33**

Table 8. Freeze–thaw performance test results of composites which containing 2% PCM by weight of cement.

First simulation		Reference	PCM_2_CF_0	PCM_2_CF_0.1	PCM_2_CF_0.3
+ 20 °C	Temperature average	20.18	19.74	20.37	20.20
	Temperature difference compared to reference sample	0	−0.44	0.19	0.02
- 20 °C	Temperature average	−19.29	−19.68	−20.30	−20.77
	Temperature difference compared to reference sample	0	0.39	1.01	1.48
	Total temperature difference compared to reference sample	**0**	**−0.05**	**1.20**	**1.50**
Second simulation		**Reference**	**PCM_2_CF_0**	**PCM_2_CF_0.1**	**PCM_2_CF_0.3**
+ 10 °C	Temperature average	10.09	9.27	10.18	9.75
	Temperature difference compared to reference sample	0	−0.82	0.09	−0.34
- 10 °C	Temperature average	−9.39	−9.79	−10.08	−10.76
	Temperature difference compared to reference sample	0	0.40	0.69	1.37
	Total temperature difference compared to reference sample	**0**	**−0.42**	**0.78**	**1.03**

Table 9. Freeze–thaw performance test results of composites which containing 4% PCM by weight of cement.

First simulation		Reference	PCM_4_CF_0	PCM_4_CF_0.1	PCM_4_CF_0.3
+ 20 °C	Temperature average	20.61	20.06	20.65	21.02
	Temperature difference compared to reference sample	0	−0.55	0.04	0.41
- 20 °C	Temperature average	−18.68	−18.91	−19.41	−19.10
	Temperature difference compared to reference sample	0	0.23	0.73	0.42
	Total temperature difference compared to reference sample	**0**	**−0.32**	**0.77**	**0.83**
Second simulation		**Reference**	**PCM_4_CF_0**	**PCM_4_CF_0.1**	**PCM_4_CF_0.3**
+ 10 °C	Temperature average	10.21	9.15	9.77	9.58
	Temperature difference compared to reference sample	0	−1.06	−0.44	−0.63
- 10 °C	Temperature average	−9.21	−9.25	−9.90	−10.32
	Temperature difference compared to reference sample	0	0.04	0.69	1.11
	Total temperature difference compared to reference sample	**0**	**−1.02**	**0.25**	**0.48**

Table 10. Freeze–thaw performance test results of composites which containing 6% PCM by weight of cement.

First simulation		Reference	PCM_6_CF_0	PCM_6_CF_0.1	PCM_6_CF_0.3
+ 20 °C	Temperature average	20.18	20.01	19.89	20.36
	Temperature difference compared to reference sample	0	−0.17	−0.29	0.18
- 20 °C	Temperature average	−20.20	−19.66	−20.62	−20.38
	Temperature difference compared to reference sample	0	−0.54	0.42	0.18
	Total temperature difference compared to reference sample	**0**	**−0.71**	**0.13**	**0.36**
Second simulation		**Reference**	**PCM_6_CF_0**	**PCM_6_CF_0.1**	**PCM_6_CF_0.3**
+ 10 °C	Temperature average	10.07	9.21	10.23	9.81
	Temperature difference compared to reference sample	0	−0.86	0.16	−0.26
- 10 °C	Temperature average	−9.31	−9.09	−10.28	−10.45
	Temperature difference compared to reference sample	0	−0.21	0.97	1.14
	Total temperature difference compared to reference sample	**0**	**−1.07**	**1.13**	**0.88**

Table 11. Freeze–thaw performance test results of composites which containing 8% PCM by weight of cement.

First simulation		Reference	PCM_8_CF_0	PCM_8_CF_0.1	PCM_8_CF_0.3
+ 20 °C	Temperature average	19.75	18.88	20.24	19.96
	Temperature difference compared to reference sample	0	−0.87	0.49	0.21
- 20 °C	Temperature average	−19.33	−19.31	−20.46	−20.71
	Temperature difference compared to reference sample	0	−0.02	1.13	1.38
	Total temperature difference compared to reference sample	**0**	**−0.89**	**1.62**	**1.59**
Second simulation		**Reference**	**PCM_8_CF_0**	**PCM_8_CF_0.1**	**PCM_8_CF_0.3**
+ 10 °C	Temperature average	10.20	8.65	10.16	9.89
	Temperature difference compared to reference sample	0	−1.55	−0.04	−0.31
- 10 °C	Temperature average	−9.33	−8.85	−10.19	−10.61
	Temperature difference compared to reference sample	0	−0.48	0.86	1.28
	Total temperature difference compared to reference sample	**0**	**−2.03**	**0.82**	**0.97**

composite and by 1.50°C in the PCM_2_CF_0.3 composite compared to the reference sample. In the second simulation, the amplitude increased by 0.78°C in the PCM_2_CF_0.1 composite and by 1.03°C in the PCM_2_CF_0.3 composite. Since the temperature range experienced by the composites (−10, +10°C) remained within the operating range of the PCM used (−14, 11°C), the amplitude increase stayed at lower levels in the second simulation. In Table 9, for the PCM_4_CF_0.1 composite, the temperature amplitude increased by 0.77°C in the first simulation and by 0.25°C in the second simulation. For the PCM_4_CF_0.3 composite with higher CF content, the amplitude increased by 0.83°C in the first simulation and 0.48°C in the second simulation. Due to the 2% PCM difference, the PCM_4_CF_0.1 composite achieved 0.43°C more restriction in the first simulation and 0.53°C more in the second simulation compared to the PCM_2_CF_0.1 composite. Also, the PCM_4_CF_0.3 composite had 0.67°C more amplitude restriction in the first simulation and 0.55°C more in the second simulation compared to the PCM_2_CF_0.3 composite. On the other hand, the amplitude increase in the PCM_6_CF_0.1 composite in the first simulation was 0.13°C, the PCM _6_CF_0.3 composite was 0.36°C, and in the second simulation, the PCM_6_CF_0.1 composite was 1.13°C and the PCM_6_CF_0.3 composite was 0.88°C (Table 10). As seen in Table 11, in general, as the PCM ratio increased, the amplitude constraint increased in both simulations and the PCM_8_CF_0 composite showed the highest performance. This composite had the potential to offer the most benefit to freeze–thaw damage by providing an amplitude restriction of 0.89°C in the first simulation and 2.03°C in the second simulation. However, the PCM was found to be insufficient against the amplitude enhancing effect of CF in the PCM_8_CF_0.1 and PCM_8_CF_0.3 composites. The amplitude increase for the PCM_8_CF_0.1 composite in the first simulation was 1.62°C, that for the PCM _8_CF_0.3 was 1.59°C, and in the second simulation, that for the PCM_8_CF_0.1 composite was 0.82°C and that for the PCM_8_CF_0.3 composite was 0.97°C.

Figure 26 shows the relationships between PCM content and temperature restriction in comparison to the reference sample. In order to monitor the effect of only PCM on temperature amplitudes in the relationships, composites with the code

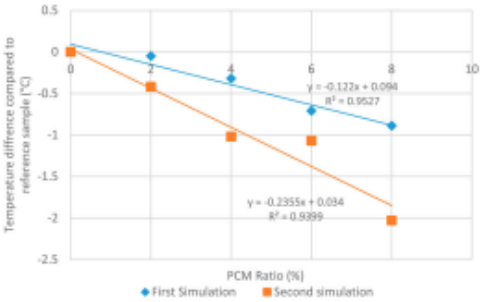

Figure 26. Relationship between PCM additions and temperature difference compared to reference sample.

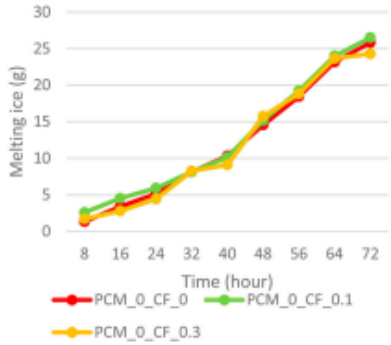

Figure 28. Amount of melting ice in composites which containing 0% PCM by weight of cement.

PCM_0_CF_0, PCM_2_CF_0, PCM_4_CF_0, PCM_6_CF_0, PCM_8_CF_0 without carbon fibre were used. The coefficients of determination of the line fitted to the relationships are determined for both simulations to be almost 1. ($R^2 = 0.9527$ for the first simulation and $R^2 = 0.9399$ for the second simulation). The results show that a 1% increase in the PCM ratio provided an amplitude restriction of 0.028°C for the first simulation and 0.20°C for the second simulation. Furthermore, it is clear that the amplitude restriction difference between the two simulations became much more as the PCM ratio increased. This demonstrates that the rise in PCM content produced a thermal effect that was nearly linear in behaviour.

4.3. Ice melting performance test

Ice melting rates of all composites are given in Figure 27. The mass of the ice melted versus time graph for the composites without the PCM for 72 h is shown in Figure 28. Since there was no PCM providing heat energy for the samples, melting of the ice layer on the surface of the samples was only due to the cabin temperature, therefore the composites showed similar performances. 25.8, 26.5 and 24.3 g of ice melted on the PCM_0_CF_0, PCM_0_CF_0.1, PCM_0_CF_0.3 composites, respectively. The average ice melting rate for the PCM_0_CF_0 composite was 0.35 g/h, while the rates for the PCM_0_CF_0.1 and PCM_0_CF_0.3 composites were 0.36 and 0.33 g/h, respectively (Figure 27). The amount of ice melted on the samples including 2% PCM relative to the cement weight is depicted in Figure 29. The PCM_2_CF_0.1 composite had an average ice melting rate of 0.66 g/h and total of 47.6 grams of ice melted. The ice melting rate of the PCM_2_CF_0 composite was 0.42 g/h, and that of the PCM_2_CF_0.3 composite was 0.44 g/h. Considering the results, the amount of ice melted for the PCM_2_CF_0.1 composite was significantly higher than those for the PCM_2_CF_0 and PCM_2_CF_0.3 composites. The reason can be the particle size of its PCMs determined. In the SEM analysis of the PCM_2_CF_0.1 composite (Figure 12), high number of small particles of microcapsules positively affected the heat transfer (Norvell *et al.* 2013, Xiong *et al.* 2015) and homogeneous distribution (Aguayo *et al.* 2016). Furthermore, it was observed that the PCM_2_CF_0.1 composite melted 21.1 grams of ice more than the PCM_0_CF_0.1 composite due to the presence of PCM. On the other hand, among the composites containing 4% PCM by cement weight, the

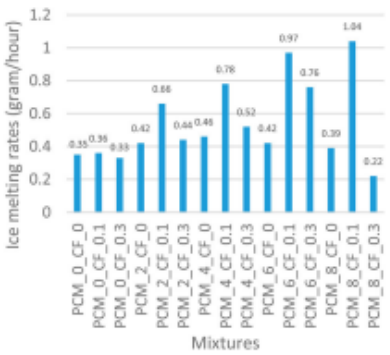

Figure 27. Ice melting rates of composites.

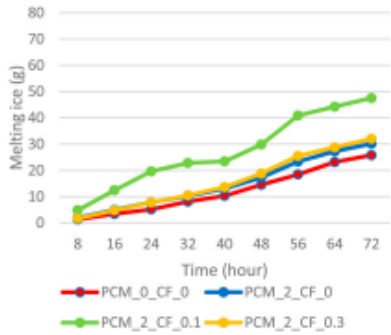

Figure 29. Amount of melting ice in composites which containing 2% PCM by weight of cement.

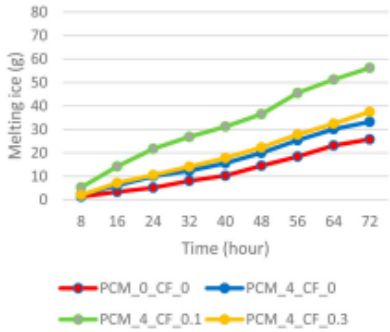

Figure 30. Amount of melting ice in composites which containing 4% PCM by weight of cement.

PCM_4_CF_0.1 composite with a moderate conductivity level demonstrated the best ice-melting performance (Figure 30). 33.3, 56.2 and 37.5 g of ice melted on the PCM_4_CF_0, PCM_4_CF_0.1, PCM_4_CF_0.3 composites, respectively. The ice melting rate for the PCM_4_CF_0 composite was 0.11 g/h higher than that for the reference. In the PCM_4_CF_0 composite, since the energy transmission is not fast, the efficiency of PCM remained low and therefore, compared to the reference sample, it created a small difference in mass of the ice melted. The amount of the ice melted for the composites containing 6% PCM, by cement weight is shown in Figure 31. The average ice melting rate of the PCM_6_CF_0.1 composite, which melted a total of 69.84 g of ice for 72 h, was 0.97 g/h, while the rate for the PCM_6_CF_0 composite was 0.42 g/h and that for the PCM_6_CF_0.3 composite was 0.76 g/h. However, the PCM_6_CF_0.1 composite having moderate conductivity melted 39.4 grams more ice than the PCM_6_CF_0 composite having low conductivity, providing a superior performance. Furthermore, the PCM_6_CF_0.1 composite melted 13.6 grams more ice compared to PCM_4_CF_0.1 composite and its average ice melting rate was 0.19 g/h higher.

Among all composites, the best performance was achieved by the PCM_8_CF_0.1 composite, which had the highest PCM ratio and was moderately conductive. This composite had an average ice melting rate of 1.04 g/h and melted a total of 75.1 grams of ice (Figure 32). The ice melting rates of the PCM_8_CF_0 and PCM_8_CF_0.3 composites were 0.39 and 0.22 g/h, respectively. The reason why PCM_8_CF_0.3 melts less ice than PCM_8_CF_0 can be that the relatively high homogeneous distribution of carbon fibres causes it to cool faster (Sakulich and Bentz 2012). Due to the CFs, the PCM_8_CF_0.1 composite performed better than the PCM_8_CF_0 composite by melting 46.7 g more ice. On the other hand, the digital image showing the form of the melting ice layers was taken during measuring the amount of ice melting in the 24th hour in Figure 33. On the image, the ice layers existing are shown by a solid line. The ice layers on the PCM_6_CF_0 and PCM_6_CF_0.3 composites maintained their square form, but this was not the case for the PCM_6_CF_0.1 composite because of more melting.

In the experiments performed on all PCM groups, the composites containing 0.1% by volume CF having moderate conductivity level showed the best performance. In these samples, the thermal energy present in the ice layer was rapidly transmitted from the sample surface to the entire sample caused faster cooling thanks to the CFs. Thus, the temperature of the samples reached the temperature limits of the heat energy release zone of the PCM (between 2°C and −14°C) more quickly. In this case, the PCM in the microcapsules frozen and released heat energy faster than the composites containing no CFs. The heat energy produced by the PCM in the samples, reached the surface quickly due to the presence of CFs and melted the ice faster. However, the mentioned situation was not detected in the ice melting rate for the composites produced having high conductivity level. This is thought to be because thermal energy of the ice reduces the high conductivity samples to lower temperatures compared to the moderate conductivity samples. It was also mentioned in previous studies that high conductivity led to rapid cooling (Sakulich and Bentz 2012). As a result, although the composites having high conductivity levels released the heat energy of the PCM earlier, this heat energy was not sufficient to heat the composites due to their lower temperature. For example, the PCM_8_CF_0.3 composite performed even worse than the PCM_0_CF_0 and PCM_8_CF_0 composites.

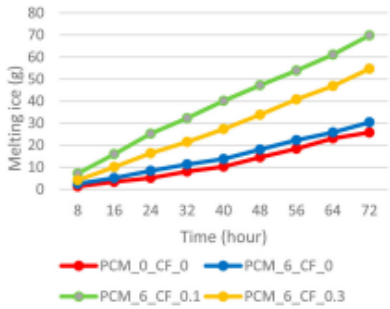

Figure 31. Amount of melting ice in composites which containing 6% PCM by weight of cement.

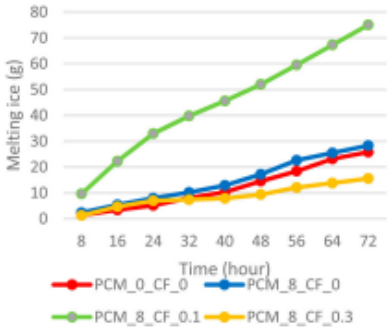

Figure 32. Amount of melting ice in composites which containing 8% PCM by weight of cement.

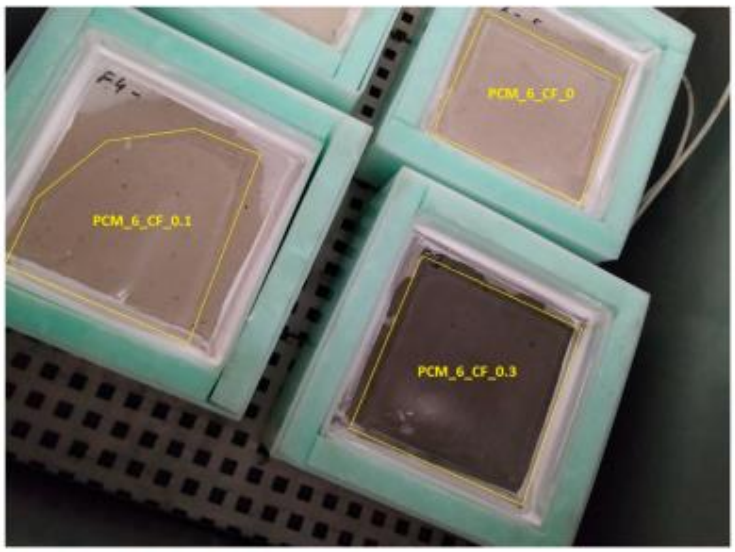

Figure 33. Condition of the ice layers on the samples at the 24th hour of the test.

Table 12. Costs and power consumptions of various heating systems.

Heating system	Installation cost	Operating cost	Power consumption
Infrared Heating Lamp	$96/m^2	Not available	75 W/m^2
Electric Cable Heating	$54/m^2	$4.8/m^2	323–430 W/m^2
Hot Water Heating	$161/m^2	$2.5/m^2	473 W/m^2
Gas Heating	$378/m^2	$2.1/m^2	Not available
Heating with Conductive Concrete	$48/m^2	$5.4/m^2	516 W/m^2

Table 13. Material costs of PCM_6_CF_0.1.

Materials	kg/m^3	Cost ($/m^2)
Cement (CEM I 52,5 R)	819	4.34
QS	598	0.6
GGBFS	493	0.5
HRWRA	3	0.3
VM	1	0.04
CF	1.8	0.3
Dispersion of PCM	180	140.4
	Total Cost	146.5

This showed that an optimum CF content should be present in snow/ice melting applications.

4.4. Cost comparison of different snow/ice melting methodologies

The removal of snow and ice depends on mechanical methods, which are costly in many countries. For snow/ice removal, Türkiye General Directorate of Highways (GDH) regional branches spent approximately 10,022,090 $ in 2020, and also the costs of the tendered were approximately 38,146,285 $. Approximately $1.11 was spent per kilometre within the scope of removal snow/ice (Karayolları Genel Müdürlüğü 2021). On the other hand, although a clear data rate is not certain, it is known that the damages caused by de-icing salts to the road pavement also cause road maintenance costs. Heated systems eliminate the damage caused by chemical solvents and de-icing salts to the environment and pavement, and help to shorten the cleaning time of snow/ice in critical areas in airports. However, the disadvantage of these systems is the complex installation procedures and costs expensive installation/maintenance requirements (Zhang and Das 2009, Anand *et al.* 2014). According to one study, the cost of installing a geothermal system with heating pipes in bridge decks will range between $1075 and $1615 per m^2. It is mentioned that using this system only in critical sections of road, bridge and airport pavements will provide economy and benefit (Lund 2005). The high costs of some heating systems based on data from different studies (Seferoğlu *et al.* 2015) are presented in Table 12. On the other hand, the material costs of the PCM pavement with self-melting snow/ice capability, which does not contain operating costs and is considered to eliminate or reduce the use of de-icing salt, are given in Table 13. With a total material cost of $146.5/m^2, it is predicted that this pavement will save maintenance and repair expenses resulting from the harm that de-icing salts to the roads. Additionally, it is anticipated that it will lower the labour and expense of mechanical methods.

5. Conclusions

The goal of this study is to create cement-based composites that have the ability to self-melting snow/ice without the use of any external power source. In order to generate thermal energy, the microencapsulated PCM was added to composites, the conductivity of which was provided by CFs. The ice melting capacities of the formed composites, as well as SEM

analysis, consistency and mechanical properties were evaluated. Investigations were also conducted into how PCM and CF affected temperature amplitudes and, consequently, the damage originated from the freeze–thaw effect.

The following conclusions were reached:

- Due to the higher water content of the PCM dispersion and weak transition zone which formed between the PCM microcapsules and composite matrix, the mechanical properties were negatively affected. Moreover, CFs created an air void, which reduced the strength.
- Due to the dispersion including water, the PCM showed consistency-enhancing effects in composites having moderate and high conductivity, but the CFs had the opposite effects.
- In SEM analysis, it was observed that the PCM and CF were homogeneously distributed without clumping. In addition, while the microcapsules were not damaged to a large extent, they continued their effectiveness without exploding thanks to their flexible structure among the developing hydration products.
- Compared to the first, the PCM inclusion reduced the temperature amplitudes more, in the second simulation of the Freeze–Thaw Performance Test. This is due to the fact that the temperature range the composite encountered in the second simulation (−10, +10°C) was within the operating range of PCM (−14, 11°C). The highest restriction values of temperature amplitudes occurred in PCM_8_CF_0 composite, which did not contain carbon fibre and had the highest PCM ratio in both simulations.
- The quick heating/cooling behaviour of the composites, whose conductivity was enhanced by CFs, led to a rise in temperature amplitudes in both simulation. This implies that the detrimental effects of freeze–thaw can be amplified by CFs.
- The heat energy released by the PCM transferred faster to the upper surface where the ice was located in composites with increased conductivity thanks to CFs.
- Compared to low-conductive and high-conductive composites, moderate conductive composites had the ability to melt more ice. The reason why high-conductivity composites did not outperform was their rapid cooling behaviour. This demonstrated that there was an optimum ratio of CF in snow/ice melting applications and for this study, this was found 0.1%.

Disclosure statement

No potential conflict of interest was reported by the author(s).

Funding

The authors gladly acknowledge the financial support granted by Türkiye's Scientific and Technical Research Council (TUBITAK) under Project: [121M943].

References

Abbas, N., Saad, M., and Habib, M, 2022. Impact of carbon fibers on mechanical and durability properties of self-compacting concrete. *Engineering Proceedings*, 22 (1), 9.

Abdulla, H., 2018. Design, construction, and performance of heated concrete pavements system. Graduate Thesis. Iowa State University.

Aguayo, M., *et al.*, 2016. The influence of microencapsulated phase change material (PCM) characteristics on the microstructure and strength of cementitious composites: experiments and finite element simulations. *Cement and Concrete Composites*, 73, 29–41.

Al-Dahawi, A., *et al.*, 2016. Effect of mixing methods on the electrical properties of cementitious composites incorporating different carbon-based materials. *Construction and Building Materials*, 104, 160–168.

Anand, P., *et al.*, 2014. Cost comparison of alternative airfield snow removal methodologies. Civil, Construction and Environmental Engineering, Iowa State University.

Anupam, B.R., Sahoo, U.C., and Rath, P, 2020. Phase change materials for pavement applications: a review. *Construction and Building Materials*, 247, 118553.

Bentz, D.P, and Turpin, R, 2007. Potential applications of phase change materials in concrete technology. *Cement and Concrete Composites*, 29 (7), 527–532.

Chuang, W., *et al.*, 2017. Dispersion of carbon fibers and conductivity of carbon fiber-reinforced cement-based composites. *Ceramics International*, 43 (17), 15122–15132.

Chung, D.D.L, 2000. Cement reinforced with short carbon fibers: a multifunctional material. *Composites Part B: Engineering*, 31 (6-7), 511–526.

Cui, H., *et al.*, 2018. Experimental study of carbon fiber reinforced alkali-activated slag composites with micro-encapsulated PCM for energy storage. *Construction and Building Materials*, 161, 442–451.

Ding, S., *et al.*, 2023. Self-heating ultra-high performance concrete with stainless steel wires for active deicing and snow-melting of transportation infrastructures. *Cement and Concrete Composites*, 138, 105005.

Faneca, G., *et al.*, 2018. Development of conductive cementitious materials using recycled carbon fibres. *Cement and Concrete Composites*, 92, 135–144.

Farnam, Y., *et al.*, 2017. Incorporating phase change materials in concrete pavement to melt snow and ice. *Cement and Concrete Composites*, 84, 134–145.

Fernandes, F., *et al.*, 2014. On the feasibility of using phase change materials (PCMs) to mitigate thermal cracking in cementitious materials. *Cement and Concrete Composites*, 51, 14–26.

Gao, Y., Huang, L., and Zhang, H, 2016. Study on anti-freezing functional design of phase change and temperature control composite bridge decks. *Construction and Building Materials*, 122, 714–720.

Gomis, J., *et al.*, 2015. Self-heating and deicing conductive cement. experimental study and modeling. *Construction and Building Materials*, 75, 442–449.

Hunger, M., *et al.*, 2009. The behavior of self-compacting concrete containing micro-encapsulated phase change materials. *Cement and Concrete Composites*, 31 (10), 731–743.

Jayalath, A., *et al.*, 2016. Properties of cementitious mortar and concrete containing micro-encapsulated phase change materials. *Construction and Building Materials*, 120, 408–417.

Kantro, D, 1980. Influence of water-reducing admixtures on properties of cement paste – a miniature slump test. *Cement, Concrete and Aggregates*, 2, 95–102.

Karayolları Genel Müdürlüğü, 2021. 2020 Yılı Devlet ve İl Yolları Bakım-İşletme Maliyetler, Ankara.

Karayolları Genel Müdürlüğü Tesisler ve Bakım Dairesi Başkanlığı, 2018. Kar ve Buzla Mücadele Rehberi, Ankara.

Kitchener, B. G., Wainwright, J., and Parsons, A.J, 2017. A review of the principles of turbidity measurement. *Progress in Physical Geography: Earth and Environment*, 41 (5), 620–642.

Lund, J.W, 2005. Pavement snow melting. Geo-Heat Center, Oregon Institute of Technology, Klamath Falls, OR.

Lv, L., *et al.*, 2016. Synthesis and characterization of a new polymeric microcapsule and feasibility investigation in self-healing cementitious materials. *Construction and Building Materials*, 105, 487–495.

Manning, B.J., *et al.*, 2015. Assessing the feasibility of incorporating phase change material in hot mix asphalt. *Sustainable Cities and Society*, 19, 11–16.

Norvell, C., Sailor, D.J., and Dusicka, P, 2013. The effect of microencapsulated phase-change material on the compressive strength of structural concrete. *Journal of Green Building*, 8 (3), 116–124.

Rangaraju, P.R., *et al.*, 2006. Potential of potassium acetate deicer to induce ASR in concrete, and its mitigation. American Society of Civil Engineers Airfield and Highway Pavements Specialty Conference, Atlanta, Georgia, United States, 683–694.

Sahmaran, M, 2020. Elektrostatik Yük Boşaltma Kabiliyetine Sahip Yeni Nesil Çimento Bağlayıcılı Kompozitler. TÜBİTAK 1002-Hızlı Destek Programı, 119M175 Numaralı Proje, Ankara.

Sahmaran, M., Christianto, H.A., and Yaman, İ.Ö., 2006. The effect of chemical admixtures and mineral additives on the properties of self-compacting mortars. *Cement and Concrete Composites*, 28 (5), 432–440.

Sakulich, A. R., and Bentz, D. P, 2012. Increasing the service life of bridge decks by incorporating phase-change materials to reduce freeze-thaw cycles. *Journal of Materials in Civil Engineering*, 24 (8), 1034–1042.

Savija, B, 2018. Smart crack control in concrete through use of phase change materials (PCMs): a review. *Materials*, 11 (5), 654.

Seferoğlu, A., Seferoğlu, M., and Akpınar, V, 2015. Karayolu ve Havayolu Kaplamalarında Kullanılan Kar ve Buzla Mücadele Yöntemlerinin Mali Analizi. *Gazi Üniversitesi Fen Bilimleri Dergisi Part C: Tasarım ve Teknoloji*, 3 (1), 407–416.

Wang, C., *et al.*, 2008. Effect of carbon fiber dispersion on the mechanical properties of carbon fiber-reinforced cement-based composites. *Materials Science and Engineering: A*, 487 (1–2), 52–57.

Wu, J., Liu, J., and Yang, F, 2015. Three-phase composite conductive concrete for pavement deicing. *Construction and Building Materials*, 75, 129–135.

Xiong, W., *et al.*, 2015. A novel capsule-based self-recovery system with a chloride ion trigger. *Scientific Reports*, 5 (1), 10866.

Xiong, T., Shah, K.W., and Kua, H.W, 2021. Thermal performance enhancement of cementitious composite containing polystyrene/n-octadecane microcapsules: an experimental and numerical study. *Renewable Energy*, 169, 335–357.

Yeon, J.H., and Kim, K.K, 2018. Potential applications of phase change materials to mitigate freeze-thaw deteriorations in concrete pavement. *Construction and Building Materials*, 177, 202–209.

Zhang, J, and Das, D.S, 2009. Selection of effective and efficient snow removal and ice control technologies for Cold-Region Bridges. *Journal of Civil, Environmental and Architectural Engineering*, 3 (1), 1–14.

APPENDIX 2 – Thesis Originality Report

CIRRICULUM VITAE